Modeling of the atmospheric dispersion of heavy metals over Poland

Janusz Zysk

AGH University of Science and Technology
Faculty of Energy and Fuels
Department of Sustainable Energy Development

University Paris-Est
Ecole des Ponts ParisTech
Centre d'Enseignement et de Recherche en Environnement Atmosphérique

DOCTORAL THESIS

Mgr inż. Janusz Zyśk

Fields of study:
Chemical Technology at Faculty of Energy and Fuels,
Science and technology of the environment at École des Ponts ParisTech

Modelling of atmospheric transport of heavy metals emitted from Polish power sector

Date of defence 30-06-2016

Supervisors:
Prof. dr hab. Janusz Gołaś
Professor Christian Seigneur Ph.D., hab.
Auxiliary supervisor:
Yelva Roustan Ph.D.

Kraków, 2016

Oświadczam, świadomy (-a) odpowiedzialności karnej za poświadczenie nieprawdy, że niniejszą pracę doktorską wykonałem (-am) osobiście i samodzielnie i że nie korzystałem (-am) ze źródeł innych niż wymienione w pracy.

.....

podpis autora pracy

Content

Acknowledgements

I would like to express my gratitude to Professors Janusz Gołaś and Christan Seignerur for their guidance as the supervisors of my Thesis. Thank you for helpful discussions and professional advice during my work on this Thesis.

I would like to express my special appreciation and thanks to Dr. Yelva Roustan, you have been a tremendous mentor for me. I would like to thank you for encouraging my research and for allowing me to grow as a research scientist.

I am greatly indebted to Dr. Artur Wyrwa for introducing me into the fascinating world of science. Your advice on both research as well as on my career has been priceless.

I would also like to thank Professors Louis Jestin, Bruno Sporitsse, Luc Musson-Genon, Wojciech Suwała, Denis Quelo, Mariusz Filipowicz for their kindness, helpful and professional advice.

I would like express my appreciation to the late professors Piotr Tomczyk and Adam Guła, who always surrounded me with unusual kindness.

1 Introduction

During the last decades many studies have been conducted to investigate the atmospheric heavy metals contamination and its deposition to ecosystems.

The increasing attention to mercury pollution has been mainly driven by the growing evidence of its negative impacts on wildlife, ecosystems and particularly human health. It should be noted, that after mercury moves through the water chain it can be transformed by aquatic microorganisms into methylmercury (MeHg), which is much more toxic than the other forms. Subsequently, MeHg is bioaccumulated in fish and seafood [1]. The predator fish can contain almost 100% of mercury in methylmercury form. Eventually, it enters the human body with consumed food. It is then transported by blood and can easily pass the blood-brain barrier and cause neurotic dysfunctions. It is reported that even relatively low doses can damage the nervous system. The symptoms that can be observed are: blurred vision, malaise, dysarthria, paraesthesia, ataxia, impairment of hearing and difficulty in walking. Symptoms appear slowly and increase gradually along with the amount of mercury accumulated in the body [1]. It should be highlighted, that mercury also passes through the placental barrier and has an immense negative impact on the foetus, decreasing the IQ of a child. In this way, the development of whole populations is influenced. It is reported that methylmercury can be the cause of a cancer, kidney dysfunction, heart and blood system diseases.

The most spectacular poisoning of methylmercury occurred in Minamata in Japan in the forties, fifties and sixties of the XX century, when the local chemical factory producing acetaldehyde released the mercury in the industrial water waste into the local gulf since 1932 until 1968. Although, the mercury concentration in water was not so high, it ensued the accumulation of mercury as methylmercury in fish and shellfish, which finally was consumed by local people and accumulated in their bodies. Until March 2001 approximately 3000 officially certified patients were identified, among them, 1784 who have already died [2]. The largest, outbreaks of mercury poisonings occurred in Iraq in winter 1971 -1972 due to the consumption of seed grain, which had been treated with fungicides containing mercury. It was estimated that around 40000 individuals were affected, 6300 were hospitalized and 450 people died [3].

Mercury can also enter the human body through inhalation of the vapours. The effects such as insomnia, memory loss, headaches, tremors are usually short lived. Results of preliminary studies on the assessment of external effects of anthropogenic mercury emissions have already been published [4]. It was reported that mercury can affect the function of kidneys,

respiratory system, heart and blood system, digestive system, immune system, liver and the reproductive system.

For the first time ever, a mass cadmium poisoning was documented, in Japan again, in the Toyama province in 1964. The people felt an intense pain of joints, muscle and spine therefore the disease was named Itai-Itai – which in Japanese means intense pain. The reason for the accumulation of cadmium in the body of the residents in Toyama was the consumption of the rice, which was polluted by cadmium compounds [5]. Cadmium enters the human body through the respiratory system, human gastrointestinal tract and skin. The high concentration of cadmium in the air causes acute poisoning. The symptoms of cough, burning sensation inside the chest, headache, dizziness, general malaise, chills, sweating, nausea, vomiting and diarrhea are mainly observed. Long exposure to cadmium, which is contained in the air has a negative effect on the skeleton (bone structure) and the kidneys. Moreover the positive correlation between cadmium exposure and cancer of the prostate and lung was observed.

Lead is also a toxic heavy metal which is being emitted into the atmosphere by anthropogenic as well as natural sources. This heavy metal has effects on the human health even at very low exposures and causes negative impacts mainly in circulatory, nervous, genitourinary systems. Intense studies were launched in the 70s of the XX century, which led to determine the dose-response functions for the impact of lead on the human health. The measurements of lead content in human blood allows for the quantification of the risk of appearance of health hazard. Long-term lead exposure can cause the level of lead in the body that finally causes the disease, which is called lead poisoning. The most common symptoms are insomnia, hallucinations, cognitive deficit and tremors. Unfortunately, also lead -as in the case of mercury - passes through the placental barrier and accumulates in the body of infants, which may lead to many diseases [6].

The harmful influence on humans and the environment of these three heavy metals was underlined in the Aarhus Protocol on Heavy Metals of 1998. The Parties of this protocol (including Poland) are obligated to reduce emissions, observe the transport and the amounts of lead, mercury and cadmium in the environment.

Moreover the European Union has made many efforts to decrease heavy metals emission and the use of those. The legislation of the European Union draws attention to control the amount of mercury, lead, cadmium and other heavy metals in air, water and food. The number of directives linked to mercury, lead and cadmium have given voice to particular concern for decreasing negative impact of heavy metals and heavy metal compounds on human health.

One can enumerate a numbers of directives and regulations, e.g.:

- 76/768/EEC, 76/769/EEC, 79/117/EEC, 91/188/EEC, 98/8/EC, 2000/53/EC, 2002/95/EC, 2002/96/EC, 2006/66/EC, 2007/51/EC restrict the use of mercury, lead and cadmium in industry, agriculture, cosmetics;
- 96/23/EEC, 2000/60/EC, 2001/22/EC, 2006/118/EC/ 2006/1881/EC are dedicated to mercury, lead and cadmium control in water and food;
- 80/68/EEC, 98/83/EEC, 2006/118/EC, 2008/105/EC limit heavy metals content in water, groundwater and drinking water;
- 2004/107/EC requires to measure the mercury background concentration with spatial resolution of 100,000km^2 and provide the long-term trends of mercury and cadmium concentration as well as arsenic and nickel in air;
- 96/61/EC (IPPC), Integrated Pollution Prevention and Control, which order to use the Best Available Techniques (BAT) to reduce pollutant emissions from power plants, chlorine production industry and cement production sector;
- 2001/80/EC (LCP) imposes limits of emissions of PM, which contains mercury, lead, cadmium and other heavy metals;
- Regulation (EC) No 1102/2008 mercury, mercury compounds, substances with containing more than 95% of mercury are prohibited to be exported out of the EU;
- 2010/75/EU (IED) replacing i.e. LCP and IPPC which will lead to considerable emission reduction via review of BREFs and adoption of BAT for industrial activities.

In 2005 the EU launched the "Community Strategy Concerning Mercury" aimed at reduction of negative impacts of mercury and the risks it poses for the environment and human health. In conclusion of the revision of this Strategy in 2011, the European Council stressed the importance for the EU to participate actively in and to give full support to the international negotiations on a new global mercury convention that have been initiated by UNEP in 2009.

The Minamata Convention on Mercury was prepared during 4 years of intergovernmental negotiations. It was opened for signature at the conference in Kumamoto, Japan in October 2013 and was signed by nearly 100 countries i.e. China, India, Germany, Brazil, South Africa, the United States and Poland. The Convention included the actions which should be taken to protect the human health and the environment from anthropogenic emissions and releases of mercury and mercury compounds [7].

The monitoring of heavy metals and above all mercury concentration and deposition over Europe is currently insufficient to provide accurate data on heavy metals concentrations and depositions. In some parts of Europe, there is a lack of sampling stations and thus such areas are not covered by monitoring at all. Therefore, it appears interesting to complement the

results of measurements by the modelling methods, keeping in mind the remaining uncertainties of mercury and other heavy metals modelling [8], [9]. The pathway of mercury dispersion in the atmosphere is complex therefore one of the key issues in reactive dispersion modelling of mercury is the chemistry model that represents the reactions and mass exchange between the gaseous, aqueous and particulate phases. During the last few decades, several chemical schemes have been implemented in different Chemical Transport Models (CTM) developed to represent the atmospheric dispersion of mercury. Some intercomparison studies were performed over Europe [10], [11], [12]. These studies were taken into account in the implementation of a chemistry scheme devoted to mercury within the framework of the Polyphemus air quality modelling system [13].

Poland is still one of the biggest emitter of mercury, lead and cadmium in Europe mainly due to emission from coal combustion processes. It should be underlined that the emissions in Poland systematically decrease mainly due to significant power sector investment in emission control equipment, which besides limiting emission of pollutants such as PM, SO_2 and NO_x, reduce significantly the emissions of other air pollutant including Hg, Cd and Pb [14].

The objectives of this work were twofold: (i) scientific and (ii) practical.

The scientific objective was to develop a model to represent the atmospheric dispersion of mercury and to implement it in the air quality modelling platform Polyphemus.

The practical objective was to run the model and perform heavy metals dispersion studies over Europe and detailed studies of the impact of the polish power sector on the air quality regarding mercury, cadmium and lead.

Some examples of questions that can be asked or hypotheses that can be verified in this work are presented below:

- does the dry deposition of gaseous elemental mercury have the greatest influence on obtained mercury deposition results?
- what is the contribution of different atmospheric reactions to atmospheric mass balance of reactive mercury?
- is most of the deposited mercury in Poland emitted outside Poland?

- what is the contribution of the power sector plants to local mercury deposition in Poland?
- does the concentration of reactive mercury and lead and cadmium depend strongly on local emission sources?

Within the scope of this work computing codes have been developed with the use of C/C++ and Fortran programing languages. Several pre-processing programs were written in C/C++ to prepare and calculate input data to model i.e. (i) dry deposition velocity for gaseous mercury species; (ii) natural emission and reemission flux of mercury, (iii) anthropogenic emission of mercury, (iv) boundary and initial contractions of mercury, (v) concentration of chlorine species, which react with mercury. The Fortran code of the chemical transport model was implemented in the Polyphemus/Polair3D system and consists of three sections dedicated to gaseous and aqueous phases and to particulate mercury (please see Appendix 1). Additionally many C/C++ codes were prepared to process obtained results e.g.: to evaluate the results of the modelling against observations.

The dissertation consists of two parts.

• Part I is devoted to a literature review of the cycle of heavy metals in the environment.

As the modelling work is based on previous laboratory research, measurements, estimations and assumptions, a review of the literature regarding emissions, chemistry and measurements of mercury, lead and cadmium was conducted. The state of the art in the development of chemical transport mercury models is described.

• Part II is devoted to the development and application of the new chemical transport model for mercury and modelling of atmospheric transport of lead and cadmium.

This part describes the development and application of the model dedicated for mercury, cadmium and lead dispersion in the atmosphere. The main assumptions and data used are presented. The obtained results are presented, evaluated and discussed. The conclusions of the Thesis, are focused on the obtained results and the scientific achievements completed in this Thesis.

In this Thesis, the term Polish power sector covers all power, cogeneration (CHP) and regional/city heating plants located in Poland which use hard or brown coal, as the main fuel. The main coal-based plants that primarily work for the industry sector but have a part of their production is designated for the market, are also included in this term.

PART I Review of the literature of the cycle of heavy metals in the environment

2 Heavy metals in the environment

2.1 Global cycle of heavy metals

Heavy metals are emitted to the atmosphere from natural and anthropogenic sources (Figure 2-1). In the atmosphere, cadmium and lead occur only as components of particulate matter (aerosols). Particulate matter is defined in its simplest form as a microscopic solid or liquid matter suspended in the Earth's atmosphere. The atmospheric aerosols are composed mainly of species/compound such as sulphates, nitrates, organics and black carbon. The share of heavy metals in aerosols is relatively low. Therefore, the atmospheric transport and behaviour of heavy metals is considered and analysed as linked to the characteristics of aerosols.

On the other hand, mercury occurs in the atmosphere in three forms:

- GEM –gaseous elemental mercury ($Hg^{0}_{(g)}$), which is a prevailing form of mercury in the atmosphere.
- RGM –reactive gaseous mercury ($Hg^{I}_{(g)}$, $Hg^{II}_{(g)}$) in organic and inorganic compounds. The inorganic compounds include compounds such as: $HgO_{(g)}$, $HgCl_{2(g)}$, $Hg(OH)_{2(g)}$, $HgBrOH_{(g)}$, $HgBr_{2(g)}$. The organic compounds are represented mainly by compounds which include one (monomethyl mercury -MMM) or two (dimethyl mercury -DMM) methyl groups e.g.: CH_3HgCl, CH_3HgOH, $Hg(CH_3)_2$.
- particulate forms of mercury (Hg_P). The mercury in aerosols could be represented by compounds such as: HgO, $HgSO_4$.

These three species exhibit different transport characteristics. Gaseous elemental mercury can be considered as a global pollutant due to its residence time in the atmosphere. Reactive gaseous and particulate forms of mercury are deposited more quickly by wet and dry deposition processes than elemental mercury [15], [8].

Heavy metals are removed from the atmosphere through wet and dry deposition process. Wet deposition is the process of removal of gaseous and particulates matter pollutants from the atmosphere where condensed water is involved. In this process, water captures pollutants and together with precipitation pollutants are moved to the Earth surface. This process occurs where ever precipitations and clouds are present. The pollutants absorbed by clouds are removed together with the removal of mass (volume) of clouds by precipitation. Precipitation also absorbs pollutant located below clouds and also remove them. Therefore the wet deposition can be split between in-cloud (rainout) and below cloud (washout) scavenging. Dry

deposition is a transport of gaseous as well as aerosols pollutants to the ground surface where those are absorbed by soil, water, flora and others materials that cover the ground during periods without precipitation. The significant part of deposited pollution is (often immediately) reemitted to the air. The heavy metals in aqueous environments undergo complex chemical and physical reactions and transformations [6], [16].

The heavy metals included in air as well as deposited to surfaces and transferred to water and food, may get in the human body, where there are usually accumulated resulting in various adverse effects, as already mentioned in the introduction chapter.

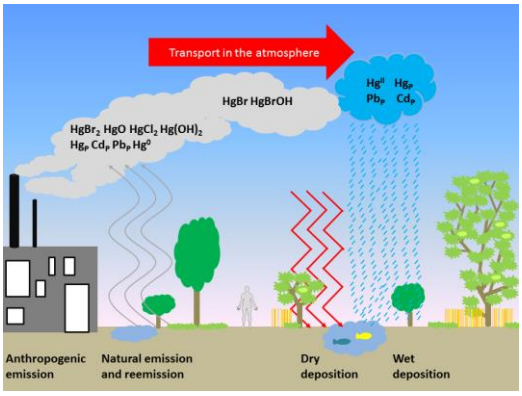

Figure 2-1. The sources, pathway and sinks of heavy metals in the atmosphere.

Naming

In the model concentration and deposition of 9 forms or compounds of mercury are being tracked. Seven in the gas phase i.e. $Hg^{0}_{(g)}$, $HgBr_{(g)}$, $HgO_{(g)}$, $HgBrOH_{(g)}$, $HgCl_{2(g)}$, $Hg(OH)_{2(g)}$, $HgBr_{2(g)}$, one in the aqueous phase ($Hg^{II}_{(aq)}$) and one in particulate form (Hg_P). The particulate form of mercury in the model is additionally split into particulate size sections. As the mercury occurs in 3 speciation forms in gaseous and aqueous phases, the common names and acronyms were used to determine chosen mercury forms. The species in gas phase are written with the index *"(g)"* and those in the aqueous phase with *"(aq)"*. In Table 2-1 all acronyms are listed along with selected species, which are included in them.

Table 2-1. Names and acronyms used in manuscript of various mercury species. "Yes" in table indicates that the specie belongs to a group described by acronym and name.

N		species track in the model				
1.	Common names and acronyms	$Hg^{0}_{(g)}$	$HgBr_{(g)}$	$HgO_{(g)}$ $HgBrOH_{(g)}$ $HgCl_{2(g)}$ $Hg(OH)_{2(g)}$ $HgBr_{2(g)}$	$Hg^{II}_{(aq)}$	Hg_P
2	Mercury	yes	yes	yes	yes	yes

3	GEM –gaseous elemental mercury	yes				
4	RGM –reactive gaseous mercury		yes	yes		
5	RGPM –reactive gaseous mercury and particulate forms of mercury		yes	yes		yes
6	RM –reactive mercury		yes	yes	yes	yes
7	RGAM –reactive gaseous mercury and reactive mercury in aqueous phase		yes	yes	yes	

2.2 Heavy metals emissions into the atmosphere

Heavy metals are emitted into the air from anthropogenic and natural (including reemissions) sources. The amounts of anthropogenic emissions of mercury are mainly estimated with the use of a top-down methodology or a bottom-up approach. To assess the natural emissions of mercury the global mercury models and measurements of mercury fluxes are applied.

2.2.1 Natural emissions of heavy metals

Mercury

Mercury is naturally emitted into the atmosphere from the Earth crust (where it occurs as the mineral of cinnabar) through the soil erosion, volcanic activities, geothermal vents, wild fires, evasion from water, and also from remission processes of previously deposited mercury. Additionally, preciously deposited mercury is reemitted from land and ocean surfaces.

The global natural emissions and reemissions of mercury are estimated as the part of global mercury fluxes and budget with use of global mercury models. The natural emissions have a significant role in the global budget of mercury, therefore the precise estimation of the amount of it is a significant issue. The estimation of mercury from natural emissions and reemissions from various sources is presented in Table 2-2.

Table 2-2. Estimation of natural emissions and reemissions of mercury using global mercury models [$Gg.y^{-1}$].

N.	Emissions from land		Emissions from ocean		Total	Reference
	natural	reemission	reemission	natural		
1	0.5	2.0	1.4	3.9		[17]
2	2.0		2.0		4.0	[18]
3	1.0		0.4	0.4	1.8	[19]
4	0.81	0.79	1.3	1.3	4.2	[20]
5	1.18	1.08	1.05	0.95	4.26	[21]
6	0.5	1.5	2.4	0.4	4.8	[22]

Estimates of natural mercury emission exist but they are based on flux measurements exist that represent limited areas and time scales [23], [24]. The most comprehensive measurements

of Hg flux in range from -0.1 to 2.7 $ng.m^{-2}.h^{-1}$ (with average 0.9 $ng.m^{-2}.h^{-1}$) from 1326 samples at 46 sites led to estimated annual natural emissions of 100Mg of mercury over the United State [23]. One of the highest upward flux was observed in China and equals 204 $ng.m^{-2}.h^{-1}$. It should be noted that the process of air-surface exchange of mercury is complex. There is bi-directional phenomena, which consists of: (i) downward flux -dry deposition processes, (ii) upward flux –natural and reemission phenomena.

Most measurements indicate the upward flux as the prevailing process. The measurements show that approximately 80% of the time the upward flux is greater than the downward flux [25].

The magnitude of the downward flux and upward flux depends on many factors such as: (i) type of surface, (ii) soil type, (iii) meteorological condition, (iv) amounts of mercury deposited previously (v) the method of measurement [26]. The conducted measurements presented in the literature give some general correlation of the amounts of the natural emission of mercury to meteorological parameters. A positive correlation between a mercury upward flux and the temperature of soil, solar radiation, wind speed was reported in many studies e.g. [24]. The increase of relative humidity slows down the natural emission of mercury [24].

To assess the natural emission and remission of mercury from various sources on limited areas, a dedicated models has been also developed. Biogenic Emission Inventory System Version 3.11 was used to estimated emission of mercury from vegetation of 44 $Mg.y^{-1}$ (from 31 to 140 $Mg.y^{-1}$) in the continental USA and from 79 to 179 $Mg.y^{-1}$ in China [27]. The Mercury Emission Model (MEM) was developed to investigate the empirical correlation of mercury flux from background soils to the atmosphere with various factors such as: surface soil temperature and moisture, solar radiation [28].

Over Europe (in the EMEP domain) annual global natural emissions over land of 1 Gg and natural emissions and reemissions over water of 0.8 Gg was spatially distributed over the Northern Hemisphere [29].

The natural flux of mercury from land is estimated based on four types of land and surface temperature dependence and can be expressed for temperatures above 273K:

$$F = A \cdot exp(-E/(R \cdot T)) \qquad \text{R.2.1}$$

where:

F –flux from soil [$ng.m^{-2}.h^{-1}$];

T –surface temperature [K];

E –activation energy [$J.mol^{-1}$] assumed $8.37 \cdot 10^4$ according to empirical results;

A –constant function of land type and equals: $3.47 \cdot 10^{14}$, $1.74 \cdot 10^{15}$, $3.47 \cdot 10^{15}$ for background soil, mercuriferous belts and deposited areas. No emission over glaciers was assumed;

R –gas constant, 8.314 [$J.mol^{-1}.K^{-1}$];

The flux from soil equals 0 for surface temperatures below 273K.

The total natural flux of mercury from water surface was distributed spatially according the proportionality of mercury emission from the ocean to the primary production of organic carbon in water [29].

The assessment of reemission of mercury in Europe of approximately 50 $Mg.y^{-1}$ were done with use of the simple box model [29]. The model calculated first the total load of mercury deposited in Europe during the last century and next the output flux from soil with the assumption of the life time of mercury according to reemission of 400 years and hydrological leaching of 950 years.

As mentioned previously the mercury can be naturally emitted not only by the process of exchange between surface and air but also by natural fires and volcanic activity. The annual global emission of mercury from volcanic activity were estimated to range from 90 Mg to 360 Mg [21]. Mercury by natural and remission processes is being emitted into the atmosphere mainly (greater than 99%) in elemental form (GEM) [30]. Although wildfires are responsible for approximately 13% of the emitted mercury, it appears mostly in particulate form [31]. On the other hand wildfires are not significant sources of mercury emission (only approx. 20 $Mg.y^{-1}$ [32]). Modelling studies and observations show that sea-salts can be significant source of mercury, the concentrations of Hg^{II} bounded to sea-salts aerosol particles are 25 -45 $pg.m^{-3}$ [33].

Lead

Lead is an element that is naturally present in many minerals, soil and rocks. The global average concentration of lead in soil equals 22 $mg.kg^{-1}$ [6]. The weathering of rocks and volcanoes are the main source of migration of lead from the lithosphere to the biosphere. The major natural sources of lead emitted into the atmosphere are sea salts, soil particles, volcanic eruptions, forest fires. The annual natural global emissions of lead into air were estimated at 12 Gg (range 0.91 -23 Gg) in 1983 [32]. According to these data the mean flux of lead from land is 54 $g.km^{-2}.y^{-1}$ while from sea surface it is 4 $g.km^{-2}.y^{-1}$. Relatively recent research led to 150 times higher with annual emissions amounting to 1.8 $Tg.y^{-1}$ (range from 0.22 to 4.9 Tg) [34]. In these two reported results, there are large differences in estimations of the amounts of lead released with soil particles, in particular during dust storms. For this source, emissions of 3.9 $Gg.y^{-1}$ and 1.7 $Tg.y^{-1}$ were estimated. Because of a high frequency of storm in deserts,

these areas cover nearly 100% of the global natural emission. The deposited lead can be reemitted into the air, e.g. through re-suspension of soil. Detailed studies in California showed that the remission is 10 times higher than direct anthropogenic emission of lead into air [6].

Cadmium

The mean natural emissions of cadmium into the air amount to 1.3 Gg (range from 0.15 -2.6 $Gg.y^{-1}$), the global average flux from sea surface amounts to 0.2 $g.km^{-2}.y^{-1}$, the global flux from land surface amounts to 3.7 $g.km^{-2}.y^{-1}$ (estimated for 1983) [32]. Most of the emissions come from: volcanoes 820 Mg, soil particles during dust storms 210 Mg, vegetation, pollen and spores 190 Mg, natural forest fires 110 Mg and sea spray 60 Mg. The relatively newest estimation shows the results of annual emission of 41 Gg [34]. According to this work, cadmium was mainly released during dust storms over deserts. The emissions from this source were estimated at 24 $Gg.y^{-1}$, from natural forest fires at 13 $Gg.y^{-1}$ and from sea salts at 2 $Gg.y^{-1}$.

2.2.2 Anthropogenic emission of mercury into the air

Mercury is emitted into air from sectors where mercury is being used intentionally in processes and from sectors where mercury is useless and undesirable and results as a by-product.

Mercury is used in artisanal and small scale gold mining to produce an amalgam, which is used to separate gold from other materials. Despite the introduction of new restrictions, it is still used in a number of products including batteries, energy-sawing lamps, electronic and electrical devices, measuring devices (thermometers, blood-pressure gauges), pesticides, pharmaceuticals, preservative in paints. In 2010 approximately 1100 Mg of mercury were used in these products [16]. Therefore, a significant amount of mercury is emitted from waste and waste treatment processes. The dental amalgam is still used for filling teeth leading to mercury, which is released into the atmosphere during body cremation and during preparation, production of fillings and from fillings which were removed. Also, in the industry, in the process of production of chlorine and caustic soda mercury-cell are also still being used.

Mercury is emitted into air from fossil combustion, mainly from coal combustion. The concentration of mercury in coal is not high but the large volume of consumption of coal (approximately 6000 $Tg.y^{-1}$) causes large emissions of mercury from this sector (25% of total anthropogenic mercury emissions to the atmosphere) [35]. According to the World Coal Quality Inventory the average content of Hg in 1500 coal samples from almost 50 countries

and regions equals 0.24 $mg.kg^{-1}$ [36]. The most extensive measurements regarding emissions of mercury from coal combustion were conducted in the United States [37]. Nearly 28 thousands samples of hard coal (bituminous) and 1 thousand samples of brown coal (lignite) were analysed. The obtained results of mercury concentration in coal were in the range of 0.0 -1.3 $mg.kg^{-1}$ and 0.02 -0.75 kg^{-1} for hard and brown coal, respectively while for both types of coal average mercury content was observed at 0.11 $mg.kg^{-1}$. The values of mercury content in coal of United States are related to dry coal. Analysis of 56 samples in China indicated the average mercury content at 0.15 $mg.kg^{-1}$ in raw hard coal and 0.28 $mg.kg^{-1}$ in raw brown coal [38]. The results ranged from 0.01 and 0.03 to 1.13 and 1.53 $mg.kg^{-1}$ for hard and brown coal, respectively. They also presented a comprehensive review of mercury content in coals from different countries and regions, which leads to the conclusion that the mercury content in Polish coals does not differ significantly from global results.

Mercury in coal is hosted in both inorganic and organic compounds. Mercury creates the inorganic compound mainly in forms of sulfanediide (e.g cinnabar -HgS), sulphate and chloride. Mercury also occurs in pyrite (FeS_2). It was observed that the concentration of mercury may be a dozen times higher in pyrite compared to directly adjacent coal [39]. Mercury from crude oil and natural gas is removed before final consumption, therefore combustion-related emissions are relatively low.

Mercury is also included in raw materials that are used in the cement production sector. Additionally, in this sector mercury is emitted from fossil fuels which are burned to produce heat. Mining, smelting, and production of iron and non-ferrous metals are also significant sources of mercury, which is included in ores use. The mercury content into Cu-Ag ores in Poland reaches even 61 $mg.kg^{-1}$, with an average value of 0.3 -2 $mg.kg^{-1}$ depending on the type of ores and the place of extraction [40]. The Zn-Pb ores includes significantly less mercury, the measurements did not exceed 0.6 $mg.kg^{-1}$. Most of the mercury contained in ores, that are captured and stockpiled or sold to be used intentionally in industrial processes and products, is eventually released to the air.

Globally, the anthropogenic emissions of mercury into air is about two times lower than by natural emissions. The global estimations show ~2000 Mg of mercury emitted annually into air from human activities (Table 2-3). The anthropogenic emissions are estimated in many countries each year e.g. in all European countries within the EMEP program [14]. Despite many efforts, which include: (i) international projects where experts are involved, (ii) measurements of mercury (e.g. emitted, in coal, deposited), (iii) estimates done for specific

counties and sectors, the range of possible global emission of mercury is still very wide. For example, the global emission of mercury is estimated to range from 1010 to 4070 $Mg.y^{-1}$ in 2010 [35]. The assessment of global anthropogenic emission during the last 2 decades presented in different publications are listed in Table 2-3.

Table 2-3. Global anthropogenic emissions of mercury into atmosphere.

N.	Year	Emission [$Mg.y^{-1}$]	Reference
1	1998	2143	[21]
2	1999*	2160	[17]
3	2000	2206	[41]
4	2000	2190	[42]
5	2002*	2400	[20]
6	2005	1480	[1]
7	2007	2320	[43]
8	2008	1287	[44]
9	2010	1554	[45]
10	2010	1960	[35], [16]

* no specific year was given, the assumption that emission inventory is for year of publication was made.

China is the biggest world emitter, with an annual emission of approx. 570 Mg in 2010 [16], [45]. Whole Asia is responsible for half of anthropogenic mercury emission to the atmosphere with an annual emission of 968 Mg (Figure 2-2).

Globally, 854 Mg of anthropogenic mercury is being emitted from sources where mercury is used intentionally and 1112 Mg from sectors where the presence of mercury is unwanted (Figure 2-3). Artisanal and small-scale gold mining and coal combustion are the most significant sources with a share in total emission of 36.7% and 24.9%, respectively. The share of anthropogenic mercury emissions into the air for different regions and activity sectors is presented in Figure 2-2 and Figure 2-3, respectively.

Figure 2-2. The contribution of regions in anthropogenic emission of mercury into the air in 2010 [%]

[35].

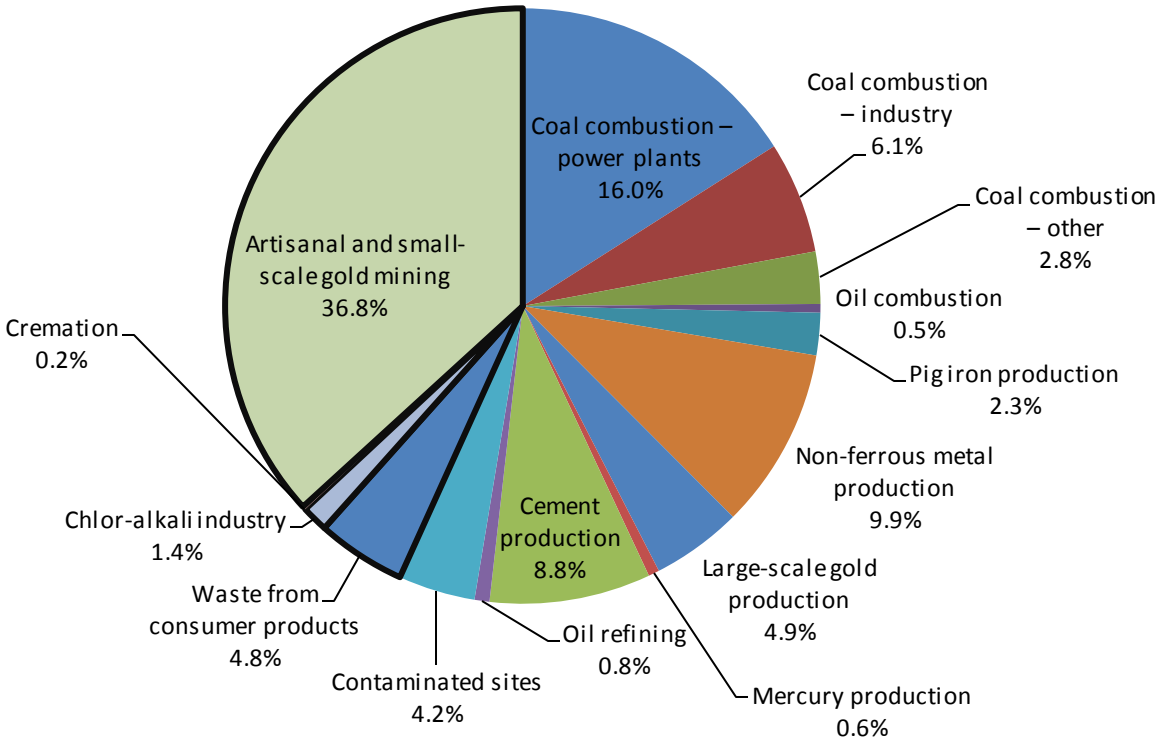

Figure 2-3. The share of different sectors in anthropogenic emission of mercury into the air in 2010 [%]. Sources with intentional use of mercury are marked with black edges [35].

In the UE-27 and other European countries, an amount of 87.5 Mg and 115 Mg of mercury were emitted in 2010, respectively [35]. However, the range of possible anthropogenic emission of mercury is wide and for instant equals 44.5 -226 Mg for UE-27 and 42.6 -289 Mg for other European countries [1]. In most of the European countries the national anthropogenic emissions of mercury are estimated each year and are reported to the European Monitoring and Evaluation Programme (EMEP), which is operating under the Convention on Long-range Transboundary Air Pollution [14]. The efforts to assess the anthropogenic emission from European countries were taken also by various research groups, operating mainly within the scope of international projects e.g. ESPREME (http://espreme.ier.uni-stuttgart.de/), EnerGEO (http://www.energeo-project.eu/) [46], [47].

Within the EMEP inventory programme, there are two types of databases. First, it includes the emission of mercury officially reported by countries which are involve in the program. For example, in Poland the emissions are prepared by the National Emission Center [48]. Second,

the database includes the mercury emissions over Europe, which were used as the input into the chemical transport models developed within the EMEP programme. The emissions of mercury are used in the models after verification of data provided by the national institutions from each country and in the case of a lack of data for some countries the estimation are introduced by experts. The estimations are mainly prepared following a top-down approach with the use of emission factors for defined sources.

The anthropogenic mercury emissions in the European Union (EU-27) were estimated at 100 Mg in 2008 [14]. The emissions of mercury in the European Union countries used in the EMEP model from 2000 until 2010 decreased by one third from 120 Mg to 80 Mg. In 2010, the highest emissions of mercury in the EU-27 were in Poland, Italy, Spain and Germany. The emissions of mercury in European countries, which do not belong to the EU were on the same level of nearly 60 Mg per year between 2000 -2010 (Table 2-4). In most EU-27 countries, the reduction of the amount of mercury emitted into the air was noticeable, during the period 2000 - 2010. The most substantial decreases in mercury emission, relatively speaking, were observed in Malta, Bulgaria and France. During that decade, the estimated amount of mercury emitted in Germany increased 2.5 times from 3.6 Mg in 2000 to 9.3 Mg in 2010. In EU countries, the share of 32%, 28% and 8% was estimated in the overall emission of mercury in sectors where coal is being burned i.e. power sector (SNAP 0101), industrial combustion (SNAP 03) and residential (SNAP 0202), respectively. In Non-EU countries, a share of 47% was estimated to come from the power sector, 19% from industrial combustion and almost 6% from residential. The EU member states emitted 20 Mg of mercury from industrial processes (SNAP 04) and 4 Mg from waste and waste treatment (SNAP 09) in 2008 (Figure 2-4). The highest emissions that originated from the power sector were observed in Poland and Germany in the EU-28, respectively 8.7 and 6.3 Mg of emitted mercury in 2008. The highest emissions from the residential sector and from industrial combustion were estimated in Italy, from industrial processes in Spain and waste treatment in UK.

The accurate emission data of mercury form European Countries can be found in the report of the Netherland's TNO Institute (Netherlands Organisation for Applied Scientific Research TNO- www.tno.nl) [49]. The data were prepared based on two different sources:

1. Projection, which was developed based on emission data for 2000, changes in activity data according to baseline scenarios developed in the context of the Clean Air For Europe (CAFÉ) program. The data for 2000 were developed with a bottom-up approach based on activities and appropriate emission factors.

2. Reported emission in the context of the EMEP programme for 2007 -note that for many countries the TNO and EMEP emissions are on the same level (Table 2-4).

The most significant difference was noticed in Russia. TNO estimated the emission in the European part of Russia to be approximately 92 Mg, which is 4 times higher than EMEP. Most of the mercury emitted in Russia is coming from the power sector. According to TNO results, the highest share in the overall mercury emission into air in Europe came from industry combustion (approx. 47% in EU-28 and 28% in Non-EU countries) and the power sector (54% in Non-EU and 36% in EU-27).

The results of mercury emissions that were published in papers by IIASA (International Institute for Applied Systems Analysis) were obtained using the GAINS (Greenhouse Gas and Air Pollution Interactions and Synergies) integrated modelling tool [46]. GAINS estimates emissions based on fuels and the sectors activity, emission factors and removal efficiency of different forms of mercury (GEM, RGM and Hg_P) by pollution control equipment [45], [47]. According to this estimation Germany represents the major source of mercury emitted into air within the EU-27 in 2010, with the total emissions being nearly two times higher than the officially reported data from EMEP and the emissions of mercury form the power sector were higher in Germany than in Poland (Figure 2-4). Overestimations of emissions of mercury in Germany using the button-up approach compared to the official data was also reported in previous work of TNO [49].

Table 2-4. Emission in European Countries in 2000, 2005, 2008 and 2010 according to the assessment of EMEP, TNO, IIASA [Mg], [14], [49], [46]. Only the countries with annual emissions over 2 Mg. Other countries i.e. Austria, Cyprus, Denmark, Estonia, Finland, Latvia, Lithuania, Luxembourg, Malta, The Netherlands, Slovenia, Sweden, Albania, Belarus, Bosnia & Herzegovina, Croatia, Iceland, Macedonia, Moldova, Norway emit together approx. 10 Mg of mercury per year.

N.	Country	Source of data						
		EMEP reported	EMEP data used into EMEP model				TNO	IIASA
		2008	2000	2005	2008	2010	2010	2010
1	Belgium	3.84	2.60	1.80	3.30	2.05	2.74	2.17
2	Bulgaria	1.39	4.20	3.40	1.60	0.88	1.61	3.05
3	Czech Republic	4.11	3.80	3.80	4.10	3.36	3.92	4.56
4	France	4.30	11.00	6.00	4.00	4.18	6.90	5.12
5	Germany	9.80	3.60	3.80	3.80	9.29	9.78	18.24
6	Greece		13.00	13.00	13.00	7.78	7.78	2.52
7	Hungary	3.01	3.60	3.00	3.00	0.78	2.83	2.46
8	Italy	10.38	9.60	10.00	11.00	9.52	10.71	5.88
9	Poland	15.65	26.00	20.00	16.00	14.85	15.83	15.20
10	Portugal	2.29	3.70	3.40	2.60	2.06	2.76	1.75
11	Romania	8.28	6.70	11.00	12.00	5.34	4.13	3.75
12	Slovakia	2.65	5.90	4.00	4.10	1.18	2.72	0.99
13	Spain	9.49	11.00	10.00	7.80	6.34	10.80	6.24
14	United Kingdom	6.52	8.10	7.10	6.20	6.29	7.19	6.02

15	Russia (European part)		10.00	14.00	23.00	22.54	92.71	17.26
16	Serbia & Montenegro	1.74	5.50	5.40	5.40	1.65	5.34	2.32
17	Switzerland	1.04	2.20	1.10	1.20	1.05	1.05	0.93
18	Turkey		18.00	20.00	22.00	22.34	22.34	15.11
19	Ukraine	6.79	26.00	6.00	6.80	6.79	7.56	7.54

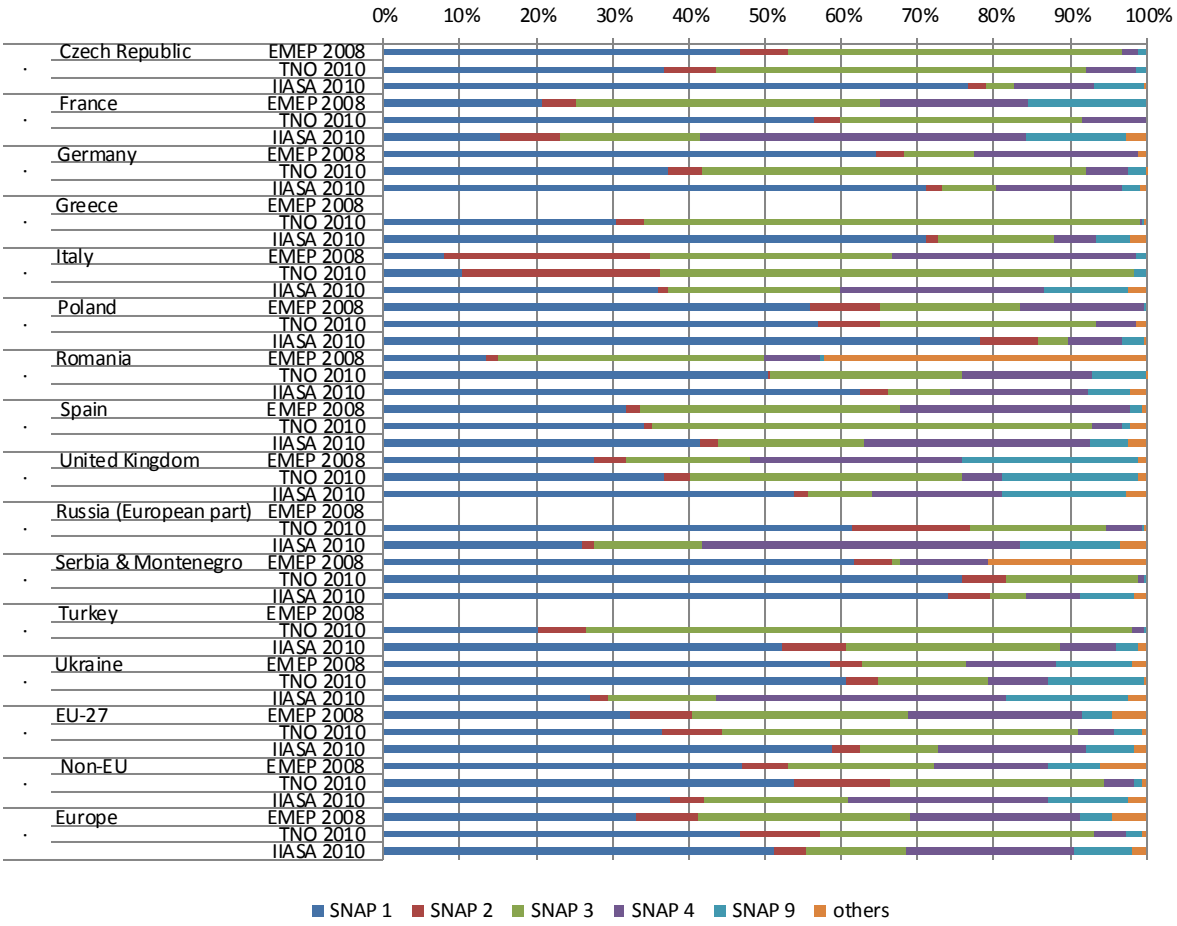

Figure 2-4. The share of mercury emissions from different sources in European countries according to the assessment of EMEP (reported emission) in 2008, TNO, and IIASA in 2010 [%] [14], [49], [46]. Data are provided only for countries with mercury emissions over 4 Mg in 2008 or 2010.

Poland belongs to the European Union countries with the highest mercury emissions. According to data estimation shown in Table 2-4 Poland emits annually approximately 15 Mg of mercury. Coal combustion in the power sector and industry sector remains the main source of mercury emitted into air (Figure 2-4). The Institute of Environmental Projection and its agencies estimates the mercury emissions in Poland for each year and divides them into emission source categories. The amount of mercury is estimated based on activity rate (chemical energy input) and respective emission factors. The mercury emission in Poland for the period 2005 -2010 is presented in Figure 2-5.

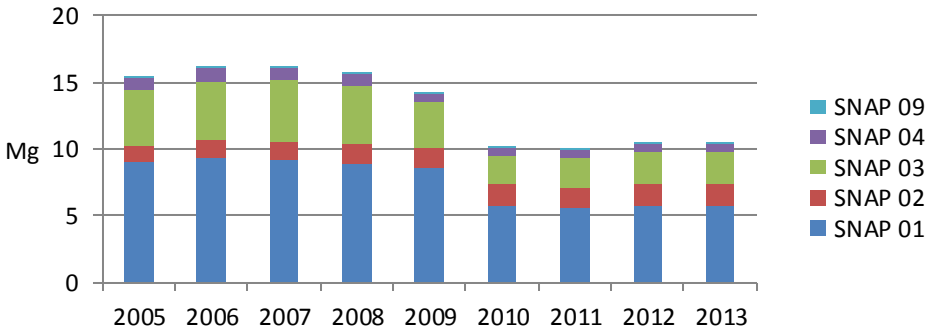

Figure 2-5. Quantity of mercury emitted into air according to the assessment of Institute of Environmental Projection and its agencies [kg] [50], [51], [52], [53], [54], [48], [55].

According to the data presented in Figure 2-5 emissions in Poland have decreased significantly and in 2011 reached the level of 10 Mg. Most of the mercury is being emitted from combustion in energy and transformation industries (SNAP 01). In this sector, mercury is emitted from public power plants (SNAP 0101) and district heating plants (SNAP 0102). Other sources in SNAP 01 i.e.: (i) petroleum refining plants (SNAP 0103), solid fuel transformation plants (SNAP 0104) and coal mining, oil/gas extraction, pipeline compressors (SNAP 0105) emit relatively low amounts of mercury. According to the national estimation from SNAP 0103 -0105, a total of 103 kg and 75 kg of mercury were emitted in 2008 and 2009, respectively. The emissions from public power plants and CHP plants (SNAP 0101) and district heating plants (SNAP 0102) are presented in Figure 2-6. Emissions from power plants and CHP were split into fuel types i.e. hard or brown coal. District heating plants use hard coal (in Poland, one heat plant, which uses brown coal operates and emits approx. 1 $kg.y^{-1}$ of mercury). Moreover, significant amounts of mercury are emitted from households (SNAP 0202), process of the production of cement and zinc (SNAP 0303, 0302) and production of coke and electric furnace steel plant (SNAP 0402).

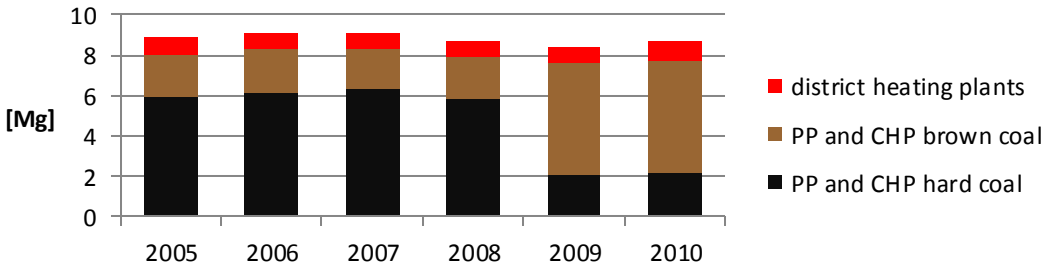

Figure 2-6. Annual emissons of mercury into air from power plants (PP), CHP (SNAP 0101) and district heating plants (SNAP 0102) in Poland in 2005 -2010 according to estimation of the Institute of Environmental Projection [Mg] [50], [51], [52], [54].

As shown in Figure 2-6, the rate of emission of mercury from burning brown and hard coal changed significantly. In the estimation which was prepared for the years 2005-2008, the emission factors of 0.0064 and 0.004 kg.TJ^{-1} were used for hard and brown coal, respectively. The estimation of mercury emission from power and CHP plants prepared for years 2009 and 2010 were based on updated emission factors of 0.0023 kg.TJ^{-1} for hard coal and 0.0114 kg.TJ^{-1} for brown coal [54]. Emission factors of 0.001498 kg.TJ^{-1} for hard coal and 0.006906 kg.TJ^{-1} for brown coal were used for 2010 [48].

The values for hard coal are similar and for brown coal are higher compared to factors provided by the European Environment Agency (EEA) [56]. The EEA recommends to use emission factors in the range from 0.001 kg.TJ^{-1} to 0.0023 kg.TJ^{-1} for hard coal and from 0.0021 kg.TJ^{-1} to 0.0049 kg.TJ^{-1} for brown coal, for the power sector in Europe. The high emission rates originating from brown coal power plants were reported in other studies which in their estimation were based on the mercury content in Polish coals [57], [58]. The estimation of mercury emission from the power sector reported in the literature (beyond results of the Institute of Environmental Projection) are presented in Table 2-5.

Table 2-5. Estimation of mercury emissions from combustion of coal in the Polish power sector [Mg].

N.	Emission of mercury [Mg.y^{-1}]		Year	Reference
	Brown coal	Hard coal		
1	15.1	5.1	2004	[57]
2	14.8	3.6	2005	[58]
3	10.7	5.0	2005	[46]

The content of mercury emission in Poland is very diversified for various deposits. However relatively new results of measurements show, that the average content in brown coal is significantly higher compared to hard coal. The summarized data of mercury content in coal used in the Polish power sector is being provided in Table 2-11.

Table 2-6. The average mercury content of Polish coal reported in the literature [mg.kg^{-1}] (range of obtained results is provided in brackets).

N.	Hard coal	Brown coal	Quality parameters of coal samples	Number of analysed samples		Reference
				hard coal	brown coal	
1	0.196 (0.095 -0.615)	0.120 (0.080-0.205)	as received	40	20	[59]
2	0.085 (0.001 -0.758)	0.322 (0.08 -1.03)	as received	143	102	[40]
3	0.141					[60]

	(0.062 -0.302)					
4	0.120 (0.05 -0.150)	0.250 (0.120 -0.370)	as received	850		[57]
5	~0.10 (0.02 -0.19)		air dried	130		[61]
6	0.0416 (0.0072 -0.0852)		air dried	25		[62]
7	0.138 (0.070 -0.276)		dry basis	17		[63]
8	(0.013 -0.156)	(0.078 -0.258)	air dried	63		[64]
9	0.073 (0.019 -0.168)	0.360 (0.097 -1.300)	dry basis	60		[65]

It should be noted that a discrepancy of mercury content in coal may appear from the preparation of coal samples and presentation of measurement data [66]. The published data should provide the information about quality parameters of the analysed coal (as received, air dried, dry basis).

2.2.3 Emissions of mercury from coal combustion in the power sector

As the combustion of coal is a main source of anthropogenic mercury emissions, the investigation of the emissions from this sector is most desirable. All three main forms of mercury usually are present in flue gases and are then emitted into the atmosphere: elemental gaseous mercury, reactive gaseous mercury and mercury associated with particulate matter. Reactive gaseous mercury may appear in compounds such as: mercuric chloride ($HgCl_{2(g)}$), mercuric bromide ($HgBr_{2(g)}$), mercury oxide ($HgO_{(g)}$), mercuric nitrate ($Hg(NO_3)_{2(g)}$) or mercuric sulphate ($HgSO_{4(g)}$). Mercury associated with particulate matter may be either elemental or oxidised.

During the combustion process when the temperatures reach approximately 1500^0C, mercury included in coal vaporizes to GEM. Elemental mercury may be transformed into other mercury forms when the flue gases are rapidly cooled and interact with other combustion products in the presence of fly ash. The adsorption of mercury on an ash surface was confirmed by the measurements of mercury content in fly and bottom ashes in operating Polish coal-fired power plants [57], [67]. They show that, the content of mercury in fly ashes is many times greater than in bottom ashes. The increase of the unburned carbon content in fly ash and the decrease of temperature of the ashes have a positive impact on the adsorption of mercury [68].

Most of the mercury from boilers enters together with flue gases and ashes to the emission control equipment. Only approximately 1% of mercury remains in bottom ash [69], [38]. The behaviour of mercury during the combustion process and consequently speciation and capture

of emitted mercury from the power sector depends on many factors such as coal characteristics (e.g. chlorine, sulphur content), temperature of combustion, residence time, type of installed post-combustion controls and flue gas cooling rate in the pathway from the boiler to the stack [70], [71]. It should be noted that the processes of mercury transformation in flue gases are very complex and many factors have various influence, at the same time, and a clear assessment of the impact of a single factor is rather difficult. Additionally, mercury is transformed through homogeneous and heterogeneous reactions. Therefore, many developed models of mercury transformation in flue gas, which were designed to predict mercury speciation, do not give a clear answer about the importance of many factors [72]. Chemical equilibrium calculations predict the complete oxidising of elemental mercury by chlorine at temperatures of flue gases below 700K. The rate of oxidised mercury in higher temperatures depends strongly on the chlorine content in coal, but in temperatures of approx. 1000K the mercury should appear mainly in elemental form. Simultaneously with $Hg^{0}_{(g)}$ may appear small amount of $HgO_{(g)}$ but only $Hg^{0}_{(g)}$ is thermodynamically stable at temperatures above 1000K [70].

The measurement results obtained by the EPA show that the share of reactive mercury emitted from hard coal plants is higher than from brown coal plants, which may be explained by the relative high concentrations of halogens (chlorine, bromine) in hard coals resulting in the oxidisation of $Hg^{0}_{(g)}$ to $Hg^{II}_{(g)}$. Additionally, brown coals have a relatively higher content of alkaline material such as sodium and calcium, which also react with halogens in flue gases resulting into lower amount of halogens available to oxidize elemental mercury [73]. Published measurement results prove that higher concentrations of chlorine and hydrogen chloride promote a mercury oxidation in flue gases [74]. The efficiency of mercury oxidation of $HCl_{(g)}$ increases together with temperatures of flue gases [75]. In contrary, $Cl_{2(g)}$ is less effective in mercury oxidation along with an increase of temperature [76].

Furthermore, mercury is oxidised by $NO_{2(g)}$ and $O_{2(g)}$ in flue gases [75]. The compounds of reactive mercury with oxygen and chlorine may further react with $SO_{2(g)}$ creating mercury sulphate in the solid phase, which is the most stable form of mercury at temperatures below 490K [77]. Therefore, $SO_{2(g)}$, can promote the oxidation of elemental mercury through a continuous regeneration of chlorine and hydrogen chloride in flue gases. Unfortunately, the impact of sulphur in coal and $SO_{2(g)}$ in flue gases is still not completely clear and many theories exist to explain the role of sulphur and sulphur compounds on mercury oxidation [78]. Some experiment results show that $SO_{2(g)}$ can inhibit the transformation of $Hg^{0}_{(g)}$ to $Hg^{II}_{(g)}$, which consequently results in lower Hg removal efficiency by existing emission

control equipment [37]. The inhibitory effect of $SO_{2(g)}$ could be explained by a theory that $SO_{2(g)}$ may react with chlorine causing the reduction of the amount of chlorine available to oxidize elemental mercury or occupies mercury reaction sites on fly-ash carbon. Experiments and modelling suggest the reaction of mercury oxidation through reactions with chlorine and hydrogen chloride as the most important in flue gases of coal-fired power plants [37]. Results of measurements also showed the inhibitory effect of $H_2O_{(g)}$ and $NO_{(g)}$ on the mercury oxidation processes [79].

The speciation of mercury leaving the boiler has a crucial impact on mercury capture in existing emission control equipment. The general measurement data the of the EPA (US Environmental Protection Agency) show that ESP (electrostatic precipitators) or FF (fabric filter) installations are very effective in capturing mercury present in particulate matter. Reactive mercury is more quickly removed by WFGD (wet flue gas desulfurization) than elemental mercury due to a significantly better solubility in water [37]. In this study, more than 230 tests of 81 power units were conducted. Mercury emissions were measured in power plants for different fuels, boilers and emission controls combinations and are presented in Table 2-7. The lowest mercury efficiency of mercury by different coal -boiler-control classes result from speciation of mercury that leaves the boiler. It was observed that the share of $Hg^0_{(g)}$ from brown coal combustion is higher compared to hard coal combustion [37], [58], [47]. For example in recent estimations, the general share for mercury leaving boilers of the European power sector -before emission control installations of 55% of GEM, 35% of RGM, 10% of Hg_P and 60% of GEM, 30% of RGM, 10% of Hg_P for respectively hard and brown coal use [47].

It was also observed that the coal cleaning method can lead to significant removal of mercury. Two measurement campaigns where 50 samples were tested showed reduction values from 3 to 78%, with average removal of 30% and 21%. The physical cleaning of coal is used primarily to reduce ash and pyritic sulphur. This results in the removal of mercury linked to sulphur compounds, which are present in coal. Additionally, the lower content of sulphur in coal may lead to more efficient transformation of elemental mercury into oxidized form, as $SO_{2(g)}$ is considered as the inhibition of this process [71]. The enrichment process of coal may remove mercury in coal up to 74% and lead to mercury emission reduction into air up to 85% [80], [64].

Table 2-7. Removal efficiency of mercury by different coal-boiler-control classes (range in brackets) [%]. Based on data [37], [80], [58].

N.	Boiler type	PM control	SO_2 control	Removal efficiency [%]	Coal type
1	GF			0	Hard coal
2	GF	CYC		0	
3	GF	ESP		20	
4	DBB	ESP		36 (0 -80)	
5	DBB	FF		90 (84 -93)	
6	DBB	ESP	SDFGD	36	
7	DBB	ESP	DFGD	36	
8	DBB	ESP	WFGD	75	
9	DBB	FF	SDFGD	98 (97 -99)	
10	FBC	ESP		70	
11	DBB	ESP		0 (0 -4)	Brown coal
12	DBB	ESP	WFGD	44 (21 -56)	
13	DBB	ESP	DFGD	20	
14	FBC	ESP		38	

DBB - Dry Bottom Boiler, FBC - Fluidized Bed Combustion, CYC - Cyclone Remove System, ESP - Electrostatic Precipitator, FF - Fabric Filter, WFGD - Wet Flue Gas Desulfurization, CS-cold-side, HS –hot-side.

Additionally, the injection of absorbent such as activated carbon can lead to a decrease of mercury emissions up to nearly zero [80]. Typical percentages of main forms of mercury emitted from power plants and from other sectors are shown in Table 2-8.

One should note that the source of mercury emissions has a significant impact on speciation of emitted mercury, however, these shares are highly variable from one plant to another (e.g. RGM from utility boilers in the US can vary from 10% to 90%) [37].

Table 2-8. Review of speciation factors for mercury emitted into air [%].

N.	Hg form	All sources [%]	SNAP's categories [%]						Reference
			01	02	03	04	09	11	
1	GEM		50				20		[81]
2	RGM		30				60		
3	Hg_P		20				20		
4	GEM	57							[82]
5	RGM	30							
6	Hg_P	13							
7	GEM		50						[83]
8	RGM		30						
9	Hg_P		20						
10	GEM		58						[37]
11	RGM		40						
12	Hg_P		2						
13	GEM	52							[29]
14	RGM	29							
15	Hg_P	19							
16	GEM	61	50	50	80	73	25	80	[84]
17	RGM	32	40	40	17	24	58	13	
18	Hg_P	7	10	10	3	3	17	7	
19	GEM		50	50	80	80	20	80	[1]
20	RGM		40	40	15	15	60	15	
21	Hg_P		10	10	5	5	20	5	

22	GEM		75						[58]
23	RGM		20						
24	Hg_P		5						
25	GEM	72							[44]
26	RGM	22							
27	Hg_P	6							
28	GEM		60						[47]
29	RGM		33						
30	Hg_P		7						

2.2.4 Anthropogenic emission of lead and cadmium into the air

Lead

The extensive global anthropogenic emissions of lead were estimated to equal 330 $Gg.y^{-1}$ and 120 $Gg.y^{-1}$, for 1983 and mid-1990s [85], [86]. At that time the main sources of emitted lead were widely used fuel additives.

In Europe, the most comprehensive database of lead emissions into the air is presented in the EMEP programme [14]. The emission amounts presented there are the total for countries (without splitting into source categories), which were used in the EMEP models. The reported data from particular countries are very fragmentary, unfortunately. According to these data, the total emission of lead into air from the whole EMEP domain was 7.2 Gg in 2008. In EU-28, annual emissions were estimated at 2688 $Mg.y^{-1}$. The highest annual emissions among EU-28 members states were in Poland, Greece, Bulgaria, Italy, Spain, Germany and France respectively: 551, 470, 297, 274, 265, 116, 95 Mg. In Russia -2602 Mg, Kazakhstan -670 Mg, Turkey -380 Mg, Ukraine -213 Mg, Uzbekistan -185 Mg of lead was emitted in 2008. In 2010, EU-28 members emitted 2237 $Mg.y^{-1}$ and No-EU countries 3389 Mg y^{-1} [87]. TNO reported emission for 2010 from EU-28 at 1994 $Mg.y^{-1}$, wherein emissions in Poland were estimated at 276 $Mg.y^{-1}$ [49].

The major sources of lead emitted into the air in EU-28 are: (i) processes of primary and secondary production of metals (SNAP 0303) -with share in total emissions in 2010 of 34%, (ii) processes in iron and steel industries and collieries (SNAP 0402) -with share of 18% and (iii) waste incineration (SNAP 0902) -9% [88].

The annual amounts of emitted lead into the atmosphere in Poland are constant and equal approximately 550 $Mg.y^{-1}$ (Figure 2-7). Nearly half of the lead is emitted from combustion in manufacturing industry (SNAP 03), in particular from processes of primary production of copper (SNAP 030306), lead (SNAP 030304) and zinc (SNAP 030314) and secondary

production of copper (SNAP 030309). In Poland were emitted 113 Mg and 14 Mg of lead from processes of primary and secondary production of copper in 2008, respectively. The primary production of lead caused emissions into the atmosphere to equal 48 $Mg.y^{-1}$ and primary production of zinc 15 $Mg.y^{-1}$. Annually approximately 111 Mg of lead was released from coal burning in households (SNAP 0202).

The share of combustion in the energy and transformation industries sector (SNAP 01) in total emission is relatively small and equals around 5%. Half of this emission, approximately 12 Mg, is coming from district heating plants (SNAP 0102). Public power plants (SNAP 0101) emitted 8.2 Mg from hard coal and 2 Mg from brown coal combustion in 2008. The annual emission of lead in the years of 2005 -2013 from public power plants were almost on the same level. The rather slight variation of emitted amounts between the years resulted from the activity of fuels. The applied emission factors were constant in the period of 2005 -2013 and equal 0.009 $kg.TJ^{-1}$ for hard coal power plants, 0.0038 $kg.TJ^{-1}$ for brown power plants and 0.1024 $kg.TJ^{-1}$ for district heat plants where hard coal was being used. The concentration of lead in world coal ranges from 0.7 to 220 $mg.kg^{-1}$ [89]. The mean concentration of lead in coal of the Upper Silesian Coal Basin equals 30.5 $mg.kg^{-1}$ and in the Polish brown coal 6.27 $mg.kg^{-1}$ [90], [91]. Lead in the analysed coal of the Upper Silesian Coal Basin is mainly from inorganic origin.

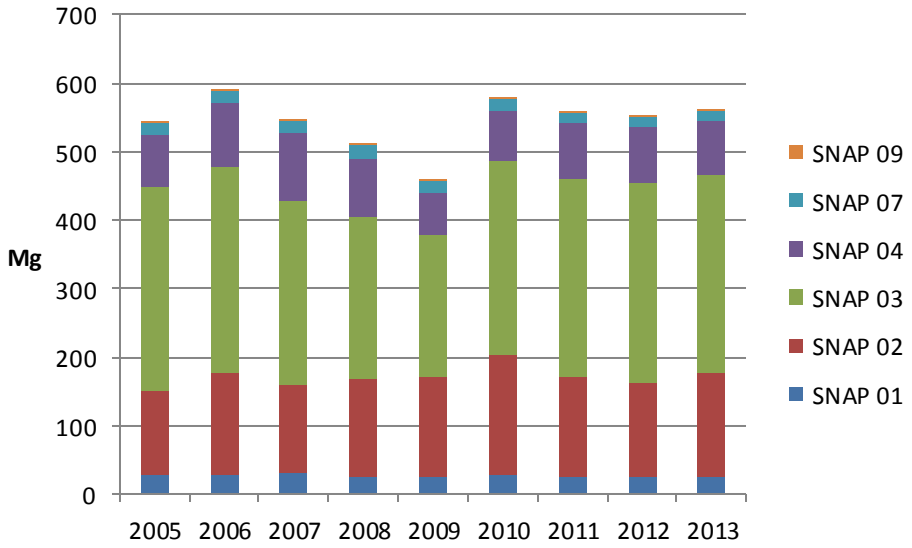

Figure 2-7. Emission of lead in Poland into air according to the assessment of the Institute of Environmental Projection and its agencies [Mg] [50], [51], [52], [53], [54], [92], [55].

Cadmium

The global emissions of cadmium into air were estimated to equal 7570 $Mg.y^{-1}$, for 1983 [85]. The emissions in the next decade (in mid-1990s) were lower and equalled 2983 $Mg.y^{-1}$ [86]. The contribution of non-ferrous metal production, stationary fossil fuel combustion, iron and steel production, cement production and waste disposal in total annual cadmium emissions were 73%, 23%, 2%, 1% and 1%, respectively.

According to the EMEP database (used in the model), annual emissions of cadmium into air from whole domain equalled 265 Mg in 2005, 286 Mg in 2008 and 137 Mg in 2010 [14]. Emissions in the EU-28 member states also decreased and equalled 139 $Mg.y^{-1}$ in 2005, 117 $Mg.y^{-1}$ in 2008 and 102 $Mg.y^{-1}$ in 2010. TNO estimated the emission of cadmium in EU-28 at 118 $Mg.y^{-1}$ in 2010 [49]. Poland is responsible for 35% of this amount. Next in order is Slovakia where annually 10 times less cadmium is emitted, compared to Poland.

In all EU-28 member states, 27% of total emission derived from residential plants (SNAP 0202), 13% from stationary combustion in manufacturing industries and construction (SNAP 03), 12% from public power sector (SNAP 0101), 10% -from iron and steel production (SNAP 0402) in 2010 [88].

In Poland in the years 2005 -2011 the main source of emission of cadmium was the non-industrial combustion plants sector (SNAP 02), mainly hard coal combustion in households (SNAP 0202). The relatively newest estimation prepared for 2012 and 2013 shows about 10 times lower emissions from this sector compared to earlier years [55]. Additionally in 2012 and 2013 the emissions from combustion in energy and transformation (SNAP 01) decreased significantly. The emissions of cadmium from this sector were 9.3% and 3.0% of the overall national emissions in Poland in 2008 and 2013, respectively. In this sector, in 2008 cadmium was released especially from district power plants (SNAP 0102) -1939 $kg.y^{-1}$ and petroleum refining plants (SNAP 0103) -1067 $kg.y^{-1}$. Hard coal power plants emitted 110 kg and brown coal power plants 68 kg of cadmium in 2008. For power plants based on both hard and brown coal, 0.0001 $kg.TJ^{-1}$ and for district heating plants 0.0164 $kg.TJ^{-1}$ emission factors for years 2005 -2011 were used. [50]. The concentration of cadmium in world coals is very diverse and ranges from 0.01 up to 300 $mg.kg^{-1}$ [89]. The Polish coal, both hard and brown is characterized by comparatively low content of cadmium. The most complex measurement campaign in Poland including 147 and 108 samples of polish hard and brown coal resulted in an average concentration of cadmium in hard coal of 0.2 $mg.kg^{-1}$ and 0.3 $mg.kg^{-1}$ in brown coal [93]. In this study, the maximum concentrations of cadmium of 7.7 $mg.kg^{-1}$ in hard coal and 2.0 $mg.kg^{-1}$ in brown coal samples were reported. Another study where 30 samples were

analysed reported concentrations of 0.10 $mg.kg^{-1}$, with minimum of 0.01 $mg.kg^{-1}$ and maximum of 0.89 $mg.kg^{-1}$ [91].

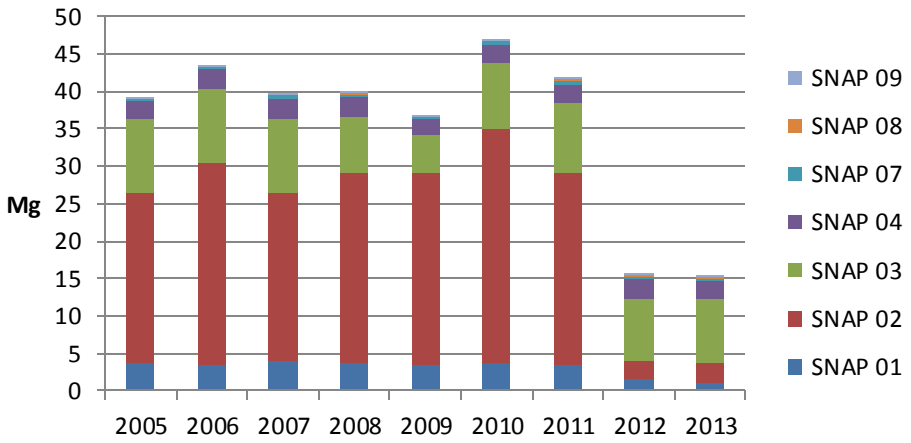

Figure 2-8. Emissions of cadmium in Poland into air according to the assessment of the Institute of Environmental Projection and its agencies [Mg] [50], [51], [52], [53], [54], [92], [55].

2.3 Reactions of mercury in the atmospheric gas phase

The various mercury forms are oxidized and reduced in homogenous and heterogeneous reactions in the gaseous and aqueous phases. The rate constants are usually estimated based on laboratory studies or theoretical calculations for laboratory conditions. As it was presented in Figure 2-9, for many reaction the estimated rate constants and concentrations of atmospheric oxidants can differ of factor 4. It makes the direct transfer of reported chemical pathways of mercury to atmospheric conditions very complicated and not always possible, taking into account observed and estimated mercury mass balance in the global atmosphere. However, many reactions with estimated rate constants are used in chemical transport models for atmospheric mercury. Major reactions are discussed below.

Oxidation of $Hg^0_{(g)}$ by ozone ($O_{3(g)}$)

Ozone is a significant oxidant of some atmospheric compounds. The observed annual average concentration of ozone in the atmosphere at ground level over Europe is approx. 50 $\mu g.m^{-3}$ [94]. Ozone during daytime is produced from photochemical reactions of NO_x and VOC-volatile organic compounds [95].

$$NO_{2(g)} + h\nu \rightarrow NO_{(g)} + O_{(g)} \qquad \text{R.2.2}$$

$$O_{(g)} + O_{2(g)} + M \rightarrow O_{3(g)} + M \qquad \text{R.2.3}$$

The reaction of mercury with ozone proceeds as follows [96], [97], [98],:

$$Hg^{0}_{(g)} + O_{3(g)} \rightarrow HgO_{(g,p)} + O_{2(g)} \qquad \text{R.2.4}$$

This reaction was first observed in 1949, but unfortunately the rate constant was not reported. However, these pioneering experimental data were subsequently used to estimate the kinetic rate constant of gaseous phase oxidation of GEM by ozone [99], [100]. Another conducted experiments led to estimation of the rate constant, although the reaction products were not experimentally verified [96], [98]. The estimations of reported rate constants of oxidation gaseous elemental mercury by ozone are presented in Table 2-9. The later experiment and theoretical calculations showed that the direct reaction R.2.4 is very endothermic, thus, the following reaction was suggested as a first stage [98]:

$$Hg^{0}_{(g)} + O_{3(g)} \rightarrow HgO_{3(g)} \qquad \text{R.2.5}$$

In the next step, gaseous $HgO_{3(g)}$ decays immediately to gaseous $O_{2(g)}$ and solid mercuric oxide $HgO_{(p)}$. This approach is consistent with the recent laboratory research with the use of high-resolution microscopy technics and theoretical studies [101], [102]. However, this heterogeneous pathway is unlikely in the atmosphere because of low concentration of atmospheric mercury [103].

However, both approaches of this reaction are considered in chemical transport models of atmospheric mercury (Table 3-1 and Table 3-2). The detailed modelling studies showed that current knowledge of GEM oxidation by $O_{3(g)}$ do not fully explain the behaviour and mass balance of GEM in the atmosphere and further laboratory studies are recommended [104].

Table 2-9. Reported values of rate constants of oxidation of mercury by ozone in gaseous phase in temperature 296 ±3K (Hall reported the temperature (T) depended rate [96]) [$cm^3.molec^{-1}.s^{-1}$].

N.	Estimation of rate constant	References
1	$4.2 \cdot 10^{-19}$	[99]
2	$1.7 \cdot 10^{-18}$	[105]
3	$4.9 \cdot 10^{-18}$	[100]
4	$2.1 \cdot 10^{-18} \exp\left(-\frac{1246}{T}\right)$	[96]
5	$(3 \pm 2) \cdot 10^{-20}$	
6	$(7.5 \pm 0.9) \cdot 10^{-19}$	[98]
7	$(6.4 \pm 2.3) \cdot 10^{-19}$	[106]
8	$(6.2 \pm 1.1) \cdot 10^{-19}$	[101]

Oxidation of $Hg^0_{(g)}$ by hydroxyl radical ($^{\bullet}OH_{(g)}$)

$$Hg^0_{(g)} + {}^{\bullet}OH_{(g)} \rightarrow products \qquad \text{R.2.6}$$

The mechanism of this reaction is still not fully clear and four products of this reaction may be simultaneously considered: gaseous mercuric hydroxide $HgOH_{(g)}$, gaseous mercury(I) hydroxide $HgOH_{(g)}$, gaseous mercuric oxide $HgO_{(g)}$ and solid mercuric oxide $HgO_{(p)}$ [9]. The $HgOH_{2(g)}$ as the product of reaction R.2.6 is included in models such as STEM-Hg, CAMx, CTM-Hg, ECHMERIT and $HgO_{(p)}$ in GLEMOS, CMAQ-Hg and MSCE-HM-hem models (Table 3-1and Table 3-2).

During the daytime, the troposphere hydroxyl radical occurs mainly form the following chemical pathway:

$$O_{3(g)} + hV \rightarrow O^{\bullet}_{(g)} + O_{2(g)} \qquad \text{R.2.7}$$

$$O^{\bullet}_{(g)} + H_2O_{(g)} \rightarrow 2{}^{\bullet}OH_{(g)} \qquad \text{R.2.8}$$

In the polluted atmosphere, the following reactions also take place:

$$HNO_{2(g)} + hv \rightarrow {}^{\bullet}OH_{(g)} + NO_{(g)} \qquad \text{R.2.9}$$

$$H_2O_{2(g)} + hv \rightarrow 2{}^{\bullet}OH_{(g)} \qquad \text{R.2.10}$$

In the upper troposphere, the photochemical reaction can lead to production of $^{\bullet}OH_{(g)}$:

$$HNO_{3(g)} + hv \rightarrow NO_{2(g)} + {}^{\bullet}OH_{(g)} \qquad \text{R.2.11}$$

The typical concentration of tropospheric $^{\bullet}OH_{(g)}$ ranges from 10^5 to 10^7 molec.cm^{-3} [15].

Table 2-10. Reported values of rate constants of oxidation of mercury by hydroxyl radical in gaseous phase at temperature of 296 ±2K [cm^3.molec^{-1}.s^{-1}].

N.	Estimation of rate constant	References
1	$(8.7 \pm 2.8)\cdot 10^{-14}$	[107]
2	$(1.6 \pm 0.2)\cdot 10^{-12}$	[108]
3	$1.2\cdot 10^{-13}$	[109]
4	$(9.0 \pm 1.3)\cdot 10^{-14}$	[110]
5	$3.2\cdot 10^{-13}\cdot (T/298)^{-3.06}$ theoretical studies	[111]

Oxidation of $Hg^0_{(g)}$ by hydrogen peroxide ($H_2O_{2(g)}$)

During the day, elemental gaseous mercury can be oxidised by hydrogen peroxide.

The scheme R.2.12 for the reaction was proposed and used in the model with the upper limit value of rate constant presented in Table 2-11 [112]:

$$Hg^{0}_{(g)} + H_2O_{2(g)} \rightarrow Hg(OH)_{2(g,p)} \qquad \text{R.2.12}$$

The performed reactor experiments found exothermic reaction R.2.12 and value of rate constant of three orders magnitude lower compared to that previously used in the model [97]. This value of rate constant should be treated as the upper limit value, and the total uncertainties were estimated at 43%.

Table 2-11. Reported values of rate constants of oxidation of mercury by hydrogen peroxide in gaseous phase at temperature of 296 ±2K [$cm^3.molec^{-1}.s^{-1}$].

N.	Estimation of rate constant	References
1	$4.1 \cdot 10^{-16}$	[112]
2	$(6.0 \pm 2.5) \cdot 10^{-19}$	[97]
3	$8.4 \cdot 10^{-6} \cdot \exp(-9021/T)$	[113]

The typical concentration of atmospheric hydrogen peroxide at ground level equals approximately 1 ppbv. The measurements done in China showed the mean concentration of 1.24 ppbv and maximum of 4.6 ppbv. The highest values were noticed in the afternoon, lower during the night and the lowest in the morning [114].

The mechanism of production of atmospheric hydrogen peroxide in gaseous phase can be expressed as follows:

$$HO_2^{\bullet}{}_{(g)} + HO_2^{\bullet}{}_{(g)} + M \rightarrow H_2O_{2(g)} + O_{2(g)} + M \qquad \text{R.2.13}$$

$HO_2^{\bullet}$-peroxyl radical arises mainly from reactions where formaldehyde (HCHO) and aldehydes (RCHO) are involved.

During the daytime, the peroxyl radical is produced in reactions R.2.14 –R.2.16 :

$$HCHO_{(g)} + h\nu \rightarrow H^{\bullet}_{(g)} + HCO^{\bullet}_{(g)} \qquad \text{R.2.14}$$

$$RCHO_{(g)} + h\nu \rightarrow R^{\bullet} + HCO^{\bullet}_{(g)} \qquad \text{R.2.15}$$

$$HCO^{\bullet}_{(g)} + O_{2(g)} \rightarrow HO_2^{\bullet}{}_{(g)} + CO_{(g)} \qquad \text{R.2.16}$$

and at night following reactions R.2.17 and R.2.18:

$$HCHO_{(g)} + NO_3^{\bullet}{}_{(g)} \rightarrow HNO_{3(g)} + HCO^{\bullet}_{(g)} \qquad \text{R.2.17}$$

$$HCO^{\bullet}_{(g)} + O_{2(g)} \rightarrow HO_2^{\bullet}{}_{(g)} + CO_{(g)} \qquad \text{R.2.18}$$

Where $NO_3^{\bullet}$ is produced in reaction:

$$NO_{2(g)} + O_{3(g)} \rightarrow NO_3^{\bullet}{}_{(g)} + O_{2(g)} \qquad \text{R.2.19}$$

Peroxy radical occurs additionally in following reaction:

$$H^{\bullet}_{(g)} + O_{2(g)} + M \rightarrow HO_2^{\bullet}{}_{(g)} + M \qquad \text{R.2.20}$$

Oxidation of $Hg^0_{(g)}$ by molecular chlorine ($Cl_{2(g)}$)

$$Hg^0_{(g)} + Cl_{2(g)} \rightarrow HgCl_{2(g)} \qquad \text{R.2.21}$$

This reaction is included in most of the chemical transport models dedicated to atmospheric mercury, nevertheless it is rather slow in comparison to other oxidation reactions of GEM [106], [9]. The reported values of rate constants of reaction R.2.21 are listed in Table 2-12. The use of various initial concentrations of GEM (50 -180 $ng.m^{-3}$) and $Cl_{2(g)}$ (3 -101 pbbv) led to estimated values of the rate constants ranging from $9.8 \cdot 10^{-18}$ to $5.0 \cdot 10^{-17}$ $cm^3.molec^{-1}.s^{-1}$ [106].

Table 2-12. Reported values of rate constants of oxidation of mercury by chlorine in gaseous phase at temperature of 296 ±2K [$cm^3.molec^{-1}.s^{-1}$].

N.	Estimation of rate constant	References
1	$4.8 \cdot 10^{-18}$	[115]
2	$5.7 \cdot 10^{-17}$	[116]
3	$(2.6 \pm 0.2) \cdot 10^{-18}$	[117]
4	$(1.82 \pm 0.05) \cdot 10^{-19}$	[118]
5	$(2.5 \pm 0.9) \cdot 10^{-18}$	[106]
6	$4.3 \cdot 10^{-15}$	[119]

Till now there is no complex model of $Cl_{2(g)}$ production in atmosphere [120]. The results from developed models to describe the behaviour of air of $Cl_{2(g)}$ are still not compatible with measurements. The evaluation of a rather recent model showed the maximum concentration of Cl_2 of 35 and 41 ppt from observation and modelling, respectively [120].

The earlier night-time measurements of $Cl_{2(g)}$ conducted at ground sites in eastern Long Island, New York, Florida coastal site, and Artic site showed concentration ranging from 9 to 150 ppt. The day-time concentration of $Cl_{2(g)}$ is significantly lower and does not exceed 15 ppt [121].

Oxidation of $Hg^0_{(g)}$ by chlorine radicals ($Cl^{\bullet}_{(g)}$)

$$Hg^0_{(g)} + Cl^{\bullet}_{(g)} \rightarrow HgCl_{(g)} \qquad \text{R.2.22}$$

The reaction R.2.22 was investigated relatively a long time ago but the uncertainty of the obtained rate coefficients were significant within a factor of three. The relatively recent studies showed the rate coefficient of 10^{-11} $cm^3.molec^{-1}.s^{-1}$ (Table 2-13), [117].

Table 2-13. Reported values of rate constants of oxidation of mercury by chlorine radicals gaseous phase.

N.	Rate constants	Units	Temperature, comments	References
1	$(3.2 \pm 1.7)\cdot 10^{-11}$	$cm^3.molec^{-1}.s^{-1}$	393-443K	[122]
2	$(1.0 \pm 0.2)\cdot 10^{-11}$	$cm^3.molec^{-1}.s^{-1}$	298K	[117]
3	$1.38\cdot 10^{-12}\cdot \exp(208.02/T)$	$cm^3.molec^{-1}.s^{-1}$	theoretical studies	[123]
4	$(2.8 \pm 0.2)\cdot 10^{-12}$	$cm^3.molec^{-1}.s^{-1}$	theoretical studies, 298K	[123]
5	$(2.2 \pm 0.5)\cdot 10^{-32}$ $\cdot \exp((680 \pm 400)(1/T-1/293))$	$cm^6.molec^{-2}.s^{-1}$	243–293 K third-order recombination rate coefficient in nitrogen buffer gas. The reaction was included into CMAQ ver. 4.7.1 model (Table 3-1).	[124]
6	$1.2\cdot 10^{-10}$	$cm^3.molec^{-1}.s^{-1}$	298K	[119]

Chlorine radicals are produced in the atmosphere by photodissociation of $Cl_{2(g)}$ with the participation of ultraviolet and visible light. The atmospheric concentration of $Cl^{\bullet}_{(g)}$ is very low and ranges from 10^3 to 10^5 $molec^{-1}.cm^3$ [125].

Oxidation of $Hg^0_{(g)}$ by hydrogen chloride ($HCl_{(g)}$)

$$Hg^0_{(g)} + 2HCl_{(g)} \rightarrow HgCl_{2(g)} + H_{2(g)} \qquad \text{R.2.23}$$

The reaction R.2.23 was investigated under various conditions (temperature and insolation) and the estimated value of the rate constant is 10^{-19} $cm^3.molec^{-1}.s^{-1}$ [126]. There is no other published measurement for comparison.

This pathway of GEM oxidation in the atmosphere was included in CTM-Hg, ECHMERIT models (Table 3-2). With the use of research on Earth's budget of chlorine the concentration of $HCl_{(g)}$ as the linear interpolation from $1.2\cdot 10^{10}$ $molec.cm^{-3}$ at surface level to 10^8 $molec.cm^{-3}$ at 10 km altitude was applied to the CTM-Hg model [127].

Reaction of mercury with bromine radical ($Br^{\bullet}_{(g)}$)

$$Hg^{0}_{(g)} + Br^{\bullet}_{(g)} \rightarrow HgBr_{(g)} \qquad \text{R.2.24}$$

The rate constant of oxidation of elemental gaseous mercury by bromine was estimated based on experimental studies and based on the direct measurements in the atmosphere [117], [128]. However, the problems with precise determination of bromine concentration in the atmosphere led to an uncertainty of 50%. Additionally, some theoretical studies of value of the rate constant are presented in Table 2-14. The bromine radicals are formed similarly to chlorine radicals in photochemical reaction:

$$Br_{2(g)} + h\nu \rightarrow 2Br^{\bullet}_{(g)} \qquad \text{R.2.25}$$

Table 2-14. Reported values of rate constants of oxidation of mercury by bromine radical in gas phase.

N.	Rate constant	Units	Comments	References
1	$(3.2 \pm 0.3)\cdot 10^{-12}$	$cm^3.molec^{-1}.s^{-1}$	T=298K	[117]
2	$1.01\cdot 10^{-12}\cdot \exp(209/T)$	$cm^3.molec^{-1}.s^{-1}$	theoretical studies	[123]
3	$1.1\cdot 10^{-12}\cdot (T/298)^{-2.37}$	$cm^3.molec^{-1}.s^{-1}$	theoretical studies	[111]
4	$(1.46 \pm 0.34)\cdot 10^{-32}\cdot (T/298)^{-(1.86\pm 1.49)}$	$cm^6.molec^{-2}.s^{-1}$	243–293 K third-order recombination rate coefficient in nitrogen buffer gas	[128]
5	$9.8\cdot 10^{-13}\cdot \exp(401\cdot (1/T-1/298))$	$cm^3.molec^{-1}.s^{-1}$	theoretical studies	[129]

The mercury bromide can be reduced or oxidized mainly by hydroxyl and bromine as follows [111]:

$$HgBr_{(g)} \rightarrow Hg^{0}_{(g)} + Br^{\bullet}_{(g)} \qquad \text{R.2.26}$$

$$HgBr_{(g)} + Br^{\bullet}_{(g)} \rightarrow HgBr_{2(g)} \qquad \text{R.2.27}$$

$$HgBr_{(g)} + OH^{\bullet}_{(g)} \rightarrow HgBrOH_{(g)} \qquad \text{R.2.28}$$

The values of the rate constants obtained for oxidation (R.2.26 +R.2.27) and reduction (R.2.28) in pressure of 1 atm equals $2.5\cdot 10^{-10}\cdot (T/298)^{-0.57}$ $cm^3.molec^{-1}.s^{-1}$ and $1.2\cdot 10^{10}\cdot \exp(-8357/T)$ s^{-1}, respectively [111]. The rate parameter of $1.2\cdot 10^{10}\cdot \exp(-8357/T)$ s^{-1} for temperatures approx. 20^0C equals $7.9\cdot 10^{-3}$ s^{-1}. This value was used in the CTM-Hg model [127].

The theoretically calculated value of the rate constant with the use of various techniques for the reaction R.2.27 is in the range of $2.98 \pm 0.14\cdot 10^{-11}$ to $1.27\ 10^{-10}$ $cm^3.molec^{-1}.s^{-1}$ [130]. In

the same studies the additional reduction reaction R.2.29 was also proposed with a theoretical rate constant of $3.89 \pm 0.17 \cdot 10^{-11}$ $cm^3.molec^{-1}.s^{-1}$ [130].

$$HgBr_{(g)} + Br^{\bullet}_{(g)} \rightarrow Hg^{0}_{(g)} + Br_{2(g)} \qquad \text{R.2.29}$$

The ambient concentration of $Br^{\bullet}_{(g)}$ ranges from 10^5 molec.cm^{-3} to 10^7 molec.cm^{-3} [117], [128]. However, it should be noted that the measurements of concentration of bromine and bromine compounds in the atmosphere are very limited and in some modelling studies the assumed concentration of $Br^{\bullet}_{(g)}$ equals 0.01 of $BrO^{\bullet}_{(g)}$ [131], [127].

Oxidation of $Hg^0_{(g)}$ by molecular bromine ($Br_{2(g)}$)

The gaseous mercury dibromide $HgBr_{2(g)}$ can also be produced in reaction:

$$Hg^{0}_{(g)} + Br_{2(g)} \rightarrow HgBr_{2(g)} \qquad \text{R.2.30}$$

The rate constant less than $0.9 \pm 02 \cdot 10^{-16}$ $cm^3.molec^{-1}.s^{-1}$ was estimated based on experimental results at 298K and 0.99 atm [117], [125]. Two other experiments were conducted with $Hg^0_{(g)}$ initial conditions of 93 and 55 ng.m^{-3}, $Br_{2(g)}$ concentration of 2 ppb and 1 ppb at 35% and 30% relative humidity (RH), respectively [106]. No evidence of $Hg^0_{(g)}$ loss in the presence of $Br_{2(g)}$ was observed, however during the experiments the concentration of RGM and Hg_P, and deposition of $Hg^0_{(g)}$ were not measured. The theoretical rate constant equals $\sim 2.8 \cdot 10^{-19}$ $cm^3.molec^{-1}.s^{-1}$ at 298K [130]. The atmospheric concentration of $Br_{2(g)}$ ranges from 10^5 molec.cm^{-3} to 10^9 molec.cm^{-3} [125], [131].

Oxidation of $Hg^0_{(g)}$ by bromine oxide radical ($BrO^{\bullet}_{(g)}$)

The oxidation of elemental gaseous mercury by $BrO^{\bullet}_{(g)}$, can lead to production of two chemical compounds [132]:

$$Hg^{0}_{(g)} + BrO^{\bullet}_{(g)} \rightarrow HgO_{(g)} + Br_{(g)} \qquad \text{R.2.31}$$

or

$$Hg^{0}_{(g)} + BrO^{\bullet}_{(g)} \rightarrow HgBr_{(g)} + O_{(g)} \qquad \text{R.2.32}$$

The experimental works provided to estimate the rate constant of $1.5 \cdot 10^{-14}$ $cm^3.molec^{-1}.s^{-1}$ and also identify $HgBrO_{(g)}$ and $HgOBr_{(g)}$ as the products of reaction [133]. This homogeneous reaction is significantly endothermic [129], [133].

The $BrO^{\bullet}_{(g)}$ is produced in the atmosphere in the reaction :

$$Br^{\bullet}_{(g)} + O_{3(g)} \rightarrow BrO^{\bullet}_{(g)} + O_{2(g)}$$ R.2.33

The atmospheric concentration of $BrO^{\bullet}_{(g)}$ equals 10^7 -10^9 molec.cm^{-3} [125], [131], [132]. $BrO^{\bullet}_{(g)}$ is mainly produced in height-latitude marine boundary layer at the beginning of the day [131].

The modelling studies showed that the reactions of elemental gaseous mercury with bromine and bromine monoxide fulfil the significant role in depletion of GEM during polar spring time in observed phenomena which are called the atmospheric mercury depletion events (AMDE) [134].

Oxidation of $Hg^0_{(g)}$ by nitrate radical ($NO_3^{\bullet}{}_{(g)}$)

$$Hg^0_{(g)} + NO_3^{\bullet}{}_{(g)} \rightarrow HgO_{(g)} + NO_{2(g)}$$ R.2.34

$NO_3^{\bullet}{}_{(g)}$ is produced in reaction of

$$NO_{2(g)} + O_{3(g)} \rightarrow NO_3^{\bullet}{}_{(g)} + O_{2(g)}$$ R.2.35

But during the day, it quickly disappears through photoreactions:

$$NO_3^{\bullet}{}_{(g)} + h\nu \rightarrow NO_{(g)} + O_{2(g)}$$ R.2.36

$$NO_3^{\bullet}{}_{(g)} + h\nu \rightarrow NO_{2(g)} + O_{(g)}$$ R.2.37

Therefore, the reactions of mercury with the nitrate radical occurs mostly at night [15].

The rate constant was assessed of $4 \cdot 10^{-15}$ cm^3.molec^{-1}.s^{-1}, but is should be treated as an upper limit value [135]. Based on this rate constant, a half-life of approximately 20 days of GEM due to $NO_3^{\bullet}{}_{(g)}$ oxidation, with assumption of $NO_3^{\bullet}{}_{(g)}$ concentration of 10^8 molec.cm^{-3} was calculated [15].

Other studies on reaction R.2.34 led to obtain three upper limit rate constants of (i) $7 \cdot 10^{-15}$, (ii) $1.3 \cdot 10^{-14}$ and (iii) $3 \cdot 10^{-14}$ cm^3.molec^{-1}.s^{-1} [106].

Till now this reaction was included only in the ECHMERIT model (Table 3-2).

Oxidation of $Hg^0_{(g)}$ by molecular iodine ($I_{2(g)}$)

$$Hg^0_{(g)} + I_{2\,(g)} \rightarrow HgI_{2(g)}$$ R.2.38

Beyond $HgI_{2(g)}$, also $HgIO_{(g)}$ or $HgOI_{(g)}$ were identified as the reaction products [136]. The estimated value of the rate constant is $(1.27 \pm 0.58) \cdot 10^{-19}$ cm^3.molec^{-1}.s^{-1}. The concentration of molecular iodine in the coastal air can reach 300 ppt, but usually the measurement stations noticed concentration of approx. 20 ppt [137].

Oxidation of $Hg^0_{(g)}$ by molecular fluorine ($F_{2(g)}$)

$$Hg^0_{(g)} + F_{2(g)} \rightarrow HgF_{2(g)} \qquad \text{R.2.39}$$

Several experiments with the use of various initial condition of $Hg^0_{(g)}$ (44 -140 $ng.m^{-3}$) and F_2 (4 -29 ppbv) led to estimates of the rate constant in a range from $1.3 \cdot 10^{-15}$ to $2.2 \cdot 10^{-15}$ with an average of $1.8 \cdot 10^{-15}$ $cm^3.molec^{-1}.s^{-1}$ [106]. The typical average annual concentration of fluorine in the air should not exceed several $\mu g.m^{-3}$. For example in Krakow the annual average concentration of approx. 1 $\mu g.m^{-3}$ was observed [138].

The half-life of atmospheric elemental gaseous mercury due to oxidation in the gaseous phase are presented in Figure 2-9. The lower half-life indicates the most effective reaction under atmospheric conditions. The ranges of concentration of most of oxidants are rather wide, because these atmospheric species are rarely measured, and many possible value of air concentration are modelled. Extensive measurements of atmospheric ozone result in rather accurate determination of it ambient concentration. Looking at Figure 2-9, the most effective oxidation of GEM can be $NO_3^{\bullet}{}_{(g)}$, $Br^{\bullet}_{(g)}$, $Cl^{\bullet}_{(g)}$, $F_{2(g)}$. However, it should be noted that most of the presented values of rate constants were calculated based on laboratory or theoretical studies and these values may not be relevant for atmospheric conditions. The next part of this manuscript is devoted to a large extent to determine the most appropriate reaction and values that should be used in the model. Furthermore, sensitivity studies are conducted to determine the influence of various reactions with different rate constants on modelling results.

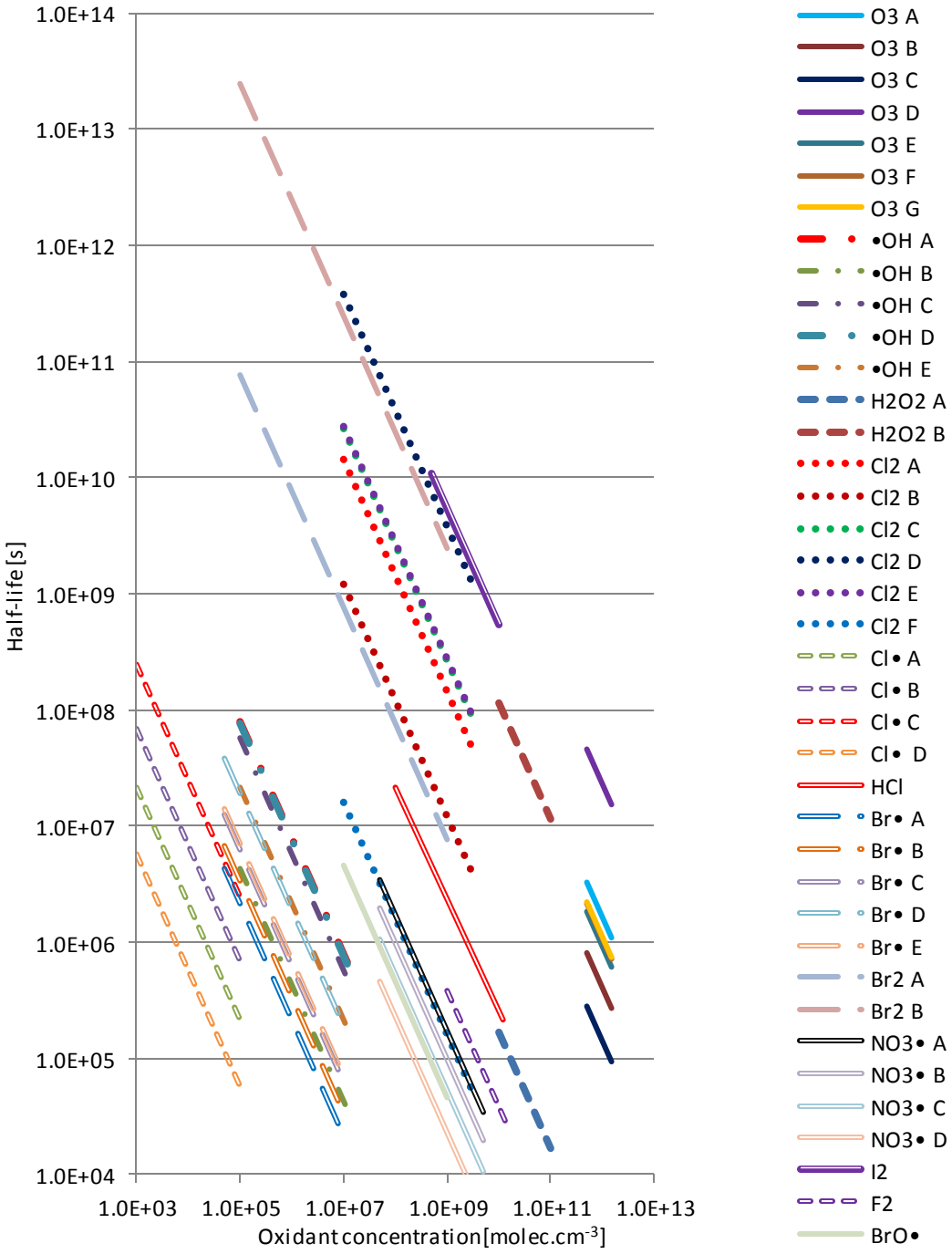

Figure 2-9. The half-life of atmospheric elemental gaseous mercury due to the oxidation in the gaseous phase. All reactions were described in the text, the list of presented reactions contains name of data series in figure, oxidant symbol, reaction rate constant in $cm^3.molec^{-1}.s^{-1}$ and reference to literature. O3 A – $O_{3(g)}$, $4.2 \cdot 10^{-19}$,[99]; O3 B – $O_{3(g)}$, $1.7 \cdot 10^{-18}$,[105]; O3 C – $O_{3(g)}$, $4.9 \cdot 10^{-18}$,[100]; O3 D – $O_{3(g)}$, $3 \cdot 10^{-20}$,[96]; O3 E – $O_{3(g)}$, $7.5 \cdot 10^{-19}$,[98]; O3 F – $O_{3(g)}$, $6.4 \cdot 10^{-19}$,[106]; O3 G – $O_{3(g)}$, $6.2 \cdot 10^{-19}$, [101]; •OH A – $^{\bullet}OH_{(g)}$, $6.2 \cdot 10^{-19}$,[107]; •OH B – $^{\bullet}OH_{(g)}$, $1.6 \cdot 10^{-12}$, [108]; •OH C – $^{\bullet}OH_{(g)}$, $1.2 \cdot 10^{-13}$,[109]; •OH D – $^{\bullet}OH_{(g)}$, $9.0 \cdot 10^{-14}$, [110]; •OH E – $^{\bullet}OH_{(g)}$, $3.2 \cdot 10^{-13}$,[111]; H2O2 A – $H_2O_{2(g)}$, $4.1 \cdot 10^{-16}$, [112]; H2O2 B – $H_2O_{2(g)}$, $6.0 \cdot 10^{-19}$,[97], [113]; Cl2 A – $Cl_{2(g)}$, $4.8 \cdot 10^{-18}$, [115]; Cl2 B – $Cl_{2(g)}$, $5.7 \cdot 10^{-17}$, [116]; Cl2 C – $Cl_{2(g)}$, $2.6 \cdot 10^{-18}$,[117]; Cl2 D – $Cl_{2(g)}$, $1.82 \cdot 10^{-19}$,[118]; Cl2 E – $Cl_{2(g)}$, $2.5 \cdot 10^{-18}$,[106]; Cl2 F – $Cl_{2(g)}$, $4.3 \cdot 10^{-15}$, [119]; Cl• A – $Cl^{\bullet}_{(g)}$, $3.2 \cdot 10^{-11}$,[122]; Cl• B – $Cl^{\bullet}_{(g)}$, $1.0 \cdot 10^{-11}$,[117]; Cl• C – $Cl^{\bullet}_{(g)}$, $2.8 \cdot 10^{-12}$, [123]; Cl• D – $Cl^{\bullet}_{(g)}$, $1.2 \cdot 10^{-10}$, [119]; HCl –$HCl_{(g)}$, $1.0 \cdot 10^{-19}$, [126]; Br• A – $Br^{\bullet}_{(g)}$, $3.2 \cdot 10^{-12}$, [117] ; Br• B – $Br^{\bullet}_{(g)}$, $2.04 \cdot 10^{-12}$, [123]; Br• C – $Br^{\bullet}_{(g)}$, $1.1 \cdot 10^{-12}$, [111]; Br• D – $Br^{\bullet}_{(g)}$, $3.6 \cdot 10^{-12}$, [128]; Br• E – $Br^{\bullet}_{(g)}$, $9.8 \cdot 10^{-19}$, [129]; Br2 A –$Br_{2(g)}$, $0.9 \cdot 10^{-16}$, [117]; Br2 B – $Br_{2(g)}$, $2.8 \cdot 10^{-19}$,[130]; BrO• A – $BrO^{\bullet}_{(g)}$, $1.5 \cdot 10^{-}$

^{14}, [133]; NO3• A – $NO_3^{\bullet}{}_{(g)}$, $4.0 \cdot 10^{-15}$, [135]; NO3• B – $NO_3^{\bullet}{}_{(g)}$, $7.0 \cdot 10^{-15}$,[106]; NO3• C – $NO_3^{\bullet}{}_{(g)}$, $1.3 \cdot 10^{-14}$,[106]; NO3• D – $NO_3^{\bullet}{}_{(g)}$, $3.0 \cdot 10^{-14}$,[106]; I2 – $I_{2\,(g)}$, $1.27 \cdot 10^{-19}$, [136]; F2 – $F_{2\,(g)}$, $1.8 \cdot 10^{-15}$, [106]. The concentrations of different oxidants were determined based on literature review [121], [15], [125], [114], [132]. Some oxidants appear only at some times of the day or over some areas (sea, coastal regions) -description in the text.

2.4 Reactions of mercury in the aqueous phase of the atmosphere

Mercury and mercury compounds as well as other elements and compounds (e.g. O_3, H_2O_2, Br_2) present in the atmosphere are dissolvable in water, according to the Henry's law.
In the aqueous phase as well as in gaseous phase, reactions of oxidation and reduction of various forms of mercury occurs.

Oxidation of $Hg^0_{(aq)}$ by ozone ($O_{3(aq)}$)

The scheme R.2.40 was proposed as the most relevant for the oxidation of $Hg^0_{(aq)}$ by $O_{3(aq)}$ of [139], [15]:

$$Hg^0_{(aq)} + O_{3(aq)} + H^+_{(aq)} \rightarrow Hg^{2+}_{(aq)} + O_{2(aq)} + OH^-_{(aq)} \qquad \text{R.2.40}$$

The value of the rate constant of $(4.7 \pm 2.2) \cdot 10^7$ $M^{-1}.s^{-1}$ of reaction R.2.40 was estimated [140]. Assuming that the atmospheric concentration of ozone in aqueous phase of $4.0 \cdot 10^{-10}$ M, the half-life of $Hg^0_{(aq)}$ due to this oxidation pathway of ~36 s was estimated [15]. Other studies assumed a higher the concentration of $O_{3(aq)}$ at $6.4 \cdot 10^{-9}$ M in atmospheric water that leads to half-life of $Hg^0_{(aq)}$ of 2.2 s [141]. However, since a very small fraction of Hg^0 is present in water, the half-life of total elemental mercury (gaseous +aqueous) is much longer.

Oxidation of $Hg^0_{(aq)}$ by hydroxyl radical ($^{\bullet}OH_{(aq)}$)

The mechanism of the oxidation of mercury by hydroxyl radical proceeds as follows [142]:

$$Hg^0_{(aq)} + {}^{\bullet}OH_{(aq)} \rightarrow Hg^+_{(aq)} + OH^-_{(aq)} \qquad \text{R.2.41}$$

$$Hg^+_{(aq)} + {}^{\bullet}OH_{(aq)} \rightarrow Hg^{2+}_{(aq)} + OH^-_{(aq)} \qquad \text{R.2.42}$$

They estimated the rate constants of $2.0 \cdot 10^9$ $M^{-1}.s^{-1}$ for reaction R.2.41. The reaction R.2.42 occurs rather quickly, therefore, the rate of the whole mechanism is controlled by the value of the rate constant of R.2.41 reaction. With the use of a peak mid-day concentration of 10^{-12} M and the value of the rate constants of $2.0 \cdot 10^9$ $M^{-1}.s^{-1}$ the half-life of 345 s of $Hg^0_{(aq)}$ was

estimated due to this pathway [15]. Several experiments conducted in laboratory conditions led to a similar estimation of this rate constant of $(2.4 \pm 0.3) \cdot 10^{9}$ $M^{-1}.s^{-1}$ [143].

Oxidation of $Hg^{0}_{(aq)}$ by molecular bromine ($Br_{2(aq)}$)

$$Hg^{0}_{(aq)} + Br_{2(aq)} \rightarrow Hg^{2+}_{(aq)} + 2Br^{-}_{(aq)} \qquad \text{R.2.43}$$

Several experiments conducted at pH =2.0 ±0.1, with initial aqueous concentration of 0.13 - 0.21 μM of $Hg^{0}_{(aq)}$, 1.1 mM and 2.21 mM of $Br_{2(aq)}$, allowed one to estimate the value of the rate constant of 2.0 ±0.03 $M^{-1}.s^{-1}$ for $Hg^{0}_{(aq)}$ oxidation by $Br_{2(aq)}$ in the aqueous phase [141]. Finally, the rate constant of 0.196 $M^{-1}.s^{-1}$ was proposed as the most appropriate. Assuming that a $Br_{2(aq)}$ concentration of $1.7 \cdot 10^{-9}$ M in atmospheric water, the half-life of $Hg^{0}_{(aq)}$ by this pathway is 66 years.

Oxidation of $Hg^{0}_{(aq)}$ by hypobromous acid ($HOBr_{(aq)}$)

In the aqueous phase, the oxidation of $Hg^{0}_{(aq)}$ by hypobromous acid (R.2.44) takes place [141]. The value of the rate constant of 0.28 ±0.02 $M^{-1}.s^{-1}$ for this pathway was estimated, based on results of experiments conducted under the following conditions: pH=6.8 ±0.1, with initial aqueous concentration 0.09 -0.17μM of $Hg^{0}_{(aq)}$, 1.1 mM and 2.13 ±0.2 mM of $HOBr_{(aq)}$.

$$Hg^{0}_{(aq)} + HOBr_{(aq)} \rightarrow Hg^{2+}_{(aq)} + OH^{-}_{(aq)} + Br^{-}_{(aq)} \qquad \text{R.2.44}$$

The half-life of $Hg^{0}_{(aq)}$ by this pathway is 53 hours for the value of the rate constant of 0.279 $M^{-1}.s^{-1}$ and $HOBr_{(aq)}$ aqueous concentration of $1.3 \cdot 10^{-5}$ M.

Oxidation of $Hg^{0}_{(aq)}$ by hypobromite anion (OBr^{-})

$$Hg^{0}_{(aq)} + OBr^{-}_{(aq)} + H^{+}_{(aq)} \rightarrow Hg^{2+}_{(aq)} + Br^{-}_{(aq)} + OH^{-}_{(aq)} \qquad \text{R.2.45}$$

The experiments conducted at pH=11.8 ±0.1, with an initial aqueous concentration 0.091-0.137 μM of $Hg^{0}_{(aq)}$, 1.21 mM and 2.25 mM of $OBr^{-}_{(aq)}$ led to the value of the rate constant of 0.27 ±0.04 $M^{-1}.s^{-1}$ [141].

Taking into account the value of the rate constant of 0.273 $M^{-1}.s^{-1}$ and $OBr^-_{(aq)}$ concentration in atmospheric water of $7.2 \cdot 10^{-7}$ M, the half-life of $Hg^0_{(aq)}$ by this pathway equals approx. 41 days [141].

Oxidation of $Hg^0_{(aq)}$ by hypochlorous acid ($HOCl_{(aq)}$) and hypochlorite anion (OCl^-)

In the aqueous phase chlorine occurs also as hypochlorous acid ($HOCl_{(aq)}$) and hypochlorite anion ($OCl_{(aq)}$). The presence of these compounds depends on the pH of the solution:

$$HOCl_{(aq)} \leftrightarrow OCl_{(aq)}^- + H^+_{(aq)} \quad \text{R.2.46}$$

with the estimated equilibrium constant of $K_{HOCl} = 3.2 \cdot 10^{-8}$ M [144].

Both species contribute to the oxidation of elemental mercury present in the aqueous phase [144]:

$$Hg^0_{(aq)} + HOCl_{(aq)} \rightarrow Hg^{2+}_{(aq)} + OH^-_{(aq)} + Cl^-_{(aq)} \quad \text{R.2.47}$$

and

$$Hg^0_{(aq)} + OCl^-_{(aq)} + H^+_{(aq)} \rightarrow Hg^{2+}_{(aq)} + OH^-_{(aq)} + Cl^-_{(aq)} \quad \text{R.2.48}$$

with the rates of $(2.09 \pm 0.06) \cdot 10^6$ and $(1.99 \pm 0.05) \cdot 10^6$ $M^{-1}.s^{-1}$ for reactions R.2.47 and R.2.48, respectively.

They also introduced the effective Henry's law constant (H_{eff}) taking into account: (i) the equilibrium R.2.46, (ii) Henry's law constant of H_{Cl_2}=0.076 $M.atm^{-1}$ for molecular chlorine (R.2.49) and (iii) equilibrium in the aqueous phase with the constant of H_{Cl_2}=$5.0 \cdot 10^{-4}$ M^2 (R.2.50):

$$Cl_{2(g)} \leftrightarrow Cl_{2(aq)} \quad \text{R.2.49}$$

$$Cl_{2(aq)} + H_2O \leftrightarrow HOCl_{(aq)} + Cl^-_{(aq)} + H^+_{(aq)} \quad \text{R.2.50}$$

The effective Henry's law constant (H_{eff}) [$M.atm^{-1}$] can be written as:

$$H_{eff} = \frac{[Cl_{2(aq)}] + [HOCl_{aq}] + [OCl^-_{(aq)}]}{Cl_{2(g)}} \quad \text{R.2.51}$$

what finally leads to the following formula:

$$H_{eff} = H_{Cl_2}\left(1 + \frac{H_{Cl2}}{[Cl^-_{(aq)}][H^+_{(qq)}]} + \frac{H_{Cl2}K_{HOCl}}{[Cl^-_{(aq)}][H^+_{(qq)}]}\right) \quad \text{R.2.52}$$

The estimated half-life of $Hg^0_{(aq)}$ by oxidation of chlorine compounds in the aqueous phase is 30 s, assuming a concentration of gaseous $Cl_{2(g)}$ of 15 pptv, chlorine ions $Cl^-_{(aq)}$ of 1mM and

pH of 4.5 [15]. Assuming a concentration of $HOCl_{(aq)}$ of $1.52 \cdot 10^{-9}$ M and $OCl^-_{(aq)}$ of $5.3 \cdot 10^{-9}$ M, this results in a half-life of $Hg^0_{(aq)}$ of 215 s and 65 s, respectively [141].

Reduction of $Hg^{2+}_{(aq)}$ by sulfite

Suflite appears in atmospheric water by scavenging of primary pollutant $SO_{2(g)}$. The solubility of SO_2 increases with pH of droplets. In the aqueous phase, two compounds of mercury and sulphur occur i.e. $HgSO_{3(aq)}$ and $Hg(SO_3)_2^{2-}{}_{(aq)}$, which are in equilibrium [145], [146]:

$$Hg^{2+}_{(aq)} + SO_3^{2-}{}_{(aq)} \leftrightarrow HgSO_{3(aq)} \quad \text{R.2.53}$$

$$HgSO_{3(aq)} + SO_3^{2-}{}_{(aq)} \leftrightarrow Hg(SO_3)_2^{2-}{}_{(aq)} \quad \text{R.2.54}$$

The value of the equilibrium constants for R.2.53 and R.2.54 are $5.0 \cdot 10^{12}$ M^{-1} and $2.1 \cdot 10^{13}$ M^{-1}, respectively [145], [146].

Mercury(II) sulfite $HgSO_{3(aq)}$ is unstable and decomposes to $Hg^0_{(aq)}$ according to the following pathway:

$$HgSO_{3(aq)} \rightarrow Hg^0_{(aq)} + products \quad \text{R.2.55}$$

The rate constant of 0.6 s^{-1} and $T \cdot \exp((31.971 \cdot T - 12595)/T)$ s^{-1}, which can be reduce to $7.7 \cdot 10^{13} T \cdot \exp(-12595/T)$ s^{-1} or 0.0106 ± 0.0009 s^{-1} at 25^0C and pH=3 were reported [145], [147].

It was reported that mercury(II) sulphite also takes part in the reduction of elemental mercury and the value of the rate constant of $0.44 \cdot 10^{-3}$ s^{-1} was estimated [145].

$$Hg(SO_3)^{2-}_{2(aq)} \rightarrow Hg^0_{(aq)} + products \quad \text{R.2.56}$$

However, later studies reported that the mercury(II) sulphite ion is stable and does dissociate to yield $Hg^0_{(aq)}$ [148], [15].

Reduction of $Hg^{2+}_{(aq)}$ by peroxyl radical ($HO_2^{\bullet}{}_{(aq)}$)

The reduction of reactive mercury to elemental mercury occurs by the following two steps (R.2.57 and R.2.58) [149]:

$$Hg^{2+}_{(aq)} + HO_2^{\bullet}{}_{(aq)} \rightarrow Hg^{+}_{(aq)} + O_{2(aq)} + H^{+}_{(aq)} \quad \text{R.2.57}$$

$$Hg^{+}_{(aq)} + HO_2^{\bullet}{}_{(aq)} \rightarrow Hg^{0}_{(aq)} + O_{2(aq)} + H^{+}_{(aq)} \quad \text{R.2.58}$$

Similar to the reduction of $Hg^{+2}_{(aq)}$ by hydroxyl radical due to a fast reduction of $Hg^{+}_{(aq)}$, reaction R.2.57 plays a leading role with the value of a rate constant of $1.7 \cdot 10^4$ $M^{-1}.s^{-1}$ or, in the case when chlorine is present in the system, of $1.1 \cdot 10^4$ $M^{-1}.s^{-1}$. However, some studies concluded that this reaction does not occur under ambient conditions and proposed not to include it into chemical transport models for atmospheric mercury [150].

Peroxyl radical occurs in the aqueous phase from the scavenging of gaseous $OH_2^{\bullet}{}_{(g)}$ or production in atmospheric water in photochemical process [151].

Assuming that the concentration in atmospheric water of $HO_2^{\bullet}{}_{(aq)}$ at 10^{-8} M the half-life of $Hg^{2+}_{(aq)}$ due to this reduction reaction is estimated to be ~1.5 h [15].

Photoreduction of $Hg^{2+}_{(aq)}$ in aqeouse phase

Mercury dihydroxide $Hg(OH)_{2(aq)}$ was found to be the most photoreactive inorganic mercury species in the aqueous phase [152]. The photoreduction occurs by the following pathway:

$$Hg(OH)_{2(aq)} + h\nu \rightarrow Hg^{0}_{(aq)} + products \quad \text{R.2.59}$$

Two sets of observations with the use of initial concentration of $Hg(OH)_{2(aq)}$ of $1.0 \cdot 10^{-6}$ M and $1.0 \cdot 10^{-7}$ M enabled to estimate the average value of the rate constant of $(1.20 \pm 0.27) \cdot 10^{-4}$ s^{-1}.

The calculated value of the rate constant with the use of midday conditions at 60^0N latitude equals $3 \cdot 10^{-7}$ s^{-1}. This value determines the half-life of $Hg(OH)_{2(aq)}$ of about 600 sunlight hours.

Moreover, the photoreduction of reactive mercury to elemental mercury in presence of dicarboxylic acids (DCA) was discovered and proposed as follows: [153], [154].

$$Hg^{2+}_{(aq)} + DCA + h\nu \rightarrow Hg^{0}_{(aq)} \quad \text{R.2.60}$$

The rate constants of (i) $1.2 \cdot 10^4$ $M^{-1}.s^{-1}$ for ethanedioic acid $(HOOC\text{-}COOH)_{(aq)}$, (ii) $1.2 \cdot 10^3$ $M^{-1}.s^{-1}$ for propanedioic acid $(HOOC\text{-}(CH_2)\text{-}COOH)_{(aq)}$ and (iii) $2.8 \cdot 10^3$ $M^{-1}.s^{-1}$ for butanedioic acid $(HOOC\text{-}(CH_2)_2\text{-}COOH)_{(aq)}$ at pH 3.0, T =296 ±2 K in a system free of oxygen and chloride ions were estimated. The ambient concentration of dicarboxylic acids was observed in a wide range from a few $ng.m^{-3}$ to a few $\mu g.m^{-3}$. Ethanedioic (oxalic) acid is the prevailing compound of DCA with the share of 50 -75% of the total DCA mass observed in the air [155].

Oxidation of Hg^{+} to Hg^{2+}

The oxidation of Hg^{+} to Hg^{2+} occurs fast and three possible pathways of this process are presented in the literature. The first considered oxidation of $Hg^{+}_{(aq)}$ by $O_{2(aq)}$ with the value of the rate constants of $1.0 \cdot 10^{9}$ $M^{-1}.s^{-1}$ [156].

$$Hg^{+}_{(aq)} + O_{2(aq)} \rightarrow Hg^{2+}_{(aq)} + O_{2}^{-}{}_{(aq)} \quad \text{R.2.61}$$

Another possible pathway with an estimated value of the rate constants of $1.0 \cdot 10^{10}$ $M^{-1}.s^{-1}$ is the oxidation of $Hg^{+}_{(aq)}$ by $^{\bullet}OH_{(aq)}$ [142].

$$Hg^{+}_{(aq)} + {}^{\bullet}OH_{(aq)} \rightarrow Hg^{2+}_{(aq)} + OH^{-}_{(aq)} \quad \text{R.2.62}$$

Additionally, it was reported that the oxidation of $Hg^{+}_{(aq)}$ by $HO_{2}^{\bullet}{}_{(aq)}$ is very fast, however no value of the constant rate was reported [149].

2.5 Mercury transformation in presence of aerosol particles

Several experiments and theoretical studies were conducted to investigate the sorption (adsorption and desorption) of various mercury forms in gaseous and aqueous phase onto/from particulate matter. As mentioned in chapter 2.3 gaseous oxidation products such as $HgO_{(g)}$ or $Hg(OH)_{2(g)}$ in air are considered to be quickly adsorbed on surfaces, mainly on aerosols [98]. It should be noted that there is still a lack of knowledge in this area, and further research is required [96], [157], [98], [158], [104], [102], [103]. However, currently a few models consider the adsorption of reactive mercury in gaseous phase. They assume simply that the whole or half amounts of $HgO_{(g)}$ and $Hg(OH)_{2(g)}$ created in reactions is adsorbed on PM.

The adsorption of elemental mercury in gaseous phase was also found through experimental and theoretical studies [157], [159]. This process is relatively inefficient and is neglected in mercury chemical transport models

On the other hand, studies focusing on divalent mercury adsorption in the aqueous phase showed that up to 35% of mercury can be adsorbed onto atmospheric aerosols [157]. Based on these experimental and theoretical results, a model of adsorption and desorption of oxidized mercury on black carbon suspended in atmospheric water was developed and widely used and in many chemical transport models for mercury [160]. The linear adsorption isotherm of black carbon in the aqueous phase was defined as follows:

$$Hg_{BC\,(air)} = [Hg_{cplx}][K_{BC}] \quad \text{R.2.63}$$

where:

$Hg_{BC(air)}$ –is the concentration of mercury adsorbed on black carbon (BC) as it is considered as the primary adsorbent of mercury [$kg_{Hg}.kg_{BC}^{-1}$];

K_{BC} is the adsorption coefficient [$m_{water}^{3}.kg_{BC}^{-1}$];

$[Hg_{cplx}]$ –aqueous concentration of dissolved reactive mercury [$kg_{Hg}.m_{water}^{-3}$].

The mass of adsorbed mercury per unit of water in cloud was defined and calculated:

$$[Hg_{p(w)}] = [Hg_{BC(air)}][\mathrm{BC}_{(w)}] \quad \text{R.2.64}$$

$[\mathrm{BC}_{(w)}]$ –concentration of black carbon suspended in atmospheric water [$kg_{BC}.m_{water}^{-3}$];

$[Hg_{p(w)}]$ –concentration of the mercury bound to black carbon suspended in atmospheric water [$kg_{Hg}.m_{water}^{-3}$].

Then they introduced the rate constant for adsorption and desorption [s^{-1}]:

$$k_S = \frac{R_{S/D}}{t^{*}\cdot(R_{S/D}+1)} \quad \text{R.2.65}$$

$$k_d = \frac{k_d}{R_{S/D}} \quad \text{R.2.66}$$

where:

t^{*} –the time constant, assumed to be 1 hour,

and

$$R_{S/D} = \frac{[Hg_{p(w)}]}{[Hg_{cplx}]} = K_{BCA}\cdot[\mathrm{BC}_{(w)}] \quad \text{R.2.67}$$

determines the ratio of adsorbed to dissolved mercury amounts in atmospheric water.

2.6 Measurements of deposition and concentration of heavy metals

The existing networks for monitoring mercury in ambient air and precipitation are mainly operating in the Northern Hemisphere within regional and national programs such as EMEP (Europe), UMAQL (US), CAMNet (Canada) and AMAP (Artic). The long-term observations of mercury were conducted mainly in Europe and North America and also at a few stations located in Asia and the Artic. However, in many other parts of the world, measurement networks dedicated to mercury observations do not exist. It should be noted that in the past few years, intensive efforts were undertaken as part of different regional programs to develop standard procedures of measurements. However, there is still a lack of worldwide standardization of measurement methods for mercury and its compounds. Consequently, the comparison of results of mercury measurements done by different operating networks is very

difficult [161]. The Global Mercury Observation System funded by the European Commission has operated since 2011. The observations are collected at about 47 ground stations located on all continents and also during oceanographic and aircraft measurements campaigns [162].

In Europe mercury measurements are done at stations of the European Monitoring and Evaluation Programme [163]. Some stations co-operate also within the HELCOM, OSPAR and AMAP programs dedicated to environmental protection of, respectively, the Baltic Sea, the North-East Atlantic and the Artic region [164], [165], [166]. The first station within the EMEP network started to operate in the seventies of the last century in Scandinavia. Some stations provide data with hourly time step, others report results once per day. The network covers mainly northern and western Europe.

The locations of stations are presented in Figure 2-10 and Figure 2-11. In years 2000-2011, only one station in the case of ambient mercury concentration and 3 stations in the case of mercury wet deposition operated continuously. Few stations have measurement data available only for one year. The measurements presented in Table 2-15 and Table 2-18 show that there is no trend (either decreasing or increasing) in annual elemental gaseous mercury concentrations and deposition values observed at stations in different years. However, analysis of long-term trends in atmospheric mercury concentrations suggest decrease at a rate of 1 to 2 % a year [167], [168].

The results show relatively low spatial differences of the GEM concentrations over Europe. On the contrary, high variations in the spatial gradient of mercury concentrations in precipitation was observed. The mean concentration of mercury in ambient air is 1.52 $ng.m^{-3}$ at all stations in years 2000 -2011. The average yearly concentration at all EMEP sites ranges from 1.34 $ng.m^{-3}$ in 2010 to 1.62 in 2002 $ng.m^{-3}$. At the PL05station located in Diabla Góra, the measurements of mercury concentration in ambient air started in 2004. The highest concentration was observed in 2004 -1.8 $ng.m^{-3}$ and the lowest in 2005 -0.9 $ng.m^{-3}$. In subsequent years, average concentrations of between 1.2 -1.5 $ng.m^{-3}$ were observed. The measured values of mercury ambient concentration are rather low at the PL05 station compared to other EMEP stations (Table 2-15).

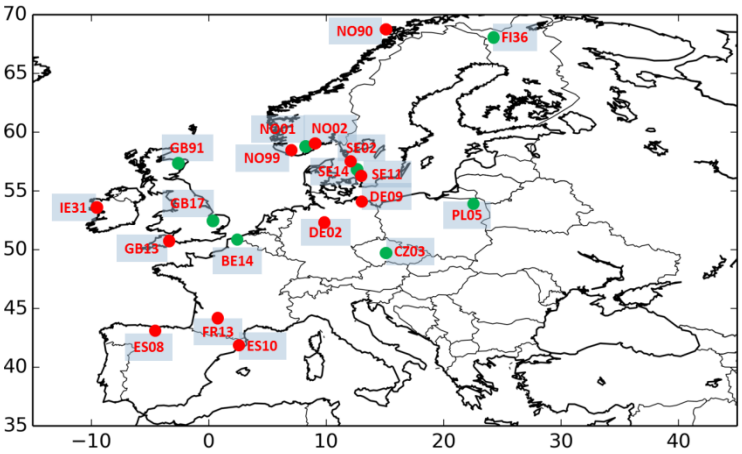

Figure 2-10. Location of EMEP stations, where measurements of ambient GEM concentrations were conducted in the period of 2000-2011. Green dots denote stations for which the observations for 2008 are available.

Table 2-15. The measured annual average concentration of total gaseous mercury in air [ng. m^{-3}]. Underlined numbers indicate results for all forms of mercury (TGM + Hg_P).

N.	Station code	2000	2001	2002	2003	2004	2005	2006	2007	2008	2009	2010	2011
1	BE14									1.81			
2	CZ03								1.18	1.58	0.67	0.48	1.94
3	DE02			1.70									
4	DE09	1.70	1.57										
5	ES08						1.78	1.84					
6	ES10						1.67	1.83					
7	FI36	1.42	1.34	1.32	1.39	1.48	1.40	1.53	1.37	1.41	1.37	1.30	1.44
8	FR13						1.34	1.21					
9	GB13				1.37		1.14		1.59				
10	GB17					1.67	1.36	1.90		1.71			
11	GB91					1.34		1.42		0.86			
12	IE31	1.78	1.64	1.75	1.67	1.63	1.55	1.48					
13	NO01						1.90	1.76	1.86	1.73	1.68	1.66	
14	NO02												1.65
15	NO90				1.66	1.62						1.67	1.61
16	NO99	1.67	1.65	1.64	1.77								
17	PL05					1.80	0.90	1.46	1.20	1.46	1.25	1.28	1.42
18	SE02	1.36	1.66								1.59	1.43	1.39
19	SE11										1.43	1.43	1.56
20	SE14			1.67	1.78	1.62	1.68	1.60	1.55	1.57	1.51	1.48	1.60

For 10 stations, the online database of EMEP provides results of concentration of Hg_P in ambient air (presented in Table 2-16).

Table 2-16. The concentration of mercury bounded to particulate matter observed at various EMEP stations [$ng.m^{-3}$]

N.	Station code	Number of samples in 2008	Average (and range) [$ng.m^{-3}$]
1	ES07	4 days	0.011 (0.005-0.0017)
2	ES08	4 days	0.002 (0.002-0.002)
3	ES10	1 day	0.002

4	ES11	4 days	0.007 (0.003-0.016)
5	ES12	4 days	0.004 (0.003-0.005)
6	ES13	4 days	0.005 (0.002-0.007)
7	FR36	36 samples –averages cover whole year	1.26 (0.1-11.2)
8	GB13	22 samples –averages cover whole year	0.677 (0.036-1.662)
9	GB48	2066 samples	1.116 (0.000-66.641)
10	SE14	100 samples –averages cover whole year	7.6 (1.2-50.2)

As presented in Table 2-16, at the stations located in Spain (ES) a low concentration of Hg_P was observed and in other countries very high, more than 1 ng.m^{-3} (three orders of magnitude difference). The concentration of Hg_P over 1 ng.m^{-3} seems to be too high. It should be noted that EMEP stations should measure the background concentration not influenced by large local sources. Only in Poland and the most polluted places in Europe, such high concentrations are observed during heating season (due to emissions from coal burnt in households) [169]. The concentration of mercury bounded to particulate matter observed at various location and reported in scientific articles are much lower and are presented in Table 2-17.

According to the EMEP reports, observed discrepancy in results may have occurred due to the use of different measuring methodology at EMEP stations and making the obtained observation results of limited use useless to evaluate models and to direct comparisons [170].

Table 2-17. The concentration of mercury bounded to particulate matter observed in various location and reported in scientific articles [ng.m^{-3}].

N.	Mean value or range in brackets [ng.m^{-3}]	Reference
1	0.098	[159]
2	0.07	[171]
3	0.11 in summer, 1.05 in winter	[169]
4	(0.061-0.186)	[172]
5	0.02	[173]
6	0.132	[174]

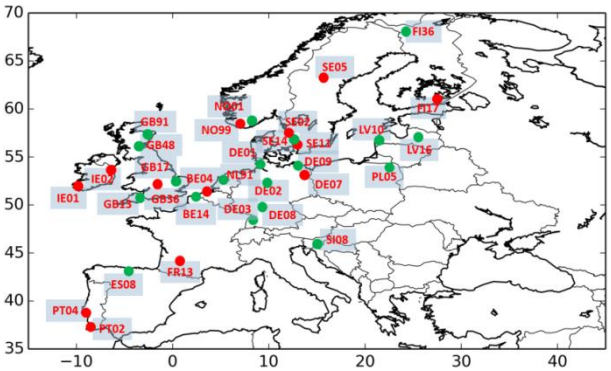

Figure 2-11. Location of EMEP stations where measurements of wet deposition of mercury were conducted in the period of 2000 -2011. Green dots denote stations for which the observations for 2008 are available.

Table 2-18. The measured annual average concentration of mercury in precipitation in years 2000-2011 and average from whole period [ng.dm^{-3}]

N.	Station code	2000	2001	2002	2003	2004	2005	2006	2007	2008	2009	2010	2011	Average
1	BE04	28.6	44.1	27.0	11.9	36.8								29.7
2	BE14						11.1	11.8	10.6	11.2	8.2	9.0	10.6	10.4
3	DE01	9.5	6.3	7.2	9.1	8.1	8.7	8.6	6.3	6.3	6.6	4.3	6.8	7.3
4	DE02			8.4	10.9	11.8	11.5		9.1	9.2	7.0	5.1	10.2	9.2
5	DE03								10.7	8.0	9.3	5.0	8.0	8.2
6	DE07					12.7	9.2							11.0
7	DE08								6.8	8.6	5.9	5.1	7.6	6.8
8	DE09	15.2	9.4	8.7	9.5	10.8	9.5	9.8	7.9	6.9	5.4			9.3
9	ES08									5.2	6.5	9.6	8.7	7.5
10	FI17												5.3	5.3
11	FI36	5.0	5.2	4.7	7.4	6.3	5.6	7.3	5.8	7.5	4.9	3.7	7.1	5.9
12	FR13							9.7	10.7					10.2
13	GB13						4.8	3.3	4.6	6.8	3.4	3.9	4.2	4.4
14	GB17						7.0	3.9	7.1	4.6	5.6	5.1	8.5	6.0
15	GB36												5.9	5.9
16	GB48							3.4	4.6	4.4	3.1	3.2	2.8	3.6
17	GB91						4.7	3.8	4.7	4.6	4.2	5.3	5.4	4.7
18	IE01										63.2	34.6	12.5	36.8
19	IE02				50.0									50.0
20	LV10								25.8	26.0	30.9	37.6	33.0	30.7
21	LV16								28.8	22.0	30.6			27.1
22	NL91	9.8	9.4	9.3	8.6	15.2	15.1	9.6	9.6	10.6	8.8	8.1	8.8	10.2
23	NO01					9.8	8.9	8.1	6.3	6.4	9.4	8.8	5.3	7.9
24	NO99	7.3	7.3	12.8	8.1									8.9
25	PL05					270.9	21.0	11.2	55.1	42.3			31.0	71.9
26	PT02										30.0	26.0	5.0	20.3
27	PT04												5.2	5.2
28	SE02	8.8	9.3											9.1
29	SE05	5.5	6.5	7.2	7.6						6.5	6.9	5.6	6.5
30	SE11	12.5	9.4	9.9	11.6						10.0	7.6	8.7	10.0
31	SE14			12.3	9.0	14.6	18.5	10.0	11.0	8.6	13.7	9.1	8.9	11.6
32	SI08									5.4	5.6	4.2	5.8	5.3

In Poland, the one-hour measurements of atmospheric concentrations of various mercury forms were conducted for the period 08/2011 -07/2012 in Zabrze and Złoty Potok, which represent respectively highly urban and background locations [175]. In Zabrze, the average concentrations of 44.46 pg.m^{-3} for Hg_P, 3.14 ng.m^{-3} for TGM including 3.13 ng.m^{-3} of GEM and 17.81 pg.m^{-3} for RGM were observed during the whole observation campaign period. During the heating season, the following concentrations were observed: 2.76 ng.m^{-3} of GEM, 20.03 pg.m^{-3} of RGM, 64.99 pg.m^{-3} of Hg_P. In the summer period, the observed concentration was higher for GEM and lower for RGM and Hg_p respectively 3.44 ng.m^{-3}, 15.21 pg.m^{-3}, 64.50 pg.m^{-3}. In Złoty Potok, the average TGM concentration of 1.84 ng.m^{-3} during heating and summer seasons was observed.

The dry deposition of pollution is a product of the concentration of species in ambient air and a parameter, which is called the dry deposition velocity. The mathematical models used to estimate the dry deposition velocity are presented in chapter 4.2.

Measurements of dry deposition of various mercury forms were conducted at various locations and periods to allow one to determine the dry deposition velocity of GEM, RGM and Hg_P [176]. The lowest mean value of dry deposition velocity was measured for surfaces covered by snow and equals 0.00025 $cm.s^{-1}$, while the highest value of 5.01 $cm.s^{-1}$ was reported in a contaminated landfill in Korea. If we assume for these two cases the air concentration of GEM to be at 1.5 $ng.m^{-3}$, the annual dry deposition load is 0.12 and 2370 $g.km^{-2}.y^{-1}$. The reported measured dry deposition velocity for forest canopies ranges from 0.0003 $cm.s^{-1}$ to 1.88 $cm.s^{-1}$, for agricultural fields from 0.05 $cm.s^{-1}$ to 0.28 $cm.s^{-1}$, grasslands from 0.003 $cm.s^{-1}$ to 0.1 $cm.s^{-1}$, wetlands 0.02 -0.19 $cm.s^{-1}$. The water surface is characterized by a low dry deposition velocity from 0.003 to 0.012 $cm.s^{-1}$.The dry deposition velocity of RGM is higher. The dry RGM deposition velocity ranges between 0.1 -6.0 $cm.s^{-1}$ for forest canopies, from 0.3 to 1.72 $cm.s^{-1}$ for grassland and 0.02 -7.6 $cm.s^{-1}$ for wetlands, that were reported [176].

The most comprehensive measurements of cadmium and lead concentrations in ambient air and in precipitation over Europe are conducted within the EMEP programme [14]. As these species are bound to aerosol particles the concentration is reported for given aerosol's size sections, usually for PM1, PM2.5, PM10 or TSP [163]. The first station where cadmium and lead concentrations were measured in Norway, and started to operate in 1974. Since that time, the EMEP measurement network was developed. In 1995, there were 23 stations, in 2000 -25, in 2005 -37, in 2008 -50 stations where concentrations of cadmium in ambient air were observed. The lead concentration were observed in these years respectively: in 24; 35; 43; 55 stations of EMEP.

In Poland, the PL05 station located in Diabla Góra has measured concentration of lead and cadmium bound to PM10 since 2005. Mean concentrations of lead 7.7; 9.5; 6.3; 5.3; 4.3; 4.1 and 5.2 $ng.m^{-3}$ in sequence in years 2005 -2011 were reported. At the PL05 station, the highest concentration of lead is being measured in January and the lowest in May. The mean concentrations of 10.6 $ng.m^{-3}$ and 1.9 $ng.m^{-3}$ from years 2005 -2011 in these months were reported. The mean annual concentration of cadmium in the years 2005 -2011 was reported to be respectively: 0.33; 0.34; 0.17; 0.16; 0.20; 0.14 and 0.24 $ng.m^{-3}$. Generally, during the summer season (May -September) the average monthly concentration of cadmium for the period 2005 -2011 is approximately 0.13 $ng.m^{-3}$, while in the rest of the months the

concentration of approximately 0.3 $ng.m^{-3}$ was reported. The highest monthly average concentration of 20.7 $ng.m^{-3}$ and 0.75 $ng.m^{-3}$ of lead and cadmium was observed at this station in November 2006. Whereas at all stations of the EMEP, the highest monthly mean concentration of lead bound to PM10 was reported at the AT02 site located in Austria in February 2003 and equalled 42.8 $ng.m^{-3}$. At the same station, the highest monthly mean concentrations of (i) 24.7 $ng.m^{-3}$ of lead bound to PM2.5, (ii) 2.00 $ng.m^{-3}$ of cadmium bound in PM10 and (iii) 1.27 of cadmium bound to PM2.5 were observed in November 2003.

The concentrations of lead and cadmium in precipitation are observed within the EMEP programme since 1973 when two stations located in Norway started to operate. In 1990, 27 stations operated, in 2000 and 2005 -57 stations. Nowadays the EMEP network consists of 62 stations spread all over Europe. Over all stations and all years, the average concentrations in precipitation of lead and cadmium equal 15.9 and 0.22 $\mu g.dm^{-3}$, respectively. The average annual wet deposition of lead at all EMEP stations was 1403 $g.km^{-2}.y^{-1}$ in 2000, in 2005 -1414 $g.km^{-2}.y^{-1}$ and 592 $g.km^{-2}.y^{-1}$ in 2010. For cadmium in these years fluxes of 69.34; 37.76; 37.18; $g.km^{-2}.y^{-1}$ were measured. The highest average monthly value of cadmium concentration in precipitation of 37.39 $\mu g.dm^{-3}$ was observed at the IT01 station (Italy, Montelibretti) in January 2007, while for lead 1651.7 $\mu g.dm^{-3}$ in August 2002 at the GB14 station (UK, High Muffles). In Poland, the lead and cadmium concentrations in precipitation have been observed since 1992 at the PL05 station located in Diabla Góra and since 1996 at the PL04 station in Łeba.

At the PL04, station the maximum monthly average concentrations of Pb in precipitation of 9.64 $\mu g.dm^{-3}$ was observed in March 1996 and the highest wet deposition of 400 $g.km^{-2}.month^{-1}$ was measured in June 2001. At PL05, the maximum observed values were 16 $\mu g.dm^{-3}$ and 713 $g.km^{-2}.month^{-1}$ in December 1992. At this station, the annual wet deposition systematically decreases. In the nineties the load of wet deposited lead above 2000 $g.km^{-2}.y^{-1}$ was observed. Whereas in 2011, depositions of only 241 $g.km^{-2}.y^{-1}$ was measured at the PL05 station.

In the XXI century, the highest monthly cadmium concentrations in precipitation of 0.23 $\mu g.dm^{-3}$ and 0.50 $\mu g.dm^{-3}$ were observed in February 2006 at the EMEP stations i.e. PL04 and PL05 operated in Poland. The maximal monthly fluxes of cadmium of 13.1 $g.km^{-2}.month^{-1}$ and 19.2 $g.km^{-2}.month^{-1}$ were measured in April 2006 at PL04 and September 2003 at PL05, respectively. At both stations, the highest wet depositions of cadmium was observed in November. Since the beginning of the operation of the stations, a downward trend in measured quantities of deposited cadmium can be observed.

3 Overview of existing mercury chemical transport models

The chemical schemes of mercury are usually implemented into the existing modelling systems developed for traditional pollutants (SO_2, NO_x, PM, O_3). The atmospheric chemistry of mercury is complex [15], [9]. Thus on one hand, the mercury models should represent well its real behaviour but on the other the computation time requirements should not be prohibitive. Many numerical mercury models of Eulerian (ADOM, CAMx, CMAQ-Hg, CMAQ ver. 4.7.1, CTM-Hg, DEHM, ECHMERIT, GEOS-Chem, GLEMOS, MOZART, MSCE-HM, MSCE-HM-Hem, STEM-Hg) and Lagrangian (HYSPLIT, RCTM-Hg) types have been developed to evaluate the atmospheric dispersion and transformation of mercury on a regional, continental and global scale [10], [11]. Developed models dedicated to atmospheric mercury consider the main chemical reactions and transformations within the aqueous and gaseous phases. However, some significant differences can be found, in chemical reactions taken into account as well as in the value of the kinetic rates. Additionally the various approaches were used to model the dry and wet deposition fluxes of mercury. The paragraphs below provide short information on the application and particular properties of those models. All main chemical reactions and transformations of mercury included in the considered models are presented in Table 3-1 and Table 3-2.

CMAQ-Hg

The version of the Community Multiscale Air Quality model with mercury scheme (CMAQ-Hg) was developed by US-EPA. The model has no explicit simulation of cloud-water transport [160]. The model assumes that the dry deposition of GEM is equivalent to emissions from natural sources. The dry deposition parameterization for gaseous nitric acid was used for the calculation of the dry deposition velocity of reactive gaseous mercury. The fields of concentration of species that react with mercury are generated simultaneously in the same simulation with the use of the algorithms of a standard CMAQ model. This Eulerian type model was applied in continental simulation over Europe and North America [177].

CMAQ ver. 4.7.1

In this version of the CMAQ model, significant features devoted to atmospheric mercury were implemented [178]. Dry deposition of reactive gaseous mercury and gaseous elemental mercury is calculated with the use of the M3Dry deposition scheme [179]. Therefore computed dry deposition depends on type of vegetation and stromatal resistance. Dry

deposition of Hg_P is calculated as a function of particle size. Wet deposition of mercury species is computed based on their concentration in cloud-water and precipitation rate.

CTM-Hg

Global chemical transport model for mercury CTM-Hg was developed by Atmospheric and Environmental Research, Inc. [180]. The model assumes the following dry deposition velocities:

-0.25 $cm.s^{-1}$ for GEM,

-0.01 $cm.s^{-1}$ over land and 0.01 $cm.s^{-1}$ over water for Hg_p,

-0.01$cm.s^{-1}$ over land and 0 $cm.s^{-1}$ over water for GEM.

Another assumption of the model is that below cloud scavenging process due to precipitation removes 10% of RGM, 50% of Hg_p and 0% of GEM.

CAMx

The Comprehensive Air Quality Model with Extensions is an Eulerian photochemical dispersion model which can be applied from sub-urban to continental scale to compute the dispersion of gaseous and particulate air pollution [181]. Dry deposition of Hg_p and RGM is calculated with the use of resistance model [182]. The model assumes that dry and wet deposition of GEM is negligible. In the model, dry deposition of GEM is not computed because of the assumption that dry deposition of GEM is equivalent to emissions from natural sources and reemission. CAMx and CMAQ ver. 4.7.1 were used in simulations performed over the eastern United States.

MSCE-HM

The MSCE-HM model is a three dimensional Eulerian type chemical transport model driven by off-line meteorological data coming from MM5 developed in the European Monitoring and Evaluation Programme by the Meteorological Synthesizing Centre-East in Moscow. The model works in the EMEP grid, which covers the whole Europe with spatial resolution of 50 km x 50 km. Dry deposition is calculated with the use of a resistance model with modification for aerosols. The wet deposition flux is calculated based on the empirical relationship derived from measurements [29]. Correlation coefficients of 0.38 and 0.5 were obtained from comparison for 2003 of measured and modelled mercury concentrations in the air and precipitation, respectively. The simulation performed for 2008 showed that difference

between modeled and observations of mercury concentrations in air and wet deposition do not exceed 15% and 30% respectively [183].

MSCE-HM-Hem

The model was developed for modelling the Northern Hemisphere and derived directly from the MSCE-HM model. The dry deposition of RGM is calculated with the use of parameters for nitric acid. The deposition of GEM to vegetation is calculated based on data of surface temperature, solar radiation and vegetation type. Value from 0 to 0.03 $cm.s^{-1}$ for dry velocity of GEM were obtained. The dry deposition of Hg_P is estimated from experimental data. The wet deposition of RGM and Hg_P is calculated based on an empirical relationship derived from measurements. The model simulations have been performed over the Northern Hemisphere with a resolution of $2.5^0 \times 2.5^0$ for the period 1990 -2004. The validation of the modelled results against measurements showed a high compatibility in the case of GEM concentrations in air and an overestimation for wet deposition fluxes of mercury [184].

GLEMOS

The Global EMEP Multi-media Modelling System is developed by the Meteorological Synthesizing Centre -East within the European Monitoring and Evaluation Programme. It can be used at global and regional scales. The chemical module of mercury is based on previous developed and tested schemes included in the MSCE-HM-Hem model but new reactions with bromine and bromine compounds were added [185]. The comparison results obtained from a simulation run for 2005 against measurement over Europe, North America and Asia showed to be satisfactory for air concentration and wet deposition [186].

ADOM mercury model

Acid Deposition and Oxidants Model (ADOM) is the Eulerian model developed under the Canada -Germany Science & Technology Co-operation Agreement. The model considers 14 mercury compounds and 21 chemical reactions. Dry deposition is calculated based on the resistance model. Mercury scavenging is calculated with the use of sub-models, which simulate vertical distribution of mercury species in clouds. Results obtained from simulations performed over Europe showed a rather good agreement with observational data [187].

DEHM

The mercury model was also implemented in the Danish Eulerian Hemispheric Model under the Danish Arctic Monitoring and Assessment Programme [188]. The chemistry of mercury implemented in DEHM is derived from ADOM model [189]. The dry deposition is calculated based on resistance model with parameters for $HNO_{3(g)}$. A simple scavenging coefficient formulation with removal rates for sulphur was applied. The model was run over the Northern Hemisphere and the obtained results showed that DEHM is able to reproduce patterns due to the mercury depletion during Polar Sunrise.

STEM-Hg

The Eulerian numerical model dedicated for mercury STEM-Hg is derived from the Sulfur Transport and Deposition Model (STEM-III), developed at the University of Iowa [190]. The wet removal rates for RGM and Hg_p were assumed to be equal to those of nitric acid and sulphate, respectively. It was assumed that the dry deposition velocity for GEM equals zero because dry deposition of GEM is equivalent to emissions from natural sources and reemission. Dry deposition velocities of RGM and Hg_p were assumed to be equal to those of gaseous $HNO_{3(g)}$ and sulphate, respectively. The model was used to investigate the atmospheric mercury budget in East Asia.

GEOS-Chem

The GEOS-Chem model is a global 3-D model of atmospheric chemistry and transport developed mainly by Harvard University [191]. Wet deposition of GEM and dry deposition of GEM over land is negligible. The dry deposition of GEM to the ocean is modelled with the use of bidirectional exchange model. For RGM and Hg_P, scavenging is computed from precipitation and in convective updrafts and dry deposition is computed with the use of resistance scheme. The surface resistance for RGM was set to zero. The performed simulation were used to study global and regional (in China and the US) budget of mercury. Overestimates of wet deposition of RGM and Hg_P were observed by a factor of 2 -5 due to high modeled concentrations of those mercury forms.

ECHMERIT

ECHMERIT is a model developed by the Institute of Atmospheric Pollution Research in Italy. The model calculates the wet and dry deposition of gaseous species and particulate matter. Mercury in the aqueous phase is considered as one lumped species. The operational validation of the model performed for 2001 showed an overestimation of wet deposition compared to stations over Europe and North America [192].

MOZART

Model for Ozone and Related Chemical Tracers (MOZART) is a global transport model developed by the National Center for Atmospheric Research (NCAR), Geophysical Fluid Dynamics Laboratory (GFDL) and Max Planck Institute for Meteorology [193]. It was modified to include gas-phase mercury chemistry [194]. The dry and wet deposition of reactive gaseous mercury is calculated with the use of parameters previously used for HNO_3. The dry and wet deposition of gaseous elemental mercury was set to 0. The model was run to investigate the impact of mercury emitted in China on global mercury mass balance and to generate boundary concentrations for simulation performed over the Great Lakes in the United States [194].

Following this review of published results of mercury modelling and their operational validation against measurements in Europe, some general conclusions can be drawn [195], [196]:

-models do not indicate peaks of concentration of GEM, or if they do then the peaks are significantly underestimated, but the average annual concentrations correspond well to the observations;

-there is a good agreement with measurements of mercury bound to aerosols.

-processes (e.g. emissions, meteorological phenomena) that take place outside the modelling domain have a strong impact on the obtained results;

-the direct anthropogenic emissions in the domain have the strongest impact on the atmospheric concentration of mercury.

-there is a weak correlation with daily measurements of RGM.

Table 3-1. Chemical reactions and transformation of mercury included in the regional/continental chemical transport models of atmospheric mercury (DCA-dicarboxylic acid). In this table, the values of reaction rates and equilibrium constants of chemical reactions, which were used in various models are presented. The blank cell indicates that reaction or equilibrium are not implemented to the model.

N.	Reaction	CMAQ ver. 4.7.1	CMAQ-Hg	MSCE-HM	MSCE-HM-Hem	STEM-Hg	ADOM/DEHM	CAMx
1	**Gas-phase oxidation**							
2	**Units: $cm^3.molec^{-1}.s^{-1}$**							
3	$Hg^0_{(g)} + O_{3(g)} \rightarrow HgO_{(g)} + O_{2(g)}$					$7.5 \cdot 10^{-19}$	$3.0 \cdot 10^{-20}$	$3.0 \cdot 10^{-20}$
4	$Hg^0_{(g)} + O_{3(g)} \rightarrow Hg_p$		$3.0 \cdot 10^{-20}$	$2.1 \cdot 10^{-18} \cdot \exp(-1247/T)$	$2.1 \cdot 10^{-18} \cdot \exp(-1247/T)$			
5	$Hg^0_{(g)} + O_{3(g)} \rightarrow 0.5 \cdot HgO_{(g)} + 0.5 \cdot Hg_p$	$3.0 \cdot 10^{-20}$						
6	$Hg^0_{(g)} + 2^{\bullet}OH_{(g)} \rightarrow Hg(OH)_{2(g)}$					$9.0 \cdot 10^{-14}$		$8 \cdot 10^{-14}$
7	$Hg^0_{(g)} + 2^{\bullet}OH_{(g)} \rightarrow Hg_p$		$8.7 \cdot 10^{-14}$	$8.7 \cdot 10^{-14}$	$8.7 \cdot 10^{-14}$			
8	$Hg^0_{(g)} + 2^{\bullet}OH_{(g)} \rightarrow 0.5 \cdot Hg(OH)_{2(g)} + 0.5 \cdot Hg_p$	$7.7 \cdot 10^{-14}$						
9	$Hg^0_{(g)} + H_2O_{2(g)} \rightarrow Hg(OH)_{2(g)}$	$8.5 \cdot 10^{-19}$						$8.5 \cdot 10^{-19}$
10	$Hg^0_{(g)} + H_2O_{2(g)} \rightarrow HgO_{(g)}$					$8.5 \cdot 10^{-19}$		
11	$Hg^0_{(g)} + H_2O_{2(g)} \rightarrow Hg_p$		$8.5 \cdot 10^{-19}$					
12	$Hg^0_{(g)} + 2Cl_{2(g)} \rightarrow HgCl_{2(g)}$	$2.6 \cdot 10^{-18}$	$4.8 \cdot 10^{-19}$	$2.6 \cdot 10^{-18}$	$2.6 \cdot 10^{-18}$	$2.6 \cdot 10^{-18}$		$2.6 \cdot 10^{-18}$
13	$2Hg^0_{(g)} + 2^{\bullet}Cl_{(g)} + M \rightarrow HgCl_{2(g)} + Hg^0_{(g)} + M$	$2.2 \cdot 10^{-32} \cdot \exp(680(1/T - 1/298))$ $cm^6.molec^{-2}.s^{-1}$						
14	$Hg^0_{(g)} + 2HCl_{(g)} \rightarrow HgCl_{2(g)}$							
15	$Hg^0_{(g)} + {}^{\bullet}BrO_{(g)} \rightarrow HgO_{(g)} + {}^{\bullet}Br_{(g)}$							
16	$Hg^0_{(g)} + {}^{\bullet}Br_{(g)} \rightarrow HgBr_{(g)}$							
17	$HgBr_{(g)} + 2^{\bullet}Br_{(g)} \rightarrow HgBr_{2(g)}$							
18	$HgBr_{(g)} + {}^{\bullet}OH_{(g)} \rightarrow HgBrOH_{(g)}$							
19	$Hg^0_{(g)} + NO_3{}^{\bullet}{}_{(g)} \rightarrow HgO_{(g)} + NO_{2(g)}$							
20	**Gas-phase reduction**							
21	**Units: s^{-1}**							
22	$HgBr_{(g)} \rightarrow Hg^0_{(g)} + Br_{(g)}$							
23	**Aqueous-phase oxidation**							
24	**Units: $M^{-1}.s^{-1}$**							
25	$Hg^0_{(aq)} + O_{3(aq)} \rightarrow Hg^{2+}_{(aq)}$	$4.7 \cdot 10^7$	$4.7 \cdot 10^7$	$4.7 \cdot 10^7$	$4.7 \cdot 10^7$	$4.7 \cdot 10^7$	$4.7 \cdot 10^7$	$4.7 \cdot 10^7$
26	$Hg^0_{(aq)} + {}^{\bullet}OH_{(aq)} \rightarrow Hg^{2+}_{(aq)}$	$2.0 \cdot 10^9$	$2.0 \cdot 10^9$	$2.4 \cdot 10^9$	$2.4 \cdot 10^9$	$2.0 \cdot 10^9$		$2.0 \cdot 10^9$
27	$Hg^0_{(aq)} + {}^{\bullet}OH_{(aq)} \rightarrow Hg^{+}_{(aq)}$							
28	$Hg^{+}_{(aq)} + {}^{\bullet}OH_{(aq)}$							

	$\rightarrow Hg^{2+}_{(aq)}$							
29	$Hg^{0}_{(aq)} + HOCl_{(aq)} \rightarrow Hg^{2+}_{(aq)}$	$2.09 \cdot 10^{6}$	$2.09 \cdot 10^{6}$			$2.09 \cdot 10^{6}$		$2.09 \cdot 10^{6}$
30	$Hg^{0}_{(aq)} + OCl^{-} \rightarrow Hg^{2+}$	$1.99 \cdot 10^{6}$	$1.99 \cdot 10^{6}$	$2.0 \cdot 10^{6}$	$2.0 \cdot 10^{6}$	$1.99 \cdot 10^{6}$		$1.99 \cdot 10^{6}$
31	$Hg^{0}_{(aq)} + HOBr_{(aq)} \rightarrow Hg^{2+}_{(aq)} + Br^{-}_{(aq)} + OH^{-}_{(aq)}$							
32	$Hg^{0}_{(aq)} + {}^{\bullet}BrO_{(aq)} \rightarrow Hg^{2+}_{(aq)} + Br^{-}_{(aq)} + OH^{-}_{(aq)}$							
33	$Hg^{0}_{(aq)} + Br_{2(aq)} \rightarrow Hg^{2+}_{(aq)} + 2Br^{-}_{(aq)}$							
34	**Aqueous-phase reduction**							
35	**Units: s^{-1}**							
36	$HgSO_{3(aq)} \rightarrow Hg^{0}_{(aq)}$	$T \cdot \exp^{((31.971T-12595)/T)}$	$T \cdot \text{expt}^{((31.971T-12595)/T)}$			0.0106	0.6	0.0106
37	$Hg(SO_3)^{2-}_{2\,(aq)} \rightarrow Hg^{0}_{(aq)}$			$4.4 \cdot 10^{-4}$	$4.4 \cdot 10^{-4}$			
38	$Hg(OH)_{2(aq)} + h\nu \rightarrow Hg^{0}_{(aq)}$	$6.0 \cdot 10^{-7}$	$6.0 \cdot 10^{-7}$			$3.0 \cdot 10^{-7}$		
39	**Units: $M^{-1}.s^{-1}$**							
40	$Hg^{2+}_{(aq)} + HO_2 \rightarrow Hg^{0}_{(aq)}$		$1.1 \cdot 10^{4}$			$1.7 \cdot 10^{4}$		$1.7 \cdot 10^{4}$
41	$Hg^{2+}_{(aq)} + DCA + h\nu \rightarrow Hg^{0}_{(aq)}$	$1.2 \cdot 10^{4}$						
42	**Gas/liquid equilibria**							
43	**Units: $M.atm^{-1}$**							
44	$Hg^{0}_{(g)} \leftrightarrow Hg^{0}_{(aq)}$		0.11	$1.76 \cdot 10^{-23} \cdot T \cdot \exp(9.08 \cdot (T_0/T-1))$	$1.76 \cdot 10^{-23} \cdot T \cdot \exp(9.08 \cdot (T_0/T-1))$	0.11		
45	$HgO_{(g)} \leftrightarrow HgO_{(aq)}$							
46	$HgCl_{2(g)} \leftrightarrow HgCl_{2(aq)}$		$1.4 \cdot 10^{6}$	$1.75 \cdot 10^{-16} \text{Texp}(18.75(T_0/T-1))$	$1.75 \cdot 10^{-16} \text{Texp}(18.75(T_0/T-1))$	$1.4 \cdot 10^{6}$		
47	$Hg(OH)_{2(g)} \leftrightarrow Hg(OH)_{2(aq)}$							
48	$HOBr_{(g)} \leftrightarrow HOBr_{(aq)}$							
49	$HgBr_{(g)} \leftrightarrow HgBr_{(aq)}$							
50	$HgBr_{2(g)} \leftrightarrow HgBr_{2(aq)}$							
51	$HgBrOH_{(g)} \leftrightarrow HgBrOH_{(aq)}$							
52	**Aqueous phase equilibria**							
53	$Hg^{2+}_{(aq)} + SO^{2-}_{3(aq)} \leftrightarrow HgSO_{3\,(aq)}$	$5 \cdot 10^{12}$ M^{-1}	$5 \cdot 10^{12}$ M^{-1}	$5 \cdot 10^{12}$ M^{-1}		$2.1 \cdot 10^{13}$ M^{-1}		$2.1 \cdot 10^{13}$ M^{-1}
54	$HgSO_{3\,(aq)} + 2SO^{2-}_{3(aq)} \leftrightarrow Hg(SO_3)^{2-}_{2(aq)}$	$2.5 \cdot 10^{11}$ M^{-1}	$2.5 \cdot 10^{11}$ M^{-1}	$1.1 \cdot 10^{-21+4pH} \cdot [SO_{2(g)}]^2$ s^{-1}	$1.1 \cdot 10^{-21+4pH} \cdot [SO_{2(g)}]^2$ s^{-1}	$1.0 \cdot 10^{10}$ M^{-1}		$1.0 \cdot 10^{10}$ M^{-1}
55	$HgCl_{2\,(aq)} \leftrightarrow Hg^{2+}_{(aq)} + 2Cl^{-}_{(aq)}$	$10^{-14}M^2$	$10^{-14}M^2$					
56	$Hg_n Cl_{m\,(dis)} \leftrightarrow Hg^{2+}_{(aq)}$			f([Cl^{-1}])	f([Cl^{-1}])			$10^{-14}M^2$
57	$HgOH^{+}_{(aq)} \leftrightarrow Hg^{2+}_{(aq)} + OH^{-}_{(aq)}$	$2.51 \cdot 10^{-11}M$	$2.51 \cdot 10^{-11}M$	$2.51 \cdot 10^{-11}M$		$2.51 \cdot 10^{-11}M$		$10^{-22}M^2$

58	$Hg(OH)_{2\,(aq)} \leftrightarrow Hg^{2+}_{(aq)} + 2OH^{-}_{(aq)}$		$10^{-22}M^2$	$10^{-22}M^2$				
59	$Hg(OH)_{2\,(aq)} \leftrightarrow HgOH^{+}_{(aq)} + OH^{-}_{(aq)}$	$6.13 \cdot 10^{-12}M$						
60	$HgOHCl_{(aq)} \leftrightarrow HgOH^{+}_{(aq)} + Cl^{-}_{(aq)}$	$3.72 \cdot 10^{-8}M$	$3.72 \cdot 10^{-8}M$	$3.72 \cdot 10^{-8}M$		$3.72 \cdot 10^{-8}M$		
61	$Hg^{2+}_{(aq)} + Br^{-}_{(aq)} \leftrightarrow HgBr^{+}_{(aq)}$							
62	$HgBr^{+}_{(aq)} + Br^{-}_{(aq)} \leftrightarrow HgBr_{2\,(aq)}$							
63	$HgBr_{2\,(aq)} + Br^{-}_{(aq)} \leftrightarrow HgBr^{-}_{3\,(aq)}$							
64	$HgBr^{-}_{3\,(aq)} + Br^{-}_{(aq)} \leftrightarrow HgBr^{2-}_{4(aq)}$							
65	$HOBr_{(aq)} \leftrightarrow H^{+}_{(aq)} + BrO^{+}_{(aq)}$							
66	$H^{+}_{(aq)} + Br^{-}_{(aq)} + Hg(OH)_{2(aq)} \leftrightarrow HgBrOH_{(aq)}$							
67	$HgOH^{+}_{(aq)} + OH^{-}_{(aq)} \leftrightarrow Hg(OH)_{2\,(aq)}$					$1.58 \cdot 10^{11}\ M^{-1}$		
68	$Hg^{2+}_{(aq)} + Cl^{-}_{(aq)} \leftrightarrow HgCl^{+}_{(aq)}$					$5.8 \cdot 10^{6}\ M^{-1}$		
69	$HgCl^{+}_{(aq)} + Cl^{-}_{(aq)} \leftrightarrow HgCl_{2\,(aq)}$					$2.5 \cdot 10^{6}\ M^{-1}$		
70	**Gas/soot equilibria**							
71	**Units: $m_{water}^{3}.m_{air}^{-3}$**							
72	$soot_{(g)} \rightarrow soot_{(aq)}$		$5 \cdot 10^{5}$	$5 \cdot 10^{5}$				
73	**Liquid /soot equilibria**							
74	$HgSO_{3\,(aq)} \leftrightarrow HgSO_{3(p)}$			0.2				
75	$HgSO^{2-}_{2\,(aq)} \leftrightarrow HgSO^{2-}_{2\,(p)}$							
76	$Hg(HO)_{2\,(aq)} \leftrightarrow Hg(HO)_{2\,(p)}$							
77	$HgCl_{2\,(aq)} \leftrightarrow HgCl_{2\,(p)}$							
78	$HgCl_{m\,(aq)} \leftrightarrow HgCl_{m\,(p)}$			0.2				
79	$HgOHCl_{(aq)} \leftrightarrow HgOHCl_{(p)}$							
80	$HgOH^{+}_{(aq)} \leftrightarrow HgOH^{+}_{(p)}$							
81	$Hg^{II}_{(aq)} \leftrightarrow Hg^{II}_{(p)}$	$45\ l.g^{-1}$						$34\ l.g^{-1}$

Table 3-2. Chemical reactions and transformation of mercury included in the global chemical transport models of atmospheric mercury (DCA-dicarboxylic acid). In this table, the values of reaction rates and equilibrium constants of chemical reactions, which were used in various models are presented. The blank cell indicates that reaction or equilibrium are not implemented to the model.

N.	Reaction	CTM-Hg	GLEMOS	MOZART	GEOS-Chem	ECHMERIT
1	**Gas-phase oxidation**					
2	**Units: $cm^3.molec^{-1}.s^{-1}$**					
3	$Hg^0_{(g)}+O_{3(g)}\rightarrow HgO_{(g)}+O_{2(g)}$	$3.0\cdot10^{-20}$		$3.0\cdot10^{-20}$	$3.0\cdot10^{-20}$	$3.0\cdot10^{-20}$
4	$Hg^0_{(g)}+O_{3(g)}\rightarrow Hg_p$		$2.1\cdot10^{-18}\cdot\exp(-1247/T)$			
5	$Hg^0_{(g)}+O_{3(g)}\rightarrow 0.5\cdot HgO_{(g)}+0.5\cdot Hg_p$					
6	$Hg^0_{(g)}+2^{\bullet}OH_{(g)}\rightarrow Hg(OH)_{2(g)}$	$8.7\cdot10^{-14}$		$8\cdot10^{-14}$	$9.0\cdot10^{-14}$	$8.7\cdot10^{-14}$
7	$Hg^0_{(g)}+2^{\bullet}OH_{(g)}\rightarrow Hg_p$		$8.7\cdot10^{-14}$			
8	$Hg^0_{(g)}+2^{\bullet}OH_{(g)}\rightarrow 0.5\cdot Hg(OH)_{2(g)}+0.5\cdot Hg_p$					
9	$Hg^0_{(g)}+H_2O_{2(g)}\rightarrow Hg(OH)_{2(g)}$	$8.5\cdot10^{-19}$		$8.5\cdot10^{-19}$		$8.5\cdot10^{-19}$
10	$Hg^0_{(g)}+H_2O_{2(g)}\rightarrow HgO_{(g)}$					
11	$Hg^0_{(g)}+H_2O_{2(g)}\rightarrow Hg_p$					
12	$Hg^0_{(g)}+2Cl_{2(g)}\rightarrow HgCl_{2(g)}$	$2.6\cdot10^{-18}$	$2.6\cdot10^{-18}$			
13	$2Hg^0_{(g)}+2^{\bullet}Cl_{(g)}+M\rightarrow HgCl_{2(g)}+Hg^0_{(g)}+M$					
14	$Hg^0_{(g)}+2HCl_{(g)}\rightarrow HgCl_{2(g)}$	10^{-19}				10^{-19}
15	$Hg^0_{(g)}+^{\bullet}BrO_{(g)}\rightarrow HgO_{(g)}+^{\bullet}Br_{(g)}$	$1.5\cdot10^{-14}$	$1.5\cdot10^{-14}$			
16	$Hg^0_{(g)}+^{\bullet}Br_{(g)}\rightarrow HgBr_{(g)}$	$3.6\cdot10^{-13}$	$1.1\cdot10^{-12}\cdot\exp(T/298)^{-2.37}$			$3.2\cdot10^{-12}$
17	$HgBr_{(g)}+2^{\bullet}Br_{(g)}\rightarrow HgBr_{2(g)}$	$2.5\cdot10^{-10}$				
18	$HgBr_{(g)}+^{\bullet}OH_{(g)}\rightarrow HgBrOH_{(g)}$	$2.5\cdot10^{-10}$				
19	$Hg^0_{(g)}+NO_3^{\bullet}{}_{(g)}\rightarrow HgO_{(g)}+NO_{2(g)}$					$4.0\cdot10^{-15}$
20	**Gas-phase reduction**					
21	**Units: s^{-1}**					
22	$HgBr_{(g)}\rightarrow Hg^0_{(g)}+Br_{(g)}$	$7.9\cdot10^{-3}$				
23	**Aqueous-phase oxidation**					
24	**Units: $M^{-1}.s^{-1}$**					
25	$Hg^0_{(aq)}+O_{3(aq)}\rightarrow Hg^{2+}_{(aq)}$	$4.7\cdot10^{7}$	$4.7\cdot10^{7}$			$4.7\cdot10^{7}$
26	$Hg^0_{(aq)}+^{\bullet}OH_{(aq)}\rightarrow Hg^{2+}_{(aq)}$	$2.0\cdot10^{9}$	$2.4\cdot10^{9}$			
27	$Hg^0_{(aq)}+^{\bullet}OH_{(aq)}\rightarrow Hg^{+}_{(aq)}$					$2.0\cdot10^{9}$
28	$Hg^{+}_{(aq)}+^{\bullet}OH_{(aq)}\rightarrow Hg^{2+}_{(aq)}$					$1.0\cdot10^{10}$
29	$Hg^0_{(aq)}+HOCl_{(aq)}\rightarrow Hg^{2+}_{(aq)}$	$2.09\cdot10^{6}$				$2.09\cdot10^{6}$
30	$Hg^0_{(aq)}+OCl^{-}\rightarrow Hg^{2+}$	$1.99\cdot10^{6}$	$2.0\cdot10^{6}$			$1.99\cdot10^{6}$
31	$Hg^0_{(aq)}+HOBr_{(aq)}\rightarrow Hg^{2+}_{(aq)}+Br^{-}_{(aq)}+OH^{-}_{(aq)}$					0.279
32	$Hg^0_{(aq)}+^{\bullet}BrO_{(aq)}\rightarrow Hg^{2+}_{(aq)}+Br_{(aq)}^{-}+OH_{(aq)}^{-}$					0.273
33	$Hg^0_{(aq)}+Br_{2(aq)}\rightarrow Hg^{2+}_{(aq)}+2Br^{-}_{(aq)}$					0.196
34	**Aqueous-phase reduction**					
35	**Units: s^{-1}**					
36	$HgSO_{3(aq)}\rightarrow Hg^0_{(aq)}$	0.0106				$T\cdot\exp((31.971\cdot$

						T-12595)/T)
37	$Hg(SO_3)^{2-}_{2(aq)} \rightarrow Hg^0_{(aq)}$					
38	$Hg(OH)_{2(aq)} + h\nu \rightarrow Hg^0_{(aq)}$				$8.4 \cdot 10^{-8} \cdot [OH]_{(aq)}$	
39	**Units: $M^{-1}.s^{-1}$**					
40	$Hg^{2+}_{(aq)} + HO_2 \rightarrow Hg^0_{(aq)}$	$1.7 \cdot 10^4$				
41	$Hg^{2+}_{(aq)} + DCA + h\nu \rightarrow Hg^0_{(aq)}$					
42	**Gas/liquid equilibria**					
43	**Units: $M.atm^{-1}$**					
44	$Hg^0_{(g)} \leftrightarrow Hg^0_{(aq)}$	0.11				0.13
45	$HgO_{(g)} \leftrightarrow HgO_{(aq)}$					$2.69 \cdot 10^{12}$
46	$HgCl_{2(g)} \leftrightarrow HgCl_{2(aq)}$	$1.4 \cdot 10^6$				$2.75 \cdot 10^6$
47	$Hg(OH)_{2(g)} \leftrightarrow Hg(OH)_{2(aq)}$	$1.2 \cdot 10^4$				
48	$HOBr_{(g)} \leftrightarrow HOBr_{(aq)}$					
49	$HgBr_{(g)} \leftrightarrow HgBr_{(aq)}$					
50	$HgBr_{2(g)} \leftrightarrow HgBr_{2(aq)}$					$2.75 \cdot 10^6$
51	$HgBrOH_{(g)} \leftrightarrow HgBrOH_{(aq)}$					
52	**Aqueous phase equilibria**					
53	$Hg^{2+}_{(aq)} + SO^{2-}_{3(aq)} \leftrightarrow HgSO_{3(aq)}$	$2.1 \cdot 10^{13}$ M^{-1}				$2.1 \cdot 10^{13}$ M^{-1}
54	$HgSO_{3(aq)} + 2SO^{2-}_{3(aq)} \leftrightarrow Hg(SO_3)^{2-}_{2(aq)}$	$1.0 \cdot 10^{10}$ M^{-1}				$1.0 \cdot 10^{10}$ M^{-1}
55	$HgCl_{2(aq)} \leftrightarrow Hg^{2+}_{(aq)} + 2Cl^-_{(aq)}$	$10^{-14} M^2$				
56	$Hg_n Cl_{m(dis)} \leftrightarrow Hg^{2+}_{(aq)}$					
57	$HgOH^+_{(aq)} \leftrightarrow Hg^{2+}_{(aq)} + OH^-_{(aq)}$	$2.51 \cdot 10^{-11} M$				$2.51 \cdot 10^{-11} M$
58	$Hg(OH)_{2(aq)} \leftrightarrow Hg^{2+}_{(aq)} + 2OH^-_{(aq)}$	$10^{-22} M^2$				
59	$Hg(OH)_{2(aq)} \leftrightarrow HgOH^+_{(aq)} + OH^-_{(aq)}$					$6.25 \cdot 10^{-12} M$
60	$HgOHCl_{(aq)} \leftrightarrow HgOH^+_{(aq)} + Cl^-_{(aq)}$	$3.72 \cdot 10^{-8} M$				$3.72 \cdot 10^{-8} M$
61	$Hg^{2+}_{(aq)} + Br^-_{(aq)} \leftrightarrow HgBr^+_{(aq)}$					$1.1 \cdot 10^9$ M^{-1}
62	$HgBr^+_{(aq)} + Br^-_{(aq)} \leftrightarrow HgBr_{2(aq)}$					$2.5 \cdot 10^8 M^{-1}$
63	$HgBr_{2(aq)} + Br^-_{(aq)} \leftrightarrow HgBr^-_{3(aq)}$					
64	$HgBr^-_{3(aq)} + Br^-_{(aq)} \leftrightarrow HgBr^{2-}_{4(aq)}$					
65	$HOBr_{(aq)} \leftrightarrow H^+_{(aq)} + BrO^+_{(aq)}$					
66	$H^+_{(aq)} + Br^-_{(aq)} + Hg(OH)_{2(aq)} \leftrightarrow HgBrOH_{(aq)}$					
67	$HgOH^+_{(aq)} + OH^-_{(aq)} \leftrightarrow Hg(OH)_{2(aq)}$					
68	$Hg^{2+}_{(aq)} + Cl^-_{(aq)} \leftrightarrow HgCl^+_{(aq)}$					$5.8 \cdot 10^6 M^{-1}$
69	$HgCl^+_{(aq)} + Cl^-_{(aq)} \leftrightarrow HgCl_{2(aq)}$					$2.5 \cdot 10^6 M^{-1}$

70	**Gas/soot equilibria**					
71	**Units: $m_{water}^3.m_{air}^{-3}$**					
72	$soot_{(g)} \rightarrow soot_{(aq)}$	$5 \cdot 10^5$				
73	**Liquid /soot equilibria**					
74	$HgSO_{3\,(aq)} \leftrightarrow HgSO_{3\,(p)}$					
75	$HgSO_{2\,(aq)}^{2-} \leftrightarrow HgSO_{2\,(p)}^{2-}$					
76	$Hg(HO)_{2\,(aq)} \leftrightarrow Hg(HO)_{2\,(p)}$					
77	$HgCl_{2\,(aq)} \leftrightarrow HgCl_{2\,(p)}$					
78	$HgCl_{m\,(aq)} \leftrightarrow HgCl_{m\,(p)}$					
79	$HgOHCl_{(aq)} \leftrightarrow HgOHCl_{(p)}$					
80	$HgOH_{(aq)}^{+} \leftrightarrow HgOH_{(p)}^{+}$					
81	$Hg_{(aq)}^{II} \leftrightarrow Hg_{(p)}^{II}$					

4 Polyphemus air quality system

The chemical transport models are typically based on one or two frameworks: (i) Eulerian e.g. EMEP, DEHM, CMAQ, Lotos-Euros or (ii) Lagrangian e.g. HYSPLIT [197]. In the Eulerian approach, the frame of reference is fixed with the respect to the Earth, whereas in the Lagrangian approach, the frame of reference is moving with the air parcel along the mean wind trajectory. Additionally, models based on the Gaussian equation are widely used for near-field calculations. At present, many air quality modelling systems often combine both type of models. Near-source emission dispersion is tackled with a Gaussian plume or puff models and subsequently at larger distances from the source an Eulerian type models is used.

Polyphemus is a comprehensive modelling system for air quality, which is developed and maintained by CEREA. It handles several dispersion models, which are based on Eulerian or Gaussian approaches, and can be applied from local to continental scale.

Its main component is an Eulerian chemical-transport-model: Polair3D, used for both gaseous and aerosol species [13]. Polair3D tracks multiphase chemistry: (i) gas, (ii) water and (iii) aerosols. Polair3D has several chemical mechanisms for traditional gaseous pollutants (SO_2, NO_x, O_3), aerosols, radioactive elements and inert compounds. One gas-phase chemical scheme is RACM and aerosol chemistry is treated differently depending on the cloud liquid water content. Inside clouds, aqueous-phase chemical reactions may be modelled using the Variable Size-Resolution Model (VSRM). Otherwise, a size-resolved aerosol model (SIREAM) treats the effects of condensation/evaporation (including the inorganic aerosol thermodynamics, modelled with ISORROPIA), coagulation and nucleation upon the particle size distribution [198].

Polair3D has a numerical solver for the chemical transport equation:

$$\frac{\partial c_i}{\partial t} = \underbrace{-div(Vc_i)}_{advection} + \underbrace{div\left(\rho K \nabla \frac{c_i}{\rho}\right)}_{diffusion} + \underbrace{\varphi_i(c_i)}_{chemistry} + S_i - L_i \qquad \text{R.4.1}$$

The concentration of the *i*-th species is c_i. The transport driven by the mean wind V is the advection term. The diffusion term essentially accounts for turbulent mixing in the vertical. Chemical production (φ_i), emissions (S_i) and losses through wet and dry deposition (L_i) of the *i*-th species are also included.

Polair3D was used in Poland to model the atmospheric dispersion of pollutants over (i) Europe, (ii) Poland, (iii) Lesser Poland, (iv) Kraków, (v) Toruń and (vi) Wrocław [199], [200], [201], [202].

The operational evaluation of Polair3D results for runs performed over Europe for 2004 showed that the correlation coefficients between simulated and observed data from background stations of EMEP [163] are 50% for $NO_{2(g)}$, 47 % for $SO_{2(g)}$, 36% for PM10 and 55% for $O_{3(g)}$ [203]. The correlation coefficients between simulated and observed data of AirBase are 41% for $NO_{2(g)}$, 44 % for $SO_{2(g)}$, 23% for PM10 and 53% for $O_{3(g)}$ [94]. The comparison of modelled results against average measurements at EMEP stations showed a slight overestimation in the case of $NO_{2(g)}$ (7.7 $\mu g.m^{-3}$ simulated against 6.5 $\mu g.m^{-3}$ in the measurements) and PM10 (20.9 $\mu g.m^{-3}$ simulated against 18.8 $\mu g.m^{-3}$ in the measurements), slight underestimation for $O_{3(g)}$ (63.1 $\mu g.m^{-3}$ simulated and 65.7 $\mu g.m^{-3}$ in the measurements) and a significant overestimation for $SO_{2(g)}$ (5.3 $\mu g.m^{-3}$ simulated and 1.7 $\mu g.m^{-3}$ in the measurements). Evaluation against data of AirBase indicated a slight overestimation of $SO_{2(g)}$ (7.7 $\mu g.m^{-3}$ simulated and 6.5 $\mu g.m^{-3}$ in the observations) and $O_{3(g)}$ (59.1 $\mu g.m^{-3}$ simulated and 51.8 $\mu g.m^{-3}$ in the observation). In the contrary, results were significantly underestimated for $NO_{2(g)}$ (13.6 $\mu g.m^{-3}$ simulated and 23.4 $\mu g.m^{-3}$ in the measurements) and PM10 (19.7 $\mu g.m^{-3}$ simulated against 26.1 $\mu g.m^{-3}$ in the measurements). The slight overestimation in case of $SO_{2(g)}$ (26.7 $\mu g.m^{-3}$ simulated against 24.7 $\mu g.m^{-3}$ in the measurements) was also observed in operational evaluation preformed for modelled results for 2005 for Poland against observation from stations located in the Krakow area [200]. Furthermore, a slight overestimation was observed for $NO_{2(g)}$ (37.8 μgm^{-3} simulated against 34.3 $\mu g.m^{-3}$ in the measurements) and a underestimation for PM10 (33.6 $\mu g.m^{-3}$ simulated against 74.3 $\mu g.m^{-3}$ in the measurements). The underestimation in Krakow can be explained by a significant uncertainty about PM low emissions from fuel combustion for heating in the domestic sector. The correlation

coefficients between simulated and observed data for all stations are 47% for $NO_{2(g)}$, 46 % for $SO_{2(g)}$, 30% for PM10.

The newest results of operational evaluation for 2000 -2008 years of quality simulation conducted over Europe with the use of Polair3D showed that the average correlation coefficients are 57% for PM10, 59% for PM2.5 and 63% for $O_{3(g)}$ [204].

Polyphemus also includes a library of physical parameterizations called AtmoData and a set of programs using AtmoData designed to generate data required by Polair3D, e.g. deposition velocities, vertical diffusion coefficients, emissions, etc. [13].

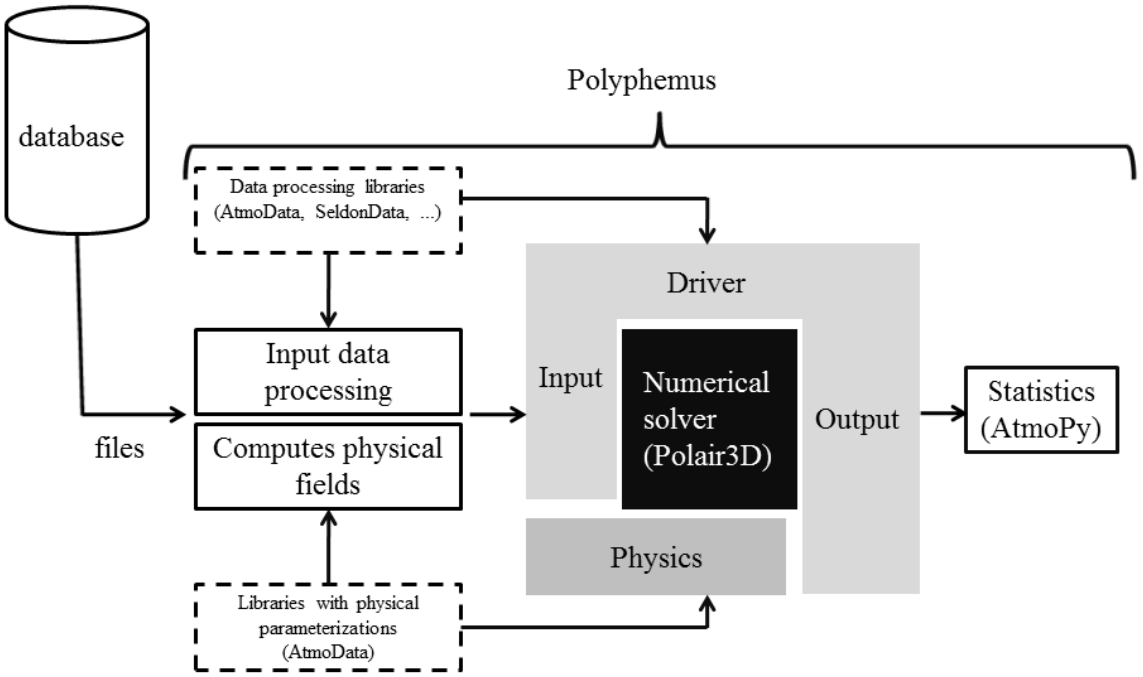

Figure 4-1. Polyphemus air quality system overall work flow. Based on [13].

4.1 Below-cloud scavenging model implemented in the Polyphemus system

The general equation for scavenging is:

$$\frac{\partial c}{\partial t} = -\lambda \cdot c \qquad \text{R.4.2}$$

where

λ –the scavenging coefficient [s^{-1}];

c –the concentration of pollutant [$kg.m^{-3}$].

Wet deposition is split between in-cloud (rainout) and below-cloud (washout) scavenging. The below-cloud scavenging was calculated based on common algorithms implemented in Polyphemus for gaseous as well as aerosol species. The in-cloud scavenging is calculated inside algorithms specific for mercury chemistry and algorithms for lead and cadmium.

Below-cloud scavenging is calculated for gaseous mercury compounds ($Hg^0_{(g)}$, $HgO_{(g)}$, $HgCl_{2(g)}$, $Hg(OH)_{2(g)}$, $HgBr_{(g)}$, $HgBr_{2(g)}$, $HgBrOH_{(g)}$).
The below cloud scavenging coefficient [s^{-1}] is given by the following relationship [205]:

$$\lambda = \frac{10^{-6} \cdot I}{3.6 \cdot U \cdot \tau_{trans}} \cdot exp\left(-\frac{z}{U \cdot \tau_{trans} \cdot H \cdot R \cdot T}\right) \qquad \text{R.4.3}$$

where:

I –intensity of rain [$m.s^{-1}$],

U –raindrop terminal fall velocity [$m.s^{-1}$],

τ_{trans} –the timescale of the mass transfer from the bulk air to the drops [s],

z –the fall distance [m],

H –Henry's law constant [$mol.\ m^{-3}.atm^{-1}$],

R –ideal gas law constant [$atm.\ m^3.mol^{-1}.K^{-1}$],

T –temperature [K].

The raindrop fall velocity U [$m.s1^{-1}$] in the model is calculated as a function of the raindrop diameter [206]:

$$U = 4854 \cdot D \cdot \exp(-195 \cdot \mathrm{D}) \qquad \text{R.4.4}$$

D –the raindrop diameter [m].
Additionally, some other functions of the raindrop diameter presented in Table 4-1 were applied to the model, but then the changes of this parameter are shown in the text.
The drop diameter can be calculated with the use of many various equations presented in Table 5-6. The model was calculated with the use of the following formula $9.7 \cdot 10^{-4} \cdot I^{0.158}$ s^{-1}. However other formulas for drop diameter were also applied to the model to investigate the sensitivity of the model to this parameter.
The timescale of the mass transfer from the bulk air to the drops is calculated as follows:

$$\tau_{trans} = \frac{D}{6\ K_T} \qquad \text{R.4.5}$$

K_T –is the mass transfer coefficient [m.s^{-1}], which is calculated as follows:

$$K_T = \frac{D_g}{D} \cdot Sh \quad \text{R.4.6}$$

where:

D_g –the gas-phase diffusivity [m^2.s^{-1}]. A gas phase diffusivity of $0.1194 \cdot 10^{-4}$ m^2.s^{-1} for GEM, and $0.1628 \cdot 10^{-4}$ m^2.s^{-1} for RGM compounds was assumed [207].

Sh –Sherwood Number which represents the ratio of convective to diffusive mass transport.

The Sherwood Number is expressed as follows:

$$Sh = 2 + 0.6 \cdot Re^{1/2} \cdot Sc^{1/3} \quad \text{R.4.7}$$

where the Reynolds number Re is defined as follows:

$$Re = U \cdot D / v_a \quad \text{R.4.8}$$

and the Schmidt number Sc is calculated as follows:

$$Sc = v_a / D_g \quad \text{R.4.9}$$

In these calculations v_a is the kinematic viscosity for air [m^2.s^{-1}] and it is calculated as the ratio of the dynamic viscosity μ [kg.s^{-1}.m^{-1}] and density of the air ρ [kg.m^{-3}].

$$v_a = \frac{\mu}{\rho} \quad \text{R.4.10}$$

The dynamic viscosity for air μ is calculated with the use of Sutherland's formula:

$$\mu = \mu_0 \cdot \frac{T_0 + C}{T + C} \cdot \left(\frac{T}{T_0}\right)^{2/3} \quad \text{R.4.11}$$

Reference viscosity μ_0, reference temperature T_0 and Sutherland's constant C – are constants with defined values for air of: $18.27 \cdot 10^6$ kg.s^{-1}.m^{-1}, 291.15 K and 120 K, respectively.

Table 4-1. Raindrop velocity [m.s^{-1}] [208].

N.	Raindrop velocity [m.s^{-1}]
1	$142 \cdot D^{0.5}$
2	$9.43 \cdot (1-\exp((-1000 \cdot D/1.77)^{1.47}))$
3	$386.577 \cdot D^{0.67}$
4	$4854.1 \cdot D \cdot \exp(-195 \cdot D)$
5	$3.075 \cdot 10^7 \cdot D^2$ for $D<10^{-4}$ $3.8 \cdot 10^3 \cdot D$ for $10^{-4} <D<10^{-3}$ $133.046 \cdot D^{0.5}$ for $D>10^{-3}$
6	$-0.193+4.96 \cdot 10^3 \cdot D-9.04 \cdot 10^5 \cdot D^2+5.66 \cdot 10^7 \cdot D^3$

The below-cloud scavenging coefficient [s^{-1}] for particulate matter is given as a function of rain intensity [$m.s^{-1}$] [209]:

$$\lambda = \frac{3}{2} \cdot \frac{E \cdot I}{D} \quad \text{R.4.12}$$

D –raindrop diameter [m] is calculated in the same way as for gases (see above).

Collision efficiency E is calculated with the use of expression R.4.13 [210]:

$$E = \frac{4}{Re \cdot Sc} \cdot \left(1 + 0.4 \cdot Re^{\frac{1}{2}} \cdot Sc^{\frac{1}{3}} + 0.16 \cdot Re^{\frac{1}{2}} \cdot Sc^{\frac{1}{2}}\right) + 4 \cdot \emptyset \cdot \left(\omega^{-1} + \left(1 + 2 \cdot Re^{\frac{1}{2}}\right) \cdot \emptyset\right) + \left(\frac{St - S^*}{St - S^* + \frac{2}{3}}\right)^{\frac{3}{2}} \cdot \left(\frac{\rho_p}{\rho_w}\right)^{\frac{1}{2}} \quad \text{R.4.13}$$

ρ_p and ρ_w are the particle and water density [$kg.m^{-3}$], with fixed values in the model of 1400 $kg.m^{-3}$ and 1000 $kg.m^{-3}$, respectively.

The Reynolds number Re is defined as follows:

$$Re = U \cdot D / v_a / 2 \quad \text{R.4.14}$$

The calculation for raindrop velocity U [m/s] and kinematic viscosity for air v_a [$m^2.s^{-1}$] are identical compared to calculation for gases above.

$\emptyset$ –ratio of diameters calculated:

$$\emptyset = d_p / D \quad \text{R.4.15}$$

where d_p is the particle diameter [m];

ω –the ratio of viscosities is defined as follows:

$$\omega = \frac{\mu_{water}}{\mu} \quad \text{R.4.16}$$

μ –the dynamic viscosity of air [$kg.s^{-1}.m^{-1}$].

μ_{water} –viscosity [$kg.s^{-1}.m^{-1}$] of water, assumed that is 1000 [$kg.s^{-1}.m^{-1}$].

The Critical Schmidt number S^* is calculated as a function of the Reynolds number:

$$S^* = \frac{1.2 + 1/12 \cdot \ln(1 + Re)}{1 + \ln(1 + Re)} \quad \text{R.4.17}$$

The Schmidt number Sc is defined as follows:

$$Sc = v_a / D_B \quad \text{R.4.18}$$

The aerosol Brownian diffusivity coefficient D_B [$m^2.s^{-1}$] is calculated as follows:

$$D_B = \frac{k \cdot T \cdot C_c}{3 \cdot \pi \cdot \mu \cdot d_p} \quad \text{R.4.19}$$

where:

k –Boltzmann constant [J.K^{-1}];

C_c –is the Cunningham correction factor for particles defined as follows:

$$C_c = 1 + \frac{2 \cdot \lambda_{air}}{d_p} \cdot \left(1.257 + 0.4 \cdot \exp\left(-0.55 \cdot \frac{d_p}{\lambda_{air}}\right)\right) \quad \text{R.4.20}$$

λ_{air} –is the mean free path of air molecules [m] calculated:

$$\lambda_{air} = \frac{2 \cdot \mu}{P \cdot \sqrt{8/\pi \cdot R \cdot T}} \quad \text{R.4.21}$$

where:

R –gas constant [J.K^{-1}.kg^{-1}];

T –temperature [K];

P –pressure [Pa].

The Stokes number *St* for particle is defined as follows:

$$St = \frac{2 \cdot u_{grav}}{g} \cdot \frac{U - u_{grav}}{D} \quad \text{R.4.22}$$

g –the gravity constant [m.s^{-2}].

u_{grav} –gravitational settling velocity [m.s^{-1}]. For small particles (diameter lower than 20μm) it is calculated with the use of Stokes formula [211]:

$$u_{grav} = \frac{d_p^2 (\rho_p - \rho) \cdot g \cdot C_c}{18 \cdot \mu} \quad \text{R.4.23}$$

ρ –the density of air [kg.m^{-3}].

4.2 Dry deposition models implemented in the Polyphemus system

4.2.1 Dry deposition for gaseous species

The dry deposition flux can be described as follows:

$$dry = V_d \cdot c \quad \text{R.4.24}$$

where:

c –the concentration of pollutant [kg.m^{-3}].

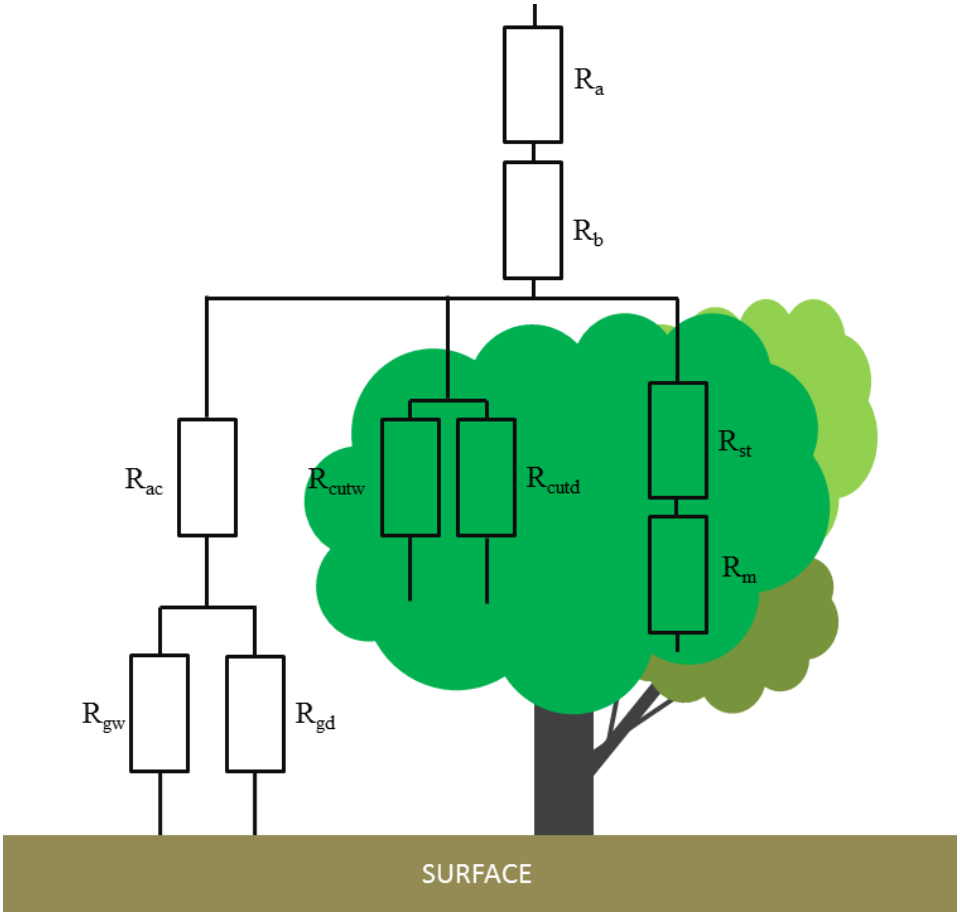

Figure 4-2. Schematic representation of a resistance model. The description of the resistances is provided in the text.

The dry deposition velocity V_d [m.s^{-1}] can be expressed with the use of a resistance model presented in Figure 4-2 as:

$$V_d = \frac{1}{R_a + R_b + R_c} \qquad \text{R.4.25}$$

R_a, R_b, R_c are called the aerodynamic resistance, the quasi-laminar sublayer resistance and the overall canopy resistance [all in s.m^{-1}], respectively.

The aerodynamic resistance depends only on meteorological conditions and surface roughness. The aerodynamic resistance is calculated based on the parametric model of vertical eddy fluxes in the atmosphere for the part of the mass transfer dominated by turbulence [212], [213].

$$R_a = (A_t A_u f_h W)^{-1} \qquad \text{R.4.26}$$

$$A_u = \frac{\kappa}{ln\left(\frac{z_0 + Z_r}{Z_r}\right)} \qquad \text{R.4.27}$$

$$A_t = \frac{\kappa}{ln\left(\frac{z_0+Z_t}{Z_t}\right)}$$ R.4.28

where:

Z_r –the roughness height [m] -calculated for various types of surface, with the use of fixed values for surface categories i.e. for water 0.0001 [m], for urban 0.8 [m];

Z_t –the roughness length [m] assumed to be Z_r/10;

κ –Von Karman constant, equals 0.4;

z_0 –reference height equals (half of height of lower vertical (surface) level of simulation) [m];

W –the horizontal wind module at the reference height [m.s^{-1}].

The stability function for the stable boundary layer f_h is defined as follows:

$$f_h \begin{cases} 1 - 3 \cdot b \cdot \frac{R_i}{1+3 \cdot c \cdot \sqrt{-Ri}} & \text{for } R_i < 0 \\ \left(1 + 3 \cdot b \cdot R_i \cdot \sqrt{(1 + d \cdot Ri)}\right)^{-1} & \text{for } R_i > 0 \end{cases}$$ R.4.29

and $c = b \cdot c_1 \cdot A_u \cdot A_t \sqrt{1 - \frac{Z_t}{z_0+Z_t}} \cdot \left(\left(\frac{z_0+Z_t}{Z_t}\right)^{1/3} - 1\right)^{3/2}$ R.4.30

b,c_1, d are the constants equal 5,

Ri is the Richardson number.

$$Ri = \frac{2 \cdot z_0 \cdot g}{W^2} \cdot \frac{\theta(z_0) - \theta_s}{\theta(z_0) + \theta_s}$$ R.4.31

where:

g –the standard acceleration due to gravity [m.s^{-2}];

θ_s –potential temperature of air close surface (approx. 0 m above surface) [K];

$\theta(z_0)$ –potential temperature of air at reference latitude [K].

The quasi-laminar sublayer resistance is computed for each species using the friction velocity [214], [215].

$$R_b = \frac{1}{\kappa \cdot u_*}\left(\frac{Sc}{Pr}\right)^{2/3}$$ R.4.32

κ –the von Karman constant,

Pr –turbulent Prandtl number, assumed 0.74 for gases in natural conditions.

The Schmidt number equals:

$$Sc = v_a / D_g$$ R.4.33

The gas phase diffusivity D_g [$m^2.s^{-1}$] and the kinematic viscosity for air v_a [$m^2.s^{-1}$], are calculated in the same way as for cloud-scavenging for gases.

The friction velocity u_* [$m.s^{-1}$] is calculated based on the following formula:

$$u_* = A_u \cdot W \cdot \sqrt{f_m} \qquad \text{R.4.34}$$

The stability function for the stable boundary layer f_m is defined as follows:

$$f_m \begin{cases} 1 - \frac{2 \cdot b \cdot Ri}{1+3 \cdot c \cdot \sqrt{-Ri}} & \text{for } R_i < 0 \\ \left(1 + 2 \cdot b \cdot Ri \cdot (1 + d \cdot Ri)^{-\frac{1}{2}}\right)^{-1} & \text{for } R_i > 0 \end{cases} \qquad \text{R.4.35}$$

The canopy resistance for gaseous species with the parameterisation for mercury is applied [216], [217], [176].

The canopy resistance is computed following the equation:

$$\frac{1}{R_c} = \frac{1-W_{st}}{R_{st}+R_m} + \frac{1-W_c}{R_{cutd}} + \frac{W_c}{R_{cutw}} + \frac{1-W_g}{R_{gd}+R_{ac}} + \frac{W_g}{R_{gw}+R_{ac}} \qquad \text{R.4.36}$$

R_{st} is the canopy stomatal resistance, which is calculated as follows:

$$R_{st} = 1/\left[G_{st} \cdot f_T \cdot f_D \cdot f_\psi \cdot D_g/D_w\right] \qquad \text{R.4.37}$$

where:

G_{st} –the unstressed canopy stomatal conductance, calculated as follows:

$$G_{st} = \frac{F_{sun}}{r_{st}(PAR_{sun})} + \frac{F_{shade}}{r_{st}(PAR_{shade})} \qquad \text{R.4.38}$$

$$r_{st}(PAR) = r_{stmin} \cdot \left(1 + \frac{b_{rs}}{PAR}\right) \qquad \text{R.4.39}$$

$$F_{sun} = 2 \cdot cos\theta \cdot \left(1 - exp\left(-0.5 \cdot \frac{LAI}{cos\theta}\right)\right) \qquad \text{R.4.40}$$

$$F_{shade} = LAI - F_{sun} \qquad \text{R.4.41}$$

for LAI < 2.5 $m^2.m^{-2}$ and RS < 200 $W.m^{-2}$:

$$PAR_{shade} = SR_{diff} \cdot \exp(0.5 \cdot LAI^{0.7}) + 0.07 \cdot SR_{dir} \cdot (1.1 - 0.1 \cdot LAI) \cdot \exp(-cos\theta) \qquad \text{R.4.42}$$

$$PAR_{sun} = SR_{dir} \cdot \frac{cos\alpha}{cos\theta} + PAR_{shade} \qquad \text{R.4.43}$$

for other conditions PAR_{shade} and PAR_{sun} are defined as follows:

$$PAR_{shade} = SR_{diff} \cdot \exp(0.5 \cdot LAI^{0.8})$$

$$+0.07 \cdot SR_{dir} \cdot (1.1 - 0.1 \cdot LAI) \cdot \exp(-cos\theta) \quad \text{R.4.44}$$

$$PAR_{sun} = SR_{dir}^{0.8} \cdot \frac{cos\alpha}{cos\theta} + PAR_{shade} \quad \text{R.4.45}$$

LAI –leaf area index [$m^2.m^{-2}$]. It is a characteristic of various types of surfaces, seasons and weather conditions.

θ –the solar zenith angle.

α –the angle between the leaf and the sun, it is assumed to be 60^0,

PAR –photosynthetically active radiation [$W.m^{-2}$],

PAR_{sun} –photosynthetically active radiation received by sunlit leaves [$W.m^{-2}$],

PAR_{shade} –photosynthetically active radiation received by shaded leaves [$W.m^{-2}$],

F_{sun} –area of sunlit leaf area index [$m^2.m^{-2}$],

F_{shade} –area of shaded leaf area index [$m^2.m^{-2}$],

SR – solar radiation [$W.m^{-2}$],

SR_{diff} –downward visible radiation fluxes above the canopy from diffused radiation [$W.m^{-2}$],

SR_{dir} –direct-beam radiation [$W.m^{-2}$],

b_{rs} –empirical light response coefficient [$W.m^{-2}$],

r_{stmin} –the minimum leaf stomatal resistance [$s.m^{-1}$],

f_T –represents the conductance-reducing effects of air temperature on leaf stomatal conductance.

$$f_T = \frac{T - T_{min}}{T_{opt} - T_{min}} \cdot \left[\frac{T_{max} - T}{T_{max} - T_{opt}}\right]^{\frac{T_{max} - T_{opt}}{T_{opt} - T_{min}}} \quad \text{R.4.46}$$

T –air temperature [^{0}C].

T_{opt} –air temperature of maximum stomatal opening [^{0}C],

T_{max} –maximum of temperature for stomatal opening [^{0}C],

T_{min} –minimum of temperature for stomatal opening [^{0}C],

f_D –represents the conductance-reducing effects of water vapour pressure deficit on leaf stomatal conductance.

$$f_D = 1 - b_{bvpd} \cdot (e^* - e) \quad \text{R.4.47}$$

e^* –the saturation water vapour pressure [kPa] at air temperature [K],

e –the ambient water vapour pressure [kPa],

b_{bvpd} –constants of water-vapour-pressure-deficit [kPa^{-1}],

f_ψ –represents the conductance-reducing effects of water stress (leaf water potential) on leaf stomatal conductance.

$$f_\psi = \frac{-0.72-0.0013SR-\psi_{c2}}{\psi_{c1}-\psi_{c2}} \quad \text{R.4.48}$$

ψ_{c1}, ψ_{c2} –parameters that specify leaf-water-potential dependency [MPa];

D_w –the diffusivity of water vapor [$m^2.s^{-1}$],

D_g –the gas-phase diffusivity of pollutants [$m^2.s^{-1}$],

R_{ac} –in-canopy aerodynamic resistance [$s.m^{-1}$]. The value of in-canopy aerodynamic resistance is calculated as follows:

$$R_{ac} = \frac{R_{ac0}\cdot LAI^{1/4}}{u_*^2} \quad \text{R.4.49}$$

R_{ac0} is the reference value [$s.m^{-1}$] for in-canopy aerodynamic resistance and its value depends on land-use coverage. For example, for surface with no canopy (e.g. water, desert) it is set to 0.

u_* –friction velocity [$m.s^{-1}$] -corresponding data for different land-use coverage and weather conditions.

Data of $T_{opt}, T_{max}, T_{min}, \psi_{c1}, \psi_{c2} b_{bvpd}, z_0, b_{rs}, r_{stmin}$ for various land use coverage [217].

Values for leaf area index LAI are presented in the literature [216].

W_{st} –represents the fraction stomatal blocking when leaves are wet. It is calculated:

$$W_{st} = \begin{cases} 0 & SR \le 200 \\ (SR-200)/800 & 200 < SR \le 600 \\ 0.5 & SR > 200 \end{cases} \quad \text{R.4.50}$$

W_c –represents the fraction of wet canopy,

W_g –represents the fraction of the wet ground surface.

The corresponding values of W_g, W_c for different humidity conditions are presented in Table 4-2.

Table 4-2 The value of constants for canopy stomatal model.

N.	constants	Conditions		
		rainy	dewy	humid
1	W_g	0.9	0.5	0.2
2	W_c	0.9	0.7	0.2

R_m is the mesophyll resistance [$s.m^{-1}$] and values of 500 and 0 were used for elemental and for reactive mercury, respectively. The mesophyll resistance is characteristic of the chemical species. Usually, the value of the mesophyll resistance is set on the basis of observation or through comparison with other species, that have similar chemical properties.

The R_{cutw}, R_{cutd}, R_{gw}, R_{gd} are resistances of: the wet cuticle, dry cuticle, wet-ground and dry-ground, respectively. They are derived from well-known data for sulfur dioxide and

ozone [216]. The sulphur dioxide and ozone dry deposition pathway is very highly documented and has been investigated in many measurement campaigns of dry deposition made for these species. The model uses results for sulphur dioxide and ozone and sets surface resistance for other species following their aqueous solubility and their chemical reactivity. The average dry deposition velocity over Europe for sulphur dioxide and ozone generated with the use of Polyphemus system are presented in Figure 4-3 and Figure 4-4.

$$\frac{1}{R_{cutw}(i)} = \frac{\alpha(i)}{R_{cutw}(SO_2)} + \frac{\beta(i)}{R_{cutw}(O_3)} \quad \text{R.4.51}$$

$$\frac{1}{R_{cutd}(i)} = \frac{\alpha(i)}{R_{cutd}(SO_2)} + \frac{\beta(i)}{R_{cutd}(O_3)} \quad \text{R.4.52}$$

$$\frac{1}{R_{gw}(i)} = \frac{\alpha(i)}{R_{gw}(SO_2)} + \frac{\beta(i)}{R_{gw}(O_3)} \quad \text{R.4.53}$$

$$\frac{1}{R_{gd}(i)} = \frac{\alpha(i)}{R_{gd}(SO_2)} + \frac{\beta(i)}{R_{gd}(O_3)} \quad \text{R.4.54}$$

Scaling parameters α = 10 and β = 10 and α = 0 and β = 0.2 were set for reactive mercury and elemental mercury, respectively. The scaling parameters were chosen with the assumption that reactive mercury is deposited in the same way as $HNO_{3(g)}$ and elemental mercury is poorly soluble.

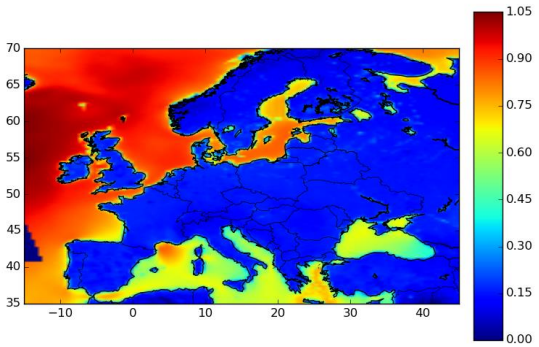

Figure 4-3. Annual average dry deposition velocity in 2008 for $SO_{2(g)}$ [cm.s^{-1}].

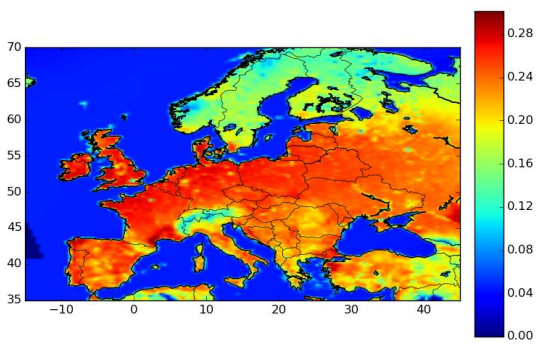

Figure 4-4. Annual average dry deposition velocity in 2008 for $O_{3(g)}$ [cm.s^{-1}].

4.2.2 Dry deposition velocity for aerosols

The dry deposition velocity V_d [m.s^{-1}] is calculated for aerosols of mercury, lead and cadmium with the following formula [218]:

$$V_d = u_{grav} + \frac{1}{(R_a + R_s)}$$ R.4.55

where:

u_{grav} –gravitational settling velocity [m.s^{-1}],

R_a –the aerodynamic resistance [s.m^{-1}] is computed as for gaseous species,

R_s –the surface resistance [s.m^{-1}].

The surface resistance [s.m^{-1}] characterizes the collection efficiency of the surface and is calculated as follows:

$$R_s = \frac{1}{\varepsilon_0 \cdot u_* \cdot (E_B + E_{IM} + E_{IN}) \cdot R_1}$$ R.4.56

where:

ε_0 –empirical constant equals 3,

u_* –friction velocity [m.s^{-1}] calculated in the same way as for gases,

E_B –the collection efficiency from Brownian diffusion is a function of the Schmidt number Sc:

$$E_B = (Sc)^{-\gamma}$$ R.4.57

γ –values depending on land use categories (usually between 1/2 and 2/3);

E_{IM} is the collection efficiency from impaction and is expressed based on a formula proposed by [219]:

$$E_{IM} = \left(\frac{St}{0.8 + St}\right)^2$$ R.4.58

The collection efficiency by interception is calculated, as follows:

$$E_{IN} = \frac{1}{2}\left(\frac{d_p}{A}\right)^2$$ R.4.59

d_p –is the particle diameter [m];

A –characteristic radius [m] of collectors is given for various seasonal and land use categories.

The correction factor R_1 representing the fraction of particles that stick to the surface and is calculated with the use of the following formula [220]:

$$R_1 = exp\left(-St^{1/2}\right)$$ R.4.60

The Stokes number *St* in this case is calculated for the vegetated surface:

$$St = \frac{u_{grav} \cdot u_*}{g \cdot A}$$ R.4.61

and for others surface categories.

$$St = \frac{u_{grav} \cdot u_*^2}{v_a}$$ R.4.62

where v_a is the kinematic viscosity for air [m^2.s^{-1}]

PART II Development and application of a new chemical transport model for mercury, modelling of atmospheric transport of lead and cadmium

5 Distribution of the emissions of heavy metals into the air by the Polish power sector with the use of the bottom-up approach

5.1 Methodology

The localization of the heavy metals sources and the speciation of emitted mercury have a significant impact on the atmospheric transport of heavy metals, particularly from relatively big sources, which are present in the power sector. Unfortunately, the EMEP programme provides the total emissions from all sectors with horizontal resolution of 50 km by 50 km [87]. Therefore, in this part of the manuscript, the vertical and horizontal localization of heavy metals sources of the power sector will need to be specified. The speciation of emitted mercury from all individual stacks will also be estimated. To that end, the ENVIRO database for 2005 has been updated for 2008 in relation to installed boilers and emission controls, as well as coal consumption and coal chemical energy (activity) based on statistics published for that year [221], [222], [223], [58], [53]. The updated database for 2008 includes information about boiler type, coal and chemical energy consumption, PM and SO_2 emission control configuration of 804 main boilers from the Polish power sector. It was assumed that the chemical energy of coal consumed by heating plants included in the database equals the chemical energy provided by the national emission inventors, (there is a possibility that some small heating plants are not included in the database) [53]. National emission inventories reported low (less than 1%) uncertainty of estimation of chemical energy of coal consumed in the power sector [48]. The operated boilers were connected to 170 stacks, which are also included together with a precise location and height in an improved database.

With the use of the chemical energy (activity) of coal consumed and the corresponding emission factor, the mercury, cadmium and lead emission into the air were calculated for all boilers. For mercury, two emission factors for 2008 and for 2009 were used. In 2008, they were 0.0064 and 0.004 $kg.TJ^{-1}$ for all hard and brown coal power plants, respectively [53]. For 2009, the emission factors were changed for power and CHP plants and amounted to 0.0023 $kg.TJ^{-1}$ for hard coal and 0.0114 $kg.TJ^{-1}$ for brown coal [54]. The obtained emissions of mercury from all boilers installed in the polish power sector were split into three mercury forms i.e.: (i) gaseous elemental mercury (GEM), (ii) reactive gaseous mercury (RGM) and (iii) mercury bound to aerosol particles (Hg_P). The share of three forms of emitted mercury for different coal -boiler type -emission control configurations were based on information

provided from measurement campaigns [37]. The corresponding numbers characterising the power, CHP and heating plants and emissions of mercury with the use of emission factor for 2008 and 2009 and speciation factors are presented in Table 5-1.

Table 5-1. Aggregated data on power sector, which operated in 2008.

N.	Boiler type	PM control	SO_2 control	Number of in-stallation	Thermal input [MW]	Activity [TJ]	Emission of Hg [kg]		Hg_p [%]	RGM [%]	GEM [%]
							EF 2008	EF 2009			
1	Hard coal power and CHP plants										
2	GF	CYC		128	3965	27144	174	62	20	40	40
3	GF	ESP		2	199	697	5	2	5	70	25
5	DBB	CYC		1	57	116	1	0	20	40	40
6	DBB	ESP		175	29489	293218	1877	671	5	60	35
7	DBB	FF		10	1101	15154	97	35	5	60	35
8	DBB	ESP	SDFGD	15	4659	80849	517	185	5	45	50
9	DBB	ESP	DFGD	4	307	2157	14	5	5	45	50
10	DBB	ESP	WFGD	47	26226	409326	2620	936	10	35	55
11	DBB	FF	SDFGD	4	1327	19280	123	44	5	35	60
12	FBC	ESP	CFB	14	3680	67663	433	155	5	10	85
13	Total for hard coal power and CHP plants			399	71010	915604	5860	2094			
14	Brown coal power plants										
15	DBB	ESP		7	1982	36541	146	415	5	15	80
16	DBB	ESP	WFGD	23	17192	347164	1389	3939	5	10	85
17	DBB	ESP	DFGD	3	1722	37792	151	429	5	10	85
18	FBC	ESP	CFB	6	3213	100926	404	1145	5	10	85
19	Total for brown coal power plants			39	24109	522423	2090	5928			
20	Hard coal heating plants										
21	GF	CYC		317	8506	53035	339		20	40	40
22	GF	FF		3	66	431	3		5	60	35
23	DBB	ESP		40	4998	56191	360		5	60	35
24	DBB	ESP	WFGD	4	464	4537	29		10	35	55
25	FBC	ESP	CFB	1	185	2382	15		5	10	85
26	Total for hard coal heating plants			365	14219	116576	746				
27	Brown coal heating plants										
28	FBC	ESP	CFB	1	78	284	1		5	10	85

GF - Grate Firing, DBB - Dry Bottom Boiler, FBC - Fluidized Bed Combustion, CYC - Cyclone Remove System, ESP - Electrostatic Precipitator, FF - Fabric Filter, SDFGD - Semi Dry Flue Gas Desulfurization, DFGD - Dry Flue Gas Desulfurization, WFGD - Wet Flue Gas Desulfurization.

The chemical energy of consumed coal by plants included in the database was also used in the distribution of emitted lead and cadmium to individual stack of the power sector. The emission factors for cadmium and lead in 2008, which are used to assess the emissions from 814 boilers installed in polish power plants are presented in Table 5-2.

The annual emissions of lead and cadmium from coal based power, cogeneration and heating plants an equalled to 22148 kg and 2087 kg, in 2008, respectively [53]. The main share falls

on the emission of heating plants. In 2008, from these sources about 12938 $kg.y^{-1}$ of lead and 1909 $kg.y^{-1}$ of cadmium were released into the atmosphere. In the power sector (SNAP 0101 and SNAP 0102), 129 kg of cadmium and 742 kg of lead are emitted annually also from combustion of natural gas, biomass, heating oil and coal gas. These emission were not assigned to point sources and remain in the EMEP gridded inventory.

Table 5-2. Emission factors of lead and cadmium used to estimate emissions from individual boilers installed in the Polish power sector [53].

N.	Fuel type	Type of plants	Emission factors [$g.TJ^{-1}$]		Emission in 2008 [kg]	
			Lead	Cadmium	Lead	Cadmium
1	Hard coal	Power and CHP plants	8.96	0.12	8203.8	109.9
2		Heating plants	102.4	16.37	11937.4	1909.5
3	Brown coal	Power plants	3.84	0.13	2006.1	67.9
4		Heating plants	3.87	0.00	1.1	0.0

5.2 Results

Locations of main emitters of mercury, lead and cadmium are presented in Figure 5-1 -Figure 5-4. The vertical distribution of these heavy metals from the power sector is presented in Figure 5-5.

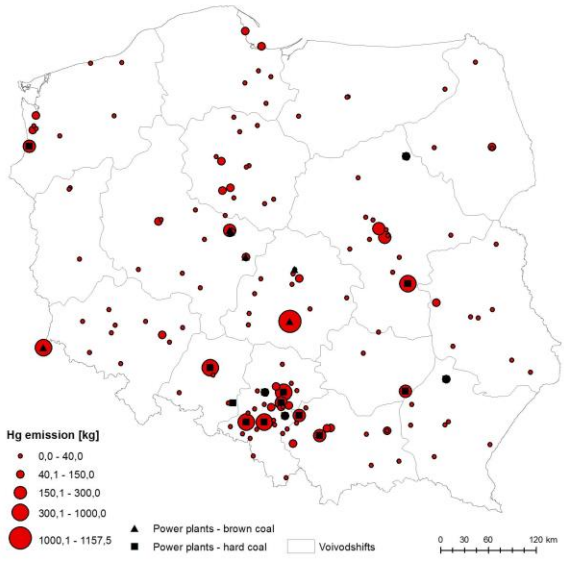

Figure 5-1. Location and emissions [kg] of main emitters of mercury. Emissions based on emission factors for 2008 (EF2008).

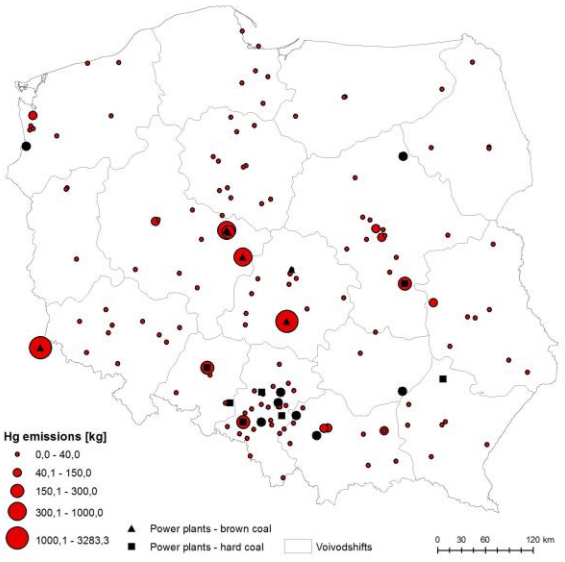

Figure 5-2. Location and emissions [kg] of main emitters of mercury. Emissions based on emission factors for 2009 (EF2009).

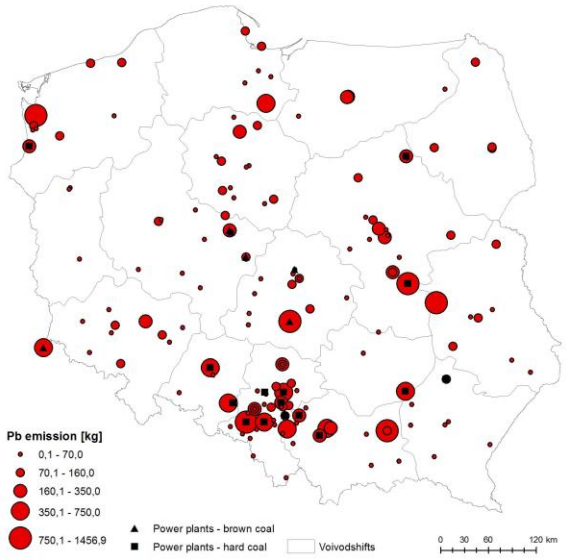

Figure 5-3. Location and emissions [kg] of main emitters of lead.

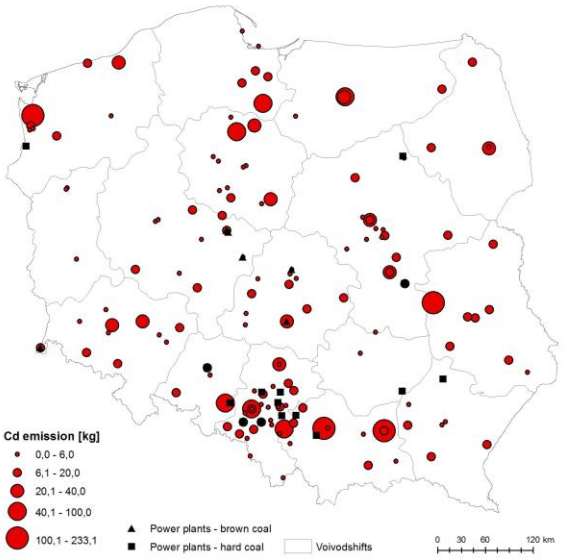

Figure 5-4. Location and emissions [kg] of main emitters of cadmium.

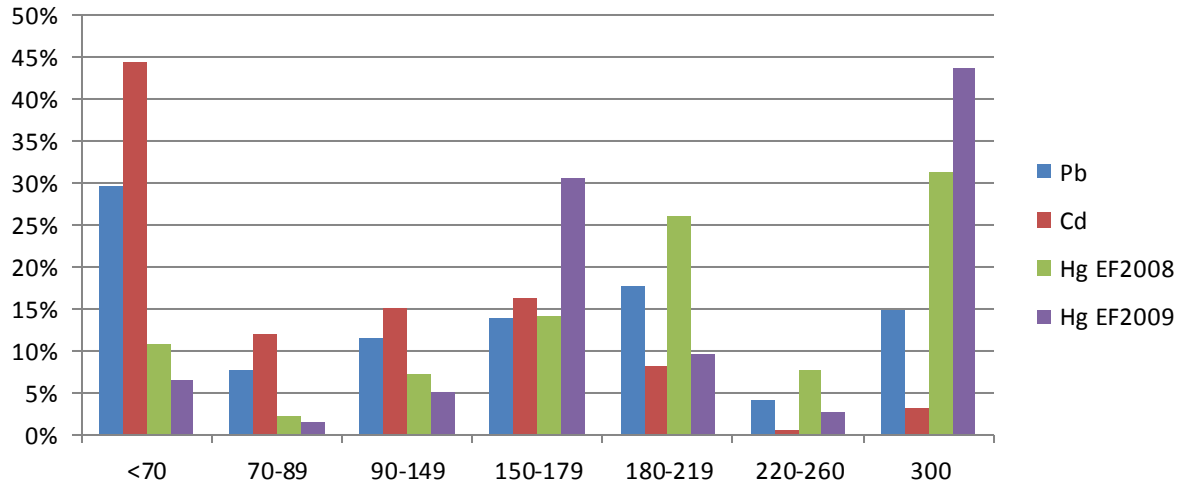

Figure 5-5. Vertical distribution of mercury, lead and cadmium emissions from Polish power sector (expressed as percentage of calculated total emission). EF2008 -emission factors for 2008, EF2009 - emission factors for 2009.

Table 5-3. Emission of various mercury forms from Polish power sector.

N	Fuel type	Type of plants	Type of estimation	Emissions [kg]			Emissions rate [%]		
				Hg_p	RGM	GEM	Hg_p	RGM	GEM
1	Hard coal	Power and CHP plants	EF2008	450	2499	2911	8	43	49
2			EF2009	161	893	1040			
3		Heating plants		90	365	291	12	49	39
4	Total for hard coal		EF2008	540	2864	3202	8	43	49
5			EF2009	251	1258	1331	9	44	47
6	Brown coal	Power plants	EF2008	105	216	1769	5	10	85
7			EF2009	296	614	5018			
8		Heating plants		0	0	1	0	0	100

9	Total for hard and brown coal	EF2008	645	3080	4972	7	35	57
10		EF2009	547	1872	6350	6	21	72

The total emissions of mercury from the power sector where coal is consumed with the use of emission factors for 2008 and 2009 are almost equal (Table 5-3). It amounted to 8697 kg and 8769 kg, respectively. The significant differences appears in the estimation of emissions of 3 forms of mercury (GEM, RGM and Hg_P). The coal type, hard or brown, strongly affects the share of emitted mercury forms. The combustion of brown coal causes high emission of GEM compared to other forms. Whilst power plants based on hard coal emit nearly the same amount of GEM and RGM. The emission of Hg_P in both cases is relatively low, because of the widespread use of PM emission control systems (Table 5-1). The final speciation of mercury emitted in the Polish power sector in the case of EF2008 emission factors i.e. 55% of GEM, 36% of RGM and 9% of Hg_P is consistent with the results reported in the literature and presented in Table 2-8 [84], [1], [47]. The results obtained with the emission factors for 2009 (EF2009) show that elemental mercury is prevailing, because mercury is mainly released from brown coal power plants.

Most of cadmium is emitted from heating plants, which have low stack heights that usually do not reach 70 meters as was presented in Figure 5-5. Lead is also mainly emitted from plants which have stack heights lower than 70 meters. The share of these stack heights in total emissions is 37% and 65% for lead and cadmium, respectively. As mercury is mainly emitted from big power plants, most of it is released into the air from stacks above 150 meters.

5.3 Implemented chemical scheme of atmospheric mercury

The chemical scheme used in this study takes into account the reactions and transitions of mercury in the gaseous, aqueous and particulate phases presented in Figure 5-6. This scheme is an upgraded version of the chemical model previously introduced in the PhD thesis of Yelva Roustan [224]. The main developments in this model are related to the reactions and transformations of mercury with bromine. It has been shown, that bromine is more effective in Hg-oxidation than chlorine to produce $HgBr_{2(g)}$ during coal combustion [225].

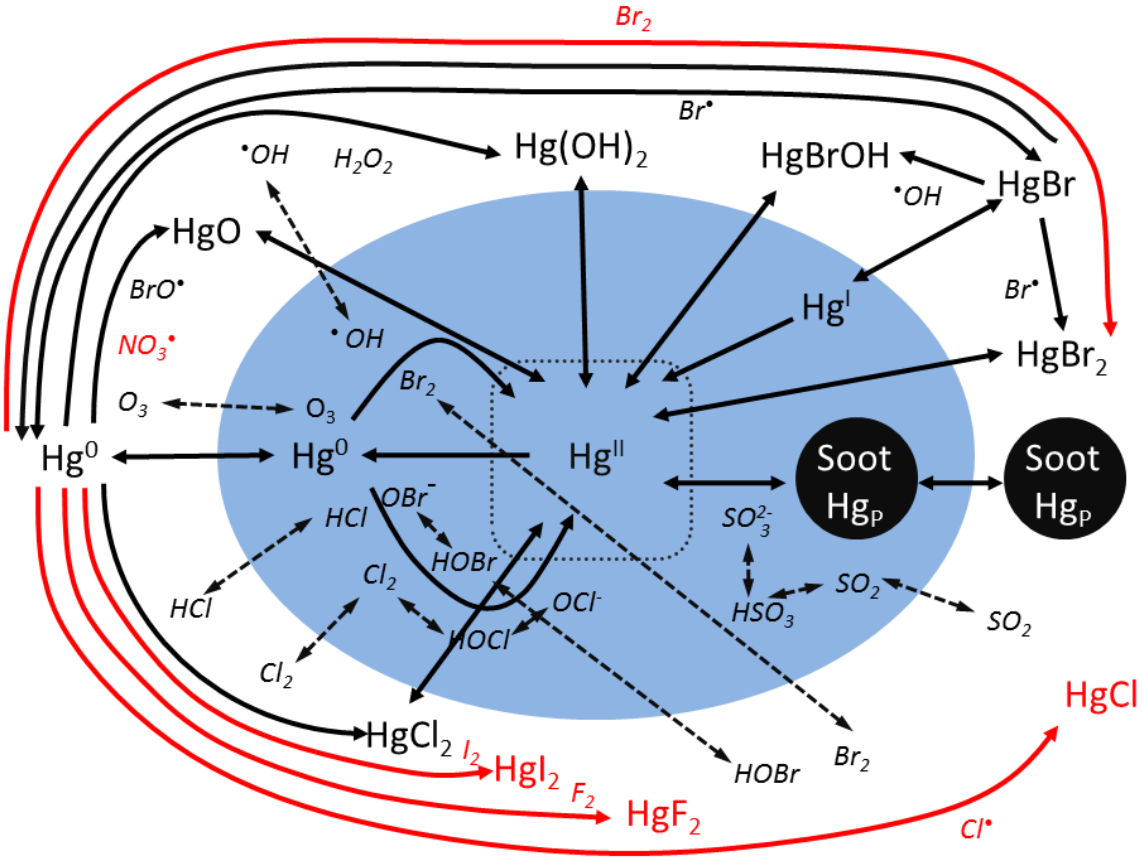

Figure 5-6. The implemented chemical model for mercury. In this picture, the gaseous and aqueous phases are marked in white and blue, respectively. The line arrows show possible transformations of mercury. The dashed arrows show additional species used in the model ,which react with mercury. The red arrows and species show the reactions implemented additionally in sensitivity analyses of the model. The species and arrows in black indicate the reactions and transformations, which were used in all simulations (otherwise the changes are marked in the text).

In this model, the user can choose a number of particles size sections and define threshold limits of size sections for modelled particulate species. All the equilibrium constants and chemical rates used to quantify the physico-chemical processes considered in the chemical scheme are presented in Table 5-4. The values of parameters were determined based on a literature review (relevant references are provided in the last column of Table 5-4).

The mechanism proposed in the CMAQ model was adopted to model the sorption and desorption of dissolved mercury compounds on particulate matter (black carbon is the primary sorbent) in the aqueous phase [160]. This mechanism was based on the previous study in which the adsorption of mercury onto black carbon is analysed in detail [157].

Table 5-4. Physico-chemical processes considered in the mercury chemistry model. In italics are written reaction which are used only in sensitivity studies.

N.	Reaction	Rate / equilibrium constant	Units	Reference
1	**Gas-phase oxidation**			
2	$Hg^0_{(g)} + O_{3(g)} \rightarrow HgO_{(g)} + O_{2(g)}$	$k_1=2.1\cdot10^{-18}\cdot\exp(-1246/T)$	$cm^3.molec^{-1}.s^{-1}$	[96]
3	$Hg^0_{(g)} + 2^{\bullet}OH_{(g)} \rightarrow Hg(OH)_{2(g)}$	$k_2=8.7\cdot10^{-14}$	$cm^3.molec^{-1}.s^{-1}$	[107]
4	$Hg^0_{(g)} + Cl_{2(g)} \rightarrow HgCl_{2(g)}$	$k_3=2.6\cdot10^{-18}$	$cm^3.molec^{-1}.s^{-1}$	[117]
5	$Hg^0_{(g)} + 2HCl_{(g)} \rightarrow HgCl_{2(g)} + H_{2(g)}$	$k_4=10^{-19}$	$cm^3.molec^{-1}.s^{-1}$	[126]
6	$Hg^0_{(g)} + H_2O_{2(g)} \rightarrow Hg(OH)_{2(g)}$	$k_4=8.4\cdot10^{-6}\cdot\exp(-9021/T)$	$cm^3.molec^{-1}.s^{-1}$	[113]
7	$Hg^0_{(g)} + BrO^{\bullet}_{(g)} \rightarrow HgO_{(g)} + Br_{(g)}$	$k_5=1.5\cdot10^{-14}$	$cm^3.molec^{-1}.s^{-1}$	[133]
8	$Hg^0_{(g)} + Br^{\bullet}_{(g)} \rightarrow HgBr_{(g)}$	$k_6=1.46\cdot10^{-32}\cdot(T/298)^{-1.86}$	$cm^6.molec^{-2}.s^{-1}$	[226]
9	$HgBr_{(g)} + Br^{\bullet}_{(g)} \rightarrow HgBr_{2(g)}$	$k_7=2.5\cdot10^{-10}\cdot\exp(T/298)^{-0.57}$	$cm^3.molec^{-1}.s^{-1}$	[111]
10	$HgBr_{(g)} + {}^{\bullet}OH_{(g)} \rightarrow HgBrOH_{(g)}$	$k_8=2.5\cdot10^{-10}\cdot\exp(T/298)^{-0.57}$	$cm^3.molec^{-1}.s^{-1}$	[111]
11	*$Hg^0_{(g)} + Br_{2\,(g)} \rightarrow HgBr_{2(g)}$*	*$k_9=0.9\cdot10^{-16}$*	*$cm^3.molec^{-1}.s^{-1}$*	*[117]*
12	*$Hg^0_{(g)} + NO_3^{\bullet}{}_{(g)} \rightarrow HgO_{(g)} + NO_{2(g)}$*	*$k_{10}=4.0\cdot10^{-15}$*	*$cm^3.molec^{-1}.s^{-1}$*	*[135]*
13	*$Hg^0_{(g)} + I_{2\,(g)} \rightarrow HgI_{2(g)}$*	*$k_{11}=1.27\cdot10^{-19}$*	*$cm^3.molec^{-1}.s^{-1}$*	*[136]*
14	*$Hg^0_{(g)} + F_{2(g)} \rightarrow HgF_{2(g)}$*	*$k_{12}=1.8\cdot10^{-15}$*	*$cm^3.molec^{-1}.s^{-1}$*	*[106]*
15	*$Hg^0_{(g)} + Cl^{\bullet}_{(g)} \rightarrow HgCl_{(g)}$*	*$k_{13}=1.0\cdot10^{-11}$*	*$cm^3.molec^{-1}.s^{-1}$*	*[117]*
16	**Gas-phase reduction**			
17	$HgBr_{(g)} \rightarrow Hg^0_{(g)} + Br^{\bullet}_{(g)}$	$k_{14}=1.2\cdot10^{10}\cdot\exp(-8357/T)$	s^{-1}	[111]
18	$HgBr_{(g)} + Br^{\bullet}_{(g)} \rightarrow Hg^0_{(g)} + Br_{2(g)}$	$k_{15}=3.9\cdot10^{-11}$	$cm^3.molec^{-1}.s^{-1}$	[130]
19	**Aqueous-phase oxidation**			
20	$Hg^0_{(aq)} + O_{3(aq)} + H^+_{(aq)} \rightarrow Hg^{2+}_{(aq)} + OH^-_{(aq)} + O_{2(aq)}$	$k_{16}=4.7\cdot10^{7}$	$M^{-1}.s^{-1}$	[140]
21	$Hg^0_{(aq)} + {}^{\bullet}OH_{(aq)} \rightarrow Hg^+_{(aq)} + OH^-_{(aq)}$	$k_{17}=2.0\cdot10^{9}$	$M^{-1}.s^{-1}$	[142]
22	$Hg^0_{(aq)} + HOCl_{(aq)} \rightarrow Hg^{2+}_{(aq)} + OH^-_{(aq)} + Cl^-_{(aq)}$	$k_{18}=2.09\cdot10^{6}$	$M^{-1}.s^{-1}$	[144]
23	$Hg^0_{(aq)} + OCl^-_{(aq)} + H^+_{(aq)} \rightarrow Hg^{2+}_{(aq)} + OH^-_{(aq)} + Cl^-_{(aq)}$	$k_{19}=1.99\cdot10^{6}$	$M^{-1}.s^{-1}$	[144]
24	$Hg^0_{(aq)} + HOBr_{(aq)} \rightarrow Hg^{2+}_{(aq)} + OH^-_{(aq)} + Br^-_{(aq)}$	$k_{20}=0.279$	$M^{-1}.s^{-1}$	[141]
25	$Hg^0_{(aq)} + OBr^-_{(aq)} + H^+_{(aq)} \rightarrow Hg^{2+}_{(aq)} + Br^-_{(aq)} + OH^-_{(aq)}$	$k_{21}=0.273$	$M^{-1}.s^{-1}$	[141]
26	$Hg^0_{(aq)} + Br_{2(aq)} \rightarrow Hg^{2+}_{(aq)} + 2Br^-_{(aq)}$	$k_{22}=0.196$	$M^{-1}.s^{-1}$	[141]
27	$Hg^+_{(aq)} + ({}^{\bullet}OH,\ O_2,\ HO_2^{\bullet})_{(aq)} \rightarrow Hg^{2+}_{(aq)}$	fast		[142] [149] [156]
28	**Aqueous-phase reduction**			
29	$HgSO_{3(aq)} \rightarrow Hg^0_{(aq)} + products(SIV)_{(aq)}$	$k_{23}=7.7\cdot10^{13}T\cdot\exp(-12595/T)$	s^{-1}	[147]
30	$Hg^{2+}_{(aq)} + HO_2^{\bullet}{}_{(aq)} \rightarrow Hg^0_{(aq)} + O_{2(aq)} + H^+_{(aq)}$	$k_{24}=1.1\cdot10^{4}$	$M^{-1}.s^{-1}$	[149]
31	**Gas/liquid equilibria**			
32	$O_{3(g)} \leftrightarrow O_{3(aq)}$	$H_1=1.13\cdot10^{-2}$	$M.atm^{-1}$	[227]
33	$SO_{2(g)} \leftrightarrow SO_{2(aq)}$	$H_2=1.23$	$M.atm^{-1}$	[228]
34	$Cl_{2(g)} \leftrightarrow Cl_{2(aq)}$	$H_3=0.076$	$M.atm^{-1}$	[229]
35	${}^{\bullet}OH_{(g)} \leftrightarrow {}^{\bullet}OH_{(aq)}$	$H_4=25$	$M.atm^{-1}$	[230]
36	$HO_2^{\bullet}{}_{(g)} \leftrightarrow HO_2^{\bullet}{}_{(aq)}$	$H_5=2\cdot10^{3}$	$M.atm^{-1}$	[231]
37	$Br_{2(g)} \leftrightarrow Br_{2(aq)}$	$H_6=0.76$	$M.atm^{-1}$	[232]

38	$HOBr_{(g)} \leftrightarrow HOBr_{(aq)}$	$H_7=6.1\cdot10^{3}$	$M.atm^{-1}$	[233]
39	$Hg^{0}_{(g)} \leftrightarrow Hg^{0}_{(aq)}$	$H_8=0.11$	$M.atm^{-1}$	[234]
40	$HgO_{(g)} \leftrightarrow HgO_{(aq)}$	$H_9=2.69\cdot10^{12}$	$M.atm^{-1}$	[235]
41	$HgCl_{2(g)} \leftrightarrow HgCl_{2(aq)}$	$H_{10}=1.4\cdot10^{6}$	$M.atm^{-1}$	[236]
42	$Hg(OH)_{2(g)} \leftrightarrow Hg(OH)_{2(aq)}$	$H_{11}=1.2\cdot10^{4}$	$M.atm^{-1}$	[236]
43	$HgBr_{(g)} \leftrightarrow HgBr_{(aq)}$	$H_{12}=1.4\cdot10^{6}$	$M.atm^{-1}$	[237]
44	$HgBr_{2(g)} \leftrightarrow HgBr_{2(aq)}$	$H_{13}=1.4\cdot10^{6}$	$M.atm^{-1}$	[134]
45	$HgBrOH_{(g)} \leftrightarrow HgBrOH_{(aq)}$	$H_{14}=1.4\cdot10^{6}$	$M.atm^{-1}$	[237]
46	**Aqueous phase equilibria**			
47	$Hg^{2+}_{(aq)} + SO_3^{2-}{}_{(aq)} \leftrightarrow HgSO_{3(aq)}$	$K_1=2.1\cdot10^{13}$	M^{-1}	[146]
48	$HgSO_{3(aq)} + SO_3^{2}{}_{(aq)}^{-} \leftrightarrow Hg(SO_3)_2^{2-}{}_{(aq)}$	$K_2=1.0\cdot10^{10}$	M^{-1}	[146]
49	$HgCl_{2(aq)} \leftrightarrow Hg^{2+}_{(aq)} + 2Cl^{-}_{(aq)}$	$K_3=10^{-14}$	M^{2}	[238]
50	$HgOH^{+}_{(aq)} \leftrightarrow Hg^{2+}_{(aq)} + OH^{-}_{(aq)}$	$K_4=2.51\cdot10^{-11}$	M	[228]
51	$Hg(OH)_{2(aq)} \leftrightarrow Hg^{2+}_{(aq)} + 2OH^{-}_{(aq)}$	$K_5=1.0\cdot10^{-22}$	M^{2}	[238]
52	$HgOHCl_{(aq)} \leftrightarrow HgOH^{+}_{(aq)} + Cl^{-}_{(aq)}$	$K_6=3.72\cdot10^{-8}$	M	[228]
53	$SO_{2(aq)} + H_2O_{(aq)} \leftrightarrow HSO_3^{-}{}_{(aq)} + H^{+}_{(aq)}$	$K_7=1.23\cdot10^{-2}$	M	[228]
54	$HSO_3^{-}{}_{(aq)} \leftrightarrow SO_3^{2-}{}_{(aq)} + H^{+}_{(aq)}$	$K_8=6.6\cdot10^{-8}$	M	[228]
55	$Cl_{2(aq)} + H_2O_{(aq)} \leftrightarrow HOCl_{(aq)} + Cl^{-}_{(aq)} + H^{+}_{(aq)}$	$K_9=5.0\cdot10^{-4}$	M^{2}	[144]
56	$HOCl_{(aq)} \leftrightarrow OCl^{-}_{(aq)} + H^{+}_{(aq)}$	$K_{10}=3.2\cdot10^{-8}$	M	[144]
57	$Hg^{2+}_{(aq)} + Br^{-}_{(aq)} \leftrightarrow HgBr^{+}_{(aq)}$	$K_{11}=1.1\cdot10^{9}$	M^{-1}	[239]
58	$HgBr^{+}_{(aq)} + Br^{-}_{(aq)} \leftrightarrow HgBr_{2(aq)}$	$K_{12}=2.5\cdot10^{8}$	M^{-1}	[239]
59	$HgBr_{2(aq)} + Br^{-}_{(aq)} \leftrightarrow HgBr_3^{-}{}_{(aq)}$	$K_{13}=1.5\cdot10^{2}$	M^{-1}	[239]
60	$HgBr_3^{-}{}_{(aq)} + Br^{-}_{(aq)} \leftrightarrow HgBr_4^{2-}{}_{(aq)}$	$K_{14}=2.3\cdot10^{1}$	M^{-1}	[239]
61	$HOBr_{(aq)} \leftrightarrow H^{+}_{(aq)} + BrO^{-}_{(aq)}$	$K_{15}=2.51\cdot10^{-9}$	M^{-1}	[141]
62	$Br_{2(aq)} + H_2O_{(aq)} \leftrightarrow HOBr_{(aq)} + Br^{-}_{(aq)} + H^{+}_{(aq)}$	$K_{16}=5.75\cdot10^{-9}$	M^{-1}	[141]
63	$H^{+}_{(aq)} + Br^{-}_{(aq)} + Hg(OH)_{2(aq)} \leftrightarrow HgBrOH_{(aq)}$	$K_{17}=2.7\cdot10^{-12}$	M^{-2}	[240]
64	**Gas/aerosol equilibrium**			
65	$BC_{(air)} \leftrightarrow BC_{(w)}$	$G_1=1\cdot10^{5}$	$m_{water}^{3}.m_{air}^{-3}$	[241]
66	**Adsorption/desorption coefficients**			
67	$HgSO_{3(aq)} \leftrightarrow HgSO_{3(p)}$	k_S, k_D	s^{-1}	Where k_S, k_D are the rate constants of sorption and desorption respectively. [160]
68	$HgSO_2^{2-}{}_{(aq)} \leftrightarrow HgSO_2^{2-}{}_{(p)}$			
69	$HgCl_{2(aq)} \leftrightarrow HgCl_{2(p)}$			
70	$HgOH^{+}_{(aq)} \leftrightarrow HgOH^{+}_{(p)}$			
71	$Hg(OH)_{2(aq)} \leftrightarrow Hg(OH)_{2(p)}$			
72	$HgOHCl_{(aq)} \leftrightarrow HgOHCl_{(p)}$			
73	$HgBrOH_{(aq)} \leftrightarrow HgBrOH_{(p)}$			
74	$HgBr^{+}_{(aq)} \leftrightarrow HgBr^{+}_{(p)}$			
75	$HgBr_{2(aq)} \leftrightarrow HgBr_{2(p)}$			
76	$HgBr_3^{-}{}_{(aq)} \leftrightarrow HgBr_3^{-}{}_{(p)}$			
77	$HgBr_4^{2-}{}_{(aq)} \leftrightarrow HgBr_4^{2-}{}_{(p)}$			

Gaseous phase

In the gaseous phase the concentration of elemental mercury ($Hg^{0}_{(g)}$) and six reactive mercury species i.e. mercury monoxide $HgO_{(g)}$, mercury(II) hydroxide $Hg(OH)_{2(g)}$, mercury(II)

chloride $HgCl_{2(g)}$, mercury bromide $HgBr_{(g)}$, mercury(II) bromide $HgBr_{2(g)}$, hydroxy mercury bromide $HgBrOH_{(g)}$ are modelled. Taken into account the mercury reactions in the gaseous phase (listed in Table 3-1) the changes of concentrations of considered species are expressed as follows:

$$\frac{d}{dt}\left[Hg^{0}_{(g)}\right] = -j_1 - j_2 - j_3 - j_4 - j_5 - j_6 - j_7 + j_{15} + j_{16} \quad \text{R.5.1}$$

$$\frac{d}{dt}\left[HgO_{(g)}\right] = j_1 + j_6 \quad \text{R.5.2}$$

$$\frac{d}{dt}\left[Hg(OH)_{2(g)}\right] = j_2 + j_5 \quad \text{R.5.3}$$

$$\frac{d}{dt}\left[HgCl_{2(g)}\right] = j_3 + j_4 \quad \text{R.5.4}$$

$$\frac{d}{dt}\left[HgBr_{(g)}\right] = j_7 - j_8 - j_9 - j_{15} - j_{16} \quad \text{R.5.5}$$

$$\frac{d}{dt}\left[HgBr_{2(g)}\right] = j_8 \quad \text{R.5.6}$$

$$\frac{d}{dt}\left[HgBrOH_{(g)}\right] = j_9 \quad \text{R.5.7}$$

where:

$$j_1 = k_1[Hg^0_{(g)}][O_{3(g)}] \quad \text{R.5.8}$$

$$j_2 = k_2[Hg^0_{(g)}][OH_{(g)}] \quad \text{R.5.9}$$

$$j_3 = k_3[Hg^0_{(g)}][Cl_{2(g)}] \quad \text{R.5.10}$$

$$j_4 = k_4[Hg^0_{(g)}][HCl_{(g)}] \quad \text{R.5.11}$$

$$j_5 = k_5[Hg^0_{(g)}][H_2O_{2(g)}] \quad \text{R.5.12}$$

$$j_6 = k_6[Hg^0_{(g)}][BrO^{\bullet}_{(g)}] \quad \text{R.5.13}$$

$$j_7 = k_7[Hg^0_{(g)}][Br^{\bullet}_{(g)}] \quad \text{R.5.14}$$

$$j_8 = k_8[HgBr_{(g)}][Br^{\bullet}_{(g)}] \quad \text{R.5.15}$$

$$j_8 = k_9[HgBr_{(g)}][{}^{\bullet}OH_{(g)}] \quad \text{R.5.16}$$

$$j_{15} = k_{15}[HgBr_{(g)}] \quad \text{R.5.17}$$

$$j_{16} = k_{16}[HgBr_{(g)}][Br^{\bullet}_{(g)}] \quad \text{R.5.18}$$

In sensitivity studies, additionally mercury(II) iodide -$HgI_{2(g)}$, mercury(II) fluoride -$HgF_{2(g)}$, mercury chloride -$HgCl_{(g)}$ are modelled. Accordingly, suitable reaction rates are added to the model.

Aqueous phase

The reactions and transformations of mercury in the aqueous phase are modelled when sufficient liquid water is diagnosed in the atmosphere at the beginning or the end of the

simulation time step. The cloud presence diagnosis is simply based on a threshold (0.05 $g.m^{-3}$) of the liquid water content in the atmosphere.

The concentration of substrates taken part in the aqueous phase are calculated based on Henry's law and equilibria presented in Table 5-4:

$$[O_{3(aq)}] = H_1 \cdot \frac{R \cdot T}{N_{av}} [O_{3(g)}] \quad \text{R.5.19}$$

$$[SO_3^{2-}{}_{(aq)}] = \frac{K_7 \cdot K_8}{[H^+]^2} \cdot H_2 \cdot \frac{R \cdot T}{N_{av}} [SO_{2(g)}] \quad \text{R.5.20}$$

$$[HOCl_{(aq)}] = \frac{K_9}{[Cl^-][H^+]} \cdot H_3 \cdot \frac{RT}{N_{av}} [Cl_{2(g)}] \quad \text{R.5.21}$$

$$[OCl^-_{(aq)}] = \frac{K_9 \cdot K_{10}}{[Cl^-][H^+]^2} \cdot H_3 \cdot \frac{R \cdot T}{N_{av}} [Cl_{2(g)}] \quad \text{R.5.22}$$

$$[{}^{\cdot}OH_{(aq)}] = H_4 \cdot \frac{R \cdot T}{N_{av}} [{}^{\cdot}OH_{(g)}] \quad \text{R.5.23}$$

$$[HO^{\cdot}_{2(aq)}] = H_5 \cdot \frac{R \cdot T}{N_{av}} [HO^{\cdot}_{2(g)}] \quad \text{R.5.24}$$

$$[Br_{2(aq)}] = H_6 \cdot \frac{R \cdot T}{N_{av}} [Br_{2(g)}] \quad \text{R.5.25}$$

$$[HOBr_{(aq)}] = H_7 \cdot \frac{R \cdot T}{N_{av}} [HOBr_{(g)}] \quad \text{R.5.26}$$

$$[OBr^-_{(aq)}] = \frac{K_{15}}{[H^+]} \cdot H_7 \cdot \frac{R \cdot T}{N_{av}} [HOBr_{(g)}] \quad \text{R.5.27}$$

where:

$$[H^+] = 10^{-pH} \quad \text{R.5.28}$$

R –ideal gas law constant, 82 $atm.cm^3.mol^{-1}.K^{-1}$ or 8.13 $J.\ mol^{-1}.K^{-1}$;

N_{av} –Avogadro constant, $6.022 \cdot 10^{23}$ $molec \cdot mol^{-1}$;

T –temperature [K];

pH –potential of hydrogen, pH of cloud water, assumed to be 4.5 [195].

In the model only total divalent mercury ($Hg^{II}_{(aq)}$), and elemental mercury $Hg^0_{(aq)}$ are specified in the aqueous phase. However, at each simulation time steps the concentrations of particular oxidized mercury compounds i.e. $HgSO_{3(aq)}$, $HgSO_2^{2-}{}_{(aq)}$, $Hg(OH)_{2(aq)}$, $HgCl_{2(aq)}$, $HgOHCl_{(aq)}$, $HgOH^+_{(aq)}$, $HgBrOH_{(aq)}$, $HgBr^+_{(aq)}$, $HgBr_{2(aq)}$, $HgBr_3^-{}_{(aq)}$, $HgBr_4^{2-}{}_{(aq)}$ is calculated, if needed. The total divalent mercury in the models equals:

$$[Hg^{II}{}_{(aq)}] = [Hg^{2+}{}_{(aq)}] + [Hg(\boxed{S})_{(aq)}] + [HgCl_{2(aq)}] + [Hg(\boxed{O})_{(aq)}] + [Hg(\boxed{Br})_{(aq)}] \quad \text{R.5.29}$$

where:

$$[\boldsymbol{Hg}(\boxed{S})_{(aq)}] = [HgSO_{3\,(aq)}] + [Hg(SO_3)_2^{2-}{}_{(aq)}] \quad \text{R.5.30}$$

$$\left[HgSO_{3(aq)}\right] = K_1\left[Hg^{2+}{}_{(aq)}\right]\left[SO_3^{2-}{}_{(aq)}\right] \quad \text{R.5.31}$$

$$\left[Hg(SO_3)_2^{2-}{}_{(aq)}\right] = K_2\left[HgSO_{3(aq)}\right]\left[SO_3^{2-}{}_{(aq)}\right] \quad \text{R.5.32}$$

$$\left[Hg(\boxed{S})_{(aq)}\right] = [Hg^{2+}]\underbrace{K_1\left[SO_3^{2-}{}_{(aq)}\right]\left(1 + K_2\left[SO_3^{2-}{}_{(aq)}\right]\right)}_{group\ A} \quad \text{R.5.33}$$

$$\left[\boldsymbol{HgCl_2}_{(aq)}\right] = [Hg^{2+}{}_{(aq)}]\underbrace{\frac{[Cl^-{}_{(aq)}]^2}{K_3}}_{group\ B} \quad \text{R.5.34}$$

$$\left[\boldsymbol{Hg}(\boxed{\boldsymbol{O}})_{(aq)}\right] = \left[HgOH^+{}_{(aq)}\right] + \left[Hg(OH)_{2(aq)}\right] + \left[HgOHCl_{(aq)}\right] + \left[HgBrOH_{(aq)}\right] \quad \text{R.5.35}$$

$$K_4\left[HgOH^+{}_{(aq)}\right] = \left[Hg^{2+}{}_{(aq)}\right]\left[OH^-{}_{(aq)}\right] \quad \text{R.5.36}$$

$$K_5\left[Hg(OH)_{2(aq)}\right] = \left[HgOH^+{}_{(aq)}\right]\left[OH^-{}_{(aq)}\right] \quad \text{R.5.37}$$

$$K_6\left[HgOHCl_{(aq)}\right] = \left[HgOH^+{}_{(aq)}\right]\left[Cl^-{}_{(aq)}\right] \quad \text{R.5.38}$$

$$K_{17}\left[Hg(OH)_{2(aq)}\right]\left[H^+{}_{(aq)}\right]\left[Br^-{}_{(aq)}\right] = \left[HgBrOH_{(aq)}\right] \quad \text{R.5.39}$$

$$\left[Hg(\boxed{O})_{(aq)}\right] = \left[Hg^{2+}{}_{(aq)}\right]\underbrace{\frac{[OH^-{}_{(aq)}]}{K_4}\left(1 + \frac{[Cl^-{}_{(aq)}]}{K_6} + \frac{[OH^-{}_{(aq)}]}{K_5}\left(1 + K_{17}\left[H^+{}_{(aq)}\right]\left[Br^-{}_{(aq)}\right]\right)\right)}_{group\ C} \quad \text{R.5.40}$$

$$\left[\boldsymbol{Hg}(\boxed{\boldsymbol{Br}})_{(aq)}\right] = \left[HgBr^+{}_{(aq)}\right] + \left[HgBr_{2\,(aq)}\right] + \left[HgBr_3^-{}_{(aq)}\right] + \left[HgBr_4^{2-}{}_{(aq)}\right] \quad \text{R.5.41}$$

$$\left[HgBr^+{}_{(aq)}\right] = K_{11}\left[Hg^{2+}{}_{(aq)}\right]\left[Br^-{}_{(aq)}\right] \quad \text{R.5.42}$$

$$\left[HgBr_{2\,(aq)}\right] = K_{12}\left[HgBr^+{}_{(aq)}\right]\left[Br^-{}_{(aq)}\right] \quad \text{R.5.43}$$

$$\left[HgBr_3^-{}_{(aq)}\right] = K_{13}\left[HgBr_{2\,(aq)}\right]\left[Br^-{}_{(aq)}\right] \quad \text{R.5.44}$$

$$\left[HgBr_4^{2-}{}_{(aq)}\right] = K_{14}\left[HgBr_3^-{}_{(aq)}\right]\left[Br^-{}_{(aq)}\right] \quad \text{R.5.45}$$

$$\left[Hg(\boxed{Br})_{(aq)}\right] = [Hg^{2+}]\underbrace{K_{11}[Br^-{}_{(aq)}]\left(1 + K_{12}[Br^-{}_{(aq)}]\left(1 + K_{13}[Br^-{}_{(aq)}](1 + K_{14}[Br^-{}_{(aq)}])\right)\right)}_{group\ D} \quad \text{R.5.46}$$

Finally, after reorganizing:

$$\left[Hg^{II}{}_{(aq)}\right] = \left[Hg^{2+}{}_{(aq)}\right](1 + group\ A + group\ B + group\ C + group\ D) \quad \text{R.5.47}$$

The concentration of divalent mercury compounds are:

$$\left[HgSO_{3(aq)}\right] = K_1\left[SO_3^{2-}{}_{(aq)}\right]\left[Hg^{II}{}_{(aq)}\right]/(1 + group\ A + group\ B + group\ C + group\ D) \quad \text{R.5.48}$$

$$\left[Hg(SO_3)_2^{2-}{}_{(aq)}\right] = \left[Hg^{II}{}_{(aq)}\right]K_2K_1\left[SO_3^{2-}{}_{(aq)}\right]^2 / (1 + group\ A + group\ B + group\ C + group\ D) \quad \text{R.5.49}$$

$$\left[HgCl_{2(aq)}\right] = \left[Hg^{II}{}_{(aq)}\right] / \left[\frac{K_3}{[Cl^-{}_{(aq)}]^2}(1 + group\ A + group\ B + group\ C + group\ D)\right] \quad \text{R.5.50}$$

$$\left[Hg(OH)_{2(aq)}\right] = \left[Hg^{II}{}_{(aq)}\right] / \left[\frac{K_4K_5}{[OH^-{}_{(aq)}]^2}(1 + group\ A + group\ B + group\ C + group\ D)\right] \quad \text{R.5.51}$$

$$\left[HgBr_{2\,(aq)}\right] = \left[Hg^{II}{}_{(aq)}\right]\left[\frac{1}{K_{12}K_{11}[Br^-]^2}(1 + group\ A + group\ B + group\ C + group\ D)\right] \quad \text{R.5.52}$$

$$\left[HgBrOH_{(aq)}\right] = \left[Hg^{II}{}_{(aq)}\right]\left[OH^-{}_{(aq)}\right]^2 K_{17}\left[H^+{}_{(aq)}\right]\left[Br^-{}_{(aq)}\right] / [K_4K_5(1 + group\ A + group\ B + group\ C + group\ D)] \quad \text{R.5.53}$$

The changes of concentrations in the aqueous phase are calculated as follows:

$$\frac{d}{dt}\left[Hg^0_{(aq)}\right] = -j_{17} - j_{18} - j_{19} - j_{20} - j_{21} - j_{22} - j_{23} + j_{24} + j_{25} \quad \text{R.5.54}$$

$$\frac{d}{dt}\left[Hg^{II}{}_{(aq)}\right] = -j_{17} - j_{18} - j_{19} - j_{20} - j_{21} - j_{22} - j_{23} - j_{24} - j_{25} + f_1^{g\to aq} + f_2^{g\to aq} - f_2^{aq\to g} + f_3^{g\to aq} - f_3^{aq\to g} + f_4^{g\to aq} + f_5^{g\to aq} - f_5^{aq\to g} + f_6^{g\to aq} + f_6^{aq\to g} \quad \text{R.5.55}$$

and the changes of gaseous species due to transformation of gaseous to aqueous phase, or inversely, are calculated in the model:

$$\frac{d}{dt}\left[HgO_{(g)}\right] = -f_1^{g\to aq}\frac{N_{av}\cdot W_T}{10^3} \quad \text{R.5.56}$$

$$\frac{d}{dt}\left[Hg(OH)_{2(g)}\right] = \left(-f_2^{g\to aq} + f_2^{aq\to g}\right)\frac{N_{av}\cdot W_T}{10^3} \quad \text{R.5.57}$$

$$\frac{d}{dt}\left[HgCl_{2(g)}\right] = \left(-f_3^{g\to aq} + f_3^{aq\to g}\right)\frac{N_{av}\cdot W_T}{10^3} \quad \text{R.5.58}$$

$$\frac{d}{dt}\left[HgBr_{(g)}\right] = -f_4^{g\to aq}\frac{N_{av}\cdot W_T}{10^3} \quad \text{R.5.59}$$

$$\frac{d}{dt}\left[HgBr_{2(g)}\right] = \left(-f_5^{g\to aq} + f_5^{aq\to g}\right)\frac{N_{av}\cdot W_T}{10^3} \quad \text{R.5.60}$$

$$\frac{d}{dt}\left[HgBrOH_{(g)}\right] = \left(-f_6^{g\to aq} + f_6^{aq\to g}\right)\frac{N_{av}\cdot W_T}{10^3} \quad \text{R.5.61}$$

where:

$j_{17}=k_{17}[Hg^0{}_{(aq)}][O_{3(aq)}]$ R.5.62

$j_{18}=k_{18}[Hg^0{}_{(aq)}][{}^{\bullet}OH_{(aq)}]$ R.5.63

$j_{19}=k_{19}[Hg^0{}_{(aq)}][HOCl_{(aq)}]$ R.5.64

$j_{20}=k_{20}[Hg^0{}_{(aq)}][OCl^-{}_{(aq)}]$ R.5.65

$j_{21}=k_{21}[Hg^0{}_{(aq)}][HOBr_{(aq)}]$ R.5.66

$j_{22}=k_{22}[Hg^0{}_{(aq)}][OBr^-{}_{(aq)}]$ R.5.67

$j_{23}=k_{23}[Hg^0{}_{(aq)}][Br_{2(aq)}]$ R.5.68

$j_{24}=k_{24}[HgSO_{3(aq)}]$ R.5.69

$j_{25}=k_{25}[Hg^{2+}{}_{(aq)}][HO_2{}^{\bullet}{}_{(aq)}]$ R.5.70

$$f_1^{g\to aq} = y_1\frac{10^3}{N_{av}}\left[HgO_{(g)}\right] \quad \text{R.5.71}$$

$$f_2^{g\to aq} = y_2\frac{10^3}{N_{av}}\left[Hg(OH)_{2(g)}\right] \quad \text{R.5.72}$$

$$f_2^{aq\to g} = y_2 \frac{1}{H_{11}\cdot R\cdot T}\left[Hg(OH)_{2(aq)}\right] \quad \text{R.5.73}$$

$$f_3^{g\to aq} = y_3 \frac{10^3}{N_{av}}\left[HgCl_{2(g)}\right] \quad \text{R.5.74}$$

$$f_3^{aq\to g} = y_3 \frac{1}{H_{10}\cdot R\cdot T}\left[HgCl_{2(aq)}\right] \quad \text{R.5.75}$$

$$f_4^{g\to aq} = y_4 \frac{10^3}{N_{av}}\left[HgBr_{(g)}\right] \quad \text{R.5.76}$$

$$f_5^{g\to aq} = y_5 \frac{10^3}{N_{av}}\left[HgBr_{2(g)}\right] \quad \text{R.5.77}$$

$$f_5^{aq\to g} = y_5 \frac{1}{H_{13}\cdot R\cdot T}\left[HgBr_{2(aq)}\right] \quad \text{R.5.78}$$

$$f_6^{g\to aq} = y_6 \frac{10^3}{N_{av}}\left[HgBrOH_{(g)}\right] \quad \text{R.5.79}$$

$$f_6^{aq\to g} = y_6 \frac{1}{H_{14}\cdot R\cdot T}\left[HgBrOH_{(aq)}\right] \quad \text{R.5.80}$$

$$y_a = \left(\frac{D^2}{D_g} + \frac{4\cdot D}{3\cdot\varphi\cdot\left(\frac{8\cdot R\cdot T}{\pi\cdot M_a}\right)^{1/2}}\right)^{-1} \quad \text{R.5.81}$$

Where:

a ranges from 1 to 6.

D_g –the gas phase diffusivity [$m^2.s^{-1}$]. A gas phase diffusivity of $0.1628\cdot10^{-4}$ $m^2.s^{-1}$ for reactive gaseous mercury compounds was assumed [207], [242],

D –representative raindrop diameter [m] -set to 10 μm,

W_T –the water content in the atmosphere [$m_{water}^3.m_{air}^{-3}$],

φ –accommodation coefficient -set to 0.1 for all species of reactive mercury [243],

y –mass transfer coefficient [s^{-1}],

M –molar mass of individual mercury compounds [$kg.mol^{-1}$].

When the aqueous phase is diagnosed the elemental mercury concentration is distributed into gaseous ($Hg^0_{(g)}$) and aqueous ($Hg^0_{(aq)}$) phases.

Assuming that the total of Hg^0 (in $molec.cm^{-1}$) present in the atmosphere is in the gaseous ($Hg^0_{(g)}$) (in $molec.cm^{-1}$) or/and in aqueous ($Hg^0_{(aq)}$) (in M) phases, the following relationship occurs:

$$[Hg^0] = \left[Hg^0_{(g)}\right] + [Hg^0_{(aq)}]\frac{N_{av}\cdot W_T}{10^3} \quad \text{R.5.82}$$

and Henry's law for elemental mercury:

$$[Hg^0_{(aq)}] = H_8 \cdot \frac{R\cdot T}{N_{av}}\left[Hg^0_{(g)}\right] \quad \text{R.5.83}$$

then:

$$\left[Hg^0_{(g)}\right] = \frac{1}{1+H_8 \cdot W_T \cdot R \cdot T \cdot 10^{-3}} [Hg^0] \quad \text{R.5.84}$$

$$\left[Hg^0_{(aq)}\right] = \frac{1}{N_{av}} \cdot \frac{H_8 \cdot R \cdot T}{1+H_8 \cdot W_T \cdot R \cdot T \cdot 10^{-3}} [Hg^0] \quad \text{R.5.85}$$

In the case when no aqueous phase occurs $\left[Hg^0_{(g)}\right]$ is equal to $[Hg^0]$.

Concentrations of aqueous and gaseous species are expressed in M and in molec.cm^{-3}, respectively. The rates are expressed in M.s^{-1} or molec.cm^{-3}.s^{-1}. In the model, the units are chosen as necessary. No mass transfer from $Hg^{II}_{(aq)}$ to $HgO_{(g)}$ and $HgBr_{(g)}$ was assumed, because of the high solubility of $HgO_{(g)}$ and because $HgBr_{(g)}$ mercury has an oxidation state of one.

In the case when the aqueous phase does not appear in the next step of a simulation run, because the liquid water content is below the given threshold, whole divalent mercury in the aqueous phase is equally splint among gaseous compounds i.e. $HgOH_{2(g)}$, $HgCl_{2(g)}$, $HgBr_{2(g)}$, $HgBrOH_{(g)}$.

Adsorption/ Desorption

The adsorption (or wider sorption) rates j_s [M.s^{-1}] of aqueous Hg compounds i.e. $HgSO_{3(aq)}$, $HgSO_2{}^{2-}{}_{(aq)}$, $Hg(OH)_{2(aq)}$, $HgCl_{2(aq)}$, $HgOHCl_{(aq)}$, $HgOH^+{}_{(aq)}$, $HgBrOH_{(aq)}$, $HgBr^+{}_{(aq)}$, $HgBr_{2(aq)}$, $HgBr_3{}^-{}_{(aq)}$, $HgBr_4{}^{2-}{}_{(aq)}$ -the sum was named Hg_{cplx} in [kg.m$_{water}^{-3}$ or M], onto black carbon aerosol ($BC_{(w)}$) suspended in atmospheric water is calculated based on the approach described in chapter 2.5 [160]:

$$j_S = k_s \cdot \left[Hg_{cplx}\right] \quad \text{R.5.86}$$

where:

$$k_S = \frac{K_{ECA} \cdot [\mathrm{BC}_{(w)}]}{t^* \cdot (K_{ECA} \cdot [\mathrm{BC}_{(w)}] + 1)} \quad \text{R.5.87}$$

$[\mathrm{BC}_{(w)}]$ –concentration of black carbon suspended in atmospheric water [kg.m$_{water}^{-3}$] which equals:

$$[\mathrm{BC}_{(w)}] = G_1 \cdot [\mathrm{BC}_{(air)}] \quad \text{R.5.88}$$

$[\mathrm{BC}_{(air)}]$ –concentration of black carbon in air [kg.m$_{air}^{-3}$],

G_1 –equilibrium (Table 5-4),

K_{BCA} –absorption coefficient, assumed to be $680 \cdot 10^{-9}$ m$_{water}^3$.µg$_{BC}^{-1}$ [157], [243],

t^* –time, constant value, assumed to be 3600 s.

$$[Hg_{cplx}] = [HgSO_{3(aq)}] + [Hg(SO_3)^{2-}_{2\ (aq)}] + [HgCl_{2(aq)}] + [HgOH^{+}_{(aq)}] + [Hg(OH)_{2(aq)}] + [HgOHCl_{(aq)}] + [HgBrOH_{(aq)}] + [HgBr^{+}_{(aq)}] + [HgBr_{2(aq)}] + [HgBr^{-}_{3\ (aq)}] + [HgBr^{2-}_{4\ (aq)}] \quad \text{R.5.89}$$

Finally, after reorganizng:

$$[Hg_{cplx}] = [Hg^{II}_{(aq)}] \cdot [1 - (1 + group\ A + group\ B + group\ C + group\ D)^{-1}] \quad \text{R.5.90}$$

The desorption rate j_d [$M.s^{-1}$] of mercury from BC can be defined as follows:

$$j_d = k_d \cdot [Hg_{p_w}] \quad \text{R.5.91}$$

$$k_d = \frac{1}{t^* \cdot (K_{BC} \cdot [BC_w] + 1)} \quad \text{R.5.92}$$

$[Hg_{p_w}]$ –concentration of mercury bound to black carbon suspended in atmospheric water [$kg.m_{water}^{-3}$ or M].

Then, the changes of the concentration of the mercury bound to black carbon suspended in atmospheric water is calculated as follows:

$$\frac{d}{dt}[Hg_{p_w}] = j_s - j_d \quad \text{R.5.93}$$

Keeping in mind that Hg_{cplx} is a part of $Hg^{II}_{(aq)}$ ($[Hg^{II}_{(aq)}]=[Hg^{2+}_{(aq)}]+[Hg_{cplx}]$) the additional rates j_d and j_s determine the changes $Hg^{II}_{(aq)}$. Finally the concentration of $Hg^{II}_{(aq)}$ in the model is calculated as follows:

$$\frac{d}{dt}[Hg^{II}_{(aq)}] = j_d - j_s \quad \text{R.5.94}$$

5.3.1 In-cloud scavenging

In the base model, the in-cloud scavenging was calculated for elemental mercury (Hg^0_{aq}), reactive mercury ($Hg^{II}_{(aq)}$) and particulate-bound heavy metals with the use of a scavenging coefficients of $8.4 \cdot 10^{-5} \cdot I^{0.79}$ [244]. However, several other scavenging coefficients presented in Table 5-5 were applied to study the impact on mercury deposition and concentration.

Table 5-5. Scavenging coefficients for in-cloud scavenging [s^{-1}] (based on [245]).

N.	Scavenging coefficient [s^{-1}]	Remarks
1	$3.5 \cdot 10^{-4} \cdot I^{0.78}$	Applied for soluble PMs, rain
2	$2.44 \cdot 10^{-4} \cdot I^{0.78}$	Applied for soluble PMs, snow
3	$8.4 \cdot 10^{-5} \cdot I^{0.79}$	Applied for PMs, dynamic rain
4	$3.36 \cdot 10^{-4} \cdot I^{0.79}$	Applied for PMs, convective rain

5	$8.0 \cdot 10^{-5} \cdot I^{0.305}$	Applied for PMs, dynamic snow
6	$3.36 \cdot 10^{-4} \cdot I^{0.79}$	Applied for PMs, convective snow
7	$\frac{1 - \exp(-\alpha \tau_{cld})}{\tau_{cld}}$	Applied for gases and PMs
8	$4.17 \cdot 10^{-7} \cdot I \cdot E \cdot D^{-1}$	Applied for soluble gases and PMs
9	$4.17 \cdot 10^{-4} \cdot I^{0.79}$	Applied for soluble PMs

I –intensity of rain [$mm.h^{-1}$],
D –representative raindrop diameter [m],
τ_{cld} –a cloud timescale (set as 1 hour),

$$\frac{1}{\alpha} = \tau_{washout} = \frac{W_T \Delta Z_{cld}}{I} \cdot 3.6 \cdot 10^6 \text{ [s]}, \qquad \text{R.5.95}$$

W_T –the total water content [$m_{water}^3.m_{air}^{-3}$],
ΔZ_{cld} –the cloud vertical thickness [m],
E –collision efficiency.

Scavenging coefficients of $4.17 \cdot 10^{-7} \cdot I \cdot E \cdot D^{-1}$ [s^{-1}] depends on the representative raindrop diameter, which was proposed to be a function of the rain intensity in several studies (Table 5-6). As the base reference value, the collision efficiency with raindrops of 0.9 for all forms of mercury was applied [211]. Additionally, one simulation was done with a collision efficiency of 0.4 [246]. This value was chosen based on studies where the collision efficiency for particulate matter from 0.3 to 0.5 was proposed.

Table 5-6. Representative raindrop diameter [m] [208].

N.	Representative raindrop diameter [m]
1	$1.238 \cdot 10^{-3} \cdot I^{0.182}$
2	$7.88 \cdot 10^{-4} \cdot I^{0.3}$
3	$3.97 \cdot 10^{-4} \cdot I^{0.37}$
4	$0.9 \cdot 10^{-3} \cdot I^{0.21}$ leads to $4.17 \cdot 10^{-4} \cdot I^{0.79}$ if E=0.9
5	$8 \cdot 10^{-4} \cdot I^{0.34}$
6	$1.3 \cdot 10^{-3} \cdot I^{0.14}$
7	$7 \cdot 10^{-4} \cdot I^{0.25}$
8	$1.18 \cdot 10^{-3} \cdot I^{0.2}$
9	$1.06 \cdot 10^{-3} \cdot I^{0.16}$
10	$9.7 \cdot 10^{-4} \cdot I^{0.158}$
11	$1.16 \cdot 10^{-3} \cdot I^{0.227}$

Modelling of the transport of cadmium and lead

The Polyphemus air quality system was also developed to track the atmospheric dispersion of lead and cadmium bound to particulate matter. It is a chemically invert version of the model where physical and chemical transformations of particulate matter are not considered. The ambient concentrations of lead and cadmium are calculated only with the use of the Polair3D transport model. The wet and dry deposition fluxes are modelled in the same way as in case of mercury bound to particulate matter.

6 Simulation setting

Simulations were performed for the year 2008 for two domains covering Poland and Europe. The main aims of the simulation over Europe were: (i) to prepare boundary conditions for the finer domain covering Poland and (ii) to evaluate the results against the measurements available through the stations network operated in the context of EMEP [163]. The year 2008 was chosen because most of the input data e.g. meteorological or emissions as well as the mercury measurement data used for the evaluation of the results were available. Moreover, the detailed inventory of the Polish power sector was prepared for 2008. The second domain was used to analyse the mercury transport over Poland in a more detailed manner. In the past, simulations had also been performed with other resolutions for 2005 [201]. Particulate mercury, lead and cadmium are distributed among 10 different size sections (between 0.01 to 10 μm with the following threshold limits : 0.01 - 0.02 - 0.0398 - 0.0794 - 0.1585 - 0.3162 - 0.6310 - 1.2589 - 2.5119 - 5.0119 - 10).

6.1 Domains of simulation

The European domain consisted of 140 x 120 cells with a horizontal resolution of 0.25^0 x 0.5^0 (along latitude and longitude respectively), starting from 36.5^0N latitude and 12.8^0W longitude with a horizontal resolution of 1.0^0. The domain over Poland consisted of 80 x 118 cells, starting from 47.95^0N latitude and 13.55^0E longitude with a horizontal resolution of 0.10 (Figure 6-1). Ten vertical levels were used with the following limits [in meters above surface]: 0; 70; 150; 300; 500; 750; 1000; 2000; 3000; 4000; 5000.

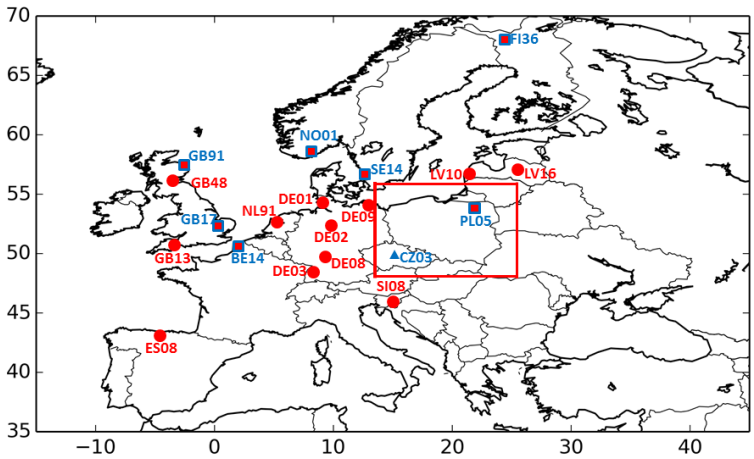

Figure 6-1. Domains of simulation and locations of measurement stations of mercury wet deposition (red circles), ambient concentration (blue triangles) or both parameters (red-blue squares) operated in 2008 in the context of [163].

6.2 Input data

6.2.1 Land use data

A database from the United States Geological Survey, the Global Land Cover Characteristics (version 2.0, Lambert Azimuthal Equal Area, 1km) was used to describe land use coverage [247]. This database includes 24 categories of land use coverage with a horizontal resolution of 1 km. The land use coverage data were used to: (i) compute the dry deposition velocity of mercury species, (ii) and conversion of mercury emission from EMEP grid into mercury model grid used in this work.

6.2.2 Meteorological data

The meteorological parameters were taken from The European Centre for Medium-Range Weather Forecasts (ECMWF) meteorological data for 2008 [248]. The ECMWF data for 2008 are provided with a horizontal resolution of 0.25^0 on 54 vertical levels every 3 hours. The vertical turbulent transport is represented through a diffusion coefficient computed using the parameterization of Troen and Mahrt within the boundary layer and the Louis parameterization above it [249], [212]. As an example of metrological parameters of ECMWF disaggregated onto the simulation grid precipitation intensity in Europe is presented in Figure 6-2.

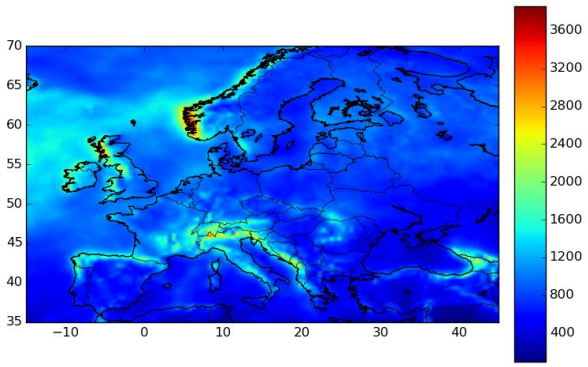

Figure 6-2. Annual precipitation intensity [$mm.y^{-1}$] over Europe due to [248].

6.2.3 Boundary and initial concentrations

The initial concentrations for both domains and boundary concentrations for the European domain were set to 0.185 ppt for $Hg^0_{(g)}$ and 0.0012 ppt for $HgO_{(g)}$, $Hg(OH)_{2(g)}$, $HgCl_{2(g)}$, Hg_P. At the first level, the concentration equals to approximately 1.5 $ng.m^{-3}$ for Hg^0 and 5 $pg.m^{-3}$

for $HgO_{(g)}$, $Hg(OH)_{2(g)}$, $HgCl_{2(g)}$, Hg_P. The concentration of 2 $ng.m^{-3}$ and 0.15 $ng.m^{-3}$ were set to 0 for lead and cadmium, respectively. The boundary and initial concentrations of Hg_P, lead and cadmium are equally distributed among the 10 size sections. The concentrations of other mercury compounds in the gas phase as well as concentrations of mercury compounds in the aqueous phase were set to 0. The chosen values were selected on the basis of simulation results and measurements of mercury compounds in the air over Europe [10], [224], [250], [251]. The modelling results from the simulation run for the European domain were used as the input boundary concentrations in the simulation over Poland.

6.2.4 Concentrations of species that react with mercury

The ambient concentrations of sulfur dioxide ($SO_{2(g)}$), hydrogen peroxide ($H_2O_{2(g)}$), ozone ($O_{3(g)}$), peroxyl radical ($HO_2^{\bullet}{}_{(g)}$), hydroxyl radical ($^{\bullet}OH_{(g)}$), hydrogen chloride ($HCl_{(g)}$), molecular chlorine ($Cl_{2(g)}$), chlorine radicals ($Cl^{\bullet}{}_{(g)}$), bromine oxide radical ($BrO^{\bullet}{}_{(g)}$) bromine radical ($Br^{\bullet}{}_{(g)}$), molecular bromine ($Br_{2(g)}$), hypobromous acid ($HOBr_{(g)}$), nitrate radical ($NO_3^{\bullet}{}_{(g)}$), molecular iodine ($I_{2(g)}$), molecular fluorine ($F_{2(g)}$), and black carbon aerosol (ECA) are provided to the model in each cell with a 3h time step. It was assumed that, if the concentrations of these species have a significant influence for mercury reactions in the atmosphere, mercury does not have an impact on the concentrations of these species, due to relatively small quantity of these species directly involved in the reactions with mercury.

The concentrations of $SO_{2(g)}$, $H_2O_{2(g)}$, $NO_3^{\bullet}{}_{(g)}$, $O_{3(g)}$, $HO_2^{\bullet}{}_{(g)}$, $^{\bullet}OH_{(g)}$ and black carbon in aerosols were generated by a simulation run for 2008 with the Polyphemus/Polair3D air quality model. The model was run for both domains (European and over Poland) with time step of 600 s and the average results were saved in each cell with a 3h time step.

In these simulations, are used:

1. Anthropogenic emissions of $SO_{2(g)}$, $PM2.5_{(g)}$, PM10, $NH_{3(g)}$, $CO_{(g)}$, $NMVOC_{(g)}$, $NO_{x(g)}$ provided by the EMEP for 2008 [87].
2. The results for the year 2000 for gaseous species of the global model MOZART as the initial concentrations for both domains and boundary concentrations for the European domain [193].
3. The results of GOCART for the year 2001 for the European domain for boundary concentrations of aerosol species [252].
4. A nesting approach, the results from a simulation run in the European domain were used as the boundary conditions for simulation over Poland.

5. Estimated natural emissions of terpenes and isoprenes [253].
6. Generated natural emission of sea salts [254].
7. Emission temporal profiles for SNAP sectors to distribute the annual emissions into months, days of the week and hours of the day [255].
8. Dry deposition velocities generated with a time step of 3 hours based on dedicated models and parameters for gaseous and aerosols species [217], [218].

The meteorological and land data were generated in the same way as for the simulations dedicated to atmospheric heavy metals dispersion. The results of concentrations in ambient air of $SO_{2(g)}$, $H_2O_{2(g)}$, $NO_3^{\bullet}{}_{(g)}$, $O_{3(g)}$, $HO_2^{\bullet}{}_{(g)}$, $OH^{\bullet}{}_{(g)}$ and black carbon from simulations run are presented in chapter 7.3. The concentrations of $HCl_{(g)}$, $Cl_{2(g)}$, $BrO^{\bullet}{}_{(g)}$, $Br^{\bullet}{}_{(g)}$, $Br_{2(g)}$, $HOBr_{(g)}$, $Cl^{-}{}_{(aq)}$, $NO_3^{\bullet}{}_{(g)}$, $I_{2(g)}$, $F_{2(g)}$, $Cl^{\bullet}{}_{(g)}$ were assumed to be as presented in Table 6-1.

Table 6-1. Concentration of species which react with mercury

N.	Species	Concentration	Units	References
1	$HCl_{(g)}$	Linear interpolation from $1.2 \cdot 10^{10}$ at surface level to 10^8 at 10 km altitude	molec.cm^{-3}	[256], [127]
2	$Cl_{2(g)}$	100 during night over sea at surface level 50 during night over sea above surface level 10 during day over sea	ppt	[121]
3	$BrO^{\bullet}{}_{(g)}$	0.3	ppt	[131]
4	$Br^{\bullet}{}_{(g)}$	0.003	ppt	[127]
5	$Br_{2(g)}$	0.003	ppt	[131]
6	$HOBr_{(g)}$	1	ppt	[131]
7	$Cl^{-}{}_{(aq)}$	$7 \cdot 10^{-5}$	M	[195]
8	$NO_3^{\bullet}{}_{(g)}$	10^8 during night 0 during day	molec.cm^{-3}	[15], [257]
9	$I_{2(g)}$	20 over sea	ppt	[137]
10	$F_{2(g)}$	1	µg.m^{-3}	[138]
11	$Cl^{\bullet}{}_{(g)}$	$4 \cdot 10^{-4}$	ppt	[125]

One should bear in mind that the concentrations of those species can vary significantly. This is very important in particular over Poland due to relatively still large emissions of pollutants into the air. The wide range of concentrations of those species reported in the literature were presented in Figure 2-9. For instance the reported atmospheric concentration of $Br_{2(g)}$ differs by a factor of four.

6.2.5 Natural emissions

Data on natural emissions and reemissions of heavy metals provided for 2005 by EMEP were used [29], [14]. It was assumed that natural emissions and reemissions of heavy metals do not change significantly during the period of 3 years (from 2005 to 2008) and theses data were used for a simulation run for 2008. The data provided by EMEP are stored as yearly average

emission fluxes with a resolution of 50 km x 50 km covering the whole Europe. For mercury EMEP accepted the global results presented in Table 2-2, row 3 [19]. Those emissions are distributed over land based on soil temperature and type of land surface: (i) background soil, (ii) soil of the geochemical mercuriferous belt, (iii) soil of mercury deposited areas and (iv) glacier with no emission of mercury. The emissions over sea water were distributed based on the assumption that it is proportional to the emission of organic carbon [258]. The natural emissions and reemissions of mercury provided by EMEP are around 15% higher than the anthropogenic emissions in the European domain. It has been assumed that all emissions of mercury from non-anthropogenic sources were in the form of $Hg^0_{(g)}$. The natural emissions are lowest in northern Europe and increase to the south with the increasing temperature (Figure 6-3). The natural emissions of lead and cadmium are spatially distributed equally over the land and water surfaces. The EMEP model, as input data, uses the assumed flux of natural emission of lead of 160 $g.km^{-2}.y^{-1}$ from sea surface and 220 $g.km^{-2}.y^{-1}$ from soil, while no emissions from the surface covered by snow were implemented. The natural flux of cadmium was assumed to be 12 $g.km^{-2}.y^{-1}$ over soil while it was 8 $g.km^{-2}.y^{-1}$ over sea surface. No emissions from the surface covered by snow were assumed and used in the EMEP model. The reemissions of lead and cadmium were calculated based on modelled historical deposition loads and measurement data. The obtained numerical results are displayed in Figure 6-3, Figure 6-4 and Figure 6-5. It was assumed that natural emission and reemission fluxes of lead and cadmium are constant over the period of a year. The amounts of naturally emitted and reemitted mercury were split into months of the given year with the assumption that in summer months (April -September) the flux is 4 times higher compared to other months. The natural emissions and reemissions occur at ground level.

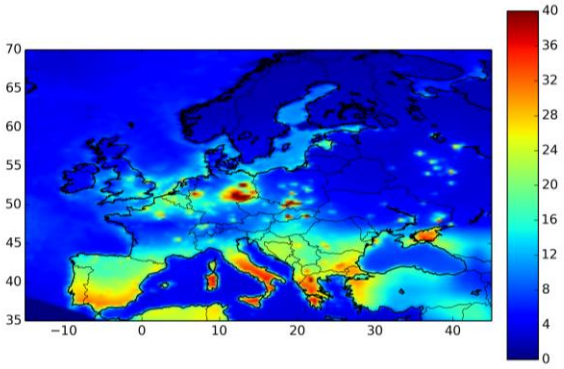

Figure 6-3. Natural emissions and reemissions of mercury over Europe [$g.km^{-2}.y^{-1}$], [29], [14].

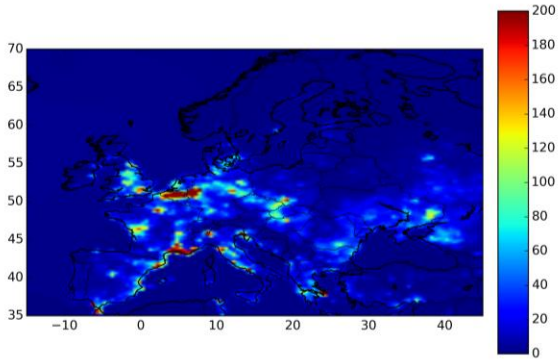

Figure 6-4. Natural emissions and reemissions of cadmium over Europe [g.km^{-2}.y^{-1}], [29], [14].

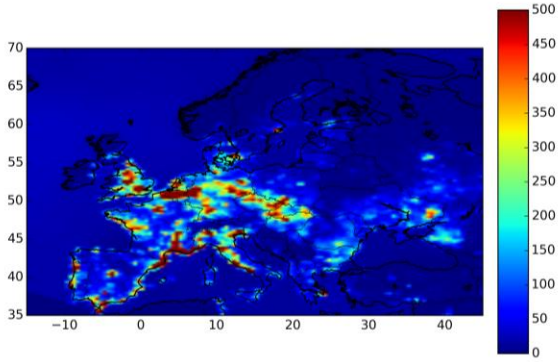

Figure 6-5. Natural emissions and reemissions of lead over Europe [g.km^{-2}.y^{-1}], [29], [14].

6.2.6 Anthropogenic emissions, simulations over Europe

For the simulation over Europe anthropogenic emission data of mercury, cadmium and lead provided by the EMEP programme were used [14]. The yearly emission fluxes (total for all sectors) are provided by EMEP with a horizontal resolution of approximately 50 km x 50 km based on emission data reported by the membership countries. The emission of heavy metals stored in a grid 50 km by 50 km were transformed to the simulation domain grids with the use of land use coverage (LUC) data with a horizontal resolution of 1 km by 1 km [247]. The 24 land use coverage categories are grouped into 4 main categories: urban, forest, water and others. The emissions from EMEP are distributed into all cells of LUC with the assumption that: (i) emissions from water equal 0, (ii) emissions of urban area cells are 16 times higher than those from cells with forests and 10 times higher than those from other areas. Finally, LUC cells and their emissions are assigned to cells of the simulations domains.

Anthropogenic emissions of these heavy metals disaggregated over the simulation domains are presented in Figure 6-6, Figure 6-7 and Figure 6-8.

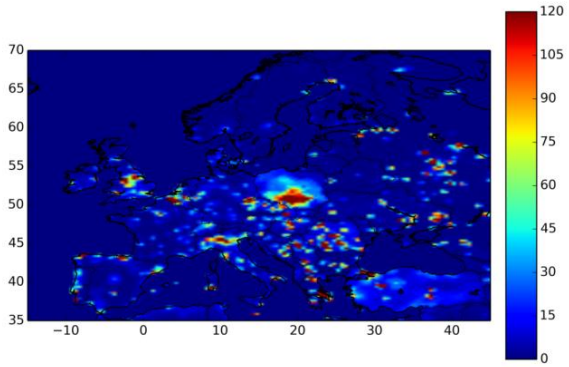

Figure 6-6. Anthropogenic emissions of mercury over Europe in 2008 due to EMEP [$g.km^{-2}.y^{-1}$], [14].

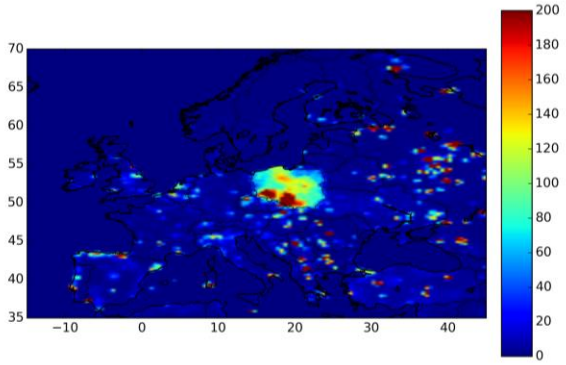

Figure 6-7. Anthropogenic emission of cadmium over Europe in 2008 due to EMEP [$g.km^{-2}.y^{-1}$], [14].

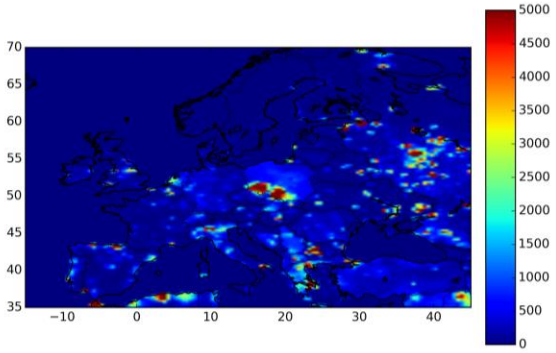

Figure 6-8. Anthropogenic emission of lead over Europe in 2008 due to EMEP [$g.km^{-2}.y^{-1}$], [14].

The anthropogenic mercury emissions provided by the EMEP inventory and presented in Figure 6-6 were disaggregated into its three main forms: GEM, RGM and Hg_P with the following speciation: 61%, 32%, 7%, respectively [84]. It was assumed that emissions of

reactive gaseous mercury (RGM) are equally distributed into four mercury compounds: $Hg(OH)_{2(g)}$, $HgBr_{2(g)}$, $HgO_{(g)}$, $HgCl_{2(g)}$ [29], [237]. Two options for distribution of the aerosol-bound mercury in ten size sections: (i) equal distribution or (ii) in proportion to the surface areas of aerosol size sections. Lead and cadmium were only equally distributed to 10 particulate matter section. This assumption was made based on measurements of physical speciation of heavy metals in inhalable particulate matter conducted in Spain [171]. The mass distribution of mercury, cadmium and lead was investigated in 6 size sections of aerosols. The mass distribution of heavy metals from measurements and considered in the simulation in PM sections are presented in Table 6-2.

Table 6-2. The mass distribution in PM size sections considered in the model and obtained from measurements.

N.	HM	PM size sections considered in the model [μm]										
1		0.01-0.02	0.02-0.0398	0.0398-0.0794	0.0794-0.1585	0.1585-0.3162	0.3162-0.631	0.631-1.289	1.2589-2.5119	2.5119-5.0119	5.0119-10	>10
2		Mass distribution of particulate-bound heavy metals tracked in simulation runs.										
3	Hg Pb Cd	10%	10%	10%	10%	10%	10%	10%	10%	10%	10%	0%
4		PM size sections of measured heavy metals content [μm] [171]										
5		0.00-0.61						0.61-1.3	1.3-2.7	2.7-4.9	4.9-10	
6		Measured mass distribution of particulate-bound heavy metals in PM sizes										
7	Hg	40%						8%	10%	13%	15%	14%
8	Pb	66%						9%	5%	4%	8%	8%
9	Cd	60%						10%	8%	6%	10%	9%

The corresponding distributions of mercury emissions into various forms, compounds and aerosol diameters are presented in Table 6-5, column B. In addition, one simulation was run with distribution of Hg_P in proportion to aerosol surfaces (Table 6-5, column B). It was assumed that the concentrations of emitted particulate matter (dust) in all considered size sections are the same. These emissions were split among the three lowest vertical levels with the rates presented in Table 6-3.

Table 6-3. Emission rates released at different levels [29].

N.	Limits of vertical levels [m]	Emission rate [%]		
		mercury	cadmium	lead
1	0-70	37	40	61
2	71-150	38	43	28
3	151-300	25	17	11

The temporal (monthly, weekly and hourly) emissions profiles presented in Table 6-4 were calculated based on: (i) EMEP data including emissions from different sectors over Europe

[87], (ii) time profiles of activity during a year for different sectors in Europe [255]. Emissions for each hour were provided as the product of these profiles. For example for 3:30 pm, 2th April 2008, the factors for April, Monday and for 4 pm were multiplied.

Table 6-4. Time profiles of emitted heavy metals in Europe.

N.												
1	hours	19-6		7-18								
2	Hg factors	0.93		1.07								
3	Cd factors	0.86		1.14								
4	Pb factors	0.87		1.13								
5	days	M	T	W	T	F	S	S				
6	Hg factors	1.05	1.06	1.07	1.06	1.06	0.86	0.84				
7	Cd factors	1.04	1.04	1.05	1.04	1.05	0.89	0.89				
8	Pb factors	1.04	1.05	1.05	1.04	1.05	0.88	0.89				
9	months	J	F	M	A	M	J	J	A	S	O	N	D
10	Hg factors	1.21	1.22	1.15	1.05	0.92	0.87	0.83	0.77	0.83	0.97	1.04	1.14
11	Cd factors	1.35	1.44	1.38	1.09	0.85	0.77	0.70	0.62	0.68	0.86	1.04	1.22
12	Pb factors	1.13	1.19	1.19	1.08	0.95	0.92	0.87	0.78	0.83	0.96	1.03	1.09

6.2.7 Anthropogenic emissions, simulation over Poland

For simulations over Poland, four variants of input sets of anthropogenic mercury emission were prepared.

1. "Base" –for all sectors (including the Polish power sector) data of anthropogenic mercury emissions of EMEP, and time profiles presented in Table 6-6 were used [84], [14]. The emissions were further split into forms, compounds and size sections of particle with the use of factors presented in Table 6-5 -column B. The horizontal and vertical transformation and disaggregation of emission proceeds identically as in the case of simulation on the European domain (chapter 6.2.6),.
2. "EF2008-fix" -calculated point emission of three forms of mercury emitted by the Polish power sector, based on emission factors for 2008 (chapter 5), fixed mercury speciation into form, compound and size section, presented in Table 6-5 -column F and time profiles from Table 6-8 were applied.
3. "EF2008" -calculated point emissions of three forms of mercury emitted by the polish power sector, based on emission factors for 2008 (chapter 5), the mercury split into mercury compound and size sections presented in Table 6-5 -column H and time profiles from Table 6-8 were used.
4. "EF2009" -point emissions of mercury, all forms, plants of Polish power sector, based on emission factors for 2009 (chapter 5), the speciation presented in Table 6-5 -column H and time profiles from Table 6-8 were also applied.

In the case of using point emissions for power sector (EF2008-fix, EF2008, EF2009) the EMEP emissions are used for other sectors i.e: (i) non-industrial combustion plants (SNAP 2), (ii) combustion in manufacturing industry (SNAP 3), (iii) production processes (SNAP 4), waste treatment and disposal (SNAP 9), (iv) petroleum refining plants (SNAP 0103), (v) solid fuel transformation plants (SNAP 0104) and (vi) coal mining, oil/gas extraction, pipeline compressors (SNAP 0105). The time profiles presented in Table 6-7 and speciation factors for mercury form presented in Table 6-5 -column D for these emission were applied. It was assumed that the emissions of mercury from sectors beyond the power sector are distributed equally into two lowest vertical level of the simulation domain. The horizontal disaggregation of these emissions were done in the same way as for the European domain (chapter 6.2.6).

In conclusion, in the sets "EF2008-fix" and "EF2008", the emissions from the Polish power sector (SNAP 0101 and SNAP 0102) are the same while the speciation into mercury form is different. On the other hand "EF2009" is characterized by different emissions of mercury from the power sector compared to previous cases.

In the case of the of different emissions from the power sector than EMEP in emission preprocessing program of Polyphemus, two additional steps were added. At the beginning, each cell of the EMEP database includes emissions for all sectors, the emissions from the Polish power sector included in "EF2008-fix", "EF2008" and "EF2009" were subtracted. Therefore, to further transformation from the EMEP grid to the simulation domain grid, disaggregation into forms/compounds of mercury (Table 6-5 -column D) and temporal profiles (Table 6-7) are applied only for emissions from all sectors beyond the Polish power sectors. Then, the emissions from the power sector of various mercury forms and compounds with relevant times profiles are added to individual cells.

The speciation factors presented in Table 2-8 were calculated based on factors proposed in the literature and emission of mercury in Poland from various source categories [84], [53]. In emission sets "Base", "EF2008-fix", "EF2008" and "EF2009", the aerosol-bound mercury was distributed equally among ten size sections (Table 6-5 -columns B, D, F, H). Additional simulation were run with the use of emissions of Hg_P distributed among ten size sections of aerosols in proportion to their surfaces (Table 6-5 -columns C, E, F, I). The emission sets were named respectively: "Base-PM", "EF2008-fix-PM", "EF2008-PM" and "EF2009-PM".

The simulations for lead and cadmium were run with two types of emissions sets. The first used only those provided by the EMEP with a resolution of 50 km by 50 km for 2008 for all sectors and the emitted cadmium and lead were split into vertical levels as presented in Table 6-3 and with temporal profiles presented in Table 6-6. The second simulation was run based

on (i) prepared amounts of emitted lead and cadmium together with location and height of stacks of power sector plants and (ii) emission from the EMEP for other sectors. The time profiles presented in Table 6-8 and Table 6-7 were applied respectively. The emissions of cadmium and lead were split equally among ten size of aerosols.

Table 6-5. Mercury distribution factors according to different forms, compounds and aerosol size sections of mercury used in simulation. The speciation in columns B-G –taken from [84].

N	A	B	C	D	E	F	G	H	I
1	Forms, species or aerosol section of mercury	All sectors, emission of EMEP, constant speciation, domain over Poland and Europe.		All sectors in except polish power sector, constant speciation, domain over Poland		Polish power sector EF2008-fix		Power sector, EF2008 and EF2009	
2	Hg^0	0.60		0.70		0.50		em_Hg^0	
3	Hg^{II}	0.32		0.23		0.40		em_Hg^{II}	
4	$Hg(OH)_2$	0.08		0.0575		0.10		$0.25 \cdot em\_Hg^{II}$	
5	$HgBr_2$	0.08		0.0575		0.10		$0.25 \cdot em\_Hg^{II}$	
6	HgO	0.08		0.0575		0.10		$0.25 \cdot em\_Hg^{II}$	
7	$HgCl_2$	0.08		0.0575		0.10		$0.25 \cdot em\_Hg^{II}$	
8	Hg_P	0.08		0.05		0.10		em_Hg_P	
9	Hg_P_0 size 0.01 - 0.02 μm	0.008	0.03996	0.005	0.02491	0.01	0.04990	$0.1 \cdot em\_Hg_P$	$0.4990 \cdot em\_Hg_P$
10	Hg_P_1 size 0.02 –0.0398 μm	0.008	0.02000	0.005	0.01250	0.01	0.02500	$0.1 \cdot em\_Hg_P$	$0.2500 \cdot em\_Hg_P$
11	Hg_P_2 size 0.0398 - 0.0794 μm	0.008	0.01004	0.005	0.00628	0.01	0.01256	$0.1 \cdot em\_Hg_P$	$0.1256 \cdot em\_Hg_P$
12	Hg_P_3 size 0.0794 –0.1585 μm	0.008	0.00503	0.005	0.00315	0.01	0.00630	$0.1 \cdot em\_Hg_P$	$0.0630 \cdot em\_Hg_P$
13	Hg_P_4 size 0.1585 –0.3162 μm	0.008	0.00252	0.005	0.00158	0.01	0.00316	$0.1 \cdot em\_Hg_P$	$0.0316 \cdot em\_Hg_P$
14	Hg_P_5 size 0.3162 –0.6310 μm	0.008	0.00126	0.005	0.00079	0.01	0.00158	$0.1 \cdot em\_Hg_P$	$0.0158 \cdot em\_Hg_P$
15	Hg_P_6 size 0.6310 –1.2589 μm	0.008	0.00063	0.005	0.00040	0.01	0.00080	$0.1 \cdot em\_Hg_P$	$0.0080 \cdot em\_Hg_P$
16	Hg_P_7 size 1.2589 –2.5119 μm	0.008	0.00032	0.005	0.00020	0.01	0.00040	$0.1 \cdot em\_Hg_P$	$0.0040 \cdot em\_Hg_P$
17	Hg_P_8 size 2.5119 –5.0119 μm	0.008	0.00016	0.005	0.00010	0.01	0.00020	$0.1 \cdot em\_Hg_P$	$0.0020 \cdot em\_Hg_P$
18	Hg_P_9 size 5.0119 –10 μm	0.008	0.00008	0.005	0.00005	0.01	0.00010	$0.1 \cdot em\_Hg_P$	$0.0010 \cdot em\_Hg_P$

The temporal (monthly, weekly and hourly) emission profiles were generated with the use of national emission data of mercury and activity data of different sectors in Poland [53], [255]. The results are presented in Table 6-6, Table 6-7 and Table 6-8.

Table 6-6. Time profiles of emitted heavy metals from all sectors in Poland.

N.			
1	hours	19-6	7-18
2	Hg factors	0.95	1.05

3	Cd factors	0.83		1.17									
4	Pb factors	0.84		1.16									
5	days	M	T	W	T	F	S	S					
6	Hg factors	1.05	1.05	1.07	1.07	1.06	0.88	0.83					
7	Cd factors	1.03	1.02	1.02	1.01	1.03	0.94	0.95					
8	Pb factors	1.05	1.05	1.05	1.05	1.05	0.87	0.88					
9	months	J	F	M	A	M	J	J	A	S	O	N	D
10	Hg factors	1.28	1.27	1.21	1.05	0.88	0.80	0.75	0.75	0.79	0.93	1.09	1.20
11	Cd factors	1.72	1.90	1.81	1.13	0.67	0.49	0.38	0.35	0.39	0.63	1.07	1.46
12	Pb factors	1.40	1.49	1.46	1.09	0.82	0.72	0.62	0.59	0.65	0.82	1.07	1.27

Table 6-7. Time profiles of emitted heavy metals from all sectors in Poland except national power sector.

N.													
1	hours	19-6		7-18									
2	Hg factors	0.88		1.12									
3	Cd factors	0.82		1.18									
4	Pb factors	0.83		1.17									
5	days	M	T	W	T	F	S	S					
6	Hg factors	1.06	1.05	1.06	1.05	1.06	0.86	0.86					
7	Cd factors	1.03	1.02	1.02	1.01	1.02	0.95	0.96					
8	Pb factors	1.05	1.05	1.05	1.04	1.05	0.87	0.88					
9	months	J	F	M	A	M	J	J	A	S	O	N	D
10	Hg factors	1.36	1.42	1.39	1.08	0.84	0.74	0.66	0.65	0.69	0.84	1.07	1.25
11	Cd factors	1.75	1.95	1.86	1.14	0.65	0.47	0.35	0.32	0.36	0.61	1.07	1.48
12	Pb factors	1.41	1.51	1.47	1.10	0.82	0.71	0.61	0.58	0.64	0.81	1.07	1.27

Table 6-8. Time profiles of emitted heavy metals (Hg, Cd, Pb) from Polish power sector.

N.													
1	hours	All hours											
2	factors	1											
5	days	M	T	W	T	F	S	S					
6	factors	1.04	1.05	1.08	1.08	1.06	0.89	0.80					
9	months	J	F	M	A	M	J	J	A	S	O	N	D
10	factors	1.21	1.15	1.06	1.03	0.91	0.85	0.82	0.83	0.87	1.00	1.10	1.17

The distribution factors presented in Table 6-5 -columns B or C and time profiles presented in Table 6-6 were used also to disaggregate emissions of mercury in neighbouring countries of Poland, which are included in the domain of the simulation. The time profiles in Table 6-6 were also used to disaggregate lead and cadmium in these countries. The EMEP emission data of mercury, cadmium and lead in all sectors in 2008 in these countries were used [14].

7 Results

In this chapter are presented the most important results. At the beginning, the generated results, which are used as the input data to mercury and other heavy metals model are presented and evaluated. From the meteorological results the evaluation of rain intensity is presented as this parameter has crucial influence on wet deposition load of heavy metals. The

dry deposition velocity for mercury forms is presented and discussed in reference to other research conducted in this area. Afterwards, the obtained results of the ambient concentrations of species that react with mercury are presented and evaluated against observations. Finally, the evaluation for mercury, lead and cadmium results is carried out. For this evaluation, the observations from the EMEP network were used. The EMEP stations measure mainly the background concentrations and deposition of pollutants. This means that the impact of local sources on the measured values is minimized, mainly thanks to site locations far away from urban and industry areas with strong emission sources. In the evaluations, the average values of observed and model results, Pearson product-moment correlation coefficient (correlation) and root mean square error (RMSE) are calculated and presented. The evaluation of modelled results is presented for the European domain because this domain covers the locations of many European observation sites. In the domain over Poland, fewer stations are located.

The Pearson product-moment correlation coefficient is defined as follows:

$$\text{correlation} = \frac{\sum_{i=1}^{n}(o_i-\overline{o})(s_i-\overline{s})}{\sqrt{\sum_{i=1}^{n}(o_i-\overline{o})^2}\sqrt{\sum_{i=1}^{n}(s_i-\overline{s})^2}} \qquad \text{R.7.1}$$

and the root mean square error (RMSE) is calculated with the following relationship

$$RMSE = \sqrt{\frac{1}{n}\sum_{i=1}^{n}(o_i - s_i)^2} \qquad \text{R.7.2}$$

o –observation results value,

s –simulation results value,

$\overline{o}$ –mean from observation results,

$\overline{s}$ –mean from observation results,

n –numbers of pairs of results (observation and simulation).

The evaluated models were used to run 150 simulations, which allowed one to obtain various results. These results are presented and discussed in this chapter as well. The selected results are dedicated mainly to: spatial distribution over Europe, sensitivity analyses, contribution of various sources to deposition in Poland, and the impact of the polish power sector. All results are for 2008.

In this thesis, only the evaluation of the modelled results for the European domain measurements is presented despite the fact that the evaluation of the results was also the conducted over Polish domain. In this work, the modelled results from the domains over

Europe and Poland and their evaluations for particular stations are quite similar and relatively small differences have been noticed. The cause for the observed differences in the modelled results from Eulerian models run which the use of various domains and modelling resolutions is very complex and may results from several main factors, such as the issue of representativeness [259]. Therefore the discussion and comparison of results from various domain sizes and resolutions was omitted here because this was not the aim of this thesis.

7.1 Evaluation of intensity of precipitation

The monthly rain intensity data provided by the ECMWF and processed by Polyphemus meteorological pre-processing program were compared against measurements conducted at the EMEP stations [248], [163]. The corresponding results are presented in Table 7-1. In this table, the results are presented for stations where mercury wet deposition was observed and aggregated results for all 53 stations operated in 2008 for EMEP and located within the European domain are also presented.

Table 7-1. Evaluation of monthly results of intensity of precipitation [mm] from the meteorological pre-processing run over the European domain with the use of ECMWF database and measurements of in stations of EMEP [248], [163].

N.	Stations code	Number of month with valid observations	Annual intensity of precipitation in EMEP stations [mm.year^{-1}]	Annual intensity of precipitation used the in model [mm.year^{-1}]	Correlation coefficient	RMSE [mm.month^{-1}]
1	BE14	12	586	1036	0.81	42
2	DE01	12	838	1156	0.96	33
3	DE02	12	658	768	0.87	18
4	DE03	12	1611	1332	0.77	36
5	DE08	12	1119	978	0.34	41
6	DE09	12	533	740	0.67	25
7	ES08	11	1453	1469	0.91	95
8	FI36	12	320	798	0.93	42
9	GB13	12	1227	1303	0.71	32
10	GB17	9	471	626	0.59	29
11	GB48	12	919	1152	0.79	35
12	GB91	12	613	986	0.29	51
13	LV10	12	939	1108	0.96	20
14	LV16	12	824	960	0.82	21
15	NL91	12	771	1119	0.91	34
16	NO01	12	1797	1660	0.95	36
17	PL04	12	674	858	0.89	21
18	PL05	12	592	805	0.54	28
19	SE14	12	718	1228	0.81	54
20	SI08	12	1159	1125	0.71	41
21	All	625	41948	53388	0.79	36

All–results for all observations from 53 stations located inside European domain, where precipitation intensity was measured together with heavy metals concentrations in precipitation.

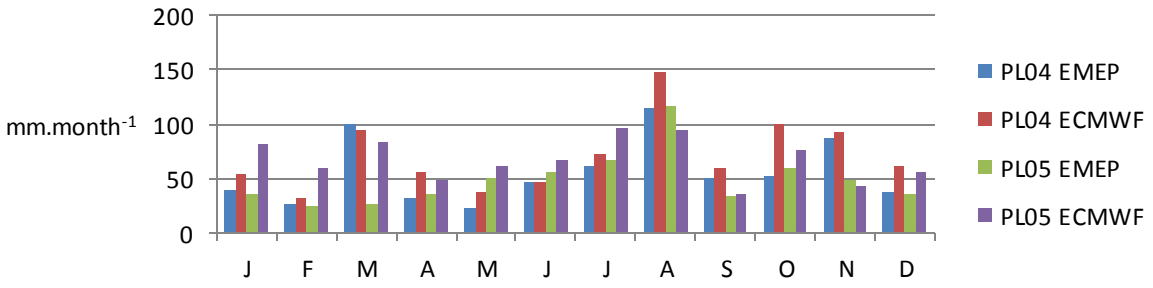

Figure 7-1. The monthly intensity of precipitation [mm] from the meteorological pre-processing run over the European domain with the use of ECMWF database and measurements at the EMEP stations located in Poland PL04 –Łeba and PL05 –Diabla Góra.

The annual amounts of precipitation intensity used in the model are 27% higher than at the EMEP stations observed. The average annual precipitation intensity observed at EMEP stations and extracted from ECMWF are 806 $mm.y^{-1}$ and 1025 $mm.y^{-1}$, respectively.

At the same stations i.e. BE14, FI36 the observed preparation rates are two times lower than in the EMCWF database. Generally, the stations located near the sea measured higher precipitation intensity compared to stations within the main land. However, the PL05 station located in Łeba has a relatively low precipitation intensity. In Poland, in 2008 the highest of precipitation rates were observed in March and in August. The monthly results from the EMEP and EMCWF are highly correlated.

7.2 Dry deposition velocity for mercury species

With the use of a pre-processing program the dry deposition velocity fields were generated and were used to calculate the dry deposition flux of mercury. The generated yearly average values of dry deposition velocities for gaseous elemental mercury (GEM) and reactive gaseous mercury (RGM) from all cells in the European domain for meteorological parameters recorded every 3 hours for different land types are presented in Figure 7-2. The average dry deposition velocity of these forms in simulation domain are presented in Figure 7-3 and Figure 7-4. The monthly average dry deposition velocity of GEM and RGM in cell where Krakow is located is presented in Figure 7-5.

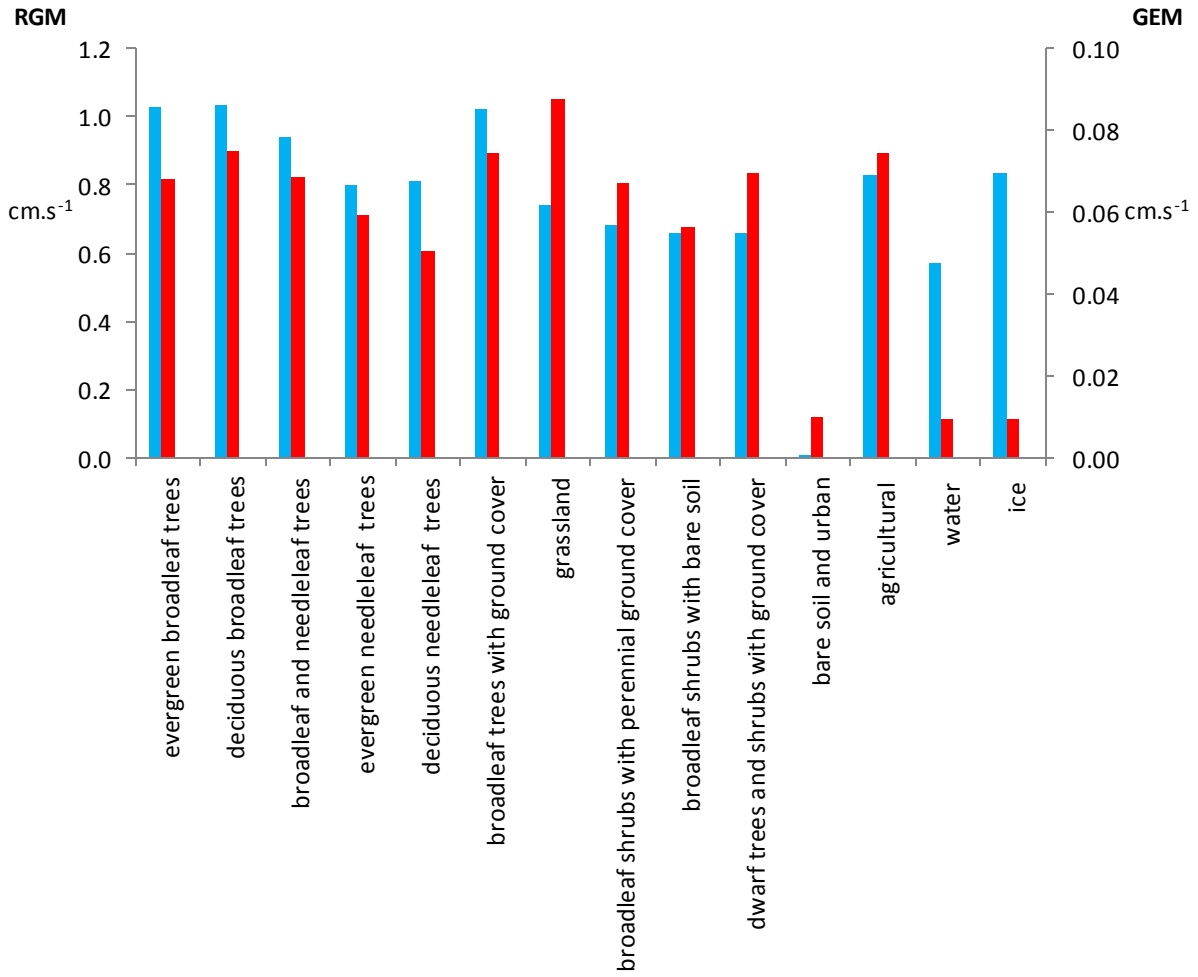

Figure 7-2. The average dry deposition velocity of RGM (blue, left axis) and GEM (red, right axis) for different land types over Europe [cm.s^{-1}].

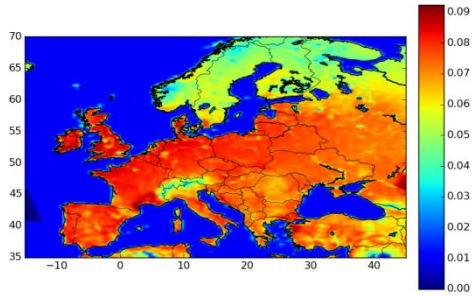

Figure 7-3. Annual average dry deposition velocity of GEM [cm.s^{-1}].

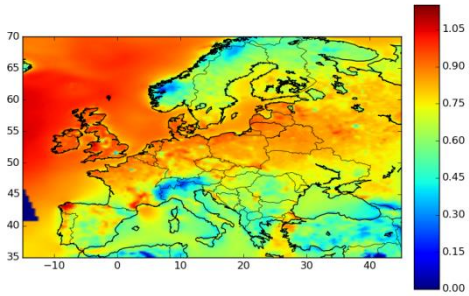

Figure 7-4. Annual average dry deposition velocity of RGM [cm.s^{-1}].

The dry deposition velocity of RGM is around 12 times higher compared to GEM (Figure 7-2). The presented results are consistent with the measurements conducted in many places of

the world [176]. Over the urban and bare soil areas, the dry deposition velocity is low for both RGM and GEM. This is contrary to the modelling results with the use of resistance model for typical daytime condition (wind 6m.s^{-1} at 10 m), which showed a relatively high dry deposition velocity for urban area [176]. Generally, the obtained results are higher than assumed in the CTM-Hg model and were calculated in MSCE-HM-Hem model. In the CTM-Hg dry deposition velocities of 0.25 cm.s^{-1} for RGM and 0.01 cm.s^{-1} over land for GEM were assumed, while in MSCE-HM-Hem a dry velocity of GEM from 0 to 0.03 cm.s^{-1} was calculated. The large differences in value of dry deposition velocity are observed between land and water surfaces (Figure 7-3). The low dry deposition velocity over water is caused by low solubility of GEM.

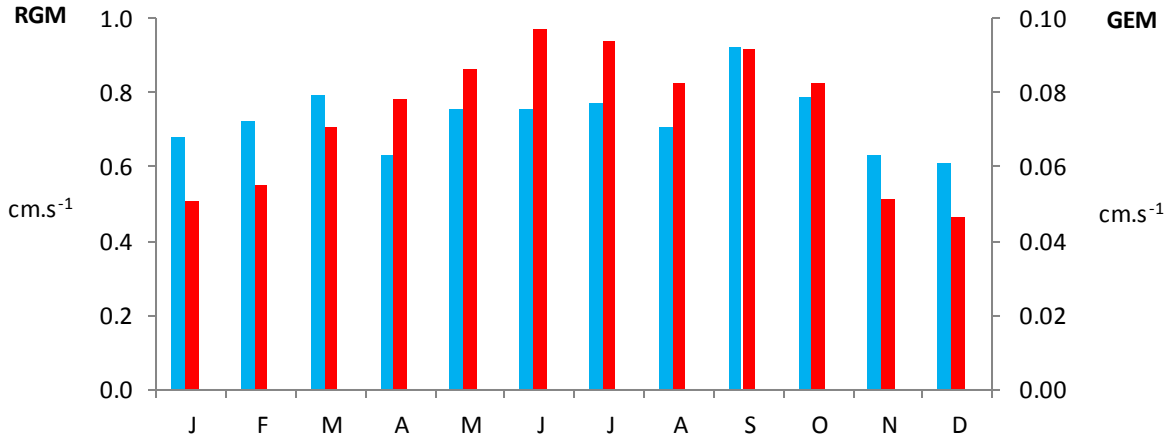

Figure 7-5. The monthly average dry deposition velocity of RGM (blue, left axis) and GEM (red, right axis) in modelling cell where Kraków is located [cm.s^{-1}].

The generated dry deposition velocity of GEM is highest in summer, while in the winter it is approximately 50% lower. For RGM, this parameter is characterized by relatively lower yearly variation, but the highest value is observed during spring and autumn, as presented in Figure 7-5.

7.3 Results and evaluation of concentrations of species that react with mercury

The concentrations of sulphur dioxide ($SO_{2(g)}$), ozone ($O_{3(g)}$), hydrogen peroxide ($H_2O_{2(g)}$), nitrate radical ($NO_3^{\bullet}{}_{(g)}$), peroxyl radical ($HO_2^{\bullet}{}_{(g)}$), hydroxyl radical ($^{\bullet}OH_{(g)}$), and black carbon

aerosol (BC) are presented in Figure 7-6 -Figure 7-31. The maps of the concentration are presented for a domain over Poland, while the time profiles of concentrations in cells where selected stations of EMEP are located and concentrations in 10 vertical levels are the results of simulations run over the European domain. It should be noted that the concentrations at 10 levels are given in $\mu g.m^{-3}$ and the changes of atmospheric pressure and density of air affect the presented quantitative results. The maps from the European domain are not presented because similar results for Europe are frequently presented in scientific reports and articles i.e. EMEP. On the other hand the maps that show the detailed modelled concentrations of compounds as hydrogen peroxide ($H_2O_{2(g)}$), peroxyl radical ($HO_2^{\bullet}{}_{(g)}$), hydroxyl radical ($^{\bullet}OH_{(g)}$) over Poland have not been presented yet and are, therefore, of interest. The nitrate radical ($NO_3^{\bullet}{}_{(g)}$) was presented for the European domain because it was modelled and then used only in this domain. The nesting approach was applied –the results in the European domain were used as the boundary condition for the domain over Poland. The evaluation of modelling results of $SO_{2(g)}$ and $O_{3(g)}$ against observations at EMEP stations was also presented in Table 7-2, Table 7-3 and Table 7-4. In these tables, the detailed results are presented for stations where mercury air concentration or wet deposition was measured in 2008 and at all stations located in Poland. The presented results were shortly discussed, but it should be noted that the atmospheric behaviour of the considered species is complex and only some possible mechanisms and explanations are presented without going into details.

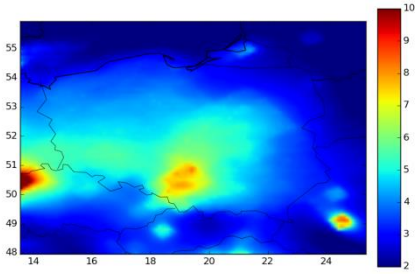

Figure 7-6. Annual average concentrations of $SO_{2(g)}$ [$\mu g.m^{-3}$] in the surface.

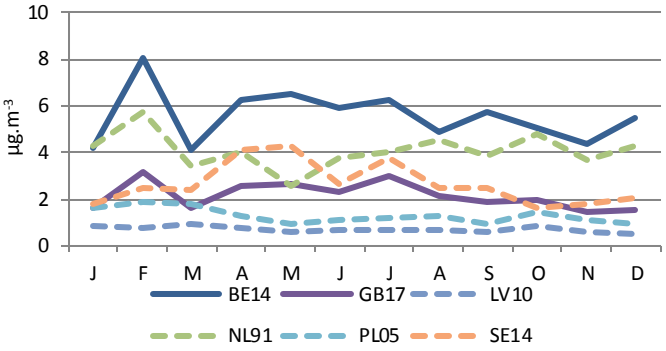

Figure 7-7. Monthly average modelled concentrations of SO_2 [$\mu g.m^{-3}$] in the surface at selected stations.

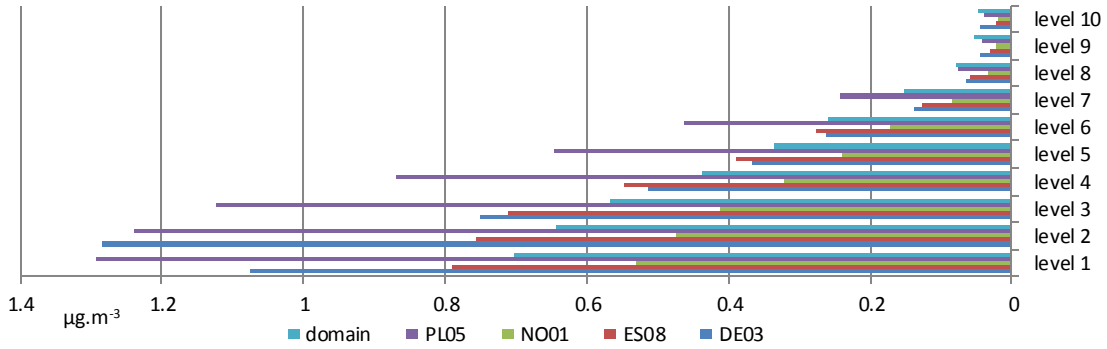

Figure 7-8. Annual average concentrations of $SO_{2(g)}$ [µg.m^{-3}] at vertical 10 levels according to the vertical split of simulation domain e.g. level 1 –the lowest, surface level from 0 to 70 m above ground, level 10 –the highest from 3000 to 5000 m above ground.

The highest concentration of $SO_{2(g)}$ occurs over southern Poland where the most of the Polish power plants are located (Figure 7-6). In Poland, more than half of sulphur dioxide is emitted from the power sector (SNAP 01), whereas a quarter of sulphur dioxide is emitted from coal combustion in the residential sector (SNAP 02). The emissions from this sector occurs mainly during the winter season, which may explain the highest $SO_{2(g)}$ concentration in winter in cells where station PL05 is located (Figure 7-7). As presented in Figure 7-9, the highest ambient concentration is observed near the surface and decreases significantly with altitude.

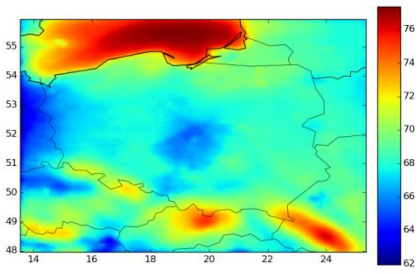

Figure 7-10. Annual average concentrations of $O_{3(g)}$ [µg.m^{-3}] at the surface.

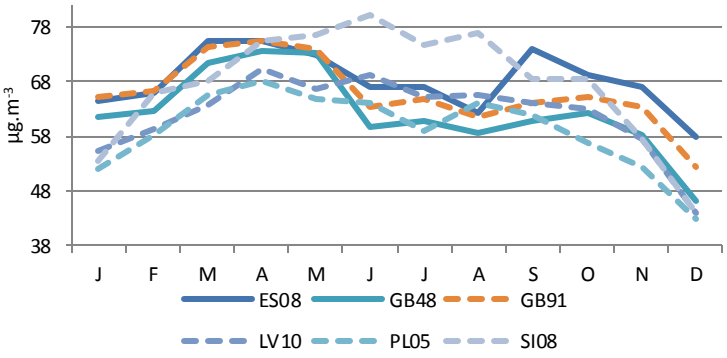

Figure 7-11. Monthly average concentrations of $O_{3(g)}$ [µg.m^{-3}] at the surface at selected stations.

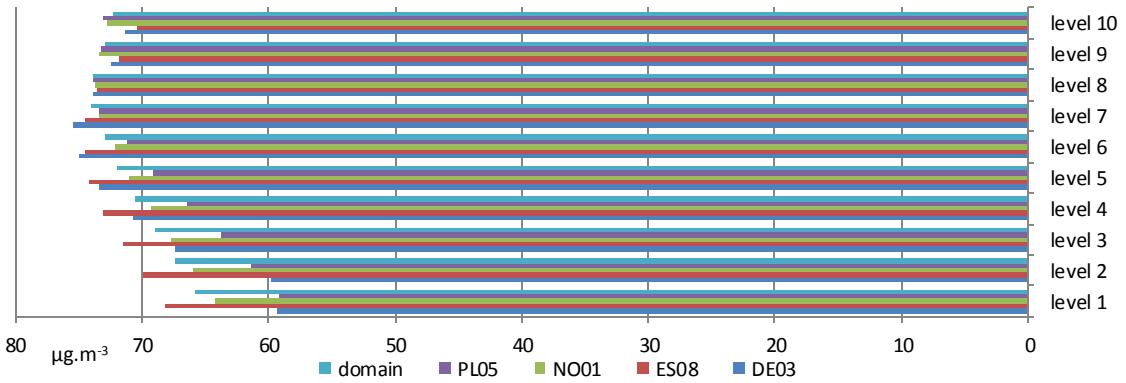

Figure 7-12. Annual average concentrations of $O_{3(g)}$ [µg.m^{-3}] at 10 vertical levels.

The ambient concentrations of ozone presented in Figure 7-10 is highest over the sea because of low dry deposition velocity over water surfaces, which is shown in Figure 4-4. The results presented in Figure 7-11 and Figure 7-12 show that the concentrations of ozone over land in Europe is relatively of the same magnitude, and the differences in annual modelled concentration in various location do not exceed 20%. The maximal modelled concentration is noticed in levels 6 -8, i.e. 750 -3000 meters above surface. At most of the stations, the lower concentration occurs during the winter season. It results from lower solar radiation in the northern hemisphere during winter.

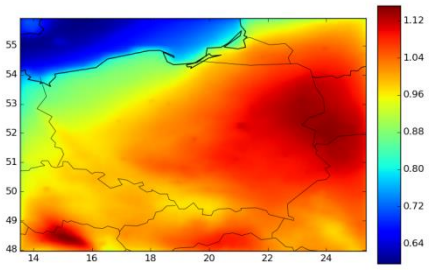

Figure 7-13. Annual average concentrations of $H_2O_{2(g)}$ [µg.m^{-3}] at the surface.

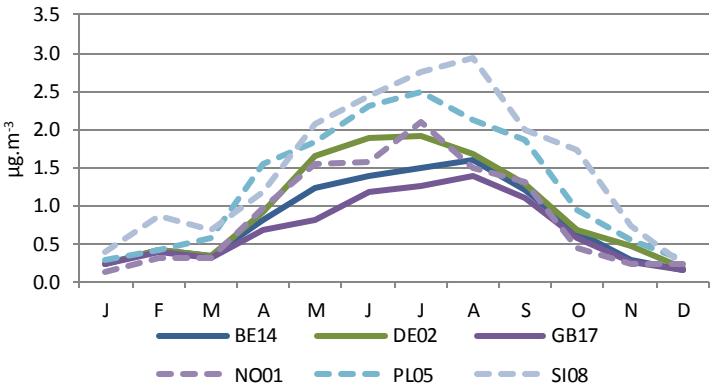

Figure 7-14. Monthly average concentrations of $H_2O_{2(g)}$ [µg.m^{-3}] at the surface at selected stations.

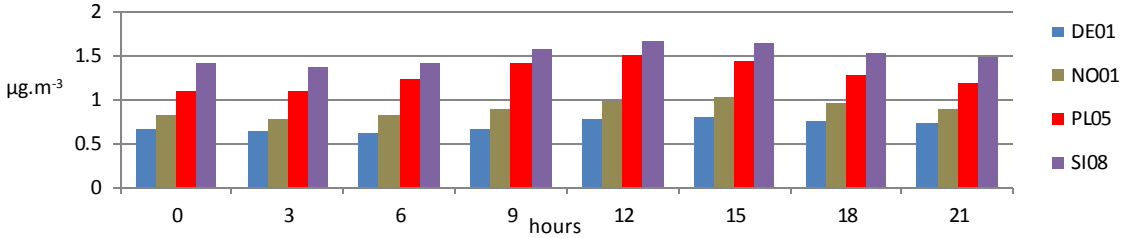

Figure 7-15. Annual average concentrations of $H_2O_{2(g)}$ [µg.m^{-3}] in hours of day at the surface level.

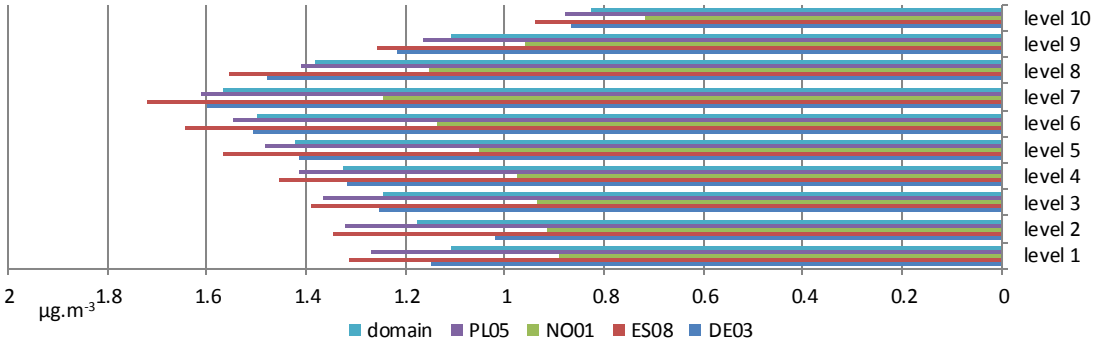

Figure 7-16. Annual average concentrations of $H_2O_{2(g)}$ [µg.m^{-3}] at 10 vertical levels.

The ambient concentrations of hydrogen peroxide show large spatial and seasonal variations (Figure 7-13 and Figure 7-14). The lower concentrations are noticed over sea and during the winter. Over land, the $H_2O_{2(g)}$ concentrations are 30-50% higher compared to concentrations over sea. During the summer, the $H_2O_{2(g)}$ concentration is 15 times higher than in winter. Vertical variations are not very large, however the clear maximum is visible in Figure 7-16 at level 7 ranging in altitudes from 1000 to 2000 meters. The results presented in Figure 7-15 show that the day and night time mechanisms of atmospheric production and consumption of $H_2O_{2(g)}$ are similarly efficient, because no high daily variation in $H_2O_{2(g)}$ ambient concentrations at the surface level are observed.

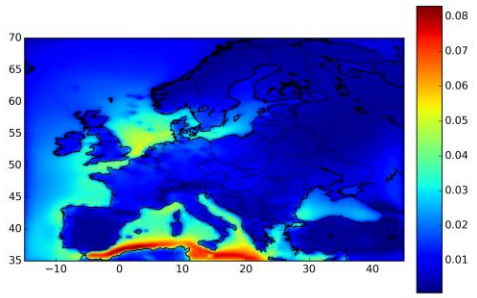

Figure 7-17. Annual average concentrations of $NO_3^{\bullet}{}_{(g)}$ [µg.m^{-3}] in the surface level.

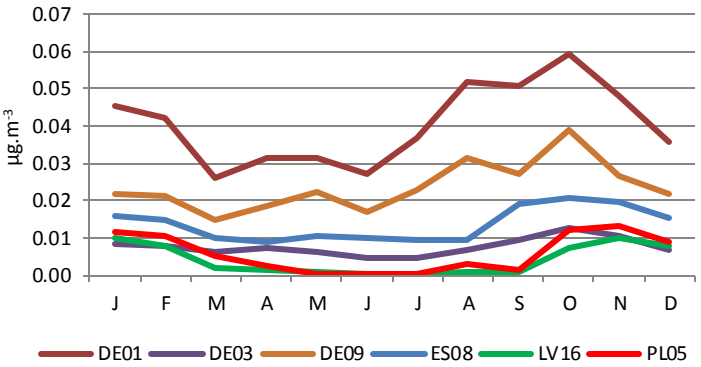

Figure 7-18. Monthly average concentrations of $NO_3^{\bullet}{}_{(g)}$ [µg.m^{-3}] at the surface level at selected stations.

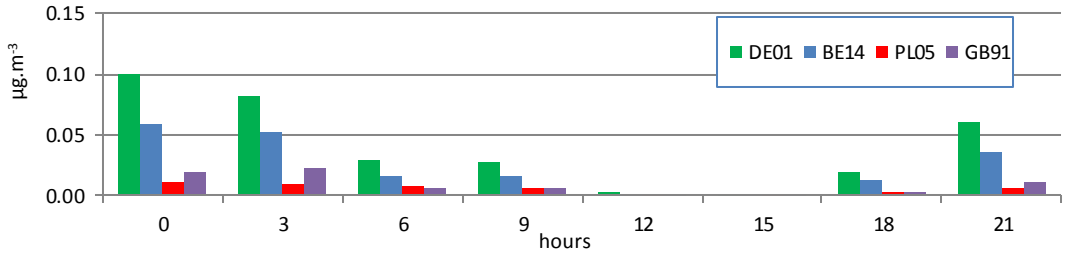

Figure 7-19. Annual average concentrations of $NO_3^{\bullet}{}_{(g)}$ [µg.m^{-3}] in hours of day at the surface.

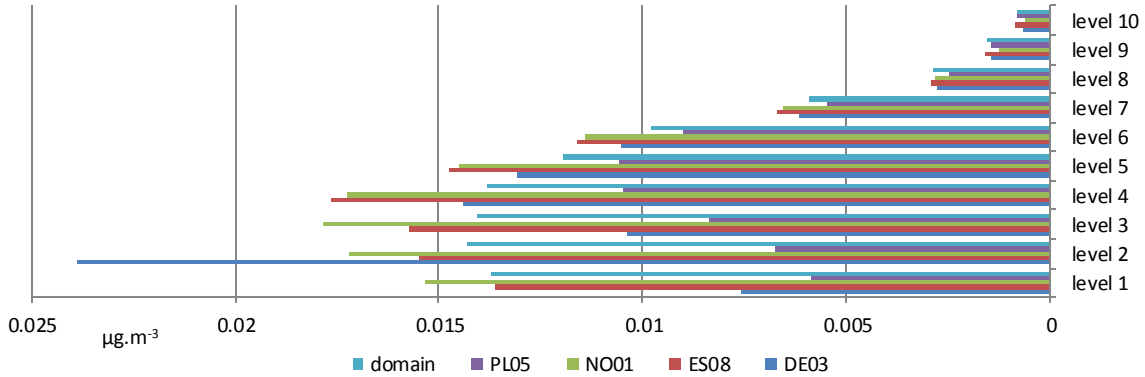

Figure 7-20. Annual average concentrations of $NO_3^{\bullet}{}_{(g)}$ [µg.m^{-3}] at 10 vertical levels.

The ambient concentration of nitrate radical is higher over the sea as shown in Figure 7-17 and Figure 7-18. The reason for this is that there are higher ozone concentrations over the sea and ozone is involved in the production reaction of $NO_3^{\bullet}{}_{(g)}$. The concentration of $NO_3^{\bullet}{}_{(g)}$ during the day quickly disappears due to photolysis, which was reported in previous articles where the reaction of $NO_3^{\bullet}{}_{(g)}$ with mercury was discussed [15]. The concentrations of $NO_3^{\bullet}{}_{(g)}$ increase with altitude up to approximately 500 meters and then decrease.

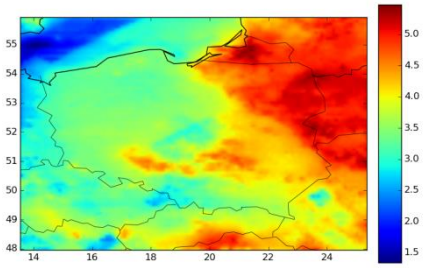

Figure 7-21. Annual average concentrations of $HO_2^{\bullet}{}_{(g)}$ [ng.m^{-3}] at the surface.

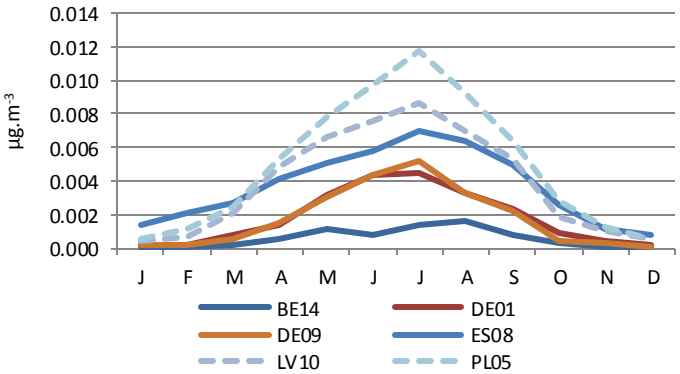

Figure 7-22. Monthly average concentrations of $HO_2^{\bullet}{}_{(g)}$ [µg.m^{-3}] at the surface at selected stations.

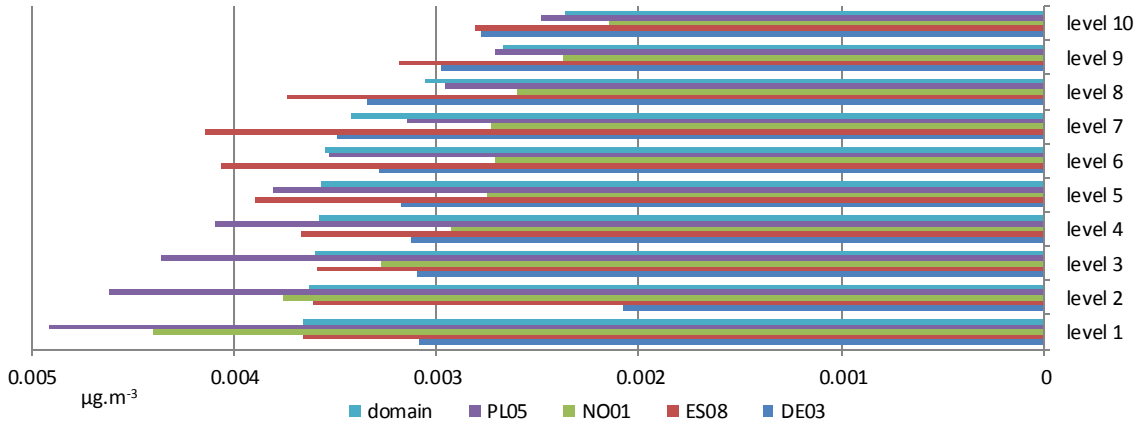

Figure 7-23. Annual average concentrations of $HO_2^{\bullet}{}_{(g)}$ [µg.m^{-3}] at vertical 10 levels.

The average yearly ambient concentration of peroxyl radical ranges from 3.0 ng.m^{-3} over the west and south of Poland to 5.0 ng.m^{-3} over north-east parts (Figure 7-21). The highest values were noticed in summer because the peroxyl radical is produced in various photochemical reactions (Figure 7-22). The vertical changes of ambient concentrations are diverse for various location (Figure 7-23).

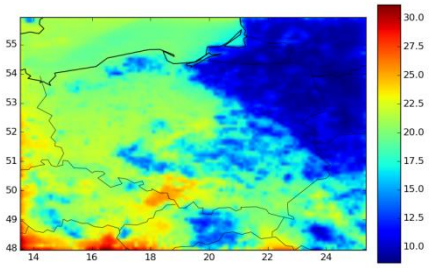

Figure 7-24. Annual average concentrations of $^{\bullet}OH_{(g)}$ [pg.m^{-3}] at the surface level.

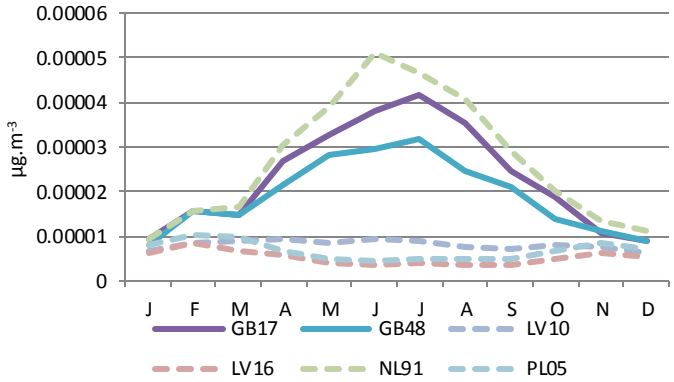

Figure 7-25. Monthly average concentrations of $^{\bullet}OH_{(g)}$ [µg.m^{-3}] in 2008 at the surface at selected stations.

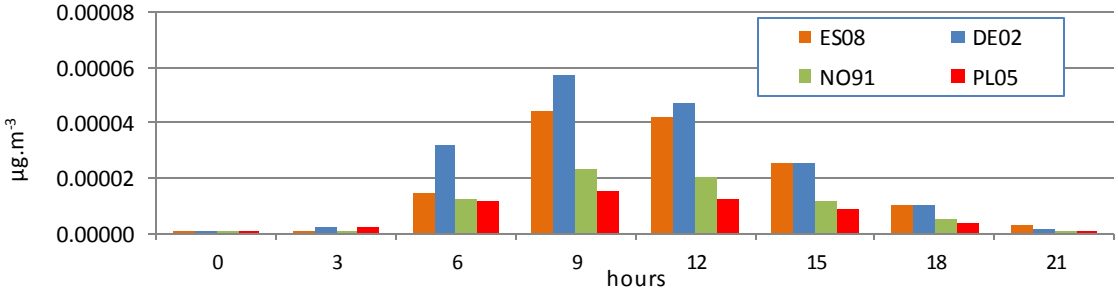

Figure 7-26. Annual average concentrations of $^{\bullet}OH_{(g)}$ [µg.m^{-3}] in hours of day at the surface.

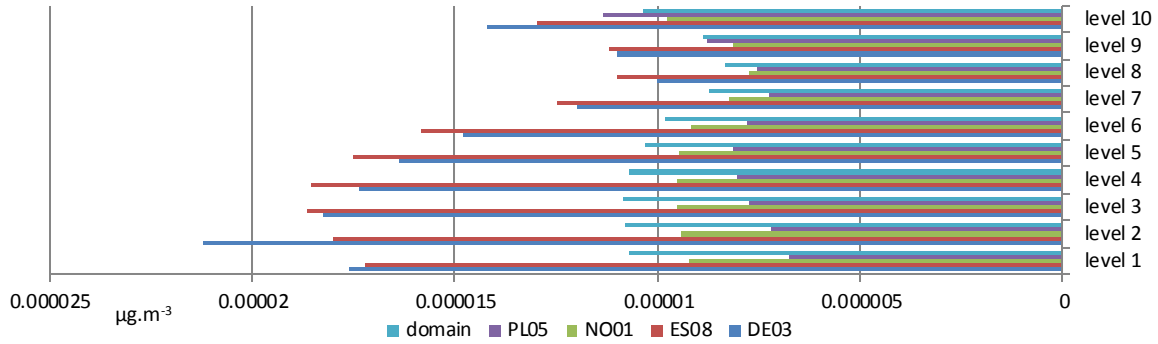

Figure 7-27. Annual average concentrations of $^{\bullet}OH_{(g)}$ [µg.m^{-3}] at vertical 10 levels.

The hydroxyl radical is produced in photochemical reactions, therefore, the maximum of generation appears in summer and during the day (Figure 7-25 and Figure 7-26). The maximum concentrations occur in the levels 2 -5 from 70 to 750 meters above ground. Over Poland, the concentrations of hydroxyl radical are inversely proportional to concentration of peroxyl radical as are presented in Figure 7-21 and Figure 7-24. In the atmosphere, there are many reactions that lead to the production of peroxyl radical from hydroxyl radical and vice-versa [95]. The results presented in Figure 7-21 and Figure 7-24 lead to the conclusion that the production hydroxyl radical from peroxyl radical is very slight, over Poland. Despite the increase of the ambient concentration of peroxyl radical the concentration of hydroxyl radical decreases. The average yearly ambient concentration of hydroxyl radicals is relatively low and reaches tens of picograms per cubic meter of air.

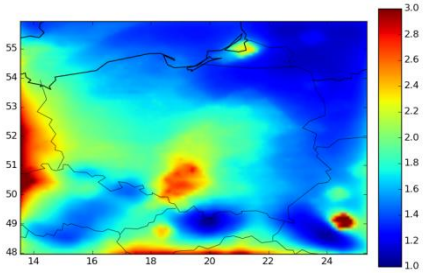

Figure 7-28. Annual average concentrations of black carbon [µg.m^{-3}] at the surface.

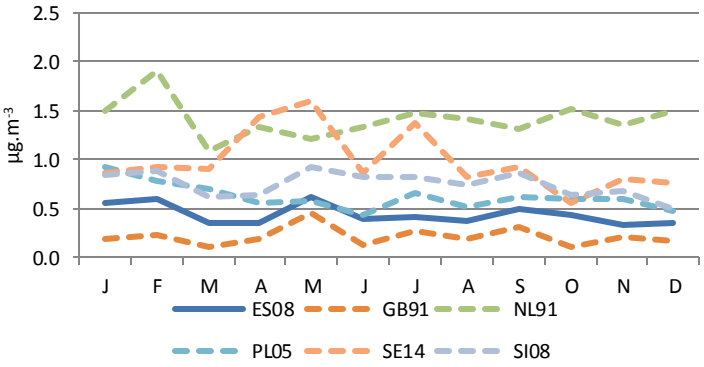

Figure 7-29. Monthly average concentrations of black carbon [µg.m^{-3}] at the surface at selected stations.

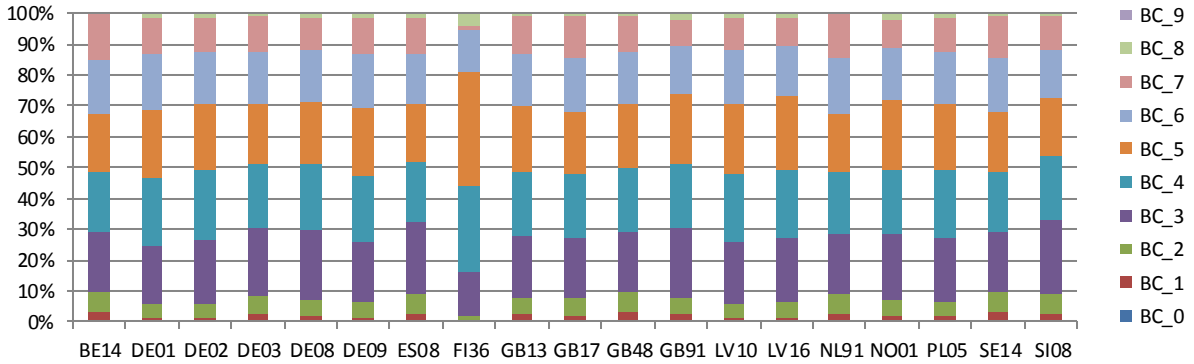

Figure 7-30. The share of different size section in total concentration of black carbon [µg.m^{-3}] in all cells at the surface. BC_0, BC_1, BC_2, BC_3, BC_1 , BC_1 , BC_1 , BC_1 are black carbon particle size sections with the following threshold limits [in µm] 0.01 - 0.02 - 0.0398 - 0.0794 - 0.1585 - 0.3162 - 0.6310 - 1.2589 - 2.5119 - 5.0119 -10, respectively.

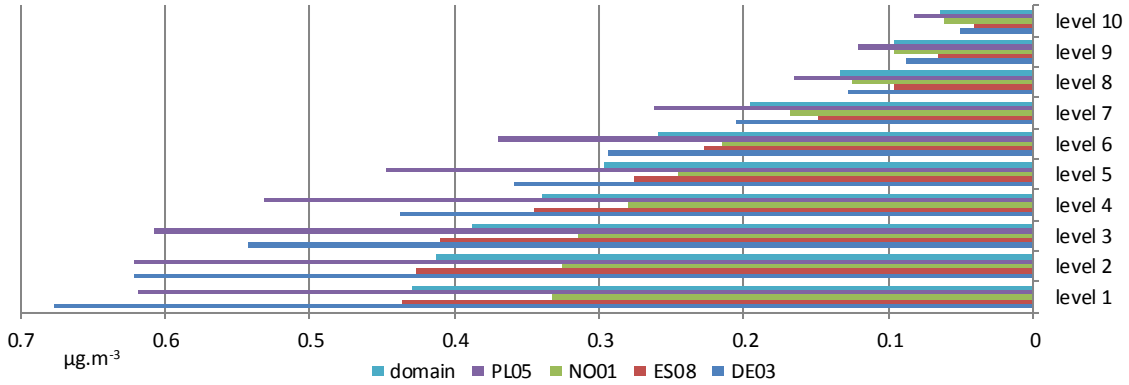

Figure 7-31. Annual average concentrations of black carbon [µg.m^{-3}] at 10 vertical levels.

The results presented in Figure 7-28 show that the most polluted area of Poland by black carbon is Silesia. The ambient concentration of black carbon does not vary significantly as it is presented in Figure 7-29. The ambient concentrations of black carbon decrease together with altitude (Figure 7-31). The main share in overall concentrations correspond to particulate matter with representative diameters from 0.1585 µm to 2.5119 µm.

Table 7-2. Evaluation of results of $O_{3(g)}$ concentrations from simulation run over the European domain at the surface against measurements of EMEP [163]. The concentrations were measured with time step of 1 hour.

N.	Stations code	Share of valid observations	Average annual observed concentration [µg.m^{-3}]	Average annual modelled concentration [µg.m^{-3}]	RMSE [µg.m^{-3}]	Correlation coefficient
1	CZ03	0.985	62.0	60.4	19.1	0.72
2	DE02	0.952	52.7	56.9	22.5	0.78
3	DE03	0.958	79.1	59.2	27.7	0.48
4	DE08	0.956	68.2	59.2	23.5	0.62
5	DE09	0.948	54.8	59.9	18.2	0.75

6	ES08	0.989	69.0	68.1	16.3	0.47
7	GB13	0.887	60.9	67.8	16.7	0.61
8	GB48	0.977	60.4	62.3	14.9	0.68
9	LV10	0.810	55.4	61.9	23.5	0.51
10	LV16	0.800	52.9	58.9	18.9	0.45
11	NL91	0.845	47.9	50.9	19.6	0.73
12	PL02	0.991	52.4	58.0	19.7	0.68
13	PL03	0.964	83.2	61.6	29.6	0.63
14	PL04	1.000	62.7	63.6	19.7	0.68
15	PL05	0.992	54.0	59.1	21.9	0.60
16	SE14	0.996	61.7	61.2	17.2	0.63
17	All	0.951	62.9	62.5	22.3	0.59

All–results for all observations from 113 stations located inside the European domain, where $O_{3(g)}$ concentrations were measured and the share of valid results exceeded 75%.

In general, the observed and modelled yearly average of ambient concentrations of ozone are similar (Table 7-2). However, at station PL03 located in Śnieżka the modelled concentration is lower approx. 20 $\mu g.m^{-3}$. The high measured concentration of ozone probably results from the location of the station at 1603 meters above sea level. The correlation coefficients are higher than 0.6 at 12 stations where mercury concentration or deposition was also observed in 2008. For all 113 stations correlation coefficients are equal 0.59.

Table 7-3. Evaluation of results of sulphur dioxide concentrations from simulation run over the European domain at the surface against measurements of EMEP [163]. The concentrations were measured with time step of 1 hour.

N.	Stations code	Share of valid observations	Average annual observed concentration [$\mu g.m^{-3}$]	Average annual modelled concentration [$\mu g.m^{-3}$]	RMSE [$\mu g.m^{-3}$]	Correlation coefficient
1	CZ03	1.000	1.15	1.25	1.13	0.22
6	ES08	0.993	0.79	0.78	1.13	0.30
11	NL91	0.750	1.07	4.05	3.67	0.23
17	All	0.965	0.82	1.11	1.62	0.23

All–results for all observations from 19 stations located inside the European domain, where $SO_{2(g)}$ concentrations were measured and the share of valid results exceeded 75%.

Table 7-4. Evaluation of results of sulphur dioxide concentration from simulation run over the European domain at the surface against measurements of EMEP [163]. The concentrations were provided with time step of 1 day.

N.	Stations code	Share of valid observations	Average annual observed concentration [$\mu g.m^{-3}$]	Average annual modelled concentration [$\mu g.m^{-3}$]	RMSE [$\mu g.m^{-3}$]	Correlation coefficient
2	DE02	0.651	0.44	1.31	1.04	0.44
3	DE03	0.676	0.20	1.11	1.11	0.04
4	DE08	1.000	0.54	1.05	0.72	0.40
5	DE09	0.648	0.50	1.46	1.16	0.46
9	LV10	1.000	0.40	0.70	0.63	0.39
10	LV16	1.000	0.29	0.34	0.35	0.31
12	PL02	0.986	1.75	3.08	1.89	0.38

13	PL03	0.997	1.06	4.79	5.53	0.01
14	PL04	0.989	1.03	1.25	0.84	0.53
15	PL05	0.986	0.58	1.29	1.07	0.51
16	SE14	0.981	0.32	2.78	2.81	0.98
17	All	0.960	0.49	1.30	1.74	0.34

All–results for all observations from 25 stations located inside he European domain, where $SO_{2(g)}$ concentrations were measured and the share of valid results exceeded 75%.

The modeled results of $SO_{2(g)}$ are in general overestimated by 2.5 times compared to observations. Moreover, the correlation coefficient is low. In case of evaluation against 1 hour observation it is equal to 0.23 and for 1 day observation it is 0.34. The performed results of $O_{3(g)}$ and $SO_{2(g)}$ evaluations agree with previous evaluation which had been done for the European simulation with the use of Polyphemus air quality system [203], [204]. The averages results and the correlation coefficient for $O_{3(g)}$ are very satisfactory, while the modelled $SO_{2(g)}$ is overestimated and the correlation coefficients are around 0.3.

7.4 Evaluation of mercury concentrations and deposition

The mercury dispersion models are usually evaluated against measurements of concentrations in ambient air and wet deposition (e.g. [183]). Due to the lack of separate measurements of the atmospheric concentrations of reactive gaseous mercury at the EMEP station, the concentration of mercury is dominated by a high concentration of elemental gaseous mercury, which is up to a dozen times higher than the concentration of its other forms. The relatively long residence time of GEM in the atmosphere makes it rather evenly distributed in the global atmosphere. Therefore, the modelled concentration of elemental gaseous mercury does not provide too much information on the scientific correctness of the applied model. However, elemental gaseous mercury is poorly removed in scavenging processes, therefore mercury measured in precipitation depends mostly on concentrations of reactive gaseous mercury and mercury bound to aerosols in ambient air. These forms are dispersed in the atmosphere locally and their deposition pattern strongly depends on local sources and chemistry of mercury in the atmosphere.

The results of the model comparison against measurements for wet mercury deposition are presented in Figure 7-32 and in Table 7-5. To mitigate the influence of the amount of precipitation, the modelling results named “rain corrected” were multiplied by the ratio of precipitation measured at EMEP stations and precipitation from meteorological input data presented in Table 7-1. In Table 7-5 and in Figure 7-33 -Figure 7-51 evaluation results from

the model run over Europe are presented. Evaluation at stations PL05 of the results from simulation run over Poland is presented in Table 7-7 [87]. The correlation coefficients of monthly precipitation intensity and wet deposition mercury fluxes for both observations and modelled results are presented in Table 7-6. The graphical distribution of the monthly modelled results of precipitation intensity and amount of mercury wet deposited is presented in Figure 7-32.

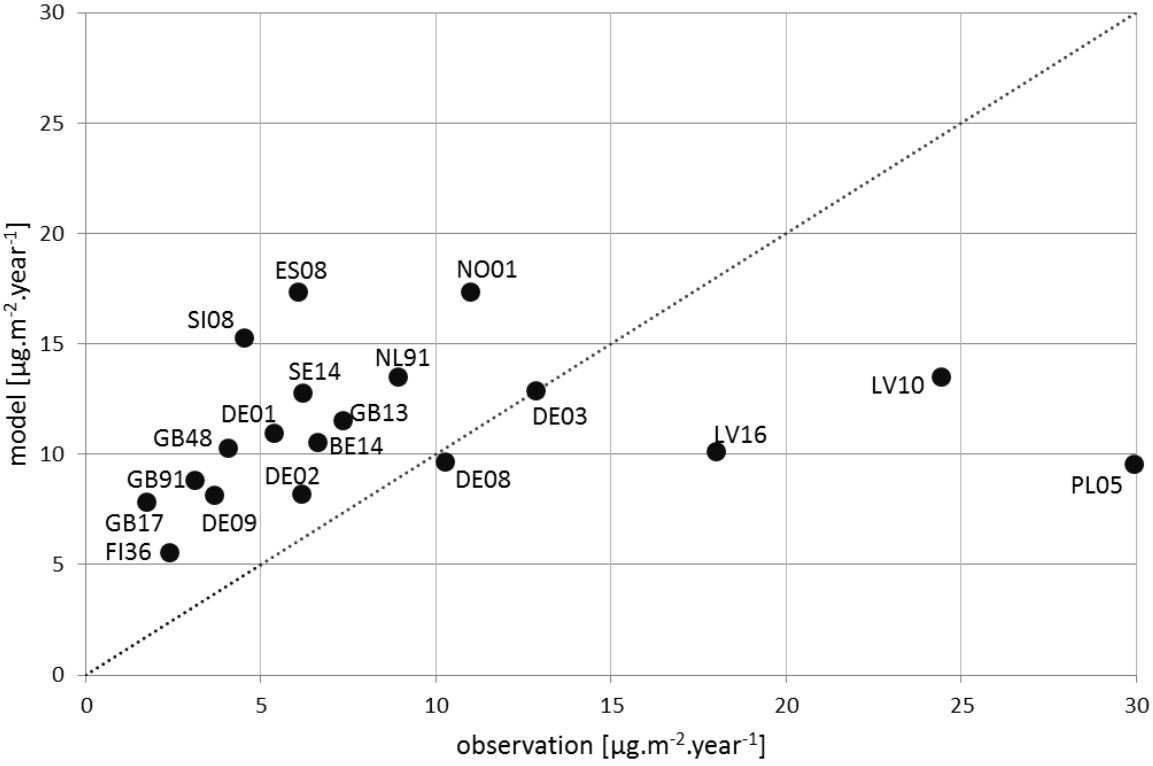

Figure 7-32. The annual modeled (model) and observed (observation) amounts of mercury wet deposition at the stations of EMEP.

Table 7-5. The evaluation of monthly results from the model run over Europe against measurements for mercury wet deposition [µg.m^{-2}.year^{-1}]. At all stations, the observations were provided for the whole except stations ES08, FI36, GB17 and SI08 where mercury wet deposition were observed in 11, 10, 6 and 7 months, respectively.

N.	Stations code	Observed annual wet deposition [µg.m^{-2} .year^{-1}]	Model			Model –"rain corrected"		
			Annual wet deposition [µg.m^{-2} .year^{-1}]	Correlation coefficient	RMSE [µg.m^{-2} .month^{-1}]	Annual wet deposition [µg.m^{-2} .year^{-1}]	Correlation coefficient	RMSE [µg.m^{-2} .month^{-1}]
1	BE14	6.64	10.53	0.70	0.57	5.85	0.57	0.54
2	DE01	5.37	10.96	0.55	0.61	8.11	0.60	0.38
3	DE02	6.17	8.21	0.50	0.36	7.21	0.54	0.31
4	DE03	12.85	12.87	0.23	0.59	15.55	0.26	0.64
5	DE08	10.28	9.65	0.23	0.46	12.44	0.31	0.54

6	DE09	3.69	8.13	0.36	0.42	5.93	0.68	0.27
7	ES08	6.09	15.53	0.57	1.02	11.95	0.58	0.74
8	FI36	2.40	5.53	0.82	0.31	1.99	0.94	0.14
9	GB13	7.36	11.52	0.11	0.61	9.50	-0.03	0.56
10	GB17	1.75	3.75	-0.05	0.46	4.03	0.66	0.71
11	GB48	4.06	10.29	0.56	0.65	8.20	0.34	0.45
12	GB91	3.14	8.82	0.50	0.60	6.09	0.49	0.35
13	LV10	24.42	13.51	0.79	1.39	11.33	0.91	1.47
14	LV16	18.02	10.09	0.50	1.02	8.74	0.50	1.09
15	NL91	8.93	13.52	0.48	0.59	10.21	0.41	0.48
16	NO01	11.00	17.34	0.36	0.81	18.97	0.26	1.09
17	PL05	29.94	9.53	0.41	2.07	7.73	0.32	2.21
18	SE14	6.20	12.75	0.08	0.78	7.09	0.47	0.28
19	SI08	4.53	10.00	0.78	0.85	7.88	0.71	0.69
20	All	172.85	202.54	0.30	0.86	168.81	0.34	0.85

At 15 stations, the modelled results are overestimated (Figure 7-32). Only at 3 stations located in Poland and Latvia, the modelled results are lower than measured fluxes of wet deposited mercury. It should be underlined that for 11 stations the differences between observed and modelled annual wet deposition fluxes do not exceed 50% of the observed annual amounts. The station located in Poland reported the highest annual wet deposition of mercury of 30 $\mu g.m^{-2}$ (Table 7-5). Generally, when the influence of the amount of precipitation is mitigated, the statistical indicators are not improved significantly. The correlation coefficient for all results increase from 0.30 to 0.34 and RMSE decreases only by 0.01 $\mu g.m^{-2}.month^{-1}$. The annual wet deposition flux at in all stations decreased from 203 to 169 $\mu g.m^{-2}$. At 10 stations the correlation coefficients were above 0.5.

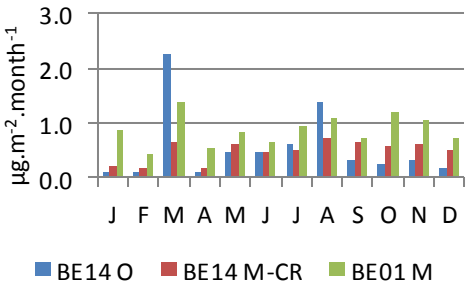

Figure 7-33. The comparison of results from the model run (M –model, M-CR –"model rain corrected") over Europe against measurements (O) at station BE14 for mercury wet deposition [$\mu g.m^{-2}.month^{-1}$].

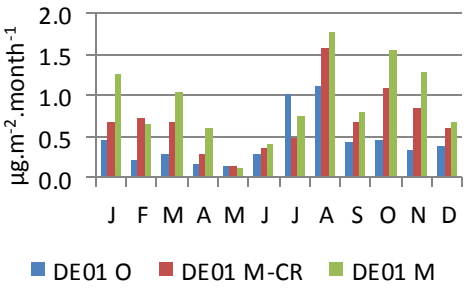

Figure 7-34. The comparison of results from the model run (M –model, M-CR –"model rain corrected") over Europe against measurements (O) at station DE04 for mercury wet deposition [$\mu g.m^{-2}.month^{-1}$].

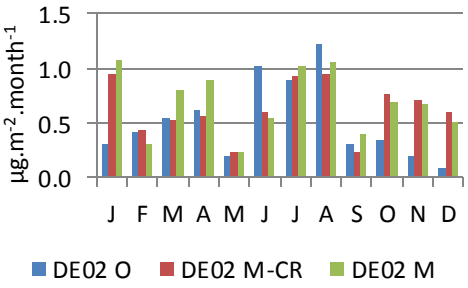

Figure 7-35. The comparison of results from the model run (M –model, M-CR –model "rain corrected") over Europe against measurements (O) at station BE14 for mercury wet deposition [µg.m^{-2}.month^{-1}].

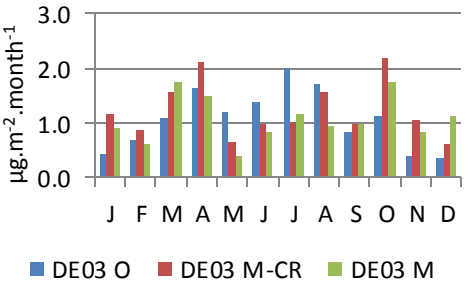

Figure 7-36. The comparison of results from the model run (M –model, M-CR –model "rain corrected") over Europe against measurements (O) at station DE04 for mercury wet deposition [µg.m^{-2}.month^{-1}].

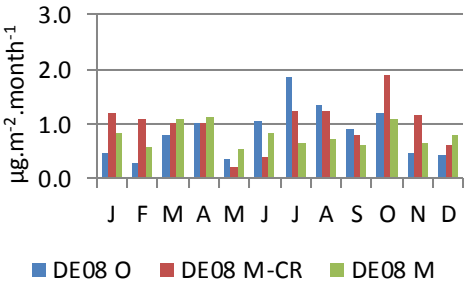

Figure 7-37. The comparison of results from the model run (M –model, M-CR –model "rain corrected") over Europe against measurements (O) at station DE08 for mercury wet deposition [µg.m^{-2}.month^{-1}].

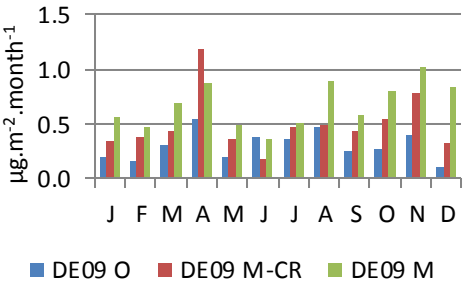

Figure 7-38. The comparison of results from the model run (M –model, M-CR –model "rain corrected") over Europe against measurements (O) at station DE09 for mercury wet deposition [µg.m^{-2}.month^{-1}].

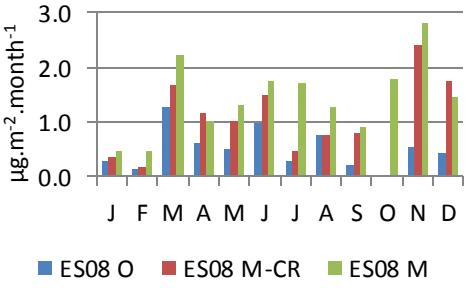

Figure 7-39. The comparison of results from the model run (M –model, M-CR –"model rain corrected") over Europe against measurements (O) at station ES08 for mercury wet deposition [µg.m^{-2}.month^{-1}].

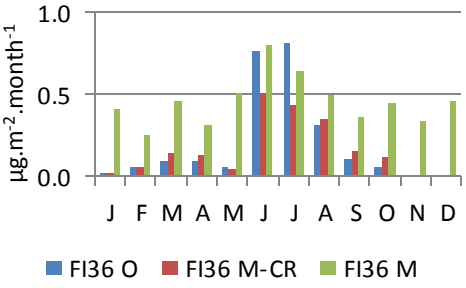

Figure 7-40. The comparison of results from the model run (M –model, M-CR –"model rain corrected") over Europe against measurements (O) at station FI36 for mercury wet deposition [µg.m^{-2}.month^{-1}].

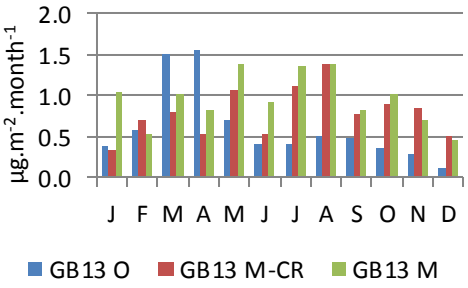

Figure 7-41. The comparison of results from the model run (M –model, M-CR –"model rain corrected") over Europe against measurements (O) at station GB13 for mercury wet deposition [µg.m^{-2}.month^{-1}].

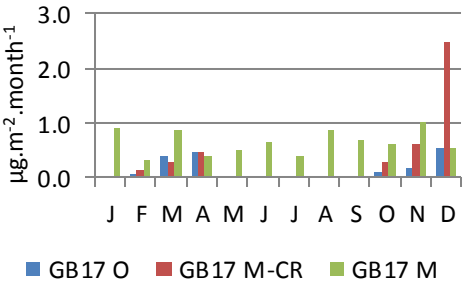

Figure 7-42. The comparison of results from the model run (M –model, M-CR –"model rain corrected") over Europe against measurements (O) at station GB17 for mercury wet deposition [µg.m^{-2}.month^{-1}].

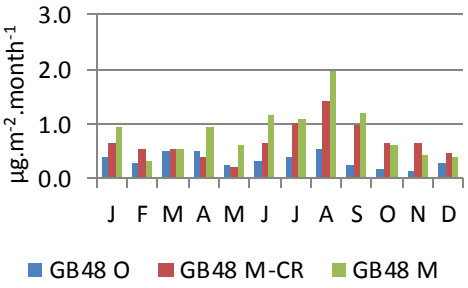

Figure 7-43. The comparison of results from the model run (M –model, M-CR –"model rain corrected") over Europe against measurements (O) at station GB48 for mercury wet deposition [µg.m^{-2}.month^{-1}].

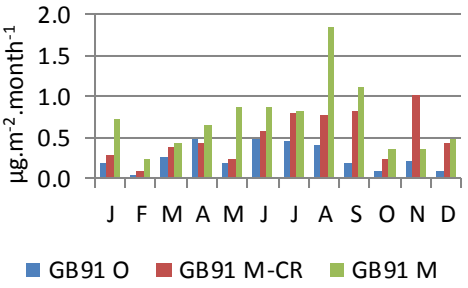

Figure 7-44. The comparison of results from the model run (M –model, M-CR –"model rain corrected") over Europe against measurements (O) at station GB48 for mercury wet deposition [µg.m^{-2}.month^{-1}].

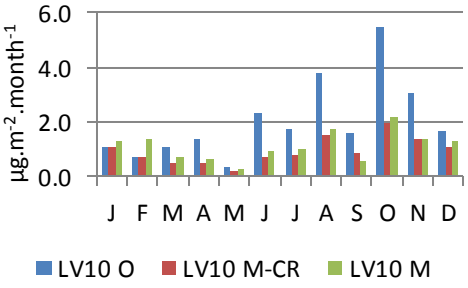

Figure 7-45. The comparison of results from the model run (M –model, M-CR –"model rain corrected") over Europe against measurements (O) at station LV10 for mercury wet deposition [µg.m^{-2}.month^{-1}].

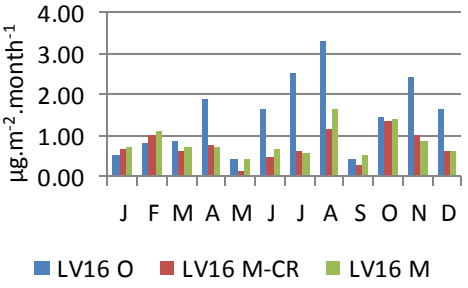

Figure 7-46. The comparison of results from the model run (M –model, M-CR –"model rain corrected") over Europe against measurements (O) at station LV16 for mercury wet deposition [µg.m^{-2}.month^{-1}].

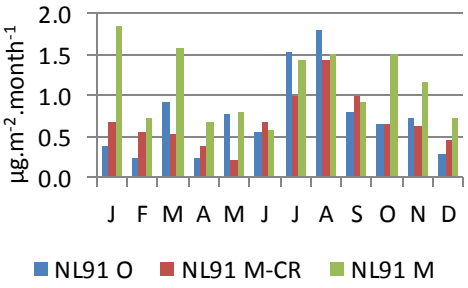

Figure 7-47. The comparison of results from the model run (M –model, M-CR –"model rain corrected") over Europe against measurements (O) at station NL91 for mercury wet deposition [µg.m^{-2}.month^{-1}].

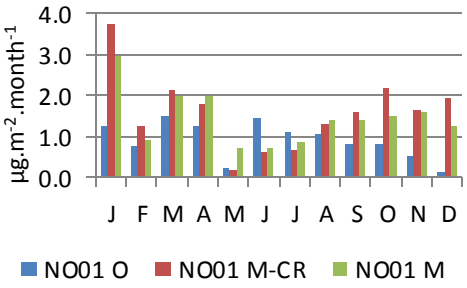

Figure 7-48. The comparison of results from the model run (M –model, M-CR –"model rain corrected") over Europe against measurements (O) at station NO01 for mercury wet deposition [µg.m^{-2}.month^{-1}].

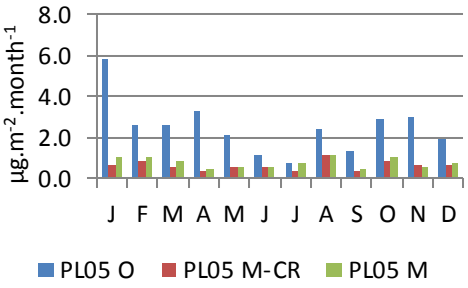

Figure 7-49. The comparison of results from the model run (M –model, M-CR –"model rain corrected") over Europe against measurements (O) at station PL05 for mercury wet deposition [µg.m^{-2}.month^{-1}].

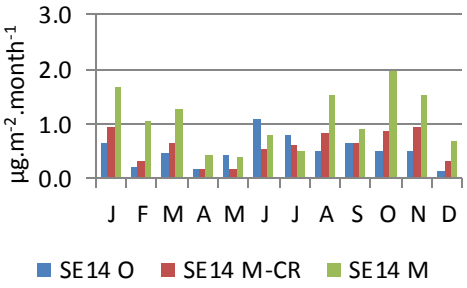

Figure 7-50. The comparison of results from the model run (M –model, M-CR –"model rain corrected") over Europe against measurements (O) at station DE04 for mercury wet deposition [µg.m^{-2}.month^{-1}].

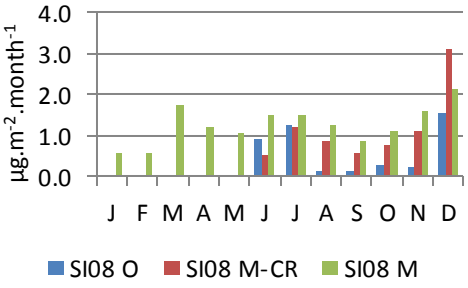

Figure 7-51. The comparison of results from the model run (M –model, M-CR –"model rain corrected") over Europe against measurements (O) at station SI08 for mercury wet deposition [µg.m^{-2}.month^{-1}].

The monthly amounts of wet deposited mercury measured at EMEP stations often change strongly from month to month e.g. at station BE14 presented in Figure 7-33. At this stations

the observed mercury wet flux was 20 times higher in March than in February and April. The precipitation intensity was 5.5 times and the concentration of mercury in precipitation was 3.7 times higher in March compared to February and April 2008. According to the observation and modeled data, the highest wet deposition of mercury was in August and the lowest in February. The maximum of monthly wet deposition of mercury of 5.88 $\mu g.m^{-2}$ was observed at a station located in Poland (PL05) in January (Figure 7-49). The modeled maximum monthly wet deposition of 2.97 $\mu g.m^{-2}$ was obtained at station NO01 in January (Figure 7-48).

Table 7-6. Correlation coefficient between monthly results of precipitation intensity and mercury wet deposition

N.	Station code	Measured both: precipitation intensity and wet deposition load	Modelled both: precipitation intensity and wet deposition load
1	BE14	0.55	0.97
2	DE01	0.70	0.95
3	DE02	0.63	0.95
4	DE03	0.56	0.89
5	DE08	0.60	0.84
6	DE09	0.75	0.68
7	ES08	0.54	0.77
8	FI36	0.96	0.89
9	GB13	-0.03	0.92
10	GB17	0.60	0.92
11	GB48	0.48	0.94
12	GB91	0.58	0.97
13	LV10	0.95	0.92
14	LV16	0.79	0.75
15	NL91	0.65	0.93
16	NO01	0.48	0.86
17	PL05	0.11	0.72
18	SE14	0.61	0.92
19	SI08	0.85	0.83

At most of the stations, there is some correlation between the monthly precipitation rate and the wet deposition load for measurements. The correlation coefficient is above 0.6 at 11 stations. There is strong correlation between modelled results. At 17 stations, the correlation coefficient is above 0.8. A significant correlation between the wet deposition flux of mercury and the amount of precipitation was reported at sites in North America and in Japan [159]. Thus, most of the variance in mercury wet deposition is explained by the amount of precipitation, whereas the remaining variance is probably caused by the local and regional sources of RGM and Hg_P and also by other meteorological conditions. The lowest correlation coefficient of 0.75 is in the cell where the PL05 station is located. Therefore, at this location the impact of the local sources of RGM and Hg_P may be the highest.

Table 7-7. The evaluation of results from the model run over Poland against measurements for mercury monthly wet deposition at PL05 station [$\mu g.m^{-2}.year^{-1}$]. Observed annual wet deposition is 30 [$\mu g.m^{-2}.year^{-1}$]. The emission option description are in chapter 6.2.7.

N.	Emission option	Model			Model –"rain corrected"		
		Annual wet deposition [$\mu g.m^{-2}.year^{-1}$]	Correlation coefficient	RMSE [$\mu g.m^{-2}.month^{-1}$]	Annual wet deposition [$\mu g.m^{-2}.year^{-1}$]	Correlation coefficient	RMSE [$\mu g.m^{-2}.month^{-1}$]
1	Base	9.60	0.28	2.09	7.80	0.22	2.22
2	EF2008-fix	10.26	0.34	2.03	8.31	0.27	2.18
3	EF2008	10.19	0.33	2.04	8.26	0.27	2.18
4	EF2009	9.88	0.32	2.06	8.01	0.25	2.20
5	EF2009-PM	9.72	0.30	2.21	7.89	0.24	2.21

The impact of the amounts, speciation and location of mercury emitted into the atmosphere has an influence on the load of wet deposited mercury. However, due to the location of the PL05 station in Diabla Góra in the north-western part of Poland, far away from the main power plants, this impact is not very significant (Table 7-7). Compared to the results presented in Table 7-5 for station PL05, the simulation with higher spatial resolution with detailed data did not improved the statistical indexes.

Table 7-8. The evaluation of results from the model run over Europe against measurements for mercury ambient air concentration [$\mu g.m^{-2}.year^{-1}$]

N.	Stations code	Average modelled concentration [$ng.m^{-3}$]	Average observed concentration [$ng.m^{-3}$]	Share of valid observation	RMSE [$ng.m^{-3}$]	Correlation coefficient	Provided observation (average)
1	BE14	1.34	1.84	1.00	0.88	-0.05	daily
2	CZ03	1.14	1.55	0.88	0.78	-0.06	weekly
3	FI36	1.25	1.37	0.24	0.22	0.14	daily
4	GB17	1.27	1.71	1 observation, average 14.03-11.04			
5	GB91	1.23	0.83	0.79	0.60	-0.20	half months
6	NO01	1.20	1.73	0.12	0.58	-0.03	daily
7	PL05	1.16	1.47	0.15	0.63	-0.07	daily
8	SE14	1.23	1.57	0.28	0.38	0.06	daily

The modelled result of air concentration of mercury are significantly lower (Table 7-8). The additional simulation were performed and further results were presented to find a possible explanation of such behaviour of the model.

7.5 Evaluation of cadmium and lead ambient concentrations and deposition

The obtained model results of cadmium and lead air concentrations and wet deposition fluxes were evaluated against measurements conducted at EMEP stations in 2008. The results of the air concentrations of cadmium and lead bound to PM10 were taken into accounting for this evaluation. The evaluation for cadmium air concentrations was done for 19 stations (Table 7-9 and Table 7-10). The other 31 stations measured the cadmium concentrations in other PM size sections (mostly in total particulate matter) or outside the modelling domain in 2008. The lead air concentration in PM10 was measured in 2008 at 23 stations located within the European modelling domain (Table 7-12 and Table 7-13. The other 32 stations measured the lead concentration outside the domain or in other particulate matter size sections than PM10. The evaluation of the wet deposition flux was done at 52 stations for both lead and cadmium.

Table 7-9. Evaluation of results of concentrations in ambient air of cadmium bound to PM10 from simulation run over the European domain at the surface against measurements of EMEP [163]. The observed concentrations were provided with time step of 1 day.

N.	Stations code	Share of valid observation	Average annual observed concentration [ng.m^{-3}]	Average annual modelled concentration [ng.m^{-3}]	RMSE [ng.m^{-3}]	Correlation coefficient
1	AT02	0.300	0.15	0.15	0.12	0.63
2	AT05	0.134	0.08	0.08	0.07	0.47
3	AT48	0.153	0.05	0.08	0.05	0.55
4	CZ01	0.139	0.19	0.19	0.16	0.53
5	CZ03	0.525	0.15	0.16	0.08	0.56
6	ES09	0.120	0.03	0.06	0.06	0.53
7	SI08	0.464	0.10	0.13	0.09	0.22
8	All	0.280	0.13	0.14	0.10	0.69

All - results for all observations from 7 stations located inside the European domain, where Cd concentrations where observed in 2008 and results were provided with temporal resolution of 1 day.

Table 7-10. Evaluation of results of concentrations in ambient air of cadmium bound to PM10 from simulation run over the European domain at the surface against measurements of EMEP [163]. The observed concentrations were provided as the average value 1 week.

N.	Stations code	Share of valid observation	Average annual observed concentration [ng.m^{-3}]	Average annual modelled concentration [ng.m^{-3}]	RMSE [ng.m^{-3}]	Correlation coefficient
1	DE01	1.000	0.08	0.08	0.06	0.58
2	DE02	0.980	0.17	0.15	0.10	0.57
3	DE03	0.942	0.05	0.15	0.10	-0.11
4	DE07	1.000	0.15	0.15	0.07	0.74
5	DE08	1.000	0.09	0.13	0.09	0.05
6	DE09	0.980	0.11	0.12	0.05	0.78
7	GB13	0.365	0.04	0.06	0.02	0.93
8	NO01	0.712	0.03	0.03	0.04	0.27

9	PL05	0.961	0.15	0.16	0.03	0.41
10	All	0.670	0.11	0.12	0.06	0.52

All- results for all observations from 12 stations located inside the European domain, where Cd concentrations where observed in 2008. Additionally to presented stations in Table 7-10, the observation were provided in GB17, GB91 and SK07, respectively only for 2, 1 and 2 weeks.

Table 7-11. The evaluation of results from the model run over Europe against measurements for cadmium wet deposition [$\mu g.m^{-2}.year^{-1}$].

N.	Stations code	Observed annual wet deposition [$g.km^{-2}.year^{-1}$]	Model			Model –"rain corrected"		
			Annual wet deposition [$g.km^{-2}.year^{-1}$]	Correlation coefficient	RMSE [$g.km^{-2}.month^{-1}$]	Annual wet deposition [$g.km^{-2}.year^{-1}$]	Correlation coefficient	RMSE [$g.km^{-2}.month^{-1}$]
1	PL04	34.6	13.8	0.12	2.35	10.2	0.35	2.53
2	PL05	31.1	20.7	-0.06	1.72	13.7	0.56	1.73
3	All	3575	663	0.13	40	521	0.11	40

All- results for all observations from 52 stations located inside the European domain, where Cd wet deposition where observed in 2008. In all stations the data for 597 months were provided.

The model tracks the transport of cadmium in the atmosphere very well. The obtained results of the evaluation of air concentrations are satisfying. Unfortunately, the results of wet deposition are significantly understated. The measured annual wet deposition of cadmium at all 52 stations is 3575 $g.km^{-2}$ and is over 6 times higher compared to results of the model.

Table 7-12. Evaluation of results of lead concentrations in ambient air from simulation run over the European domain at the surface against measurements of EMEP [163]. The observed concentrations were provided with time step of 1 day.

N.	Stations code	Share of valid observation	Average annual observed concentration [$ng.m^{-3}$]	Average annual modelled concentration [$ng.m^{-3}$]	RMSE [$ng.m^{-3}$]	Correlation coefficient
1	AT02	0.306	6.43	7.52	5.32	0.48
2	AT05	0.144	4.96	5.70	3.86	0.56
3	AT48	0.156	2.56	3.89	2.62	0.24
4	CZ01	0.139	5.85	9.43	6.07	0.47
5	CZ03	0.527	5.40	8.06	4.57	0.32
6	DK03	0.948	2.96	3.12	2.44	0.53
7	DK05	0.926	3.78	4.91	3.62	0.50
8	DK08	0.918	2.54	3.06	3.54	0.42
9	DK31	0.950	2.66	2.50	2.19	0.66
10	ES09	0.120	0.82	2.90	2.66	0.52
11	SI08	0.464	3.82	4.62	4.00	0.24
12	All	0.518	3.60	4.55	4.04	0.50

All -results for all observations from 11 stations located inside the European domain, where Pb concentrations where observed in 2008 and results were provided with temporal resolution of 1 day

Table 7-13. Evaluation of results of lead concentrations in ambient air from simulation run over the European domain at surface against measurements of EMEP [163]. The observed concentrations were provided as the average value 1 week.

N.	Stations code	Share of valid observation	Average annual observed concentration [ng.m^{-3}]	Average annual modelled concentration [ng.m^{-3}]	RMSE [ng.m^{-3}]	Correlation coefficient
1	DE01	1.000	2.88	3.13	1.64	0.61
2	DE02	0.980	4.93	5.85	2.46	0.65
3	DE03	0.942	2.04	8.14	6.16	-0.18
4	DE07	1.000	5.01	5.74	2.76	0.61
5	DE08	1.000	2.96	6.96	4.63	0.16
6	DE09	0.980	3.72	4.19	2.10	0.61
7	GB13	0.365	1.77	3.26	1.72	0.93
8	NO01	0.712	1.06	1.05	1.65	0.28
9	PL05	0.961	5.38	2.92	1.13	0.72
10	All	0.660	3.57	4.97	2.65	0.32

All -results for all observations from 12 stations located inside the European domain, where Pb concentrations where observed in 2008. Additionally to presented stations in Table 7-13, the observation were provided in GB17, GB91 and SK07, respectively only for 2, 1 and 2 weeks.

Table 7-14. The evaluation of results from the model run over Europe against measurements for lead wet deposition [μg.m^{-2}.year^{-1}].

N.	Stations code	Observed annual wet deposition [g.km^{-2}.year^{-1}]	Model			Model –"rain corrected"		
			Annual wet deposition [g.km^{-2}.year^{-1}]	Correlation	RMSE [g.km^{-2}.month^{-1}]	Annual wet deposition [g.km^{-2}.year^{-1}]	Correlation coefficient	RMSE [g.km^{-2}.month^{-1}]
1	PL04	525	438	-0.30	25	329	-0.31	27
2	PL05	409	525	0.56	20	371	0.82	11
3	All	42347	27910	0.30	117	22558	0.34	118

All- results for all observations from 52 stations located inside the European domain, where lead wet deposition where observed in 2008. In all stations the data for 592 months were provided.

The modelling results of lead air concentrations are overestimated. The correlation coefficients for the majority of the presented stations are above 0.5 (Table 7-12 Table 7-13). On the other hand, the modelled amount of lead wet deposition are underestimated.

One very important thing to be noticed, is that an average the observed the air concentration of cadmium is 30 times lower than the air concentration of lead, while the measured wet deposition of cadmium is only 12 times lower than the wet deposition of lead. The modelling ratios of lead and cadmium for both air concentration and wet deposition are approx. 40. This is understandable because the lead and cadmium in the air are associated together in similar particles. Therefore, the atmospheric transport, as well as, the removal processes are the same for both heavy metals. The differences in observation rates may result from different distributions of lead and cadmium in size sections of particulate matter. Most of cadmium is associated in PM with a diameter above 10 μm. The measurement of air concentration is

given for PM10 while deposition covers all particles, also above 10 μm. The underestimated results of air concentration and amount of wet deposition of lead and cadmium were obtained from simulation run with the use of the MSCE-HM model for 2008 [183].

7.6 Results of ambient concentrations and deposition of mercury

The concentration of various mercury forms over Europe at the surface are presented in Figure 7-52 -Figure 7-54.

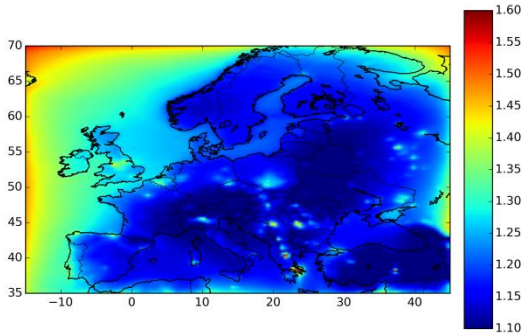

Figure 7-52. Annual average concentration of GEM [ng.m^{-3}] at the surface.

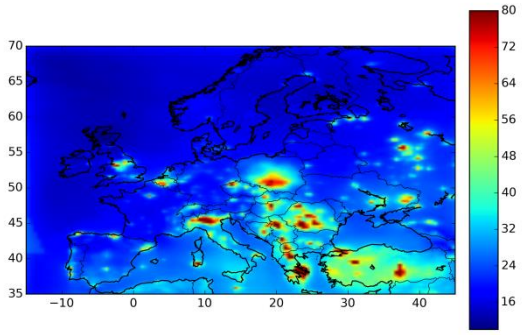

Figure 7-53. Annual average ambient concentration of RGM [pg.m^{-3}] at the surface.

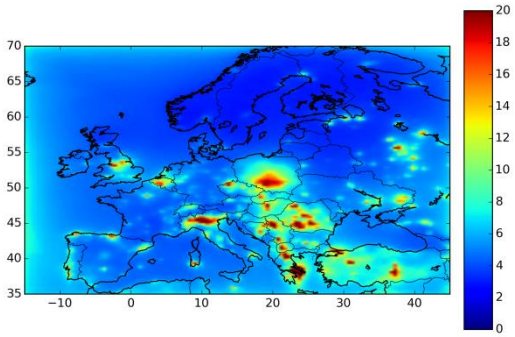

Figure 7-54. Annual average ambient concentration of Hg_P [pg.m^{-3}] at the surface.

The ambient concentrations of elemental gaseous mercury ranges from 1.10 -1.60 ng.m^{-3}. The high value is noticed near the boundary of the domain, where the concentration of approx. 1.50 ng.m^{-3} at the surface level was assumed. Inside the domain, mainly over land the

concentration is lower. It seems that there is a high sink of GEM. On the map, some parts with high anthropogenic emission are visible i.e. south Poland, the Czech Republic, the Netherlands, and Greece. However, the concentrations of GEM in these areas is about 0.20 $ng.m^{-3}$ higher (about 15% higher) compared to other places over land. On the contrary high variations in the spatial gradient of RGM ambient concentrations over Europe occur. Over the areas presented in Figure 6-6 where the high anthropogenic emissions of mercury occur the ambient concentration shown in Figure 7-53 reaches 80 $pg.m^{-3}$. Whereas over other areas the concentrations oscillates at a value of 20 $pg.m^{-3}$. Similarly to RGM, high variations in the spatial gradient of Hg_P ambient concentration occur. The places with high concentration correlate with location of large anthropogenic mercury emissions. Looking at Figure 7-54, one can notice that the boundary concentration of Hg_P used in simulations are overestimated. On the other hand the results obtained with MSCE-HM model show a higher air concentration of mercury over Europe. According to that result, the air concentration exceeds 1.7 $ng.m^{-3}$ over southern Poland, the Czech Republic, Hungary, Romania, Greece and northern Italy. The global simulation with the use of the GLEMOS model shows that over most of Europe the air concentration of GEM exceeds 2 $ng.m^{-3}$ in 2010 [260].

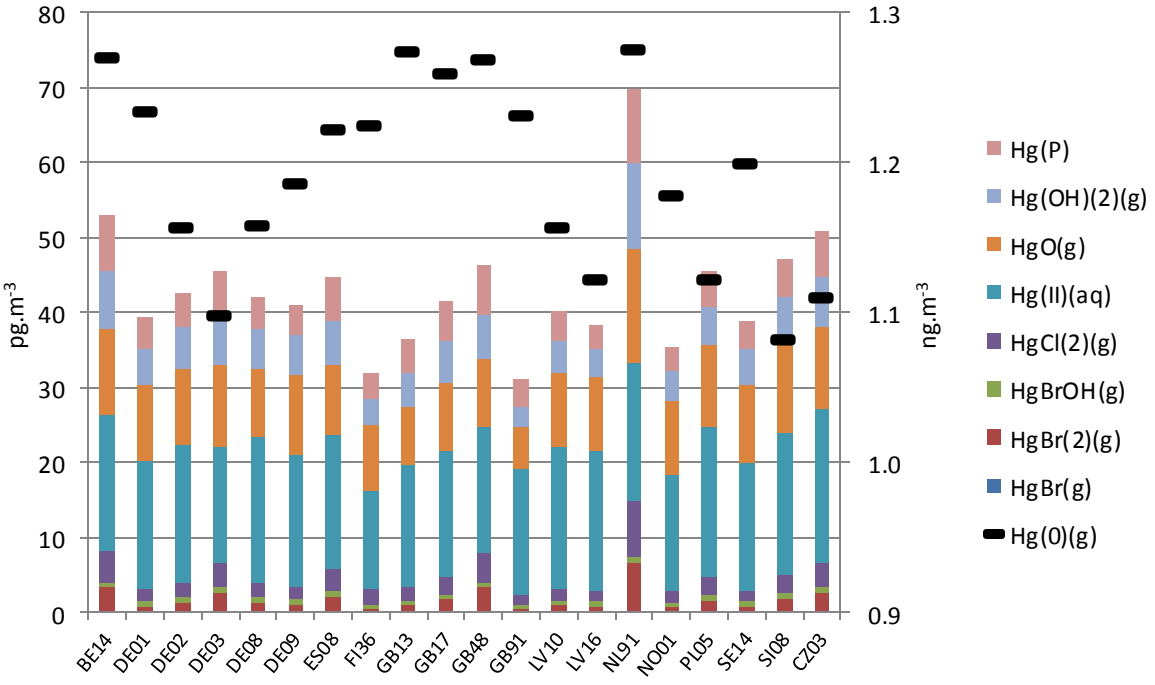

Figure 7-55. Annual average ambient air concentration of mercury forms and species at the surface at locations of EMEP measurement sites. The concentrations of reactive mercury are shown on the left [$pg.m^3$] and GEM on the right [$ng.m^3$] axis.

In the atmosphere, at the surface, 41% of reactive mercury is in the aqueous phase ($Hg^{II}_{(aq)}$). Among the gaseous compounds, $HgO_{(g)}$ is prevailing with an average share in total reactive mercury atmospheric concentration of 23%, at all stations. The shares of Hg_P and $Hg(OH)_{2(g)}$ are almost on the same level and equal 12%. The contributions of $HgCl_{2(g)}$, $HgBr_{2(g)}$, $HgBrOH_{(g)}$ and $HgBr_{(g)}$ are 5.5%, 3.8%, 1.6% and 0.1% respectively. In the model, $HgCl_{2(g)}$, $HgBr_{2(g)}$, $HgO_{(g)}$ and $Hg(OH)_{2(g)}$ were equally emitted into the air, and the similar boundary and initial concentrations were applied for these compounds.

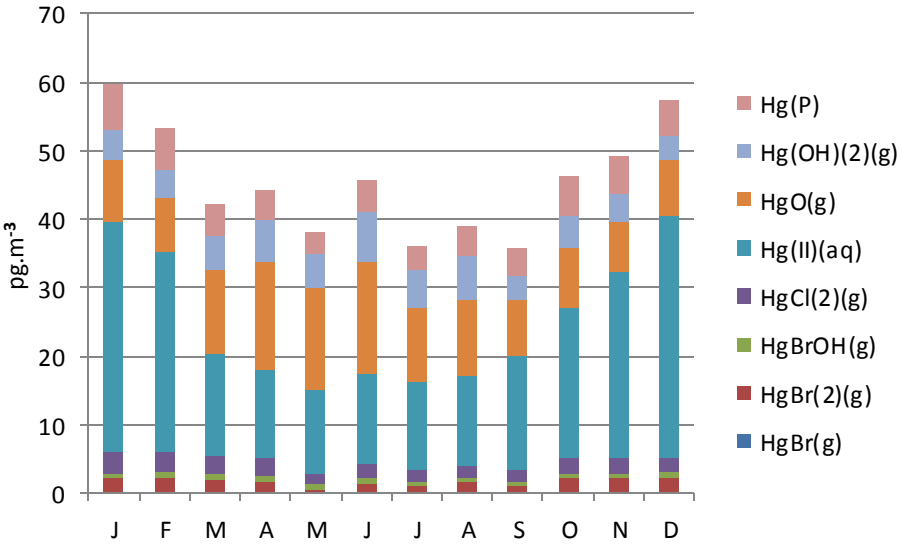

Figure 7-56. Monthly average ambient air concentration of mercury forms and species at the surface at the PL05 observation site [$pg.m^3$]. The results are from simulation over Europe.

At the PL05 station, the highest concentration of atmospheric reactive mercury occurs in the winter (Figure 7-56). During this season, more than 50% of the total reactive mercury is in the aqueous phase, while in summer the share decreases down to 28%. In April, May and June, $HgO_{(g)}$ was a main component of reactive mercury present in the atmosphere.

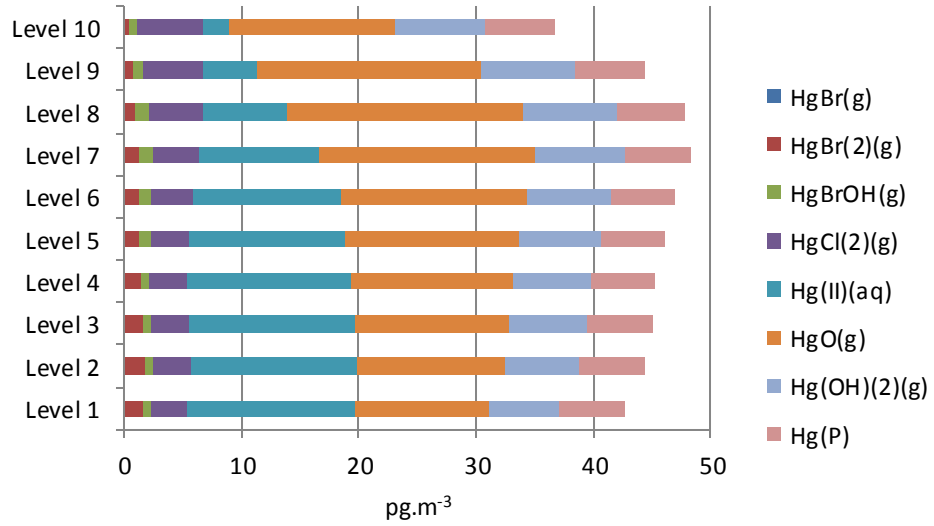

Figure 7-57. Annual average ambient air concentrations of mercury forms and species in the whole European domain at 10 vertical levels.

The concentration of reactive mercury slightly increases with the altitude up to 2000 meters and then decreases fairly quickly (Figure 7-57). Near the surface, mercury in the aqueous phase is prevailing, up to the third modelling level. At the fourth level, the concentrations of $HgO_{(g)}$ and $Hg^{II}_{(aq)}$ are equal. Then, $HgO_{(g)}$ is a dominant form of reactive mercury. The concentration of $Hg(OH)_{2(g)}$ and $HgCl_{2(g)}$ increase with the altitude while $HgBr_{2(g)}$ decreases.

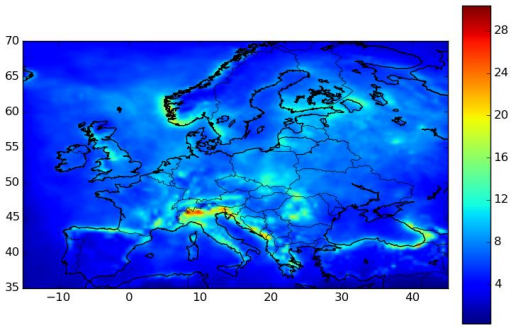

Figure 7-58. Annual wet deposition of RGAM [$g.km^{-2}.y^{-1}$].

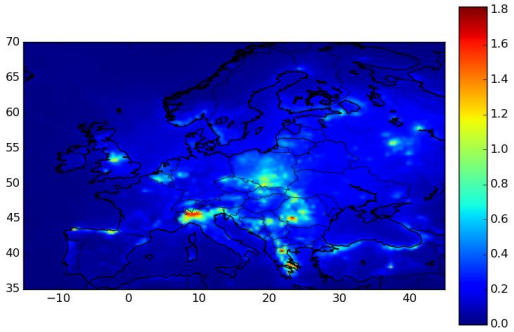

Figure 7-59. Annual wet deposition of Hg_P [$g.km^{-2}.y^{-1}$].

Looking at Figure 7-58 and Figure 7-59, the significant variations in the spatial gradient of wet deposition of reactive mercury in gaseous, aqueous and particulate forms appears. The highest deposition fluxes occur near large emission sources and over areas with the highest precipitation intensity (Figure 6-6 and Figure 6-2). The wet deposition flux of GEM is very

low and can be neglected. Rather similar results of wet deposition over Europe were calculated with the GLEMOS model [260].

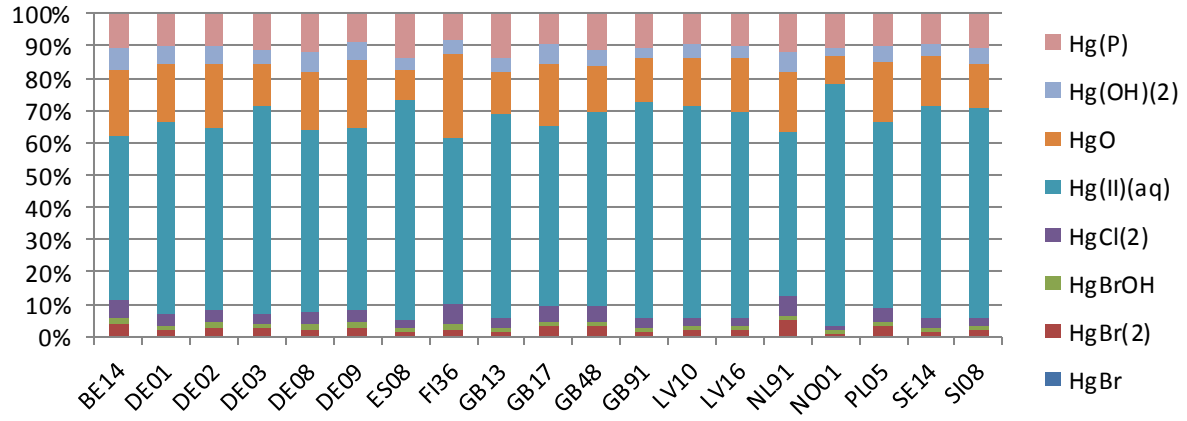

Figure 7-60. Contribution of mercury forms and species to overall wet deposition at locations of EMEP measurement sites.

The in-cloud scavenging for $Hg^{II}_{(aq)}$, Hg_P and $Hg^0_{(aq)}$ and the below-cloud scavenging for RGM and Hg_P were implemented in to the model. The prevailing share of $Hg^{II}_{(aq)}$ in the wet deposition flux of mercury is seen in Figure 7-60. Therefore, the aqueous chemistry and mass transfer as well as the implemented approach of in-cloud scavenging have a principal influence on the modeled amounts of deposited mercury. Additionally, as the mercury chemistry transport models are evaluated against wet deposition observations, the in-cloud scavenging models were carefully analyzed and the results are presented in the latter part of the manuscript.

Looking at Figure 7-55 and Figure 7-60, one notes that the below-cloud scavenging is more effective for particulate matter than for gaseous mercury. Despite the fact that the average annual ambient concentrations of Hg_P and $Hg(OH)_2$ were on the same magnitude, the wet deposition of Hg_P is higher than that of $Hg(OH)_2$.

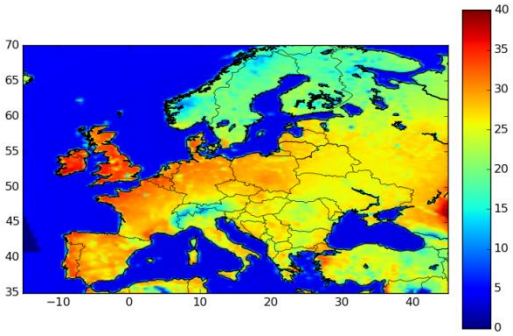

Figure 7-61. Annual dry deposition of GEM [g.km^{-2}.y^{-1}].

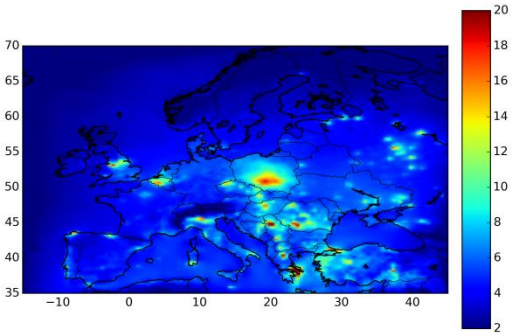

Figure 7-62. Annual dry deposition of RGM [g.km^{-2}.y^{-1}].

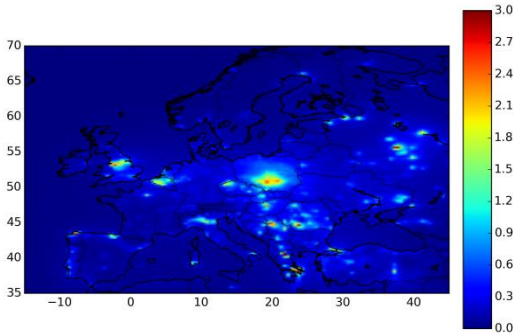

Figure 7-63. Annual dry deposition of Hg_P [g.km^{-2}.y^{-1}].

The large local mercury emission sources are not visible in Figure 7-61, and the deposition process of GEM is mainly led by dry deposition velocity of GEM. GEM is mainly deposited over the land, because the dry velocity deposition over the land is significantly higher compared to that oversea. On the contrary, the highest dry depositions of RGM and Hg_P are observed near large emission sources (Figure 7-62 and Figure 7-63).

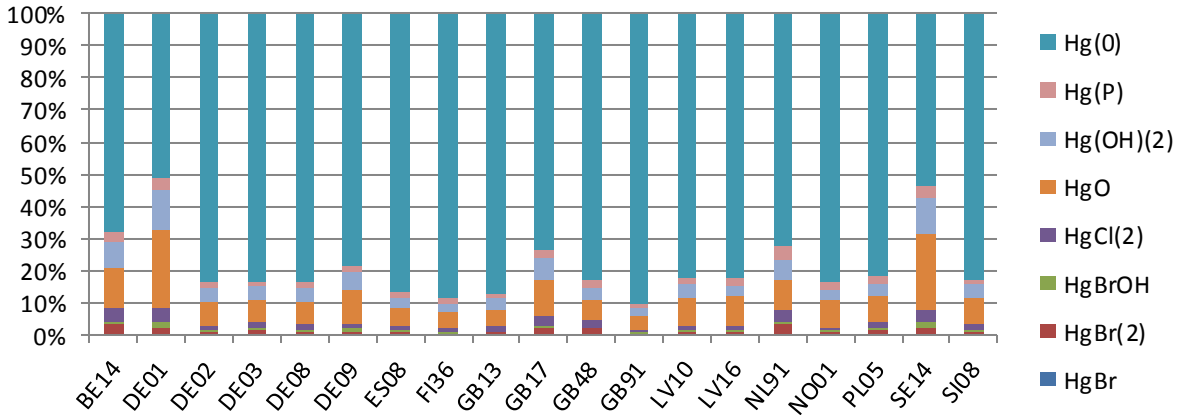

Figure 7-64. Contribution of mercury forms and species to overall dry deposition at locations of EMEP measurement sites.

Despite the fact that the dry deposition velocities of GEM are much lower compared to those of RGM (Figure 7-2, Figure 7-3, Figure 7-4), GEM is the prevailing form being dry deposited over land (Figure 7-64), because most of atmospheric mercury is in this mercury form (Figure 7-52, Figure 7-53, Figure 7-55). In other model simulations, i.e. CMAx, STEM-Hg, MOZART, dry deposition of GEM was not calculated because it was assumed by default that the dry deposition of GEM is equivalent to emissions from natural sources and remission [181], [261], [194]. The obtained results from the model presented here in Figure 7-61 for GEM dry deposition over land are significantly higher in the north and similar in the south of the simulation domain compared to natural emission and reemission of GEM presented in Figure 6-3. Moreover, over the sea the fluxes of deposited GEM are lower than the natural upward flux of GEM.

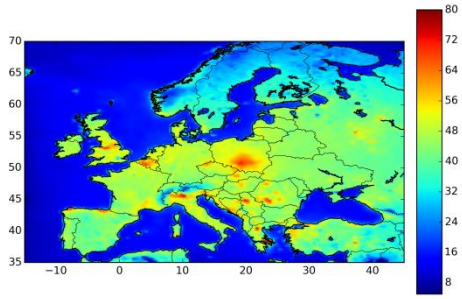

Figure 7-65. Annual deposition (wet +dry) of mercury [$g.km^{-2}.y^{-1}$].

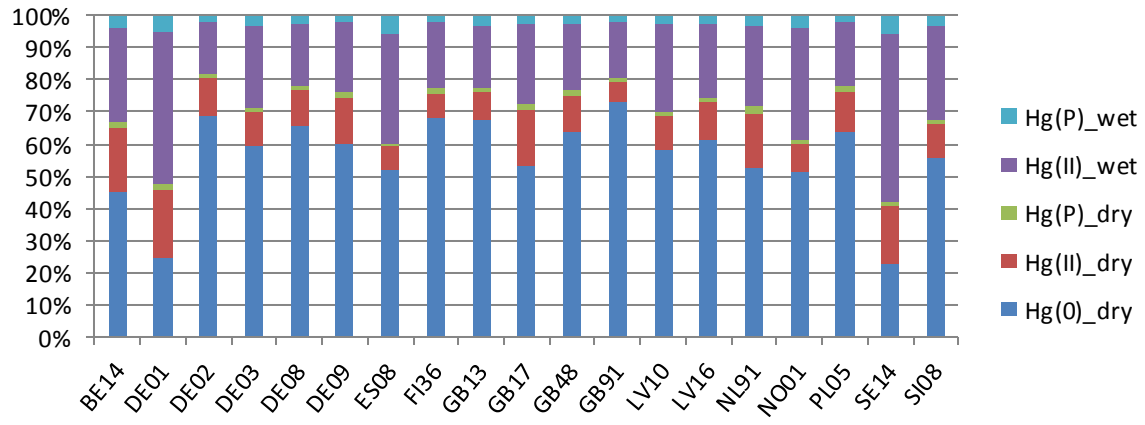

Figure 7-66. Contribution of mercury forms to overall deposition (dry and wet) at locations of EMEP measurement sites.

The final results of the spatial distribution of all mercury forms for wet and dry deposition within the domain, show that mercury is mostly deposited over land (Figure 7-65). This is the result of the GEM dry deposition process, which is the pervading compound for mercury removal from the atmosphere. The results presented in Figure 7-66 show that the share of GEM reaches even 75% in the overall mercury deposition flux. Moreover, in Figure 7-65 the highest deposition occurs near locations with intensive mercury emissions e.g. southern Poland, Greece or northern Italy. There, a lot of mercury is removed from atmosphere through the wet scavenging. From the results presented in Figure 7-66, it can be concluded that the dry deposition of GEM and in-cloud scavenging play a crucial role in the atmospheric mercury mass balance. The result obtained over Europe are higher compared to the average deposition fluxes of 21 $g.km^{-2}.y^{-1}$, 12 $g.km^{-2}.y^{-1}$ and 14 $g.km^{-2}.y^{-1}$ calculated with the use of GEOS-Chem, GLEMOS and CMAQ-Hg models, respectively [262] .

7.7 Results of ambient concentrations and deposition of cadmium and lead

The modelled results of concentrations and deposition in Europe in 2008 are presented in Figure 7-67 - Figure 7-72.

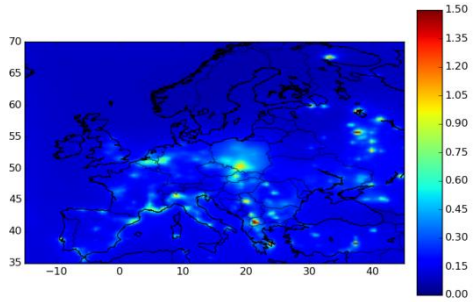

Figure 7-67. Annual average concentration of cadmium [ng.m^{-3}] at the surface.

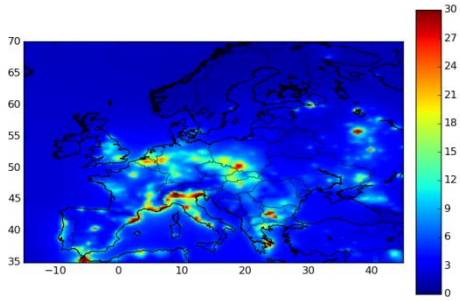

Figure 7-68. Annual average concentration of lead [ng.m^{-3}] at the surface.

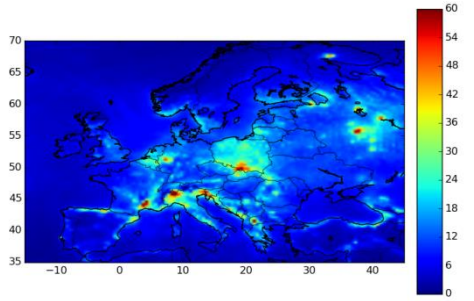

Figure 7-69. Annual wet deposition of cadmium [g.km^{-2}.y^{-1}].

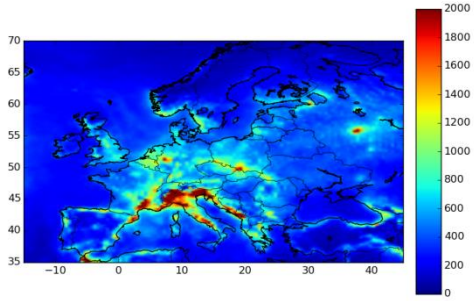

Figure 7-70. Annual wet deposition of lead [g.km^{-2}.y^{-1}].

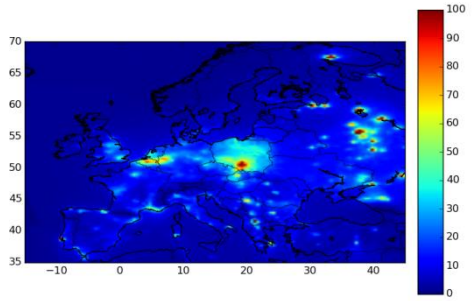

Figure 7-71. Annual dry deposition of cadmium [g.km^{-2}.y^{-1}].

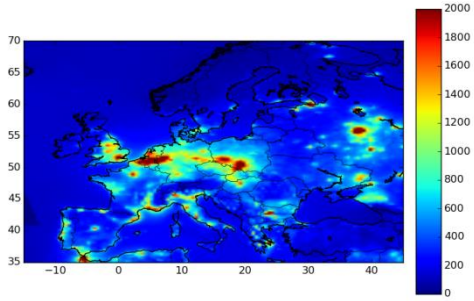

Figure 7-72. Annual dry deposition of lead [g.km^{-2}.y^{-1}].

The high variability of average concentration and annual deposition fluxes of cadmium and lead is noted. The highest concentration and deposition fluxes occurs over industrial areas where cadmium and lead are intensively released into the atmosphere, mainly by the sector of production of various metals and alloys. Southern Poland is one of the most polluted areas in Europe. The ambient concentration of Cd is relatively very low and over a majority of the simulation domain does not exceed 0.5 ng.m^{-3}. In some areas of the simulation domain, over 4kg.km^{-2} of lead are deposited during the year. The obtained air concentration spatial

distribution of lead is similar to the calculations preformed with the MSCE-HM model [183], [262]. This model calculated a significantly higher ambient concentration of cadmium. Over the south of Poland, results exceed 0.5 ng.m^{-3}. Rather similar results were obtained for deposition of lead and cadmium, e.g. the average annual deposition flux of lead of 1.6 kg.km^{-2} and flux of cadmium of 90 g.km^{-2} over Poland were estimated with the MSCE-HM model.

7.8 Sensitivity analysis of the mercury model

To better understand the obtained modelling results and study the response of various factors on those modelling results, tens of sensitivity simulations were run. The sensitive analyses include the chemistry of mercury in gaseous and aqueous phases, the input data and scavenging models. The most valuable results are presented and discussed in this chapter.

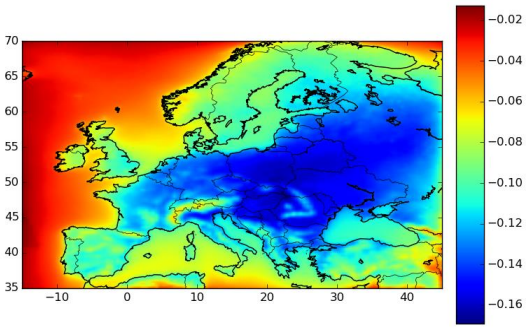

Figure 7-73. Differences in concentrations of GEM at the surface between base model run and model without dry deposition of GEM [ng.m^{-3}].

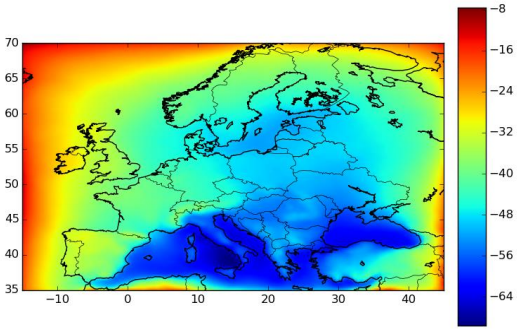

Figure 7-74. Differences in concentrations of GEM at the surface between base model run and model without atmospheric chemistry of mercury [pg.m^{-3}].

The results presented in Figure 7-52 show that the concentration of GEM close to the simulation domain boundary is higher than its concentration inside the domain, which means that this region is a sink area. To investigate the possible causes of such results, the model was run without dry deposition and without atmospheric chemistry of GEM. The obtained results are presented in Figure 7-73 and Figure 7-74. The dry deposition of GEM, which is the main process for removing mercury from the atmosphere (Figure 7-66), reduces the ambient concentration of GEM by a maximum of 0.18 ng.m^{-3}. The chemistry applied in the model

reduces the GEM concentration at the surface level above land by approx. 0.05 ng.m^{-3} (Figure 7-74). The third possible way to explain the sink of mercury from surface level is its transport to upper modelling levels. The results of the influence of model run without chemistry of mercury on the ambient concentration and deposition flux of mercury is presented in Table 7-15.

Table 7-15. The relative changes of amount of air concentration and deposition on the European domain by use of various options of model run. The presented values are ratios of the amounts of deposited and ambient concentrations of mercury from model run with the use of listed options to results of simulation with the use of reference options in base model.

N.	Model run option	Ambient concentration			Dry deposition			Wet deposition		
		Hg^0	RGAM	Hg_P	Hg^0	RGM	Hg_P	Hg^0	RGAM	Hg_P
1	No chemistry of mercury in gaseous phase	1.04	0.42	1.00	1.04	0.43	1.01	1.03	0.42	1.01
2	No chemistry of mercury	1.03	0.48	1.00	1.04	0.44	1.01	1.03	0.50	1.00
3	No in-cloud scavenging of mercury	1.00	1.10	1.09	1.00	1.01	1.08	0.91	0.46	0.37
4	No below-cloud scavenging of mercury	1.00	1.14	1.08	1.00	1.17	1.14	0.10	0.64	0.78

The reactions of mercury in the gaseous phase play a crucial role in the mass balance of reactive gaseous compounds in the atmosphere (Table 7-15). The mass of produced RGM in these reactions is higher than the emissions of RGM from anthropogenic sources. The chemistry in the aqueous phase causes the reduction of quantity of RGAM in the atmosphere it can be concluded that the reduction processes of $Hg^{II}_{(aq)}$ are prevailing over $Hg^0_{(aq)}$ oxidation. In Figure 7-60, it was concluded that divalent mercury in the aqueous phase ($Hg^{II}_{(aq)}$) has the largest contribution in the overall wet deposition of mercury. This form of mercury in the model is removed through in-cloud scavenging. The conclusions from Figure 7-60 are confirmed by the results presented in Table 7-15. The in-cloud scavenging takes a main role in removal reactive mercury (RGM and Hg_P) by wet deposition. However, below-cloud scavenging is also very important and is responsible for approx. 30% of the amount of wet deposited mercury in the simulation domain. The more detailed analyses of mercury chemistry and mercury scavenging are presented in Figure 7-75, Table 7-16,Table 7-17 and Table 7-18.

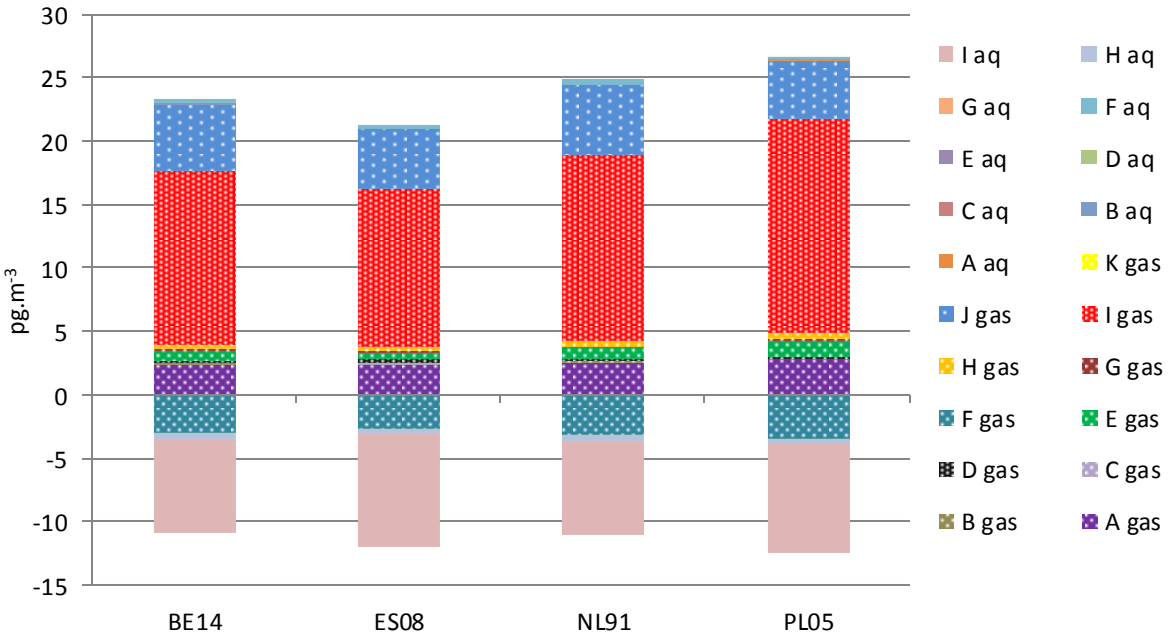

Figure 7-75.The increase or decrease of air concentration of reactive mercury (RGM+Hg_P) at selected stations at surface due to implementation of various reactions of mercury in gaseous and aqueous phases [pg.m^{-3}]. **A gas** - $Hg^0+O_3 \rightarrow HgO+O_2$, **B gas** - $Hg^0+Cl_2 \rightarrow HgCl_2$,**C gas** - $Hg^0+2HCl \rightarrow HgCl_2+H_2$, **D gas** - $Hg^0+H_2O_2 \rightarrow Hg(OH)_2$,**E gas** - $HgBr+2Br^{\bullet} \rightarrow HgBr_2$, **F gas** - $HgBr \rightarrow Hg^0+ Br^{\bullet}$, **G gas** - $HgBr+Br^{\bullet} \rightarrow HgBr_2$, **H gas** - $HgBr+{}^{\bullet}OH \rightarrow HgBrOH$, **I gas** - $Hg^0+BrO^{\bullet} \rightarrow HgO+Br$, **J gas** - $Hg^0+2{}^{\bullet}OH \rightarrow Hg(OH)_2$, **K gas** - $HgBr+Br^{\bullet} \rightarrow Hg^0+ Br_2$,
A aq - $Hg^0+O_3+H^+ \rightarrow Hg^{2+}+OH^-+O_2$, **B aq** - $Hg^0+{}^{\bullet}OH \rightarrow Hg^+ + OH^-$,
C aq - $Hg^0+HOBr \rightarrow Hg^{2+}+OH^-+Br^-$, **D aq** - $Hg^0+Br_2 \rightarrow Hg^{2+}+2Br^-$,
E aq - $Hg^0+OBr^-+H^+ \rightarrow Hg^{2+}+Br^-+OH^-$, **F aq** - $Hg^0+HOCl \rightarrow Hg^{2+}+OH^-+Cl^-$,
G aq - $Hg^0+OCl^-+H^+ \rightarrow Hg^{2+}+OH^-+Cl^-$, **H aq** - $HgSO_3 \rightarrow Hg^0 + product(SIV)$,
I aq - $Hg^{2+}+HO_2^{\bullet} \rightarrow Hg^0+O_2+H^+$.

The analysis of the results (Figure 7-75) shows that the oxidation of $Hg^0_{(g)}$ by bromine oxide radical is the most important. The second most effective oxidant of GEM is the hydroxyl radical, and the third place is the ozone reaction. In the aqueous phase, the reduction reactions of $Hg^{II}_{(aq)}$ are much more effective than oxidation of $Hg^0_{(aq)}$. The reduction of $Hg^{II}_{(aq)}$ by $HO_2{}^{\bullet}_{(aq)}$ plays a significant role in the mass balance of atmospheric mercury. The reaction with chlorine and chlorine compounds in the gaseous phase and all oxidation reactions in aqueous phase have a rather low impact on the atmospheric concentrations of reactive mercury.

Table 7-16. The relative changes amounts of air concentrations and deposition in the European domain by use of different coefficients for in-cloud scavenging. The presented values are ratios of the amounts of deposition and ambient concentrations of mercury from model run with the use of listed scavenging coefficients to results of simulation with the use of reference scavenging coefficients in base model of $8.4 \cdot 10^{-5} \cdot I^{0.79}$ [244], [245].

N.			scavenging coefficient [s^{-1}]			
			$3.5 \cdot 10^{-4} \cdot I^{0.78}$	$3.36 \cdot 10^{-4} \cdot I^{0.79}$	$4.17 \cdot 10^{-4} \cdot I^{0.79}$	$\frac{1-\exp(-\alpha\tau_{cld})}{\tau_{cld}}$
1	Ambient	Hg^0	1.01	1.00	1.00	0.99

2	concentration	RGAM	0.92	0.90	0.89	0.66
3		Hg_P	1.00	0.91	0.89	0.71
4	Dry deposition	Hg^0	1.00	1.00	1.00	0.99
5		RGM	0.99	0.98	0.98	0.94
6		Hg_P	1.05	0.92	0.91	0.74
7	Wet deposition	Hg^0	1.33	1.26	1.33	4.24
8		RGAM	1.51	1.44	1.51	2.30
9		Hg_P	1.57	1.45	1.52	2.25

Table 7-17. The relative changes of amounts of mercury of air concentrations and deposition in European domain by use of scavenging coefficients of $4.17 \cdot 10^{-7} \cdot I \cdot E \cdot D^{-1}$ proposed in CAMx model [263] and implementation of different representative raindrop diameter for in-cloud scavenging model. The presented values are the ratio of the deposition and ambient concentrations of mercury from model run with the use of listed representative raindrop diameter to results of simulation with the use of base model. E- collision efficiency with raindrops was assumed to be 0.9 for all forms of mercury [211]. One simulation is done with collision efficiency of 0.4 and representative raindrop diameter of $0.9 \cdot 10^{3} \cdot I^{0.21}$ [246]. In case of use of representative raindrop diameter of $0.9 \cdot 10^{3} \cdot I^{0.21}$ and collision efficiency of 0.9, the scavenging coefficient equals $4.17 \cdot 10^{-4} \cdot I^{0.79}$ and the results are presented in Table 7-16.

N.			collision efficiency										
			0.9										0.4
			representative raindrop diameter D [m]										
			$1.238 \cdot 10^{-3} \cdot I^{0.182}$	$7.88 \cdot 10^{-4} \cdot I^{0.3}$	$3.97 \cdot 10^{-4} \cdot I^{0.37}$	$8 \cdot 10^{-4} \cdot I^{0.34}$	$1.3 \cdot 10^{-3} \cdot I^{0.14}$	$7 \cdot 10^{-4} \cdot I^{0.25}$	$1.18 \cdot 10^{-3} \cdot I^{0.2}$	$1.06 \cdot 10^{-3} \cdot I^{0.16}$	$9.7 \cdot 10^{-4} \cdot I^{0.158}$	$1.16 \cdot 10^{-3} \cdot I^{0.227}$	$0.9 \cdot 10^{3} \cdot I^{0.21}$
1	Ambient concentration	Hg^0	0.99	1.00	1.00	1.00	1.00	1.00	1.00	1.00	1.00	1.00	1.00
2		RGAM	0.75	0.86	0.79	0.85	0.92	0.86	0.91	0.91	0.90	0.90	0.95
3		Hg_P	0.79	0.88	0.82	0.87	0.92	0.88	0.92	0.92	0.91	0.91	0.95
4	Dry deposition	Hg^0	0.99	1.00	0.99	1.00	1.00	1.00	1.00	1.00	1.00	1.00	1.00
5		RGM	0.96	0.98	0.97	0.98	0.99	0.98	0.99	0.99	0.98	0.98	0.99
6		Hg_P	0.81	0.89	0.84	0.89	0.94	0.89	0.93	0.93	1.00	0.92	0.96
7	Wet deposition	Hg^0	2.65	1.40	1.82	1.41	1.21	1.45	1.24	1.27	1.30	1.25	1.11
8		RGAM	2.04	1.60	1.85	1.62	1.36	1.61	1.42	1.44	1.46	1.44	1.25
9		Hg_P	2.01	1.61	1.85	1.63	1.38	1.62	1.43	1.45	1.47	1.45	1.26

The applied different scavenging coefficients for in-cloud scavenging presented in Table 7-16 and representative raindrop diameters presented in Table 7-17 give the highest results of wet deposition compared to results from modelling with the use of reference value. Therefore, despite the fact that the modelling results are overestimated (Figure 7-32), there is no possibility to decrease the results of wet deposition by applying another scavenging coefficient reported in literature.

Table 7-18. The relative changes amount of air concentrations and deposition in the European domain by use of different raindrop velocity for below-cloud scavenging model. The presented values are ratio of the amounts of deposition and ambient concentrations of mercury from model run with the use of listed raindrop velocity to results of simulation with the use of reference raindrop velocity in base model of $4854.1 \cdot D \cdot \exp(-195 \cdot D)$, [206], [208]. D - representative raindrop diameter D [m].

N.	Raindrop velocity [$m.s^{-1}$]	Ambient concentration			Dry deposition			Wet deposition		
		GEM	RGAM	Hg_P	GEM	RGM	Hg_P	Hg^0	RGAM	Hg_P
1	$142 \cdot D^{0.5}$	1.00	1.01	0.99	1.00	1.01	0.99	1.00	0.97	1.02
2	$9.43 \cdot (1-\exp((-1000 \cdot D/1.77)^{1.47}))$	1.00	0.98	1.01	1.00	0.98	1.01	1.00	1.05	0.97
3	$386.577 \cdot D^{0.67}$	1.00	1.00	1.00	1.00	1.00	1.00	1.00	1.00	1.00
4	$3.075 \cdot 10^{7} \cdot D^2$ for $D<10^{-4}$ $3.8 \cdot 10^{3} \cdot D$ for $10^{-4} <D<10^{-3}$ $133.046 \cdot D^{0.5}$ for $D>10^{-3}$	1.00	1.01	0.99	1.00	1.01	0.99	1.00	0.98	1.01
5	$-0.193+4.96 \cdot 10^{3} \cdot D-9.04 \cdot 10^{5} \cdot D^2+5.66 \cdot 10^{7} \cdot D^3$	1.00	0.99	1.00	1.00	0.99	1.00	1.00	1.02	0.99

All reported raindrop velocities for below-cloud scavenging model give very close results (Table 7-18). The relative changes of wet deposition of RGAM range from 0.97 to 1.05.

Table 7-19. The relative changes amounts of mercury wet deposition in the European domain by use of various rate constants [$cm^3.molec^{-1}.s^{-1}$] applied for oxidation of GEM by ozone and hydrogen peroxide. The presented values are the ratio of the amounts of deposition and ambient concentrations of mercury from model run with the use of listed rate constants to results of simulation with the use of base model. In the base model, the rate constants of $2.1 \cdot 10^{-18} \cdot \exp(-1246/T)$ [$cm^3.molec^{-1}.s^{-1}$] and $8.4 \cdot 10^{-6} \cdot \exp(-9021/T)$ [$cm^3.molec^{-1}.s^{-1}$] for oxidation by ozone and hydrogen peroxide were applied [96], [113].

N.			$Hg^0_{(g)}+O_{3(g)} \rightarrow HgO_{(g)}+O_{2(g)}$				$Hg^0_{(g)}+H_2O_{2(g)} \rightarrow Hg(OH)_{2(g)}$	
			Rate constants [$cm^3.molec^{-1}.s^{-1}$]					
			$4.2 \cdot 10^{-19}$	$1.7 \cdot 10^{-18}$	$4.9 \cdot 10^{-18}$	$7.5 \cdot 10^{-19}$	$4.1 \cdot 10^{-16}$	$6.0 \cdot 10^{-19}$
1	Ambient concentration	GEM	0.93	0.76	0.51	0.88	0.48	1.00
2		RGAM	2.10	4.77	8.48	2.90	9.84	1.03
3		Hg_P	1.00	1.00	1.00	1.00	1.00	1.00
4	Dry deposition	GEM	0.92	0.73	0.48	0.87	0.39	1.00
5		RGM	2.07	4.71	8.38	2.86	9.46	1.03
6		Hg_P	0.99	0.99	0.99	0.99	0.99	1.00
7	Wet deposition	Hg^0	0.94	0.79	0.57	0.90	0.53	1.00
8		RGAM	2.20	5.22	9.76	3.08	9.13	1.03
9		Hg_P	1.00	0.99	0.99	0.99	0.99	1.00

The gaseous oxidation of $Hg^0_{(g)}$ with ozone plays one of the most important role in the mass balance of reactive mercury (Figure 7-75). Therefore, the model is very sensitive to the changes of the value of this rate constant. Application of a rate constant of $4.9 \cdot 10^{-18}$ causes the octuple increase of concentration and deposition of reactive mercury. Similar changes are noticed when the rate constant of $4.1 \cdot 10^{-16}$ is applied for the oxidations of $Hg^0_{(g)}$ by hydrogen peroxide.

Table 7-20. The relative changes of amounts of mercury of air concentrations and deposition in the European domain by use of various rate constants applied for oxidation of GEM by molecular chlorine and hydroxyl radical. The presented values are the ratio of the amounts of deposition and ambient concentrations of mercury from model run with the use of listed rate constants to results of simulation with the use of base model. In the base model, the rate constant of $2.6 \cdot 10^{-18}$ [$cm^3.molec^{-1}.s^{-1}$] and $8.7 \cdot 10^{-14}$ [$cm^3.molec^{-1}.s^{-1}$] for oxidation respectively by molecular chlorine and hydroxyl radical were applied [117], [107].

N.			$Hg^0_{(g)}+Cl_{2(g)} \rightarrow HgCl_{2(g)}$				$Hg^0_{(g)}+2^{\bullet}OH_{(g)} \rightarrow Hg(OH)_{2(g)}$		
			Rate constants [$cm^3.molec^{-1}.s^{-1}$]						
			$4.8 \cdot 10^{-18}$	$5.7 \cdot 10^{-17}$	$1.82 \cdot 10^{-19}$	$4.3 \cdot 10^{-15}$	$1.6 \cdot 10^{-12}$	$1.2 \cdot 10^{-13}$	$3.2 \cdot 10^{-13} \cdot (T/298)^{-3.06}$
1	Ambient concentration	GEM	1.00	1.00	1.00	0.92	0.90	1.00	0.93
2		RGAM	1.00	1.01	1.00	2.05	2.64	1.04	2.22
3		Hg_P	1.00	1.00	1.00	1.00	1.00	1.00	1.00
4	Dry deposition	GEM	1.00	1.00	1.00	0.95	0.88	1.00	0.91
5		RGM	1.00	1.02	1.00	2.33	2.68	1.04	2.24
6		Hg_P	1.00	1.00	1.00	1.00	0.99	1.00	0.99
7	Wet deposition	Hg^0	1.00	1.00	1.00	0.94	0.92	1.00	0.94
8		RGAM	1.00	1.01	1.00	2.02	2.27	1.03	1.94
9		Hg_P	1.00	1.00	1.00	1.00	0.99	1.00	1.00

As the oxidation of GEM by chlorine is low (Figure 7-75), the changes of the value of the rate constants by factor of 4, as presented in Table 7-20, results are very similar. On the contrary, the changes of rate the constant of the reaction $Hg^0_{(g)}$ with hydroxyl radical affects significantly the reactive mercury concentrations and deposition, resulting in a threefold increase.

Table 7-21. The relative changes of amounts of mercury air concentrations and deposition in the European domain by use of various rate constant applied to oxidation of $Hg^0_{(g)}$ by bromine radical. The presented values are the ratio of the amounts of deposition and ambient concentration of mercury from model run with the use of listed rate constants to results of simulation with the use of base model. In the base model the rate constant of $1.46 \cdot 10^{-32} \cdot (T/298)^{-1.86}$ [$cm^6.molec^{-2}.s^{-1}$] by bromine radical was applied [226].

N.			$Hg^0_{(g)}+Br^{\bullet}_{(g)} \rightarrow HgBr_{(g)}$		
			Rate constants [$cm^3.molec^{-1}.s^{-1}$]		
			$3.2 \cdot 10^{-12}$	$1.01 \cdot 10^{-12} \cdot \exp(209/T)$	$9.8 \cdot 10^{-13} \cdot \exp(401 \cdot (1/T-1/298))$
1	Ambient concentration	GEM	0.99	0.99	0.99
2		RGAM	1.16	1.10	1.22
3		Hg_P	1.00	1.00	1.00
4	Dry deposition	GEM	0.99	0.99	0.99
5		RGM	1.13	1.09	1.19
6		Hg_P	1.00	1.00	1.00
7	Wet deposition	Hg^0	0.99	0.99	0.99
8		RGAM	1.20	1.13	1.28
9		Hg_P	1.00	1.00	1.00

The value applied in the base model for the reference rate constant of GEM oxidation by bromine radical is the least effective. The application of other possible values of the rate constant causes the increase of RGAM concentrations and deposition (Table 7-21).

Additional reactions in the gaseous phase were also implemented in to the model. The oxidation of $Hg^0_{(g)}$ by molecular bromine, nitrate radical, molecular iodine, molecular fluorine and chlorine radicals were separately added to the base model. These reactions were confirmed in laboratory research studies, however, they have not been widely applied to mercury chemical transport models (Table 3-1and Table 3-2). The obtained results are presented in Table 7-22.

Table 7-22. The relative changes amounts of mercury of air concentrations and deposition in the European domain by use of additional reactions of oxidation of $Hg^0_{(g)}$ by molecular bromine, nitrate radical, molecular iodine, molecular fluorine and chlorine radicals. The presented values are the ratio of the amounts of air concentrations and deposition of mercury from model run with the use of listed reactions to results of simulation with the use of base model (without listed reaction).

N.	Reaction	Ambient concentration			Dry deposition			Wet deposition		
		GEM	RGAM	Hg_P	GEM	RGM	Hg_P	Hg^0	RGAM	Hg_P
1	$Hg^0_{(g)} + Br_{2(g)} \rightarrow HgBr_{2(g)}$	1.00	1.00	1.00	1.00	1.00	1.00	1.00	1.00	1.00
2	$Hg^0_{(g)} + NO_3^{\bullet}{}_{(g)} \rightarrow HgO_{(g)} + NO_{2(g)}$	0.98	1.32	1.00	0.98	1.30	1.00	0.98	1.34	1.00
3	$Hg^0_{(g)} + I_{2(g)} \rightarrow HgI_{2(g)}$	1.00	1.00	1.00	1.00	1.00	1.00	1.00	1.00	1.00
4	$Hg^0_{(g)} + F_{2(g)} \rightarrow HgF_{2(g)}$	0.25	12.43	1.00	0.21	12.29	0.99	0.31	15.22	1.34
5	$Hg^0_{(g)} + Cl^{\bullet}_{(g)} \rightarrow HgCl_{(g)}$	0.99	1.17	1.00	0.99	1.17	1.00	0.99	1.19	1.00

The oxidation of GEM by molecular bromine and molecular iodine is not very effective. The changes in depiction of concentrations over the domain are not visible (Table 7-22). The nitrate radical and chlorine radicals are significant oxidants of $Hg^0_{(g)}$. The ambient concentrations of RGAM increases by 32% and 17%, respectively. The implementation into the model of the reaction with molecular fluorine causes a large loss of gaseous elemental mercury and a quick rise of concentration of reactive mercury (RGAM and Hg_P).

The obtained results from the model run are reconciled with the data presented in Figure 2-9. The most effective oxidants of GEM may be molecular fluorine, nitrate radical, ozone, hydroxyl radical and bromine oxide radical. It should be noted that the relatively narrow range of concentrations of oxidants were used in the model. For many oxidants only one fixed value of concentration was implemented. The rate constants used in the model were estimated in

laboratory conditions or were theoretically calculated with the use of the dedicated models. Another subject to keep in mind is that the many rate constants applied to this model as well as to other mercury chemical models are not given as a function of temperature and pressure. The value of the rate constants is applied to the model for all possible atmospheric conditions. The relative changes of value of five rate constants reported as a function of temperature are plotted in Figure 7-76.

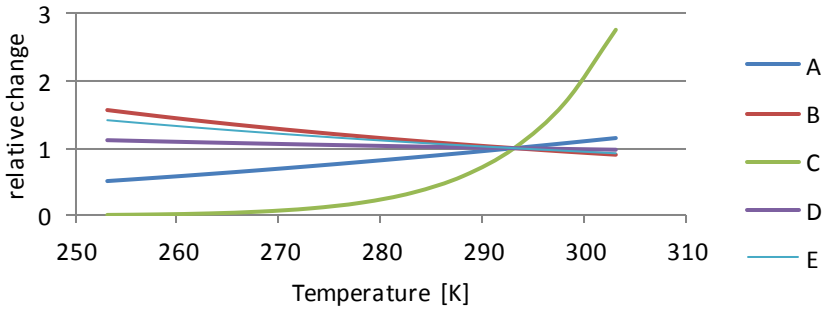

Figure 7-76. The relative changes of rate constants the temperature. The presented values are the ratio of the value of the rate constant at different temperatures to the value of the rate constant at a temperature of 20^0C (293.16K). All rate constant linked to oxidation of $Hg^0_{(g)}$ by: **A** –ozone – $2.1 \cdot 10^{-18} \exp\left(-\frac{1246}{T}\right)$,[96]; **B** –hydroxyl radical $-3.2 \cdot 10^{-13} \cdot (T/298)^{-3.06}$,[111]; **C** –hydrogen peroxide $-8.4 \cdot 10^{-6} \cdot \exp(-9021/T)$, [113], **D** –chlorine radicals $-1.38 \cdot 10^{-12} \cdot \exp(208.02/T)$, [123], **E** –bromine radical – $1.1 \cdot 10^{-12} \cdot (T/298)^{-2.37}$, [111].

The plotted curves in Figure 7-76 of relative changes of the value of rates constants at temperatures ranging from -20^0C up to 40^0C show that the temperature has a rather significant influence on values of rate constants. The value of rate constants for oxidation of GEM by hydrogen peroxide increases 350 times in the considered temperature range. On the other hand, it should be noted that for many reactions, the rate constant differing by 4 orders of magnitude, gives similar modelling results of concentrations and deposition (Table 7-19 and Table 7-20)

To analyse the possible influence of the implementation of reactive mercury adsorption onto particulate matter in the gaseous phase the model in which $HgO_{(g)}$ was assumed to be immediately adsorbed to PM was developed. The adsorbed $HgO_{(P)}$ was split into 10 size sections based on the surface area of aerosols. Equal concentrations in all sections of particulate matter onto which surface the $HgO_{(g)}$ is adsorbed were assumed.

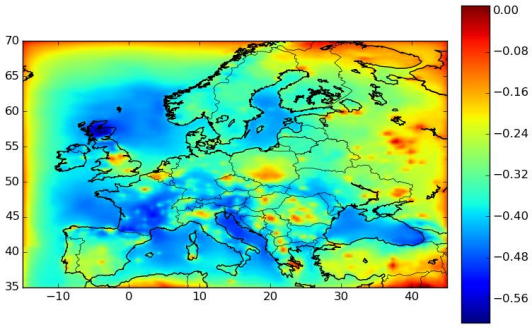

Figure 7-77. Fractional bias (FB) of results of ambient concentration of RGPM (RGM + Hg_P) at the surface from models run when formed HgO is in gaseous ([gas_{HgO}]) and particulate forms ([PM_{HgO}]).
FB = 2·([gas_{HgO}] - [PM_{HgO}]) /([gas_{HgO}] + [PM_{HgO}]).

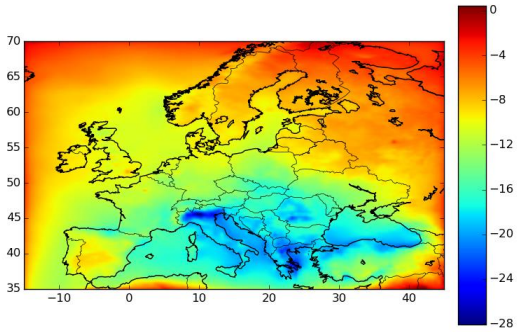

Figure 7-78. Differences (Diff) in ambient concentration of RGPM (RGM + Hg_P) at the surface from model runs when formed HgO is in gaseous ([gas_{HgO}]) and particulate forms ([PM_{HgO}]) [$pg.m^{-3}$].
Diff=[gas_{HgO}] - [PM_{HgO}].

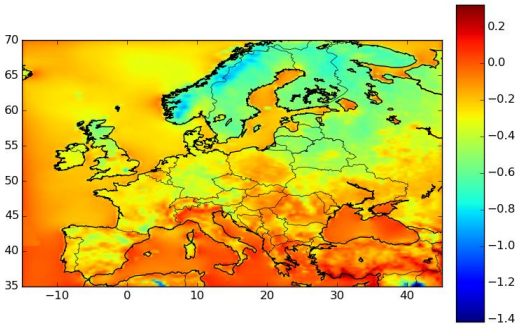

Figure 7-79. Fractional bias (FB) of results of dry deposition load of RGPM (RGM + Hg_P) at the surface from model runs when formed HgO is in gaseous ([gas_{HgO}]) and particulate forms ([PM_{HgO}]).
FB = 2·([gas_{HgO}] - [PM_{HgO}]) /([gas_{HgO}] + [PM_{HgO}]).

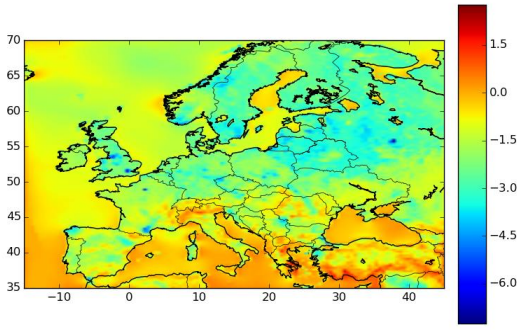

Figure 7-80. Differences (Diff) in dry deposition load of RGPM (RGM + Hg_P) at the surface from model runs when formed HgO is in gaseous ([gas_{HgO}]) and particulate forms ([PM_{HgO}]) [$g.km^{-2}.y^{-1}$].
Diff=[gas_{HgO}] - [PM_{HgO}].

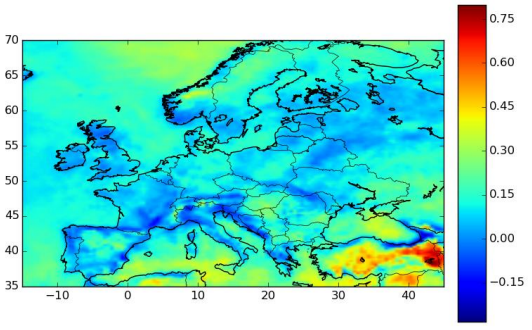

Figure 7-81. Fractional bias (FB) of results of wet deposition load of RM ($RGM+Hg^{II}_{(aq)}+Hg_P$) at the surface from model runs when formed HgO is in gaseous ([gas_{HgO}]) and particulate forms ([PM_{HgO}]).
FB = 2·([gas_{HgO}] - [PM_{HgO}]) /([gas_{HgO}] + [PM_{HgO}]).

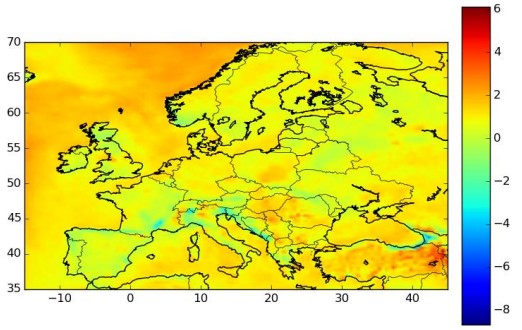

Figure 7-82. Differences (Diff) in wet deposition load of RM ($RGM+Hg^{II}_{(aq)}+Hg_P$) at the surface from model runs when formed HgO is in gaseous ([gas_{HgO}]) and particulate forms ([PM_{HgO}]) [$pg.m^{-3}$].
Diff=[gas_{HgO}] - [PM_{HgO}].

In general, the adsorption of $HgO_{(g)}$ onto particulate matters decreases the concentration and dry deposition and increases the wet deposition of reactive mercury. The changes in results are significant in many places of the simulation domain. For example, over the Mediterranean Sea the ambient concentration of reactive mercury (RGPM) decreased by 28 $pg.m^{-3}$. The fractional bias over the majority of the domain does not exceed an absolute value of 0.5 for concentration as well as for deposition (wet and dry). It should be noted that the concentration of particulate matter, here assumed to be equal, varies widely for various aerosol size sections. Generally, a higher concentration is observed for small particles with the representative diameter up to 2.5 μm. This can cause that most of the mercury will be mainly adsorbed on very small particles, bearing in mind also that the total area of particles increases with the decreasing diameter of the particular particles (Table 6-5). Furthermore, the adsorption of mercury already exists in the process of release of mercury into the atmosphere. For example, during the coal combustion process in the boiler a part of mercury is adsorbed onto dust. In the base model the emission of Hg_P was assumed to be uniform across all considered PM size sections. Taking into consideration the adsorption process of mercury onto particles of dust, the model was also run with a distribution of Hg_p in proportion to particle surface areas. In this case, the assumption that the concentration of aerosols is uniform across 10 the size sections of particulate matter was done. The corresponding results are shown in Figure 7-83 – Figure 7-88.

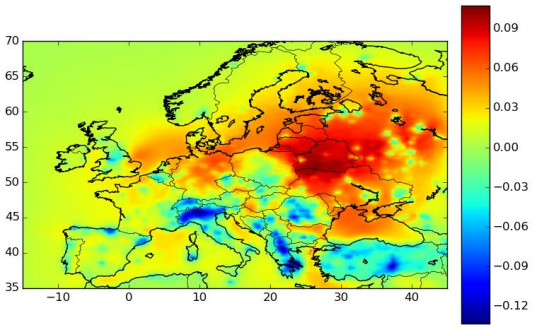

Figure 7-83. Fractional bias (FB) of results of ambient concentration of mercury bound to particulate matter at the surface from base model runs when emission of Hg_P were distributed equally ($[Hg_{P(eq)}]$) and in proportion to aerosol surface areas ($[Hg_{P(sf)}]$). $FB = 2\cdot([Hg_{P(eq)}] - [Hg_{P(sf)}]) / ([Hg_{P(eq)}] + [Hg_{P(sf)}])$.

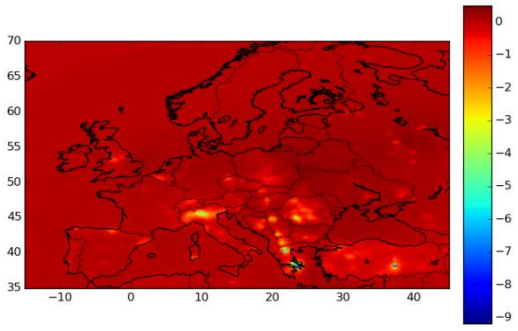

Figure 7-84. Differences (Diff) in ambient concentration of mercury bound to particulate matter at the surface from base model runs when emission of Hg_P were distributed equally ($[Hg_{P(eq)}]$) and in proportion to aerosol surface areas ($[Hg_{P(sf)}]$) $[pg.m^{-3}]$. $Diff=[Hg_{P(eq)}] - [Hg_{P(sf)}]$.

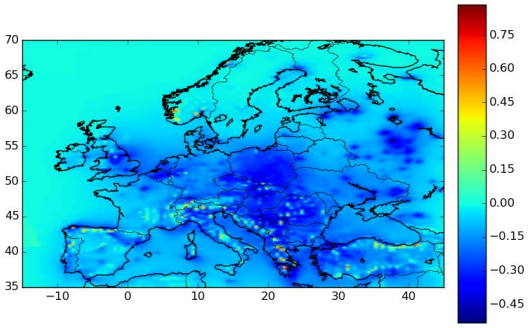

Figure 7-85. Fractional bias (FB) of results of dry deposition of mercury bound to particulate matter at the surface from base model runs when emission of Hg_P were distributed equally ($[Hg_{P(eq)}]$) and in proportion to aerosol surface areas ($[Hg_{P(sf)}]$).
$FB = 2 \cdot ([Hg_{P(eq)}] - [Hg_{P(sf)}]) / ([Hg_{P(eq)}] + [Hg_{P(sf)}])$.

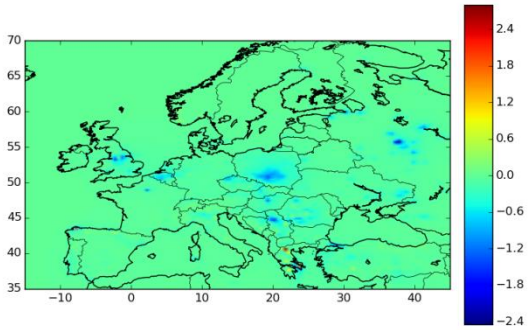

Figure 7-86. Differences (Diff) in dry deposition load of mercury bound to particulate matter at the surface level from base model runs when emission of Hg_P were distributed equally ($[Hg_{P(eq)}]$) and in proportion to aerosol surface areas ($[Hg_{P(sf)}]$) [$g.km^{-2}.y^{-1}$].
$Diff = [Hg_{P(eq)}] - [Hg_{P(sf)}]$.

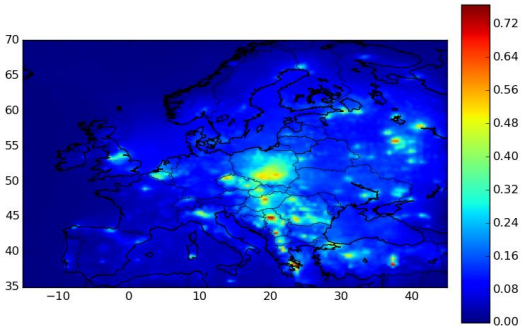

Figure 7-87. Fractional bias (FB) of results of wet deposition of mercury bound to particulate matter at the surface from base models run when emission of Hg_P were distributed equally ($[Hg_{P(eq)}]$) and in proportion to aerosol surface areas ($[Hg_{P(sf)}]$).
$FB = 2 \cdot ([Hg_{P(eq)}] - [Hg_{P(sf)}]) / ([Hg_{P(eq)}] + [Hg_{P(sf)}])$.

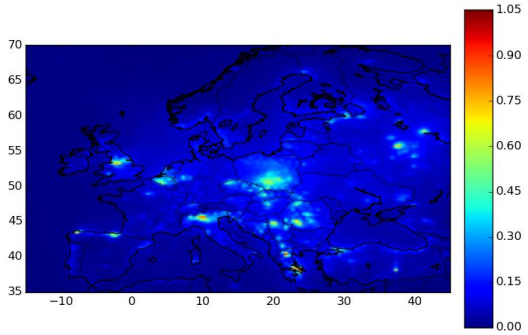

Figure 7-88. Differences (Diff) in wet deposition load of mercury bound to particulate matter at the surface from base model runs when emission of Hg_P were distributed equally ($[Hg_{P(eq)}]$) and in proportion to aerosol surface areas ($[Hg_{P(sf)}]$) [$g.km^{-2}.y^{-1}$].
$Diff = [Hg_{P(eq)}] - [Hg_{P(sf)}]$.

The biggest changes in ambient concentrations and deposition of Hg_P are noted over Poland, as it is the place with the most intensive emission of mercury in Europe. The obtained ambient concentrations of Hg_P are higher compared to the results from the base model (Figure 7-86). It is the result of a lower dry deposition flux of Hg_P (Figure 7-88). The small particles are removed slowly from the atmosphere [95]. In case of the use of the distribution in proportion to the particle surface areas most of Hg_P is bound to small particles as is presented in Table

6-5. The modeling results for wet deposition show a high spatial variation over the whole simulation domain (Figure 7-87 and Figure 7-88).

One of the most important issue in modeling of the quality are the input data used in the simulation run [183]. As an example of meteorological parameters the evaluation of precipitation intensity was presented in Table 7-1. The evaluation of ambient concentrations of the species that react with mercury was presented in chapter 7.3. Moreover, various combinations of anthropogenic emission of mercury were used in this work (e.g. Table 7-7, Figure 7-86). The sensitivity of the model to changes in input data provided to the model is presented in Table 7-23.

Table 7-23. The relative changes amounts of mercury air concentrations and deposition in the European domain by use of various input data. The presented values are the ratio of results from base model run with the use of listed changed input data to modelling results with the use of reference input data.

N.	Changes in input data	Ambient concentration			Dry deposition			Wet deposition		
		GEM	RGAM	Hg_P	GEM	RGM	Hg_P	Hg^0	RGAM	Hg_P
1	Concentration of species which react with mercury less than 20%	1.01	0.90	1.00	1.01	0.89	1.00	1.01	0.91	1.00
2	Concentration of species which react with mercury is greater than 20%	0.99	1.09	1.00	0.99	1.11	1.00	0.99	1.09	1.00
3	The boundary concentration of mercury species less than 20%	0.82	0.84	0.86	0.81	0.84	0.85	0.81	0.82	0.83
4	The boundary concentration of mercury species is greater than 20%	1.18	1.16	1.14	1.19	1.16	1.15	1.19	1.18	1.17
5	The initial concentration of mercury species less than 20%	1.00	1.00	1.00	1.00	1.00	1.00	1.00	1.00	1.00
6	The initial concentration of mercury species is greater than 20%	1.00	1.00	1.00	1.00	1.00	1.00	1.00	1.00	1.00
7	The natural emission of mercury less than 20%	0.99	1.00	1.00	0.99	1.00	1.00	1.00	1.00	1.00
8	The natural emission of mercury is greater than 20%	1.01	1.00	1.00	1.01	1.00	1.00	1.00	1.00	1.00
9	The anthropogenic emission of mercury less than 20%	1.00	0.97	0.94	1.00	0.97	0.95	1.00	0.98	0.97
10	The anthropogenic emission of mercury is greater than 20%	1.00	1.03	1.06	1.00	1.03	1.05	1.00	1.02	1.03

The model is most sensitive to changes to boundary concentrations of mercury. The decreasing or increasing of concentrations of mercury of 20% at boundaries of modelling domain, causes the changes in the concentrations of GEM, RGAM and Hg_P of 18%, 16% and 14%, respectively. The air concentration of mercury oxidation and reduction compounds have also a significant influence on the quantity of RGAM in the simulation domain. The model response is a 10% change in the concentration of RGAM due to changes in concentration of

these species of 20%. It should be noted that the measurement and modelling of ambient concentrations of these species give a wide spectrum of possible results, which are presented in Figure 2-9. The implementation of the detailed concentration fields of all of the species taking part in the reactions with mercury will be a great improvement in the modelling of mercury atmospheric transport. The amounts of emitted mercury from both anthropogenic and natural sources has a rather low influence on mercury mass balance in the modelling domain. However, the detailed information of the amount of emissions of mercury and location of sources has a great influence on the local quantity of deposited mercury.

7.9 Contribution of different sources to mercury deposition in Poland

The results of the simulations run (i) with all emissions, (ii) without natural emissions and reemissions (iii) without all anthropogenic sources, (iv) without anthropogenic sources in Poland and (v) without emission from the Polish power sector were used to investigate the contribution of different emission sources to total mercury deposition in Poland in the year 2008 (Figure 7-89). In the simulation only emissions provided by EMEP were used.

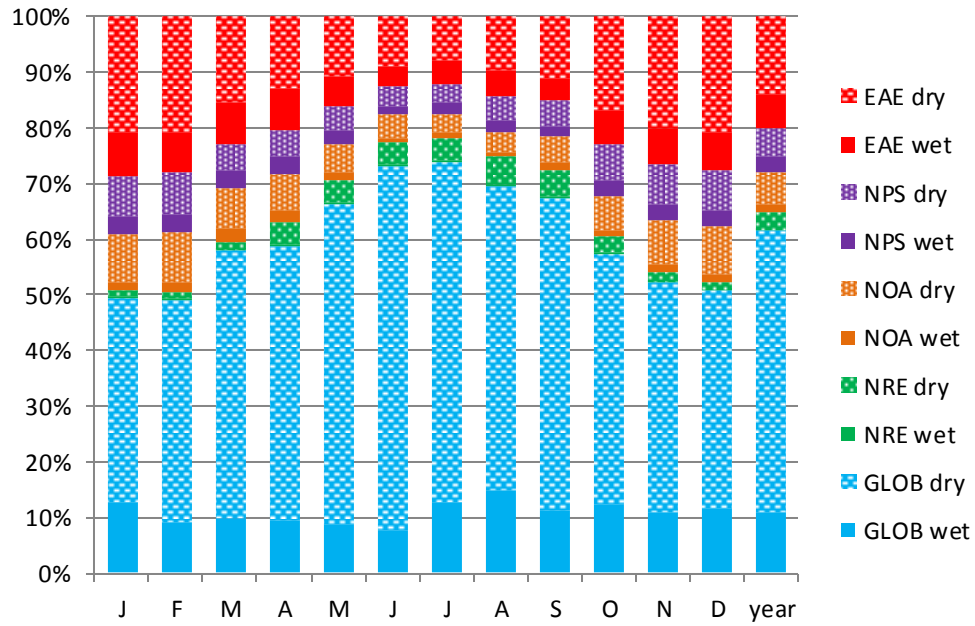

Figure 7-89. Contribution of national (Polish) power sector (NPS), national other anthropogenic (NOS), European anthropogenic (EAE), global (GLOB), and natural and re-emission sources (NRE) to total mercury deposition (dry +wet) in Poland in 2008.

The results in Figure 7-89 show the major contribution of global sources (GLOB) and a rather low contribution of natural and reemission sources (NRE). The contribution of the Polish power sector (NPS) varies in different months from 5% to 11% and national other anthropogenic sources (NOS) from 4% to 10%. The other anthropogenic European sources (EAE) contribute up to 20% to the overall annual deposition of mercury in Poland. The highest share of national sources (NPS +NOS) occurs during the winter heating season when large quantities of coal are combusted in the domestic sector and additionally the power sector activity is at its highest. The contribution of the national power sector (NPS) to all national sources varies from 45 to 55%. The majority of mercury is deposited in Poland through dry deposition process. The dry deposition contribution to the overall deposition ranges from 74% in January to 86% in June, with the annual average share of 79%. The obtained results of contribution of national sources are in contradiction with modelling results for 1999, where the Polish anthropogenic sources contributed the most to the deposition over Poland (range from 45% according to HYSPLIT model for August to 80% according to MSCE-HM model in February) [12]. The discrepancies between those results come from the amounts of deposited GEM from global sources (GLOB). In these models, dry deposition of mercury of 2 -6 $g.km^{-2}.y^{-1}$ over land was estimated. The results presented in Figure 7-61 show dry deposition of GEM over land of approx. 29 $g.km^{-2}.y^{-1}$ [217]. This value of the dry deposition flux over land compared to recent studies does not seem to be overestimated [264]. The emissions of mercury in Poland of 25.6 Mg in 2000 were used in those studies, while in this work national emissions were reduced by 10 Mg (Figure 2-6). The contribution of anthropogenic European sources (NPS +NOS +EAS) over 50% to the overall mercury deposition was obtained from simulations preformed with use of GLEMOS model [260]. That model also calculates the lower dry deposition flux compared to the model presented in this work. The results presented in Figure 7-89 are similar to the relative contribution of global, natural and re-emission sources (GLOB +NRE) and anthropogenic sources located in Europe (NPS +NOS +EAS) in Europe for 2005 obtained with GEOS-Chem, GLEMOS and CMAQ-Hg models [262].

7.10 The impact of the Polish power sector

The simulation runs over Poland allowed one to estimate the contribution of emissions from the Polish power sector to the overall deposition and air concentrations of mercury, lead and

cadmium. In this chapter, the detailed spatial results of the impact of the Polish power sector regarding mercury, lead and cadmium are presented in Figure 7-90 -Figure 7-114.

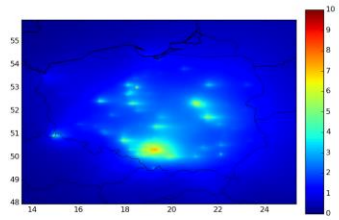

Figure 7-90. The impact of the Polish power sector. The percentage rate of emissions from power sector to overall average ambient concentration of GEM [%]. EF2008-fix emission was applied.

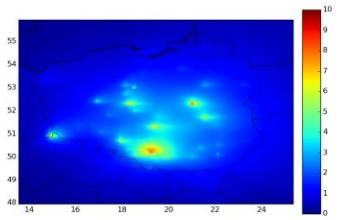

Figure 7-91. The impact of the Polish power sector. The percentage rate of emissions from power sector to overall average ambient concentration of GEM [%]. EF2008 emission was applied.

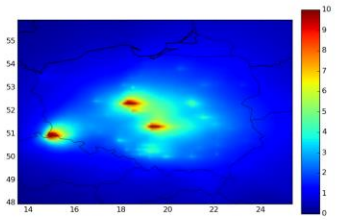

Figure 7-92. The impact of the Polish power sector. The percentage rate of emissions from power sector to overall average ambient concentration of GEM [%]. EF2009 emission was applied.

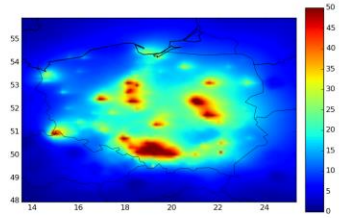

Figure 7-93. The impact of the Polish power sector. The percentage rate of emissions from power sector to overall average ambient concentration of RGM [%]. EF2008-fix emission was applied.

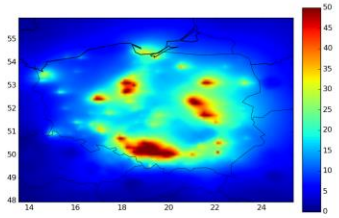

Figure 7-94. The impact of the Polish power sector. The percentage rate of emissions from power sector to overall average ambient concentration of RGM [%]. EF2008 emission was applied.

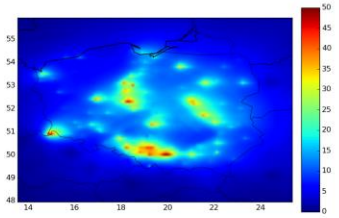

Figure 7-95. The impact of the Polish power sector. The percentage rate of emissions from power sector to overall average ambient concentration of RGM [%]. EF2009 emission was applied.

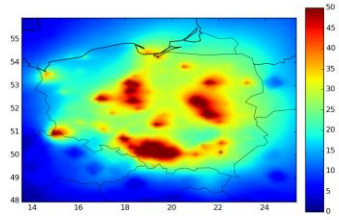

Figure 7-96. The impact of the Polish power sector. The percentage rate of emissions from power sector to overall average ambient concentration of Hg_P [%]. EF2008-fix emission was applied.

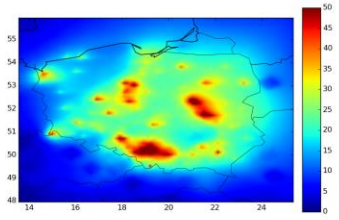

Figure 7-97. The impact of the Polish power sector. The percentage rate of emissions from power sector to overall average ambient concentration of Hg_P [%]. EF2008 emission was applied.

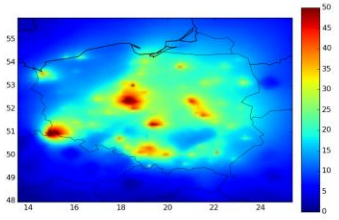

Figure 7-98. The impact of the Polish power sector. The percentage rate of emissions from power sector to overall average ambient concentration of Hg_P [%]. EF2009 emission was applied.

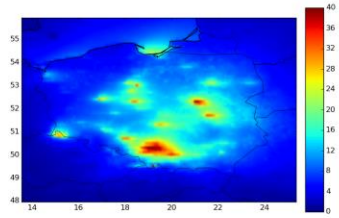

Figure 7-99. The impact of the Polish power sector. The percentage rate of emissions from power sector to overall dry deposition of mercury [%].
EF2008-fix emission was applied.

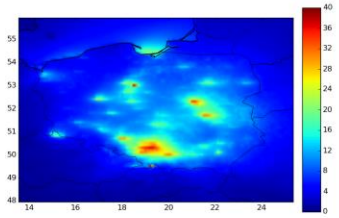

Figure 7-100. The impact of the Polish power sector. The percentage rate of emissions from power sector to overall dry deposition of mercury [%].
EF2008 emission was applied.

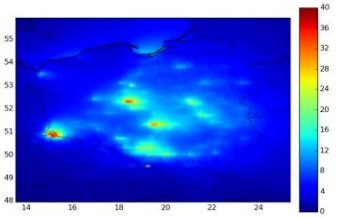

Figure 7-101. The impact of the Polish power sector. The percentage rate of emissions from power sector to overall dry deposition of mercury [%].
EF2009 emission was applied.

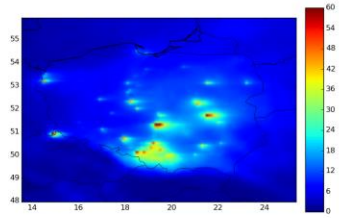

Figure 7-102. The impact of the Polish power sector. The percentage rate of emissions from power sector to overall wet deposition of mercury [%].
EF2008-fix emission was applied.

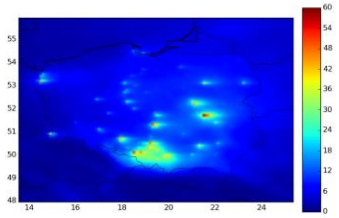

Figure 7-103. The impact of the Polish power sector. The percentage rate of emissions from power sector to overall wet deposition of mercury [%].
EF2008 emission was applied.

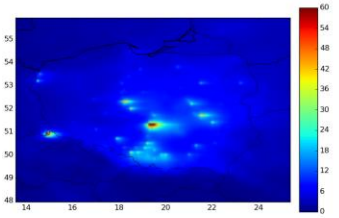

Figure 7-104. The impact of the Polish power sector. The percentage rate of emissions from power sector to overall wet deposition of mercury [%].
EF2009 emission was applied.

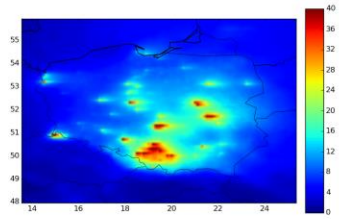

Figure 7-105. The impact of the Polish power sector. The percentage rate of emissions from power sector to overall deposition of mercury [%].
EF2008-fix emission was applied.

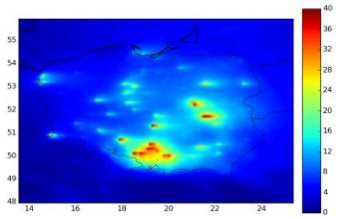

Figure 7-106. The impact of the Polish power sector. The percentage rate of emissions from power sector to overall deposition of mercury [%].
EF2008 emission was applied.

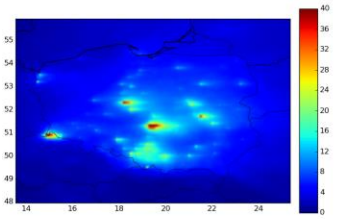

Figure 7-107. The impact of the Polish power sector. The percentage rate of emissions from power sector to overall deposition of mercury [%].
EF2009 emission was applied.

The atmospheric behaviour of forms of mercury, determines the contribution of mercury emission sources to the ambient mercury concentration and deposition at local and regional scale. As GEM is transported for long distances, the local contribution of even very

productive sources is relatively low and equals to at most 10%. While the contribution of mercury emissions from the power sector to the overall air concentration of reactive gaseous mercury and mercury bound to particulate matter exceed 50% near the large emission sources. The high influence of local sources on ambient concentrations of RGM and Hg_P determines the results presented in Figure 7-102, Figure 7-103 and Figure 7-104, which show that in many areas in Poland the power sector is responsible for more than 60% of the total wet deposition, because in the wet deposition process only mercury bound to particulate matter and reactive gaseous mercury are removed as Hg^0 scavenging is very insignificant. Therefore, the high amount of mercury deposited with precipitation indicates a high concentration of mercury included in particulate matter and reactive gaseous mercury. These forms are deposited locally and can be treated as the indicators of local mercury emissions. The local impact of the power sector on the dry deposition flux is slightly lower compared to the wet deposition (Figure 7-99, Figure 7-100, Figure 7-101), because the dry deposition results are mainly led by the amounts of deposited GEM (Figure 7-64). Its impact is lower on the local air concentration compared RGM or Hg_P.

The speciation and the quantity of emitted mercury by particular stacks have a significant influence on the obtained results. In three applied emission databases, the total emission from the power sector was nearly at the same level and equalled approx. 8.7 $Mg.y^{-1}$. However, the structure of these emission was different. In case of emission databases EF2008-fix and EF2008, mercury was mainly emitted from hard coal power, CHP and heating plants, while in the EF2009 database most of the mercury was emitted from 5 power plants that were based on brown coal. This implies that in Figure 7-92 the high impact of brown coal power plants occurs, while in Figure 7-90 and Figure 7-91, the impact of these plants is slightly visible. In the Figure 7-90 and Figure 7-91 the highest percentage rate of emissions from power sector to overall average ambient concentrations of GEM are noted for hard coal power and CHP plants. In general, application of the emissions included in the EF2009 database resulting in significant reduction of the influence of the emission of the power sector to air quality regarding mercury air concentrations over Silesia where most of Polish power plants that are based on hard coal are located. The differences in the obtained results of the impact of the Polish power sector to the overall average ambient concentrations of the various mercury forms governs the observed differences in the results of the deposition presented in Figure 7-99 -Figure 7-107. The role of the speciation of the emitted mercury is visible in Figure 7-108. Despite the fact that the annual total emissions of mercury in all used databases was at

the same level, the applied speciation of emitted mercury from the power sector was different. This results in significant differences in the average of results of percentage rate of emissions from power sector to overall wet and dry deposition of mercury over the whole of Poland (Figure 7-108). In case of EF2009, emission the impact is lowest (6% to overall deposition) because in this database the share of reactive mercury (RGM +Hg_P) to the overall emission was also lowest and equalled 27%. In contrary, the highest share of reactive mercury of 50 % was in EF2008-fix. This caused that the yearly average impact of emissions from the power sector to overall deposition (wet +dry) is 9%. The share of reactive mercury in EF2008 and in emissions used in model runs over Europe (the results market as NPS) is 42% and 39%, respectively.

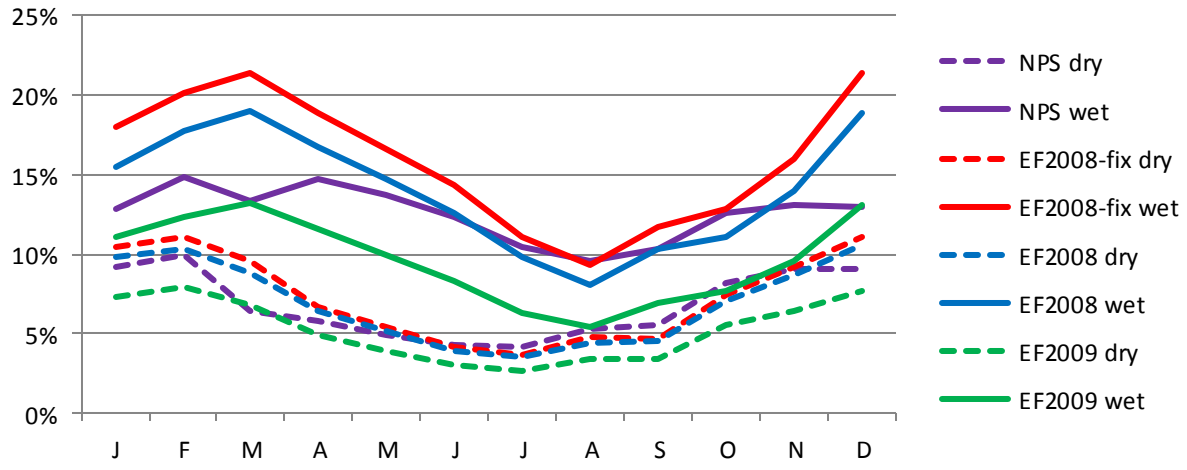

Figure 7-108. The impact of the Polish power sector. The percentage rate of emissions from the power sector to overall wet and dry deposition of mercury [%]. NPS -national power sector, results from model runs over Europe, presented also in Figure 7-89.

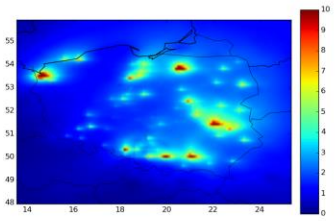

Figure 7-109. The impact of the Polish power sector. The percentage rate of emissions from the power sector to overall average ambient concentration of cadmium [%].

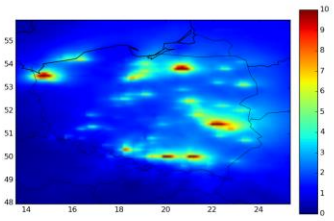

Figure 7-110. The impact of the Polish power sector. The percentage rate of emissions from the power sector to overall dry deposition of cadmium [%].

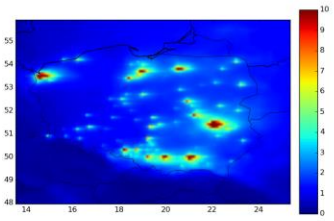

Figure 7-111. The impact of the Polish power sector. The percentage rate of emissions from the power sector to overall wet deposition of cadmium [%].

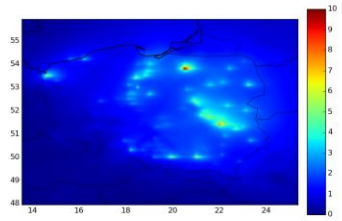

Figure 7-112. The impact of the Polish power sector. The percentage rate of emissions from the power sector to overall average ambient concentration of lead [%].

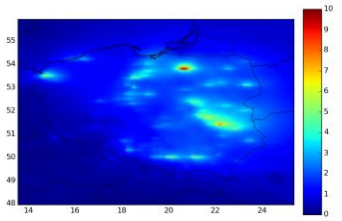

Figure 7-113. The impact of the Polish power sector. The percentage rate of emissions from the power sector to overall dry deposition of lead [%].

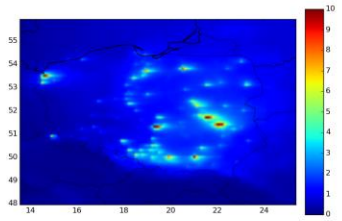

Figure 7-114. The impact of the Polish power sector. The percentage rate of emissions from the power sector to overall wet deposition of lead [%].

The impact of emissions of the power sector of lead and cadmium on ambient concentration and deposition is relatively low. The obtained results presented in Figure 7-109 -Figure 7-114 show that the impact of emissions from the Polish power sector reaches at most 10%. This rather in significant impact is due to the fact that the share of emissions from the power sector is low compared to the total emissions of lead and cadmium in Poland. The share of coal-based emission from the power sector in comparison to the overall cadmium and lead emissions, was approx. 5% in 2008. The highest rate in ambient concentration and deposition of lead and cadmium emitted from the power sector occurs near the largest emission sources. In Poland these are the brown coal power plants and hard coal industry heating plants.

8 Conclusions

The main aim of this work was to study the impact of the emissions of heavy metals (cadmium, lead and mercury) from the power sector on the air quality. To meet the declared aim, the new mercury chemical model was implemented into the Polyphemus air quality system. The main developments in this model are related to the reactions and transformations of mercury with bromine and the implementation of different sizes sections for mercury bound to aerosols. It should be underlined that the mercury chemistry in the atmosphere is very complex. The modelling of mercury behaviour in the atmosphere needs to be addressed with caution reviewed in detail. In this work, the scientific literature was reviewed in detail regarding mercury chemistry and mercury chemical models. In this part, it can be concluded that the chemistry of mercury is still not well known. There are many different reactions and transformations that were discovered under laboratory conditions but their occurrence in the

atmosphere is still not confirmed. Additionally for many reactions, the mechanism as well as the products of reactions were not fully investigated. For most of the mercury reactions, distinct values of rate constants exist. It implies that the chemistry of mercury implemented in the models may affect significantly among models. The models also differ in the way of calculating the dry and wet deposition of mercury. Additionally, the high uncertainties of the modelling results are related to the concentrations of compounds that react with mercury. Some of them are measured rarely and their air concentrations are only modelled. Overall, there are not many processes regarding mercury modelling which are common to all models. This causes the results of various models to differ significantly.

In order to analyse the problem of the contribution of heavy metals emitted from the Polish power sector in more detail, a database of the Polish power sector was prepared. It contains detailed information about boilers, emission controls equipment, fuel consumption and stack location. Thanks to this, the emissions of the power sector were desegregated into plants and speciation of mercury was estimated with a bottom-up approach. The simulations of heavy metals dispersion into the atmosphere were done on the European domain and the domain covering Poland with finer resolution. The fields of ambient concentrations and deposition of mercury over Europe and Poland were modelled. The results revealed the areas that are most polluted by heavy metals and showed where the Polish power sector has the higher impacts. The elemental gaseous mercury ambient concentrations are evenly distributed (relatively low spatial variations exist). On the contrary, high variations in the spatial gradients of reactive gaseous and particulate forms of mercury air concentrations and deposition fluxes were noted.

This detailed study shows that many components of the developed model have crucial impacts on the obtained results. In the model of mercury chemistry, the most effective pathway in the gaseous phase are the oxidation of gaseous elemental mercury by hydroxyl radical, ozone and most of all bromine oxide radicals, while in the aqueous phase the reduction reactions of elemental mercury dominate. These reactions have a crucial influence on the mass balance of reactive mercury, but a rather low influence on gaseous elemental mercury. The significant impact of the mass balance of gaseous elemental mercury includes the dry deposition process and implemented values of boundary concentrations. In this model, dry deposition of gaseous elemental mercury is the prevailing process for removing mercury from the atmosphere. Dry deposition of GEM over land is equally distributed, due to almost uniform ambient concentrations of this form. The relatively high dry deposition flux of gaseous elemental mercury has a huge influence on the presented results and differs significantly from other models where the dry deposition of GEM is often not taken into account in the models. It was

also shown that a change in the calculation of the scavenging coefficients or representative raindrop diameter for in-cloud scavenging has a significant impact on the amount of wet deposited reactive mercury. Equally important are also meteorological data, because the wet deposited amount of mercury is correlated with the precipitation intensity. The natural emissions as well as anthropogenic emissions have a rather low impact on the mass balance of mercury in the whole modelling domain, however, they have a crucial impact in particular areas. The detailed results show that the Polish power sector can be responsible for up to 80% of wet deposited mercury near large emission sources. However, the contribution from national sources over whole Poland is low and reaches only 21% during the winter heating season when large quantities of coal are burned in the domestic sector and additionally the power sector activity is at its highest. The fact that the spatial variations in GEM concentrations over Europe are moderate, on the contrary the high concentration of reactive mercury exists mainly near the emission sources which makes the latter mercury form a more relevant indicator of coal combustion. This mercury form plays an important role and has a large impact on mercury air concentrations and deposition, particularly at the local and regional scales. That is why national estimations of the amounts of emitted mercury should include the emissions of individual mercury forms and not only total emissions of mercury. However, the highest share in the total deposition in Poland derives from global sources of mercury and it is the reason why the adverse impact of mercury in Poland should be mainly reduced by global efforts to decrease mercury emissions and use.

The impact of emissions of cadmium and lead from the power sector is lower compared to the obtained results for mercury. The modelling results showed maximal impacts of 30% and 10% for cadmium and lead near large power sector sources on the ambient concentrations and deposition. The emissions of these heavy metals from the power sector where all plants are equipped with PM emission control systems are relatively low compared to other sources.

In this work, several scientific achievements were completed. The national emissions of mercury were split into mercury speciation forms with the use of a bottom-up approach. The detailed locations of emissions of mercury, lead and cadmium from the power sector was indicated. An update mercury chemistry model was developed and implemented to Polyphemus air quality system. For the first time, many reactions of mercury were applied to the chemical model, i.e. reactions with bromine, fluorine, iodine and chlorine radicals. The complex chemistry of mercury and bromine compounds were implemented into the model. The particulate matter dispersion of mercury, lead and cadmium were modelled using 10 particle size sections. The impact of many parts of the model (chemistry, deposition, input

data) on the results was investigated. The results on the impact of heavy metals emission from the Polish power sector and other sources were modelled. It should be emphasized that the scientific literature was reviewed in detail. However, it should be noted that in this scientific area there is still some lack of knowledge and the presented results show one possible solution and should be not treated as better than others obtained by different groups. To better understand the heavy metals behaviour, the model can be used to support measurements of mercury. This work shows that wide measurements of heavy metals are very much needed. The measurement stations in Europe should be mainly located in areas with high concentrations/deposition which were indicated in the modelling results. Due to a high uncertainty and simplification in the current assessment of mercury emissions, the amount of different mercury forms in exhaust gases should be monitored as well.
In conclusion let us come back to the exemplary questions and theses mentioned at the beginning of this work.

The first of them was *"does the dry deposition of gaseous elemental mercury have the greatest influence on obtained mercury deposition results?*"
The obtained results of the model show that the share of dry deposition of gaseous elemental mercury in the overall mercury deposition over land is the highest. At all stations, on average nearly 60% of deposited mercury come from dry deposition of GEM. This process has also the crucial impact on the obtained results of impact of the Polish power sector on mercury deposition in Poland.

The second question that was asked, was *"what is the contribution of different atmospheric reactions to the atmospheric mass balance of reactive mercury?"*.
The contribution of various reactions is very diverse. The most effective reaction of gaseous elemental mercury is that with bromine oxide radical, it contribute nearly 60% to the atmospheric production of reactive forms of mercury. The second reaction is the oxidation of GEM by hydroxyl radical, which contributes 20% of RGM atmospheric production. The aqueous reduction of $Hg^{II}_{(aq)}$ by $HO_2^{\bullet}{}_{(aq)}$ covers 70% of the mass of the whole atmospheric flux of reduction of reactive mercury to elemental mercury.

Another thesis was *"is most of the deposited mercury in Poland emitted outside Poland?".*
Yes, definitely. Three-quarters of deposited mercury in Poland was emitted outside Poland. The vast part comes even from outside the modelling domain, that is from outside Europe.

The other question that was asked, was *"what is the contribution of the power plant sector to local mercury deposition in Poland?*"
Overall taking into account the whole territory of Poland, this contribution in not very high and reaches 22% of overall deposition in the winter season. However, the results differ very much for various estimations of emissions the from the power sector. Near the large sources, the impact is significantly higher and reaches even 60% of the overall wet deposition of mercury.

The last question was *"does the concentration of reactive mercury and lead and cadmium depend strongly on local emission sources?".*
Yes, the high concentrations of reactive mercury and lead and cadmium are observed over areas were such species are emitted. In the maps of concentration of those species over Europe as well as maps showing the impact of the Polish power sector, the red spots indicate the areas with the high local emissions.

Results obtained in this work are very important in the context of preparing a national strategy on mercury reduction as they show to what extent mercury concentrations and deposition can be reduced over Poland by means of cutting national emissions. They also show that mercury, to a large extent, is a global pollutant and international agreements and strategies on mercury reduction are necessary to effectively tackle the problem. The model can be used as a tool supporting decision making to improve the situation in areas with the highest mercury concentrations and deposition.

References

1. AMAP/UNEP, *Technical Background Report of the Global Atmospheric Mercury Assessment*, 2008, Arctic Monitoring and Assessment Program/ UNEP Chemical Branch. p. 159.
2. Ministry of the Environment Government of Japan. *Minamata Disease The History and Measures*. 2002 [cited 2014; Available from: www.env.go.jp/en/chemi/hs/minamata.html.
3. Bakir, F., Damluji, S., Amin-Zaki, L., Murtadha, M., Khalidi, A., NY., a.-R., Tikriti, S., Dahahir, H., Clarkson, T., Smith, J.,Doherty, R., *Methylmercury poisoning in Iraq*. Science, 1973. 181 (4096): p. 230-241
4. Rabl, A.,Spadaro, J.V., *Estimating the uncertainty of damage costs of pollution: A simple transparent method and typical results*. Environmental Impact Assessment Review Volume, 2008. 28: p. 166–183.
5. UNEP, *Final review of scientific information on cadmium*, 2010, UNEP Chemicals Branch, DTIE, Geneva, Switzerland. p. 332.
6. UNEP, *Final review of scientific information on lead*, 2010, UNEP Chemicals Branch, DTIE, Geneva, Switzerland. p. 332.
7. UNEP. *Minamata Convention on Mercury* 2014; Available from: http://www.mercuryconvention.org/.
8. Lindberg, S.E., Bullock, R., Ebinghaus, R., Engstrom, D., Feng, X., Fitzgerald, W., Pirrone, N., Prestbo, E.,Seigneur, C., *A Synthesis of Progress and Uncertainties in Attributing the Sources of Mercury in Deposition*. A Journal of the Human Environment, 2007. 36 (1): p. 19–33.
9. Subir, M., Ariya, P.A.,Dastoor, A.P., *A review of uncertainties in atmospheric modeling of mercury chemistry I. Uncertainties in existing kinetic parameters - Fundamental limitations and the importance of heterogeneous chemistry*. Atmospheric Environment, 2011. 45 (doi:10.1016/j.atmosenv.2011.04.046).
10. Ryaboshapko, A., Bulloc, R., Ebinghaus, R., Ilyin, I., Lohman, K., Munthe, J., Petersen, G., Seigneur, C.,Wangberg, I., *Comparison of mercury chemistry models*. Atmospheric Environment, 2002. 36: p. 3881–3898.
11. Ryaboshapko, A., Bulloc, R., Christensen, J., Cohen, M., Dastoor, A., Ilyin, I., Petersen, G., Syrakov, D., Artz, R., Davignon, D., Draxler, R.,Munthe, J., *Intercomparison study of atmospheric mercury models, 1. Comparison of models with short-term measurements*. Science of the Total Environment, 2007a. 376: p. 228–240.
12. Ryaboshapko, A., Bullock, R., Christensen, J., Cohen, M., Dastoor, A., Ilyin, I., Petersen, G., Syrakov, D., Travnikov, O., Artz, R.S., Davignon, D., Draxler, R.R., Munthe, J.,Pacyna, E.J., *Intercomparison study of atmospheric mercury models: 2. Modelling results vs. long-term observations and comparison of country deposition budgets*. Science of the Total Environment, 2007b. 377 (2–3): p. 319–333.
13. Mallet, V., Quello, D., Sportisse, B., Ahmed de Biasi, M., Debry, E., Korsakissok, I., Wu, L., Roustan, Y., Sartelet, K., Tombette, M.,Foudhil, H., *Technical Note: The air quality modeling system Polyphemus*. Atmos. Chem. Phys., 2007. 7 (20): p. 5479–5487.
14. EMEP, *The European Monitoring and Evaluation Programme* 2014.
15. Lin, C.,Pehkonen, S.O., *The chemistry of atmospheric mercury: a review*. Atmospheric Environment, 1999. 33: p. 2067-2079

16. AMAP/UNEP, *Technical Background Report for the Global Mercury Assessment 2013.*, 2013, Arctic Monitoring and Assessment Programme, Oslo, Norway/UNEP Chemicals Branch, Geneva, Switzerland. p. 263.
17. Bergan, T., Gallardo, L.,Rodhe, H., *Mercury in the global troposphere: a three-dimensional model study*. Atmospheric Environment, 1999. 33: p. 1575-1585.
18. Shia, R.L., Seigneur, C., Pai, P., Ko, M.,Sze, N.D., *Global simulation of atmospheric mercury concentrations and deposition fluxes.* Journal of Geophysical Research, 1999. 104: p. 23747–23760.
19. Lamborg, C.H., Fitzgerald, W.F., O'Donnell, J.,Torgersen, T., *A non–steady-state compartmental model of global-scale mercury biogeochemistry with interhemispheric atmospheric gradients.* Geochimica et Cosmochimica Acta, 2002. 66 (7): p. 1105–1118.
20. Mason, R.P.,Sheu, G.R., *Role of ocean in the global mercury cycle.* Global Biogeochemical Cycles., 2002. 16 (DOI 10.1029/2001GB001440).
21. Seigneur, C., Vijayaraghavan, K., Lohman, K., Karamchandani, P.,Scott, C., *Global source attribution for mercury deposition in the United States.* Environmental Science & Technology, 2004. 38: p. 555–569.
22. Selin, N.E., Jacob, D.J., Park, R.J., Yantosca, R., M., Strode, S.,Jaegle, L., *Chemical cycling and deposition of atmospheric mercury: Global constraints from observations.* Journal of Geophysical Research, 2007. 112 (D02308, doi:10.1029/2006JD007450).
23. Ericksen, J.A., Gustin, M.S., Xin, M., Weisberg, P.J.,Fernandez, G.C.J., *Air–soil exchange of mercury from background soils in the United States.* Science of the Total Environment, 2006. 366: p. 851– 863.
24. Wang, D., He, L., Shi, X., Wei, S.,Feng, X., *Release flux of mercury from different environmental surfaces in Chongqing, China.* Chemosphere, 2006. 64: p. 1845–1854.
25. Kuiken, T., Zhang, H., Gustin, M.,Lindberg, S., *Mercury emission from terrestrial background surfaces in the eastern USA. Part I: Air/surface exchange of mercury within a southeastern deciduous forest (Tennessee) over one year.* Applied Geochemistry, 2008. 23: p. 345–355.
26. Gustin, M.S., *Are mercury emissions from geologic sources significant? A status report*. The Science of the Total Environment, 2003. 304: p. 153–167.
27. Quan, J., Zhang, X.,Shim, S.G., *Estimation of vegetative mercury emissions in China.* Journal of Environmental Sciences, 2008. 20: p. 1070–1074.
28. Scholtza, M.T., Van Heysta, B.J.,Schroederb, W.H., *Modelling of mercury emissions from background soils.* The Science of the Total Environment, 2003. 3004: p. 185–207.
29. Travnikov, O.,Ilyin, I., *Regional Model MSCE-HM of Heavy Metal Transboundary Air Pollution in Europe. Technical Report 6/2005*, 2005, EMEP/MSC-E Moscow.
30. Ci, Z., Zhang, X.,Wang, Z., *Elemental mercury in coastal seawater of Yellow Sea, China: Temporal variation and airesea exchange.* Atmospheric Environment, 2011. 45: p. 183–190.
31. Friedli, H.R., Radke, L.F., Lu, J.Y., Banic, C.M., Leaitch, W.R.,MacPherson, J.I., *Mercury emissions from burning of biomass from temperate North American forests:laboratory and airborne measurements.* AE International – North America, 2003. 37: p. 253–267.
32. Nriagu, J.O., *A global assessment of natural sources of atmospheric trace metals.* Nature, 1989. 338: p. 47–49.
33. Holmes, C.D., Jacob, D.J., Mason, R.P.,Jaffe, D.A., *Sources and deposition of reactive gaseous mercury in the marine atmosphere.* Atmospheric Environment, 2009. 43: p. 2278–2285.

34. Richardson, G.M., Garrett, R., Mitchell, I., Mah-Poulson, M.,Hackbarth, T., *Critical review on natural global and regional emissions of six trace metals to the atmosphere. Prepared for the International Lead Zinc Research Organisation, the International Copper Association, and the Nickel Producers Environmental Research Association.* 2001.
35. UNEP, *Global Mercury Assessment 2013: Sources, Emissions, Releases and Environmental Transport*, 2013, UNEP Chemicals Branch: Geneva, Switzerland.
36. USGS, *Chemical Analyses in the World Coal Quality Inventory, Version 1, Open-File Report 2010–1196*, 2010, U.S. Geological Survey: Reston, Virginia: 2010.
37. USEPA, *Control of Mercury Emissions from Coal-Fired Electric Utility Boilers: Interim Report Including Errata Dated 3-21-02*, National Risk Management Research Laboratory Research Triangle Park, Editor 2002, U.S.-EPA Research and Development. : NC 27711.
38. UNEP, *Reducing mercury emissions from coal combustion in the energy sector*, U.N.E.P.U. Chemicals, Editor 2011, Department of Environmental Science and Engineering Tsinghua University, Beijing, 100084, China: Geneva, Switzerland. p. 63.
39. Diehl, S.F., Goldhaber, M.B.,Hatch, J.R., *Modes of occurrence of mercury and other trace elements in coals from the warrior field, Black Warrior Basin, Northwestern Alabama.* International Journal of Coal Geology, 2004. 59: p. 193– 208.
40. Bojakowska, I.,Karmasz, D., *Mercury in raw materials excavated in Poland (in Polish).* in *Rtęć w środowisku : identyfikacja zagrożeń dla zdrowia człowieka*, L. Falkowska. 2010, Fundacja Rozwoju Uniwersytetu Gdańskiego: Gdańsk, Poland. p. 145–150.
41. Lohman, K., Seigneur, C., Gustin, M.,Lindberg, S., *Sensitivity of the global atmospheric cycle of mercury to emissions.* Applied Geochemistry, 2008. 23: p. 454-466.
42. Pacyna, E., Pacyna, J., Steenhuisen, F.,Wilson, S., *Global anthropogenic mercury emission inventory for 2000.* Atmospheric Environment, 2006. 40 (22): p. 4048–4063
43. Pirrone, N., Cinnirella, S., Feng, X., Finkelman, R.B., Friedli, H.R., Leaner, J., Mason, R., Mukherjee, A.B., Stracher, G.B., Streets, D.G.,Telmer, K., *Global mercury emissions to the atmosphere from anthropogenic and natural sources.* Atmospheric Chemistry and Physics, 2010. 10: p. 5951–5964.
44. Muntean, M., Janssens-Maenhout, G., Song , S., Selin, N.E., Olivier, J.G.J., Guizzardi, D., Maas, R.,Dentener, F., *Trend analysis from 1970 to 2008 and model evaluation of EDGARv4 global gridded anthropogenic mercury emissions.* Science of the Total Environment, 2014. 494–495: p. 337–350.
45. Rafaj, P., Bertok, I., Cofala, J.,Schöpp, W., *Scenarios of global mercury emissions from anthropogenic sources.* Atmospheric Environment, 2013. 79: p. 472–479.
46. GAINS. *GAINS-model Greenhouse Gas and Air Pollution Interactions and Synergies, IIASA The International Institute for Applied Systems Analysis*. 2014; Available from: http://gains.iiasa.ac.at/index.php/gains-europe-online.
47. Rafaj, P., Cofala, J., Kuenen, J., Wyrwa, A.,Zyśk, J., *Benefits of European Climate Policies for Mercury Air Pollution.* Atmosphere 2014. 5: p. 45–59.
48. KOBIZE, *Poland's Informative Inventory Report 2013. Submission under UN ECE Convention on Long-range Transboundary Air Pollution.*, 2013, National Centre for Emissions Management: Warszawa.
49. Visschedijk, A., van der Gon, H.D., Kuenen, J.,van der Brugh, H., *Emissions, emission reductions and cost of options for a revision of UNECE Heavy Metal Protocol for the priority heavy metals cadmium, mercury and lead*, in *TNO report*2010, TNO: Utrecht.

50. NEC/IEP, *Atmospheric emission inventory for SO_2, NO2, NH3,CO, PM, HM, VOCs in Poland in 2005 (In Polish)*, 2009, National Emission Centre: Warszawa.
51. NEC/IEP, *Atmospheric emission inventory for SO_2, NO2, NH3,CO, PM, HM, VOCs in Poland in 2006 (In Polish)*, 2009, National Emission Centre: Warszawa.
52. KASHUE-KOBIZE, *Atmospheric emission inventory for SO_2, NOx, NH3, CO, PM, HM, VOCs in Poland in 2008 (In Polish)*, 2009, Institute of Environmental Protection: Warszawa.
53. KOBiZE, *National emission inventory for SO_2, NOx, NH3, CO, PM, HM, VOCs in 2008-2009 in SNAP and NFR classification (in Polish)*, 2011, National Centre for Emissions Management: Warszawa.
54. KOBiZE, *National emission inventory for SO_2, NOx, NH3, CO, PM, HM, VOCs in 2009-2010 in SNAP and NFR classification (In Polish)*, 2012, National Centre for Emissions Management: Warszawa.
55. KOBiZE, *National emission inventory for SO_2, NOx, NH3, CO, PM, HM, VOCs in 2010-2011 in SNAP and NFR classification (In Polish)*, 2015, National Centre for Emissions Management: Warszawa.
56. EEA. *EMEP/EEA air pollutant emission inventory guidebook - 2009, Technical rapport 9/2009, Chapter 1.A.1*. 2009; Available from: http://www.eea.europa.eu/publications/emep-eea-emission-inventory-guidebook-2009.
57. Wojnar, K.,Wisz, J., *Mercury in Polish power sector (In Polish).* Energetyka 2006. 4 (622): p. 59–63.
58. Zyśk, J., Wyrwa, A.,Pluta, M., *Emissions of mercury from the power sector in Poland.* Atmospheric Environment, 2011. 45 (3): p. 605–610.
59. Mniszek, W., *Determination of mercury emissions from industrial sources (In Polish)*. , ed. Z.N.n. 1331995, Gliwice: Politechnika Śląska,.
60. Bojarska, K. *Concentration of mercury in Polish hard coals*. in *MEC3 Third International Expert's workshop*. 2006. Katowice, Poland.
61. Michalska, A.,Białecka, B., *The mercury content in coal and waste from processes of the coal mining (in Polish).* Research Reports Mining And Environment, 2012. 3: p. 73-87.
62. Klojzy-Kaczmarczyk, B.,Mazurek, J., *Studies of mercury content in coal intended for indywidual customers (in Polish).* Polityka eneregtyczna, 2013. 16 (4): p. 151-161.
63. Okońska, A., Uruski, Ł., Górecki, J.,Gołaś, J., *Mercury in coal – determination of total mercury in steam coals by cold vapor atomic absorption spectrometry (CV-AAS) (in Polish).* Polityka eneregtyczna, 2013. 29 (2): p. 39–49.
64. Wichliński, M., Kobyłecki, R.,Bis, Z., *The investigation of mercury contents in Polish coal samples.* Archives of Environmental Protection, 2013. 39 (2): p. 141–150.
65. Misztal, E., Chmielniak, T.,Mazurek, I., *Mercury content in Polish coals used in power sector and possibility of its reduction during treatment of fuels before comustion process (in Polish)*, in *Rtęć w środowisku : identyfikacja zagrożeń dla zdrowia człowieka*, L. Falkowska. 2013, Wydawnictwo Uniwersytetu Gdańskiego.: Gdańsk, Poland. p. 235-246.
66. Dziok, T., Strugała, A.,Rozwadowski, A., *Examinations of mercury content in coal – comments on the way results are presented (in Polish).* Polityka eneregtyczna, 2013. 16 (3): p. 273-284.
67. Styszko, K., Stanowski, T., Macherzyński, M., Górecki, J.,Szramowiat, K., *Mercury content in fly ashes from coal-fired power plants (in Polish)*, in *Rtęć w środowisku : identyfikacja zagrożeń dla zdrowia człowieka*, L. Falkowska. 2013, Wydawnictwo Uniwersytetu Gdańskiego.: Gdańsk, Poland. p. 247–252.

68. Wilcox, J., Rupp, E., Ying, S.C., Lim a, D.-H., Negreira, A.S., Kirchofer, A., Feng, F.,Lee, K., *Mercury adsorption and oxidation in coal combustion and gasification processes.* International Journal of Coal Geology, 2012. 90–91: p. 4–20.
69. Lee, S.J., Seo, Y., Jang, H., Park, K., Baek, J., An, H.S.,Song, K., *Speciation and mass distribution of mercury in a bituminous coal-fired power plant*. Atmospheric Environment, 2006. 40: p. 2215–2224.
70. Pavlish, J.H., Sondreal, E.A., Mann, M.D., Olson, E.S., Galbreath, K.C., Laudal, D.L.,Benson, S.A., *Status review of mercury control options for coal-fired power plants.* Fuel Processing Technology, 2003. 82: p. 89–165.
71. Kolker, A., Senior, C.L.,Quick, J.C., *Mercury in coal and the impact of coal quality on mercury emissions from combustion systems.* Applied Geochemistry, 2006. 21: p. 1821–1836.
72. Agarwal, H., Romero, C.E., Rosales, F.H.,Mendoza-Covarrubias, C., *A Global Kinetic Mechanism for the Prediction of Hg Oxidation by a Chlorine Species.* Energy Science and Technology, 2012. 4 (1): p. 41-54.
73. UNEP/DTIE, *Process Optimization Guidance for Reducing Mercury Emissions from Coal Combustion in Power Plants*, 2010, Division of Technology, Industry and Economics (DTIE) Chemicals Branch: Geneva, Switzerland. p. 94.
74. Wang, Y., Duan, Y., Yang, L., Zhao, C., Shen, X., Zhang, M., Zhuo, Y.,Chen, C., *Experimental study on mercury transformation and removal in coal-fired boiler flue gases.* Fuel Processing Technology, 2009. 90: p. 643–651.
75. Hall, B., Schager, P.,Lindqvist, O., *Chemical Reactions of Mercury in Combustion Flue Gases.* Water Air & Soil Pollution, 1991. 56 (1): p. 3-14.
76. Agarwal, H., Stenger, H.G., Wu, S.,Fan, Z., *Effects of H2O, SO2, and NO on Homogeneous Hg Oxidation by Cl2*. Energy Fuels, 2006. 20 (3): p. 1068–1075.
77. Frandsen, F., Dam-Johansen, K.,Rasmussen, P., *Trace elements from combustion and gasification of coal—An equilibrium approach.* Progress in Energy and Combustion Science, 1994. 20: p. 115–138.
78. Cao, Y., Duan, Y., Kellie, S., Li, L., Xu, W., Riley, J.T., Pan, W.-P., Chu, P., Mehta, A.K.,Carty, R., *Impact of Coal Chlorine on Mercury Speciation and Emission from a 100-MW Utility Boiler with Cold-Side Electrostatic Precipitators and Low-NOx Burners.* Energy & Fuels, 2005. 19: p. 842-854.
79. Suriyawong, A.,Biswas, P., *Homogeneous Mercury Oxidation under Simulated Flue Gas of Oxy-coal Combustion.* Engineering Journal, 2013. 17 (4): p. 35–45.
80. Hławiczka, S., *Mercury in the atmospheric environment (in Polish)*. Works & Studies, ed. C. Rosik-Dulewska. Vol. 73. 2008, Zabrze: Institute of Environmental Engineering of the Polish Academy of Sciences. 158.
81. Lindqvist, O., Johanson, K., Aastrup, M., Anderson, A., Bringmark, L., Hovsenius, G., Hakanson, L., Iverfeld, A., Meili, M.,Timm, B., *Mercury in the Swedish environment - recent research on causes, consequences and corrective methods.* Water, Air and Soil Pollution,, 1991. 55: p. 1-261.
82. Ryaboshapko, A.,Korolev, V., *Mercury in the atmosphere: estimates of model parameters.*, in *Report 7/97*1997, EMEP/MSC-E: Moscow.
83. Ryaboshapko, A., Ilyin, I., Gusev, A.,Afinogenova, O., *Mercury in the atmosphere of europe : concentrations, deposition patterns, transboundary fluxes.*, 1998, EMEP/MSC-E: Moscow.
84. Pacyna, E., Pacyna, J., Fudala, J., Strzelecka-Jastrząb, E., Hławiczka, S.,Panasiuk, D., *Mercury emissions to the atmosphere from anthropogenic sources in Europe in 2000 and their scenarios until 2020.* Science of the Total Environment, 2006. 370: p. 147–156.

85. Nriagu, J.O.,Pacyna, J.M., *Quantitative assessment of worldwide contamination of air, water and soils by trace metals.* Nature, 1988. 333: p. 134–139.
86. Pacyna, J.M.,Pacyna, E.G., *An assessment of global and regional emissions of trace metals to the atmosphere from anthropogenic sources worldwide.* Environmental Reviews, 2001. 9: p. 269–298.
87. CEIP/EMEP, *The EMEP Centre on Emission Inventories and Projections*, 2013.
88. Travnikov, O., Ilyin, I., Rozovskaya, O., Varygina, M., Aas, W., Uggerud, H.T., Mareckova, K.,Wankmueller, R., *Long-term Changes of Heavy Metal Transboundary Pollution of the Environment (1990-2010). EMEP/MSC-E/CCC/CEIP Technical Report 2/2012*, 2012, EMEP/MSC-E/MSC-W: Moscow/Oslo.
89. Pacyna, J.M., *Atmospheric Emissions of Arsenic, Cadmium, Lead and Mercury from High Temperature Processes in Power Generation and Industry*, in *ead, Mercury, Cadmium and Arsenic in the Environment*, T.C. Hutchinson and K.M. Meema. 1987, John Wiley & Sons: Chichester, New York, Brisbane, Toronto,. p. 69–89.
90. Parzentny, H., *Lead distribution in coal and coaly shales in the Upper Silesian Coal Basin*. Geological Quarterly, 1994. 38: p. 43–58.
91. Bielowicz, B., *Selected harmful elements in Polish lignite (in Polish).* Gospodarka Surowcami Mineralnymi, 2013. 29: p. 47–51.
92. KOBiZE, *National emission inventory for SO_2, NOx, NH3, CO, PM, HM, VOCs in 2010-2011 in SNAP and NFR classification (In Polish)*, 2013, National Centre for Emissions Management: Warszawa.
93. Bojakowska, I., *Cadmium in mineral resources of Poland and its potential emission in the environment (in Polish).* Ochrona Środowiska i Zasobów Naturalnych, 2009. 40: p. 22–30.
94. Eionet. *AirBase - the European Air quality database*. 2011; Available from: http://acm.eionet.europa.eu/.
95. Markiewicz, M.T., *Basics of modeling of the dispersion of pollutants in ambient air (in Polish).*2004, Warszawa: Oficyna Wydwnicza Politechniki Warszawskiej
96. Hall, B., *The gas phase oxidation of elemental mercury by ozone.* . Water, Air, & Soil Pollution, 1995. 80 (1-4): p. 301-315.
97. Tokos, J.J.S., Hall, B., Calhoun, J.A.,Prestbo, E.M., *Homogeneous gas-phase reaction of Hgo with H2O2, O3, CH3I, and (CH3)2S: implications for atmospheric Hg cycling.* Atmospheric Environment, 1998. 32: p. 823–827.
98. Pal, B.,Ariya, P.A., *Studies of ozone initiated reactions of gaseous mercury: kinetics, product studies, and atmospheric implications.* Physical Chemistry Chemical Physics, 2004a. 6: p. 572–579.
99. Slemr, F., Schuster, G.,Seiler, W., *Distribution, speciation, and budget of atmospheric mercury*. Jurnal of Atmospheric Chemistry, 1985. 3: p. 407–434.
100. Schroeder, W.H., Yarwood, G.,Niki, H., *Involving Mercury Species in the Atmosphere - Results from a Literature Survey*. Water, Air, & Soil Pollution, 1991. 56: p. 653–666.
101. Snider, G., Raofie, F.,Ariya, P.A., *Effects of relative humidity and CO(g) on the O3-initiated oxidation reaction of Hg0(g): kinetic & product studies.* . Physical Chemistry Chemical Physics, 2008. 10 (36): p. 5616–5623.
102. Castro, L., Dommergue, A., Ferrari, C.,Maron, L., *A DFT study of the reactions of O3 with Hg(0) or Br-*. Atmospheric Environment, 2009. 43: p. 5708–5711.
103. Hynes, A.J., Donohoue, D.L., Goodsite, M.E.,Hedgecock, I.M., *Our current understanding of major chemical and physical processes affecting mercury dynamics in the atmosphere and at the air-water/terrestrial interfaces*, in *Mercury Fate and Transport in the Global Atmosphere*, N. Pirrone and R. Mason. 2009, Springer: Lodon, New York. p. 427–457.

104. Seigneur , C., Vijayaraghavan, K.,Lohman , K., *Atmospheirc mercury chemistry: Sensitivity of global model simulations to chemical reactions.* Journal of Geophysical Research, 2006. 111: p. DOI: 10.1029/2005JD006780.
105. Iverfeldt, A.,Lindqvist, O., *Atmospheric oxidation of elemental mercury by ozone in the aqueous phase.* Atmospheric Environment, 1986. 20: p. 1567-1573.
106. Sumner, A.L., Spicer, C.W., Satola, J., Mangaraj, R., Cowen, K.A., Landis, M.S., Stevens, R.K.,Atkeson, T.D., *Environmental Chamber Studies of Mercury Reactions in the Atmosphere*, in *Dynamics of mercury pollution on regional and global scales : atmospheric processes and human exposures around the world*, N. Pirrone and K.R. Mahaffey. 2005, Springer: New York,. p. 193–212.
107. Sommar, J., Gardfeldt, K., Stromberg, D.,Feng, X., *A kinetic study of the gas-phase reaction between the hydroxyl radical and atomic mercury.* Atmospheric Environment, 2001. 35: p. 3049–3054.
108. Miller, G.C., Quashnick, J.,Hebert, V., *Reaction rate of metallic mercury with hydroxyl radical in the gas phase. Abstract of Papers of American Chemical Society.* 2001. U47: p. 221.
109. Bauer, D., D'Ottone, L., Campuzaon-Jos, P.,Hynes, A., *Gas phase elemental mercury a comparison of LIF detection techniques and study of the kinetics of reaction with the hydroxyl radical.* Journal of Photochemistry Photobiology, 2003. 157: p. 247-256.
110. Pal, B.,Ariya, P.A., *Gas-phase Reaction of Hydroxyl Initiated Reaction of Elemental Mercury Kinetics and Product Studies.* Environmental Science & Technology, 2004b. 38 (21): p. 5555–5566
111. Goodsite, M.E., Plane, J.M.C.,Skov, H., *A theoretical study of the oxidation of Hg^0 to $HgBr_2$ in the troposphere.* Environmental Science & Technology, 2004. 38: p. 1772–1776.
112. Seigneur, C., Wrobel, J.,Constantinou, E., *A chemical kinetic mechanism for atmospheric inorganic mercury.* Environmental Science and Technology, 1994. 28: p. 1589–1597.
113. Travnikov, O.,Ryaboshapko, A., *Modeling of mercury hemispheric transport and depositions*, in *EMEP Raport 6/2002*2002, EMEP/MSC-E: Moscow.
114. Hua, W., Chen, Z.M., Jie, C.Y., Kondo, Y., Hofzumahaus, A., Takegawa, N., Chang, C.C., Lu, K.D., Miyazaki, Y., Kita, K., Wang, H.L., Zhang, Y.H.,Hu, M., *Atmospheric hydrogen peroxide and organic hydroperoxides during PRIDE-PRD'06, China: their concentration, formation mechanism and contribution to secondary aerosols.* Atmospheric Chemistry and Physics, 2008. 8: p. 6755–6773.
115. Calhoun, J.A.,Prestbo, E., *Kinetic study of the gas phase oxidation of elemental mercury Hg by molecular chlorine (Cl_2). Frontier Geosciences, Inc., Seattle, WA, unpublished manuscript*. 1998.
116. Spicer, C.W., Satola, J., Abbgy, A.A., Plastridge, R.A.,Cowen, K.A., *Kinetics of Gas-Phase Elemental Mercury Reactions with Halogen Species, Ozone, and Nitrate Radical Under Atmospheric Conditions. Final Report to Florida Department of Environmental Protection under Contract AQ174*, 2002, Battelle: Columbus(US).
117. Ariya, P.A., Khalizov, A.,Gidas, A., *Reactions of Gaseous Mercury with Atomic and Molecular Halogens: Kinetics, Product Studies, and Atmospheric Implications.* The Journal of Physical Chemistry A,, 2002. 106: p. 7310–7320.
118. Yan, N.-Q., Liu, S.-H.,Chang, S.-G., *Method for the Study of Gaseous Oxidants for the Oxidation of Mercury Gas.* Industrial & Engineering Chemistry Research, 2005. 444: p. 5567–5574.

119. Byun, Y., Cho, M., Namkung, W., Lee, K., D.J., K.,Shin, D.N., *Insight into the unique oxidation chemistry of elemental mercury by chlorine-containing species: experiment and simulation.* Environmental Science & Technology, 2010. 44: p. 1624–1629.
120. Lawler, M.J., Sander, R., Carpenter, L.J., Lee, J.D., Glasow, R., Sommariva, R.,Saltzman, E.S., *HOCl and Cl2 observations in marine air.* Atmospheric Chemistry and Physics, 2011. 11: p. 7617–7628.
121. Spicer, C.W., Chapman, E.G., Finlayson-Pitts, B.J., Plastridge, R.A., Hubbe, J.M., Fast, J.D.,Berkowitz, C.M., *Unexpectedly high concentrations of molecular chlorine in coastal air.* Nature 1998. 394: p. 353–356.
122. Horne, D.G., Gosavi, R.,Strausz, O.P., *Reactions of Metal Atoms. I. The Combination of Mercury and Chlorine Atoms and the Dimerization of HgCl.* J. Chem. Phys., 1968. 48 (4758-4764).
123. Khalizov, A.F., Viswanathan, B., Larregaray, P.,Ariya, P.A., *A theoretical study on the reaction of Hg with halogens: Atmospheric implications.* Journal of Physical Chemistry A, 2003. 107: p. 6360–6365.
124. Donohoue, D.L., Bauer, D.,Hynes, A., *Temperature and pressure dependent rate coefficients for the reaction of Hg with Cl and the reaction of Cl with Cl: a pulsed laser photolysis-pulsed laser induced fluorescence study.* J. Phys. Chem. A,, 2005. 109 (34): p. 7732–7741.
125. Ariya, P.A.,Peterson, K.A., *Chemical Transformation of Gaseous Elemental Mercury in the Atmosphere*, in *Dynamics of mercury pollution on regional and global scales: atmospheric processes and human exposures around the world*, N. Pirrone and K.R. Mahaffey. 2005, Springer: New York,. p. 261-294.
126. Hall, B.,Bloom, N.S., *Annual report to the Electric Power Research*, 1993, EPRI: Palo Alto, US.
127. Seigneur, C., Vijayaraghavan, K., Lohman , K.,Levin, L., *The AER/EPRI Global Chemical Transport Model for Mercury (CTM-HG)*, in *Mercury Fate and Transport in the Global Atmosphere*, N. Pirrone and R. Mason. 2009, Springer: Lodon, New York. p. 589–602.
128. Donohoue , D.L., Bauer , D., Cossairt , B.,Hynes , A., *Temperature and pressure dependent rate coefficients for the reaction of Hg with Br and the reaction of Br with Br: A pulsed laser photolysis - pulsed laser induced fluorescence study.* J. Phys, Chem. A., 2006. 110: p. 6623 - 6632.
129. Shepler, B.C., Balabanov, N.B.,Peterson, K.A., *Hg + Br ->HgBr recombination and collision-induced dissociation dynamics.* Journal of Physical Chemistry, 2007. 127: p. 164–304.
130. Balabanov, N.B., Shepler, B.C.,A., P.K., *Accurate Global Potential Energy Surface and Reaction Dynamics for the Ground State of HgBr2.* J. Phys. Chem, 2005. 109: p. 765-8773.
131. Yang, X., Cox, R.A., Warwick, N.J., Pyle, J.A., Carver, G.D., O'Connor, F.M.,Savage, B.H., *Tropospheric bromine chemistry and its impacts on ozone: A model study.* Journal of Geophysical Research, 2005. 110: p. D23311.
132. Seigneur , C.,Lohman , K., *Effect of bromine chemistry on the atmospheric mercury cycle.* Journal of Geophysical Research, 2008. 113: p. D23309.
133. Raofie, F.,Ariya, P.A., *Reactions of BrO with mercury: kinetic studies.* Journal de Physique IV France, 2003. 107: p. 1119–1121.
134. Xie, Z.Q., Sander, R., Poschl, U.,Slemr, F., *Simulation of atmospheric mercury depletion events (AMDEs) during polar springtime using the MECCA box model.* Atmospheric Chemistry and Physics, 2008. 8: p. 7165–7180.

135. Sommar, J., Hallquist, M., Ljungstrom, E.,Lindqvist, O., *On the Gas Phase Reactions Between Volatile Biogenic Mercury Species and the Nitrate Radical.* Journal of Atmospheric Chemistry, 1997. 27: p. 233–247.
136. Raofie, F., Snider, G.,Ariya, P.A., *Reaction of gaseous mercury with molecular iodine, atomic iodine, and iodine oxide radicals — Kinetics, product studies, and atmospheric implications.* Canadian Journal of Chemistry, 2008. 86 (8): p. 811–820.
137. Huang, R.J., Seitz, K., Neary, T., O'Dowd, C.D., Platt, U.,Hoffmann, T., *Observations of high concentrations of I2 and IO in coastal air supporting iodine-oxide driven coastal new particle formation.* Geophysical Research Letters, 2010. 37: p. L03803 (1-5).
138. Turzański, K.P.,Wertz, J., *Report about the state of the environment in the Malopolska voivodeship in 1999 (in Polish)*, 2000, The Regional Inspectorate of Environmental Protection in Krakow, Małopolska Provincial Office in Krakow: Krakow, Poland.
139. Pleijel, K.,Munthe, J., *Modeling the Atmospheric Mercury Cycle - Chemistry in Fog Droplets.* Atmospheric Environment, 1995. 29: p. 1441–1457.
140. Munthe, J., *The aqueous oxidation of elemental mercury by ozone.* Atmospheric Environment, 1992. 26A: p. 1461–1468.
141. Wang, Z.,Pehkonen, S.O., *Oxidation of elemental mercury by aqueous bromine: atmospheric implications.* Atmospheric Environment, 2004. 38: p. 3675–3688.
142. Lin, C.,Pehkonen, S.O., *Aqueous free radical chemistry of mercury in the presence of iron oxides and ambient aerosol.* Atmospheric Environment, 1997. 31: p. 4125–4137.
143. Gardfeldt, K., Sommar, J., Stroemberg, D.,Feng, X., *Oxidation of atomic mercury by hydroxyl radicals and photoinduced decomposition of methylmercury in the aqueous phase,.* Atmospheric Environment, 2001. 35: p. 3039– 3047.
144. Lin, C.,Pehkonen, S.O., *Oxidation of elemental mercury by aqueous chlorine ($HOCl/OCl^-$): Implications for tropospheric mercury chemistry.* Journal of Geophysical Research, 1998a. 103: p. 28093–28102.
145. Munthe, J., Xiao, Z.F.,Lindqvist, O., *The aqueous reduction of divalent mercury by sulfite.* Water, Air, and Soil Pollution, 1991. 56: p. 621–630.
146. Van Loon, L.L., Mader, E.A.,Scott, S.L., *Sulfite stabilization and reduction of the aqueous mercuric ion: kinetic determination of sequential formation constants.* Journal of Physical Chemistry, 2001. 105: p. 3190–3195.
147. Van Loon, L., Mader, E.,Scott, S.L., *Reduction of the aqueous mercuric ion by sulfite: UV spectrum of $HgSO_3$ and its intramolecular redox reaction.* Journal of Physical Chemistry, 2000. 104: p. 1621–1626.
148. Munthe, J., *The atmospheric chemistry of mercury: kinetic studies of redox reactions (Chapter II.9).* in *Mercury Pollution: Integration and Synthesis*, C.J. Watras, Huckabee, J.W.,. 1994, Lewis Publisher–CRC Press: Boca Raton, Florida, US. p. 273–279.
149. Pehkonen, S.O.,Lin, C., *Aqueous Photochemistry of Mercury with Organic Acids.* Journal of the Air & Waste Management Association, 1998. 48:2: p. 144–150.
150. Gardfeldt, K.,Jonsson, M., *Is Bimolecular Reduction of Hg(II) Complexes Possible in Aqueous Systems of Environmental Importance.* The Journal of Physical Chemistry A, 2003. 107: p. 4478–4482.
151. Faust, B.C.,Allen, J.M., *Aqueous-phase photochemical sources of peroxyl radicals and singlet molecular oxygen in clouds and fog.* Atmospheres 2012. 97 (D12): p. 12913–12926.
152. Xiao, Z.F., Munthe, J., Stromberg, D.,Lindqvist, O., *Photochemical behavior of inorganic Hg compounds in aqueous solution. (Chapter VI.6).* in *Mercury Pollution:*

Integration and Synthesis, C.J. Watras, Huckabee, J.W.,. 1994, Lewis Publisher–CRC Press: Boca Raton, Florida, US. p. 273–279.
153. Xiao, Z.F., Stromberg, D.,Lindqvist, O., *Influence of humic substances on photolysis of divalent mercury in aqueous-solution.* Water Air and Soil Pollution, 1995. 80: p. 789–798.
154. Si, L.,Ariya, P.A., *Reduction of oxidized mercury species by dicarboxylic acids (C2-C4): kinetic and product studies.* Environmental Science & Technology, 2008. 42: p. 5150–5155.
155. Rozaini, M.Z.H., *The Chemistry of Dicarboxylic Acids in the Atmospheric Aerosols (Chapter 11).* in *Atmospheric Aerosols - Regional Characteristics - Chemistry and Physics.*, H. Abdul-Razzak. 2012, InTech: Rijeka, Croatia. p. 490.
156. Nazhat, N.B.,Asmus, K.D., *Reduction of mercuric chloride by hydrated electrons and reducing radicals in aqueous solutions. Formation and reactions of mercury chloride (HgCl).* The Journal of Physical Chemistry, 1973. 77 (5): p. 614–620.
157. Seigneur, C., Abeck, H., Chia, G., Reinhard, M., Bloom, N.S., Prestbo, E.,Pradeep, S., *Mercury adsorption to elemental carbon (soot) particles and atmospheric particulate matter.* Atmospheric Environment, 1998. 32: p. 2649–2657.
158. Calvert, J.G.,Lindberg, S.E., *Mechanisms of mercury removal by O3 and OH in the atmosphere.* Atmospheric Environment, 2005. 39: p. 3355–3367.
159. Sakata, M.,Marumoto, K., *Formation of atmospheric particulate mercury in the Tokyo metropolitan area.* Atmospheric Environment, 2002. 36: p. 239–246.
160. Bullock, R.,Brehme, K., *Atmospheric mercury simulation using the CMAQ model formulation description and analysis of wet deposition results.* Atmospheric Environment, 2002. 36: p. 2135–2146.
161. Pirrone, N., Aas, W., Cinnirella, S., Ebinghaus, R., Hedgecock, I.M., Pacyna, J., Sprovieri, F.,Sunderland, E.M., *Toward the next generation of air quality monitoring: Mercury.* Atmospheric Environment, 2013. 80: p. 599–611.
162. GMOS. *Global Mercury Observation System* 2014; Available from: http://www.gmos.eu/.
163. EMEP-CCC. *Chemical Co-ordinating Centre of EMEP (CCC).* 2013; Available from: http://www.nilu.no/projects/ccc/index.html.
164. HELCOM. *Baltic Marine Environment Protection Commission - Helsinki Commission*. 2014; Available from: http://helcom.fi/.
165. OSPAR. *The Convention for the Protection of the marine Environment of the North-East Atlantic*. 2014.
166. AMAP. *Arctic Monitoring and Assessment Programme - an Arctic Council Working Group*. 2014.
167. Slemr, F., Brunke, E.G., Ebinghaus, R.,Kuss, J., *Worldwide trend of atmospheric mercury since 1995.* Atmospheric Chemistry and Physics, 2011. 11: p. 4779–4787.
168. Weigelt, A., Ebinghaus, R., Manning, A.J., Derwent, R.G., Simmonds, P.G., Spain, T.G., Jennings, S.G.,Slemr, F., *Analysis and interpretation of 18 years of mercury observations since 1996 at Mace Head, Ireland.* Atmospheric Environment, 2015. 100: p. 85–93.
169. Zielonka, U., Hlawiczka, S., Fudala, J., Wängberg, I.,Munthe, J., *Seasonal mercury concentrations measured in rural air in Southern Poland: Contribution from local and regional coal combustion.* 2005. 39 (39): p. 7580–7586.
170. Aas, W.,Breivik, K., *Heavy metals and POP measurements, 2011. EMEP/CCC-Report 4/2013*, 2007, Norwegian Institute for Air Research: Kjeller, Norway. p. 136.

171. Alvarez, F.F., Rodrıguez, M.T., Espinosa, A.J.F.,Dabán, A.G., *Physical speciation of arsenic, mercury, lead, cadmium and nickel in inhalable atmospheric particles.* Analytica Chimica Acta, 2004. 524: p. 33–40.
172. Pyta, H., Rosik-Dulewska, C.,Czaplicka, M., *Speciation of Ambient Mercury in the Upper Silesia Region, Poland.* Water, Air, & Soil Pollution,, 2009. 197: p. 233–240.
173. Beldowska, M., Saniewska, D., Falkowska, L.,Lewandowska, A., *Mercury in particulate matter over Polish zone of the southern Baltic Sea.* Atmospheric Environment, 2012. 46: p. 397–404.
174. Nowak, B., Korszun-Kłak, K.,Zielonka, U., *Long-term measurements of atmospheric mercury species (TGM, TPM) and hg deposition in the Silesian region, Poland – concept of the mercury deposition coefficient*. Archives of Environmental Protection, 2014. 40 (3): p. 43 - 60.
175. Pyta, H., *The occurrence of different mercury forms in the air of Upper Silesia Agglomeration and at the station of regional background (in Polish)*, in *Rtęć w środowisku : identyfikacja zagrożeń dla zdrowia człowieka*, L. Falkowska. 2013, Wydawnictwo Uniwersytetu Gdańskiego.: Gdańsk, Poland. p. 29–37.
176. Zhang, L., Wright, L.P.,Blanchard, P., *A review of current knowledge concerning dry deposition of atmospheric mercury.* Atmospheric Environment, 2009. 43: p. 5853–5864.
177. Lin, C., Pongprieksa, P., Bulloc, R., Lindberg, S., Pehkonen, S.O., Jang, C., Braverman, T.,Ho, T., *Scientific uncertainties in atmospheric mercury models II, Sensitivity analysis in the CONUS domain.* Atmospheric Environment, 2007. 41: p. 6544–6560.
178. Grant, S.L., Kim, M., Lin, P., Crist, K.C., Ghosh, S.,Kotamarthi, V.R., *A simulation study of atmospheric mercury and its deposition in the Great Lakes.* Atmospheric Environment, 2014. 94: p. 164–172.
179. Pleim, J.,Byun, D., *Application of a new land-surface, dry deposition, and PBL model in the Models-3 Community Multi-scale Air Quality (CMAQ) model system*, in *Air pollution modeling and its application XIV*, S.E. Gryning and F.A. Schiermeier. 2004, Kluwer Academic Publisher: New York, Boston, Dordrecht, London, Moscow. p. 297–305.
180. Seigneur , C., Vijayaraghavan, K., Lohman , K.,Levin, L., *The AER/EPRI Global Chemical Transport Model for Mercury (CTM-HG)*, in *Mercury Fate and Transport in the Global Atmosphere*, N. Pirrone and R. Mason. 2009, Springer: Lodon, New York. p. 589-602.
181. Baker, K.R.,Bash, J.O., *Regional scale photochemical model evaluation of total mercury wet deposition and speciated ambient mercury.* Atmospheric Environment, 2012. 49: p. 151-162.
182. Wesely, M.L., *Parameterization of surface resistances to gaseous dry deposition in regional-scale numerical models.* Atmospheric Environment, 1989. 23 (6): p. 1293–1304.
183. Ilyin, I., Gusev, A., Rozovskaya, O., Shatalov, V., Sokovykh, V.,Travnikov, O., *Modelling of heavy metals and persistent organic pollutants: New developments. Technical Report 1/2010 (Draft)*, 2010, EMEP/MSC-E Moscow.
184. Travnikov , O.,Ilyin, I., *The EMEP/MSC-E Mercury Modeling System*, in *Mercury Fate and Transport in the Global Atmosphere*, N. Pirrone and R. Mason. 2009, Springer: Lodon, New York. p. 589–602.
185. Jonson, J.E.E., Travnikov, O.E., Dastoor, A., Gauss, M., Gusev, A., Hollander, A., Iyin, I., Lin, C.-J., MacLeod, M., Shatalov, V., Sokovykh, V., Valdebenito, A., Valiyaveetil, S.,Wind, P., *Development of the EMEP global modelling framework:*

Progress report. *EMEP/MSC-W Technical Report 1/2010*, 2010, EMEP/MSC-E/MSC-W: Moscow/Oslo.
186. Travnikov, O., Jonson, J.E., Amann, M., Angelbratt, J., Gauss, M., Griesfeller, J., Gusev, A., Heyes, C., Ilyin, I., Klimont, Z., Rozovskaya, O., Schulz, M., Simpson, D., Sokovyh, V.,Steensen, B.M., *Global scale modelling within EMEP: Progress report*. *EMEP/MSC-E Technical Report 1/2011*, 2011, EMEP/MSC-E/MSC-W: Moscow/Oslo.
187. Schmolkea, S.R.,Petersen, G., *A comprehensive Eulerian modelingframework for airborne mercury species: comparison of model results with data from measurement campaigns in Europe.* Atmospheric Environment, 2003. 37: p. S51–S62.
188. Christensen, J.H., Brandt, J., Frohn, L.M.,Skov, H., *Modelling of mercury with the Danish Eulerian Hemispheric Model.* Atmospheric Chemistry and Physics Discussions, 2003. 3: p. 3525–3541.
189. Petersena, G., Bloxamb, R., Wongb, S., Munthec, J., Krugerd, O., Schmolkea, S.R.,Vinod Kumar, A., *A comprehensive Eulerian modelling framework for airborne mercury species: model development and applications in Europe.* 2001. 35: p. 3063–3074.
190. Pan, L., Lin, C.-J., Carmichael, G.R., Streets, D.G., Youhua Tang, Y., Jung-Hun Woo , J.H., S.K, S., Chu, H.W., Ho, T.C., Friedli, H.R.,Feng, X., *Study of atmospheric mercury budget in East Asia using STEM-Hg modeling system*. Science of the Total Environment, 2010. 408: p. 3277–3291.
191. Wang, L., Wang, S., Zhang, L., Wang, Y., Zhang, Y., Nielsen, C., McElroy, M.B.,Hao, J., *Source apportionment of atmospheric mercury pollution in China using the GEOS-Chem model.* Environmental Pollution, 2014. 190: p. 166–175.
192. Jung, G., Hedgecock, I.M.,Pirrone, N., *ECHMERIT V1.0 – a new global fully coupled mercury-chemistry and transport model.* Geoscientific Model Development, 2009. 2: p. 175–195.
193. Horowitz, L.W., Walters, S., Mauzerall, D.L., Emmons, L.K., Rasch, P.J., Granier, C., Tie, X., Lamarque, J.F., Schultz, M.G., Tyndall, G.S., Orlando, J.J.,Brasseur, G.P., *A global simulation of tropospheric ozone and related tracers: Description and evaluation of MOZART, version 2,*. Journal of Geophysical Research, 2003. 108 (D24).
194. Drewniak, B.A., Kotamarthi, V.R., Streets, D., Kim, M.,Crist, K., *Estimates of mercury flux into the United States from non-local and global sources: results from a 3-D CTM simulation.* Atmos. Chem. Phys. Discuss, 2008. 8: p. 19861–19890.
195. Ryaboshapko, A., Artz, R., Bullock, R., Christensen, J., Cohen, M., Dastoor, A., Davignon, D., Draxler, R., Ilyin, I., Munthe, J., Pacyna, J., Petersen, G., Syrakov, D.,Travnikov, O., *Intercomparison study of numerical models for long-range atmospheric transport of mercury. Stage II : Comparison of modeling results with observations obtained during short-term measuring campaigns.*, 2003, EMEP/MSC-E.
196. Ilyin, I., Rozovskaya, O.,Travnikov, O., *Heavy Metals: Transboundary Pollution of the Environment*. *EMEP Status Report 2/2008*, 2008, MSC-E of EMEP: Moscow.
197. Draxler, R.R.,Rolph, G.D. *HYSPLIT (HYbrid Single-Particle Lagrangian Integrated Trajectory) Model access via NOAA ARL READY Website (http://ready.arl.noaa.gov/HYSPLIT.php)*. 2014.
198. Debry, E., Fahey, K.M., Sartelet, K., Sportisse, B.,Tombette, M., *Technical Note: A new Size Resolved Aerosol Model (SIREAM).* Atmospheric Chemistry and Physics, 2007. 37: p. 950–966.

199. Cuvelier, C., Muntean, M., Thunis, P., Kamiński, J., Wyrwa, A., Łobocki, L., Strużewska, J., Zdunek, M., Kamiński, K., Kamiński, W., Petera, J., Piątek, A., Głodek, A., Quelo, D., Śliż, B., Zyśk, J.,Burzyński, J. *Air Quality Modelling in the greater-Kraków area*. in *Outcome of the Kraków Integrated Project. Particulate Matter: From Emissions to Health Effects*. 2006. Krakow.
200. Wyrwa, A., Zyśk, J., Stężały, A., Śliż, B., Pluta, M., J., B.,Jestin, L. *Towards an Integrated Assessment of Environmental and Health Impact of Energy Sector in Poland*. in *Environmental Informatics and Systems Research*. 2007. Warsaw: Shaker Verlag
201. Zyśk, J., Wyrwa, A., Roustan, Y.,Pluta, M., *Integrated impact analysis of mercury emitted from the Polish power sector (in Polish).* in *Rtęć w środowisku : identyfikacja zagrożeń dla zdrowia człowieka*, L. Falkowska. 2010, Fundacja Rozwoju Uniwersytetu Gdańskiego: Gdańsk, Poland. p. 51–56.
202. Jestin, L., Wyrwa, A., Stężały, A., Zyśk, J., Pluta, M.,Śliż, B., *Environmental challenges of the Polish energy sector* Polish Journal of Environmental Studies, 2010. 19 (2): p. 331–335.
203. Zyśk, J., Stężały, A., Pluta, M., Wyrwa, A., Roustan, Y.,Sportisse, B., eds. *The Polyphemus system to model of transport of pollutants (in Polish).* Aktualne problemy w ochronie powietrza atmosferycznego. , ed. A. Musialik-Piotrowska and J.D. Rutkowski2008, Polskie Zrzeszenie Inżynierów i Techników Sanitarnych.: Wrocław. 191.
204. Lecœur, E.,Seigneur, C., *Dynamic evaluation of a multi-year model simulation of particulate matter concentrations over Europe.* Atmospheric Chemistry and Physics, 2013. 13: p. 4319–4337.
205. Sportisse, B.,du Bois, L., *Numerical and theoretical investigation of a simplified model for the parameterization of below-cloud scavenging by falling raindrops.* Atmospheric Environment, 2002. 36 (36–37): p. 5719–5727.
206. Uplinger, W.G. *A new formula for raindrop terminal velocity*. in *20th Conference on Radar Meteorology. American Meteorological Society*. 1981. Boston, Massachusetts, US.
207. USEPA, *Mercury StudyReport to Congress. Volume III: Fate and Transport of Mercury in the Environment*, 1997, Office of Air Quality Planning and Standards and Office of Research and Development U.S. Environmental Protection Agency. p. 376.
208. Duhanyan, N.,Roustan, Y., *Below-cloud scavenging by rain of atmospheric gases and particulates.* Atmospheric Environment, 2011. 45: p. 7201–7217.
209. Seinfeld, J., *Atmospheric Physics and Chemistry of Air Pollution*1985: Wiley.
210. Slinn, W.G.N., *Atmospheric Sciences and Power Production-1979. Chatpter 11 - Precipitation scavenging*, 1983, Division of Biomedical Environment Research, U.S. Department of Energy.: Washington, D.C. US.
211. Seinfeld, J.H.,Pandis, S.N., *Atmospheric Chemistry and Physics : from air pollution to climate change.*1997, New York: Wiley-Interscience.
212. Louis, J.F., *A parametric model of vertical eddy fluxes in the atmosphere.* Boundary-Layer Meteorology, 1979. 17: p. 187–202.
213. Njomgang, H., Mallet, W.,Musson-Genon, L., *AtmoData Scientific documentation; Version 1 for AtmoData 1.1*, 2007, CEREA – ENPC/EDF R&D: Champs sur Marne.
214. Louis J.F, *A parametric model of vertical eddy fluxes in the atmosphere.* Bound Layer Meteor., 1979. 17: p. 187-202.
215. Louis J.F, Tiedtke M.,Geleyn J.F. *A short history of the PBL parametrization at the ECMWF*. in *ECMWF workshop on planetary boundary layer parametrization*. 1982.

216. Zhang, L., Moran, M.D., Makar, P.A., Brook, J.R.,Gong, S., *Modelling gaseous dry deposition in AURAMS: a unified regional air-quality modelling system*. Atmospheric Environment, 2002a. 36: p. 537–560.
217. Zhang, L., Brook, J.R.,Vet, R., *A revised parameterization for gaseous dry deposition in air-quality models*. Atmospheric Chemistry and Physics, 2003. 3: p. 2067–2082.
218. Zhang, L., Gong, S., Padro, J.,Berrie, L., *A size-segregated particle dry deposition scheme for an atmospheric aerosol module*. Atmospheric Environment, 2001. 35: p. 549–560.
219. Peters, K.,Eiden, R., *Modelling the dry deposition velocity of aerosol particles to a spruce forest*. Atmospheric Environment, 1992. 26: p. 5555-2564.
220. Slinn, W.G.N., *Predictions for particle deposition to vegetative canopies.* Atmospheric Environment, 1982. 16 (7): p. 1785–1794.
221. ENVIRO Database. *The database of the Environmental Investments Resource Optimisation Project*. 2007; Available from: http://149.156.122.159:8988/Enviro-Enviro-context-root//home.jsp.
222. ARE, *Catalog of Power and Cogeneration Plants year 2009 as at 31.12.2008 (in Polish).* ed. A.R.E. S.A.2009a, Warszawa, Poland.
223. ARE, *EMITOR 2008 - The emission of pollution from power and cogeneration plants (in Polish).* ed. A.R.E. S.A.2009b, Warszawa, Poland.
224. Roustan, Y., Bocquet, M., Musson Genon, L.,Sportisse, B. *Modeling atmospheric mercury at European scale with the Chemistry Transport Model Polair 3D.* in *2nd GLOREAM/ EURASAP Workshop*. 2005. Copenhagen: National Environmental Research Institute (Denamark).
225. Vosteen, B.W., Kanefke, R.,Köser, H., *Bromine-enhanced Mercury Abatement from Combustion Flue Gases –Recent Industrial Applications and Laboratory Research.* International Journal for Electricity and Heat Generation, 2006. 86 (3/2006): p. 70-75.
226. Donohoue, D.L., Bauer, D., Cossairt, B.,Hynes, A., *Temperature and pressure dependent rate coefficients for the reaction of Hg with Br and the reaction of Br with Br: A pulsed laser photolysis - pulsed laser induced fluorescence study*. The Journal of Physical Chemistry A., 2006. 110: p. 6623–6632.
227. Kosak-Channing, L.F.,Helz, G.R., *Solubility of ozone in aqueous solutions of 0–0.6 M ionic strength at 5–30^{0}C*. Environmental Science and Technology, 1983. 17: p. 581–591.
228. Smith, R.M.,Martell, A.E., *Critical Stability Constants,Vol. 4, Inorganic Complexes*1976, New York: Plenum.
229. Lin, C.,Pehkonen, S.O., *Two-phase model of mercury chemistry in the atmosphere.* Atmospheric Environment, 1998b. 32: p. 2543–2558.
230. Jacob, D.J., *Chemistry of OH in remote clouds and its role in the production of formic acid and peroxymonosulfate*. Journal of Geophysical Research, 1986. 91D: p. 9807–9826.
231. Schwartz, S.E., *Gas- and aqueous-phase chemistry of HO2 in liquid water clouds.* Journal of Geophysical Research, 1984. 89 (D7): p. 11589–11598.
232. Dean, J.A., *Lange`s Handbook of Chemistry*1992, New York ... McGRAWHILL, INC.
233. Frenzel, A., Scheer, V., Sikorski, R., George, C., Behnke, W.,Zetzsch, C., *Heterogeneous interconversion reactions of $BrNO_2$, $ClNO_2$, Br_2 and Cl_2*. The Journal of Physical Chemistry A., 1998. 102: p. 1329–1337.
234. Sanemasa, I., *The solubility of elemental mercury vapor in water*. Bulletin of the Chemical Society of Japan 1975. 48: p. 1795–1798.

235. Schroeder, W.H.,Munthe, J., *Atmospheric Mercury - an overview*. Atmospheric Environment, 1998. 32: p. 809–822.
236. Lindqvist , O.,Rodhe, H., *Atmospheric mercury – a review*. Vol. 37B. 1985: Tellus.
237. Zyśk, J., Roustan, Y.,Wyrwa, A., *Modelling of the atmospheric dispersion of mercury emitted from the power sector in Poland.* Atmospheric Environment, 2015. 112: p. 246–256.
238. Sillen, G.L.,Martell, A.E., *Stability Constants of Metal Ion Complexes.*, in *Special Publication of the Chemical Society*1964: London. p. 17.
239. Hepler, L.G.,Olofsson, G., *Mercury. Thermodynamic properties, chemical equilibriums, and standard potentials.* Chemical Reviews, 1975. 75: p. 585–602.
240. Poulain, A.J., Garcia, E., Amyot, M., Campbell, P.G.C.,c, P.A.A., *Mercury distribution, partitioning and speciation in coastal vs. inland High Arctic snow*. Geochimica et Cosmochimica Acta 2007. 71: p. 3419–3431.
241. Petersen, G., Munthe, J.,Iverfeldt, A., *Atmospheric mercury species over Central and Northern Europe. Model calculations and comparison with observations from the nordic air and precipitation network for 1987 and 1988.* Atmospheric Environment, 1995. 29: p. 47–67.
242. Massman, W.J., *Molecular diffusivities of Hg vapor in air, O2 and N2 near STP and the kinematic viscosity and thermal diffusivity of air near STP*. Atmospheric Environment, 1999. 33 (3): p. 453–457.
243. Roustan, Y., *Modélisation de la dispersion atmosphérique du mercure, du plomb et du cadmium à l'échelle européenne*, in *ENPC*2005: Champ sur Marne.
244. Maryon, R.H., Saltbones, J., Ryall, D.B., Bartnicki, J., Jakobsen, H.A.,Berge, E., *An intercomparison of three long range dispersion models developed for the UK Meteorological Office, DNMI and EMEP.* , in *UK Met Office Turbulence and Diffusion Note 234*1996, UK Meteorological Office.: Bracknell, United Kingdom.
245. Duhanyan, N., *Parameterisation of the In-Cloud Wet Scavenging of the Atmosphere*, 2012, CEREA , Ecole des Ponts, ParisTech: Champs-sur-Marne, France.
246. Kitada, T.,Nishizawa, M., *Modeling study of the long range transport of acidic pollutants over east asia and the west pacific ocean - sensitivity of acid deposition to scavenging model parameters and emission source distribution.* Journal of Global Environment Engineering, 1998. 4 p. 1–29.
247. GLCC/USGS. *Global Land Cover Characteristics*. 2008; Available from: http://edc2.usgs.gov/glcc/glcc.php.
248. ECMWF. *Provides medium-range weather forecast support to European meteorological organizations*. Available from: www.ecmwf.int.
249. Troen, I.B.,Mahrt, L., *A simple model of the atmospheric boundary layer; sensitivity to surface evaporation.* Boundary-Layer Meteorology, 1986. 37: p. 129–148.
250. Roustan, Y.,Bocquet, M., *Inverse modelling for mercury over Europe.* Atmospheric Chemistry and Physics 2006. 6: p. 3085–3098.
251. Ilyin, I., Rozovskaya, O., Travnikov, O.,Aas, W., *Heavy Metals: Transboundary Pollution of the Environment. EMEP Status Report 2/2007*, 2007, MSC-E of EMEP: Moscow.
252. Chin, M., Rood, R.B., Lin, S.-J., Muller, J.-F.,Thompson, A.M., *Atmospheric sulfur cycle simulated in the global model GOCART: Model description and global properties.* . Journal of Geophysical Research: Atmospheres, 2000. 105 (D20): p. 24671–24687.
253. Simpson, D., Winiwarter, W., Borjesson, G., Cinderby, S., Ferreiro, A., Guenther, A., Hewitt, C.N., Janson, R., Khalil, M.A.K., Owen, S., Pierce, T.E., Puxbaum, H., Shearer, M., Skiba, U., Steinbrecher, R., Tarrason, L.,Oquist, M.G., *Inventorying*

emissions from nature in Europe. Journal of Geophysical Research: Atmospheres 1999. 104 (D7): p. 8113–8152.
254. Monahan, E.C., Spiel, D.E.,Davidson, K.L., *A Model of Marine Aerosol Generation Via Whitecaps and Wave Disruption*, in *Oceanic Whitecaps*, 1986, Springer Netherlands. p. 167– 174.
255. Friedrich, R.,Reis, S., *Emissions of Air Pollutants - Measurements, Calculation, Uncertainties - Results from the EUROTRAC-2 Subproject GENEMIS*,2004, Berlin, Heidelberg, Germany: Springer Publishers.
256. Graede, T.E.,Keene, W.C., *The budget and cycle of Earth's natural chlorine.* Pure and Applied Chemistry, 1996. 68: p. 1689–1697.
257. Stark, H., Brown, S.S., Goldan, P.D., Aldener, M., Kuster, W.C., Jakoubek, R., Fehsenfeld, F.C., Meagher, J., Bates, T.S.,Ravishankara, A.R., *Influence of nitrate radical on the oxidation of dimethyl sulfide in a polluted marine environment*. Journal of Geophysical Research, 2007. 112 (D10S10): p. 11.
258. Kim, J.P.,Fitzgerald, W.F., *Sea-air partitioning of mercury in the Equatorial Pacific Ocean.* Science, 1986. 231: p. 1131-1133.
259. Seigneur, C., Karamchandani, P., Vijayaraghavan, K., Lohman, K., Shia, R.,Levin, L., *On the effect of spatial resolution on atmospheric mercury modeling.* Science of the Total Environment, 2003. 304: p. 73–81.
260. Shatalov, V., I., I., A., G., O., R.,O., T., *Heavy Metals and Persistent Organic Pollutants: Model Assessment of Pollution and Research Activities. MSC-E Technical Report 1/2014*, 2014, MCS-E: Moscow.
261. Pan, L., Carmichael, G.R., Adhikary, B., Tang, Y., Streets, D., Wooc, J.-H., Friedlid, H.R.,Radke, L.F., *A regional analysis of the fate and transport of mercury in East Asia and an assessment of major uncertainties.* Atmospheric Environment, 2008. 42: p. 1144–1159.
262. Ilyin, I., Rozovskaya, O., Shatalov, V., Sokovykh, V., Travnikov, O., Varygina, M., Aas, W.,Uggerud, H.T., *Heavy Metals: Transboundary Pollution of the Environment. EMEP Status Report 2/2010*, 2010, EMEP/MSC-E EMEP-CCC/NILU: Moscow.
263. CAMx, *User's Guide of Comprehensive Air Quality Model, Version 4.20, with extensions.*, 2005, ENVIRON International Corporation Novato, US. p. 235.
264. Zhang, L., P. Blanchard, P., Johnson, D., Dastoor, A., Ryzhkov , A., Lin, C.J., Vijayaraghavan, K., Gay, D., Holsen, T.M., Huang, J., Graydon, J.A., St. Louis, V.L., Castro, M.S., Miller, E.K., Marsik, F., Luk, J., Poissant, L., Pilote, M.,Zhang, K.M., *Assessment of modeled mercury dry deposition over the Great Lakes region.* Environmental Pollution, 2012. 161: p. 272–283.

List of Tables

List of Figures

Appendix 1

History of the development of the Polyphemus air quality system.

N	File name	File role and task	History of development
1	HeavyMetal.cxx	Connection of code C++ code with fortan routines dedicated for heavy metals	Author(s): **Janusz Zysk**, Yelva Roustan 2010-2012
2	aerosol.f	Main routine for heavy metals in aqueous and aerosol phases	AUTHOR(S) **Janusz Zysk**, CEREA, January 2010. MODIFICATIONS 2012/02/01: Cleaning (Yelva Roustan, CEREA).
3	chem.f	Main routine for chemistry of mercury in gaseous phase	-- AUTHOR(S) Denis Quélo, CEREA, June 2001. -- MODIFICATIONS 2012/02/01: Cleaning (Yelva Roustan, CEREA). 2010/01/01: Upgrading and inclusion in Polyphemus (**Janusz Zysk**, CEREA). 2005/09/01: Adaptation for the Polair3D mercury mechanism (Yelva Roustan, CEREA).
4	fexchem.f	Computes the chemical production term for the mercury gas-phase chemical kinetic mechanism.	AUTHOR(S) Yelva Roustan, CEREA, September 2005. MODIFICATIONS 2012/02/01: Cleaning (Yelva Roustan, CEREA). 2010/01/01: Upgrading and inclusion in Polyphemus (**Janusz Zysk**, CEREA).
5	jacdchemdc.f	Computes the jacobian matrix for the mercurygas-phase chemical kinetic mechanism.	AUTHOR(S) Yelva Roustan, CEREA, September 2005. MODIFICATIONS 2012/02/01: Cleaning (Yelva Roustan, CEREA). 2010/01/01: Upgrading and inclusion in Polyphemus (**Janusz Zysk**, CEREA).
6	kinetic.f	Computes the chemical reaction rate coefficients for the mercury gas-phase chemical kinetic mechanism.	AUTHOR(S) Yelva Roustan, CEREA, September 2005. MODIFICATIONS 2010/01/01: Upgrading and inclusion in Polyphemus (**Janusz Zysk**, CEREA). 2012/02/01: Cleaning (Yelva Roustan, CEREA).
7	roschem.f	Computes one time step for the mercury gas-phase chemical kinetic mechanism.	-- AUTHOR(S) Denis Quélo, CEREA, June 2001. -- MODIFICATIONS 2012/02/01: Cleaning (Yelva Roustan, CEREA). 2010/01/01: Upgrading and inclusion in Polyphemus (**Janusz Zysk**, CEREA). 2005/09/01: Adaptation for the Polair3D mercury mechanism (Yelva Roustan, CEREA).
8	chem_aq.f	This routine computes one time step for the aqueous phase mercury chemical kinetic mechanism. Chemical kinetics is solved in each grid cell.	-- MODIFICATIONS 2012/02/01: Cleaning (Yelva Roustan, CEREA). -- AUTHOR(S) **Janusz Zysk,** CEREA, January 2010.
9	fexchem_aq.f	This routine computes the chemical production term for the mercury aqueous-phase chemical kinetic mechanism.	-- MODIFICATIONS 2012/02/01: Cleaning (Yelva Roustan, CEREA). -- AUTHOR(S) **Janusz Zysk,** CEREA, January 2010.

10	jacdchemdc_aq.f	This routine computes the jacobian matrix for the mercury aqueous-phase chemical kinetic mechanism.	-- MODIFICATIONS 2012/02/01: Cleaning (Yelva Roustan, CEREA). -- AUTHOR(S) **Janusz Zysk**, CEREA, January 2010.
11	kinetic_aq.f	This routine computes the chemical reaction rate coefficients for the mercury aqueous phase chemical kinetic mechanism.	-- MODIFICATIONS 2012/02/01: Cleaning (Yelva Roustan, CEREA). -- AUTHOR(S) **Janusz Zysk**, CEREA, January 2010.
12	roschem_aq.f	This routine computes one time step for the mercury aqueous phase chemical kinetic mechanism. The solver is based on a second-order Rosenbrock method The linear systems to be solved are optimized.	-- MODIFICATIONS 2012/02/01: Cleaning (Yelva Roustan, CEREA). -- AUTHOR(S) **Janusz Zysk,** CEREA, January 2010.
13	chem_aer.f	This routine computes one time step for the heterogeneous mercury chemical kinetic mechanism. Chemical kinetics is solved in each grid cell.	-- MODIFICATIONS 2012/02/01: Cleaning (Yelva Roustan, CEREA). -- AUTHOR(S) **Janusz Zysk**, CEREA, January 2010.
14	fexchem_aer.f	This routine computes the chemical production term for the mercury heterogeneous chemical kinetic mechanism.	-- MODIFICATIONS 2012/02/01: Cleaning (Yelva Roustan, CEREA). -- AUTHOR(S) Janusz Zysk, CEREA, January 2010.
15	jacdchemdc_aer.f	This routine computes the Jacobian matrix for the mercury heterogeneous chemical kinetic mechanism.	-- MODIFICATIONS 2012/02/01: Cleaning (Yelva Roustan, CEREA). -- AUTHOR(S) **Janusz Zysk**, CEREA, January 2010.
16	kinetic_aer.f	This routine computes the chemical reaction rate coefficients for the mercury heterogeneous mercury chemical kinetic mechanism.	-- MODIFICATIONS 2012/02/01: Cleaning (Yelva Roustan, CEREA). -- AUTHOR(S) **Janusz Zysk,** CEREA, January 2010.
17	roschem_aer.f	This routine computes one time step for the mercury heterogeneous chemical kinetic mechanism. The solver is based on a second-order Rosenbrock method (see the user's guide). The linear systems to be solved are optimized.	-- MODIFICATIONS 2012/02/01: Cleaning (Yelva Roustan, CEREA). -- AUTHOR(S) **Janusz Zysk**, CEREA, January 2010.
18	solvlin.f	Matrix decomposition	AUTHOR(S) Denis Quélo, CEREA, June 2001. MODIFICATIONS 2012/02/01: Cleaning (Yelva Roustan, CEREA). 2010/01/01: Upgrading and inclusion in Polyphemus (**Janusz Zysk**, CEREA).

			2004/08/11: Adaptation for the Polair3D mercury mechanism (Yelva Roustan, CEREA). 2001/11/05: Adaptation for the EMEP chemical mechanism (Jaouad Boutahar, CEREA).

ACC CYFRONET AGH (PL-Grid Plus) is acknowledged for the computing time.